

**Some pages of this thesis may have been removed for copyright restrictions.**

If you have discovered material in AURA which is unlawful e.g. breaches copyright, (either yours or that of a third party) or any other law, including but not limited to those relating to patent, trademark, confidentiality, data protection, obscenity, defamation, libel, then please read our [Takedown Policy](#) and [contact the service](#) immediately

**RUTHENIUM COMPLEXES AS POTENTIAL  
AQUEOUS ROMP CATALYSTS**

**PHILLIP JOSEPH BOUIC**

**Doctor of Philosophy**

**THE UNIVERSITY OF ASTON IN BIRMINGHAM**

**March 1996**

**This copy of the thesis has been supplied on condition that anyone who consults it is understood to recognise that its copyright rests with its author and that no quotation from the thesis and no information derived from it may be published without proper acknowledgement.**

The University of Aston in Birmingham.

Ruthenium Complexes as Potential Aqueous ROMP Catalysts.

Phillip Joseph Bouic

Submitted for the Degree  
of Doctor of Philosophy

March 1996

SUMMARY

The research described herein relates to studies into the Aqueous Ring-Opening Metathesis Polymerisation (ROMP) of bicyclic monomers using ruthenium complex catalysts. Two monomers were synthesised for the purpose of these studies, namely *exo*, *exo*-7-oxabicyclo[2.2.1]hept-5-ene-2,3-dicarboxylic acid (7-oxanorbornenedicarboxylic acid) and *exo*, *exo*-bicyclo[2.2.1]hept-5-ene-2,3-dicarboxylic acid (norbornene dicarboxylic acid).

A number of ruthenium complexes were synthesised, amongst them a novel complex containing the water soluble phosphine ligand tris(hydroxymethyl)phosphine  $P(CH_2OH)_3$ . Its synthesis and characterisation are described and its physical properties compared and contrasted to analogous compounds of platinum and palladium. Its peculiar properties are ascribed to a *trans*- placement of the phosphine ligands.

Dilatometry was investigated as a technique for the acquisition of kinetic data from aqueous metathesis reactions. For the attempted polymerisation of 7-oxanorbornenedicarboxylic acid the results are explained in terms of a reverse Diels-Alder reaction of the monomer.

The reaction between  $Ru(CO)Cl_2(H_2O)$  and 7-oxanorbornenedicarboxylic acid was monitored using UV/Vis spectrometry and kinetic data retrieved. The data are explained in terms of a two stage reaction consisting of consecutive first order processes.

The reaction between 7-oxanorbornenedicarboxylic acid and  $Ru(CO)Cl_2(H_2O)$  or  $Ru(P(CH_2OH)_3)_3Cl_2$  was found to produce fumaric acid as one of the major products. This reaction is previously unreported in the literature and a mechanism is proposed.

**Keywords:** Aqueous Ring-Opening Metathesis Polymerisation,  
Ruthenium,  
Tris(hydroxymethyl)phosphine,  
Isomerisation,  
Fumaric acid.

*To my parents.*

## ACKNOWLEDGEMENTS

Firstly considerable thanks are due to Dr. J.D. Miller for his support, advice, encouragement and help as I have perspired, panicked and struggled my way through the last three and a half years. I have been very lucky in having a supervisor who was not only incredibly easy to find when problems needed solving but who was also good enough to leave me on my own when I felt I had to make my own mistakes. Thank you.

Thanks are due to E.P.S.R.C for financial support and Albright and Wilson and Johnson Matthey for the provision of essential chemicals without which this research would not have been possible.

Many thanks to Dr. M. Perry for the acquisition of all the NMR spectra contained in this thesis and also for being a final year PhD student's best friend - thanks to your help and patience I could now queue jump for England! Thanks to Steve Tonge and Scott Goodall for molecular modelling on ChemX, and thanks also to Dr. A.J Amass, Mike Houghton, Denise Ingram and Maurizio Santoro for practical help and advice when needed and a good chinwag when I needed to forget about my work.

I could not have asked for better friends to spend my university career with - in particular I'd like to thank Mark Smith and Andy Hall for too many things to mention. I suppose you only really appreciate how much you need your friends when they are no longer around - enough said. However, I would not like to thank Mark 'Twig-legs' Smith for financial advice in the form of enticing me to HMV and Virgin. Thanks to you I now have the "dogs" of a C.D. collection and a huge credit card bill! Thanks are also not due to Andy 'Fatty' Hall for being a glory hunter - mind you I suppose you gave me something to laugh about on Coca-Cola Cup Final day! I am also indebted to the reprobates who have occupied Labs 208/209 over the last however many years, namely Mike, Rob, Colin, Fred, Karine, Babs, Monali, Luke and Val (I think that's all of you!). Specifically, Mike for his shirts and a ticket for Leicester vs Villa, Fred and Karine for a stonking holiday, Monali for giving me somebody else's work to do when I wasn't too busy doing my own and Babs for possessing that rare and elusive personal trait - certifiable insanity! Also a big "Thanks" to the all on the third floor, and of course not forgetting two Crunchy Frogs not mentioned elsewhere on this page - Leon and Iain.

The only person left to thank knows who she is. You've put up with a lot from this occasionally grouchy, short-tempered, depressed, terminally unemployed bag of nerves whilst I've been trying to write this thesis - and I'll be eternally grateful. Thank you for hanging around and believing in me.

## List of Contents.

<u>Section Number</u>	<u>Title</u>	<u>Page Number</u>
	<b>Title Page.</b>	1
	<b>Summary.</b>	2
	<b>Dedication.</b>	3
	<b>Acknowledgements.</b>	4
	<b>List of Contents.</b>	5
	<b>List of Tables.</b>	11
	<b>List of Figures.</b>	17
<b>Chapter 1</b>	<b>INTRODUCTION.</b>	<b>27</b>
1.1	Background to Metathesis.	27
1.2	The Mechanism of Metathesis.	28
1.3	Metathesis Catalysts.	32
1.3.1	One Component (Unary) Catalytic Systems.	32
1.3.2	Two Component (Binary) Catalytic Systems.	35
1.3.3	Three Component (Ternary) Catalytic Systems.	36
1.4	Aqueous ROMP.	36
1.5	Summary.	46
<b>Chapter 2</b>	<b>MATERIALS AND METHODS.</b>	<b>47</b>
2.1	Materials.	47
2.2	Methods.	47
2.2.1	General Synthetic Methods.	47
2.2.2	Dilatometry.	47
2.2.3	Ultra-Violet/Visible Spectroscopy.	49

<u>Section Number</u>	<u>Title</u>	<u>Page Number</u>
2.2.4	Infra-Red Spectroscopy.	52
2.2.5	Nuclear Magnetic Resonance Spectroscopy.	52
2.2.6	Size Exclusion Chromatography.	52
2.2.7	Elemental Analysis.	52
2.2.8	Melting Points.	52
<b>Chapter 3</b>	<b>SYNTHESIS OF BICYCLIC MONOMERS.</b>	<b>53</b>
3.1	Introduction.	53
3.2	The Diels-Alder Reaction.	55
3.3	Synthesis No.1 - <i>Exo, exo</i> -7-oxabicyclo[2.2.1]hept-5-ene-2,3-dimethanol.	56
3.4	Synthesis No.2 - <i>Exo</i> -oxabicyclo[2.2.1]hept-5-ene-2,3-dicarboxylic anhydride.	58
3.5	Synthesis No.3 - <i>Endo, endo</i> -bicyclo[2.2.1]hept-5-ene-2,3-dicarboxylic acid.	61
3.6	Synthesis No.4 - <i>Exo</i> -bicyclo[2.2.1]hept-5-ene-2,3-dicarboxylic anhydride.	62
3.7	Comparison of <i>Endo</i> - and <i>Exo</i> -bicyclo[2.2.1]hept-5-ene dicarboxylic anhydride.	62
<b>Chapter 4</b>	<b>SYNTHESIS OF WATER SOLUBLE PHOSPHINE COMPOUNDS.</b>	<b>64</b>
4.1	Synthesis No.5 - Tris(hydroxymethyl)phosphine (THMP).	64
4.2	Synthesis No.6 - Trisodium salt of tris( <i>m</i> -sulfophenyl)phosphine (TPPTS).	69

<u>Section Number</u>	<u>Title</u>	<u>Page Number</u>
<b>Chapter 5</b>	<b>RUTHENIUM COMPLEXES AND THEIR SYNTHESSES.</b>	<b>73</b>
5.1	The Element.	73
5.2	The Complex Chemistry of Ruthenium.	73
5.3	Some Kinetic Aspects of Ruthenium Chemistry.	83
5.3.1	Reduction-Oxidation (Redox) Reactions.	83
5.3.2	Substitution Reactions.	87
5.4	Complex Synthesis.	91
5.4.1	Synthesis No.7 - Hexammineruthenium(II)chloride.	91
5.4.2	Synthesis No.8 - Hexammineruthenium(II) tetrachlorozincate.	92
5.4.3	Synthesis No.9 - Pentamminechlororuthenium(III) dichloride.	93
5.4.4	Synthesis No.10 - Dichlorodicarbonylruthenium(II).	94
5.4.5	Synthesis No.11 - Dichloroaquocarbonyl ruthenium(II).	94
5.4.6	Synthesis No.12 - Ruthenium(II)tris (triphenylphosphine)dichloride.	94
5.4.7	Synthesis No.13 - Ruthenium(II)cyclooctadiene dichloride.	95
5.4.8	Synthesis No.14 - Dinitrosylbis(triphenyl- phosphine)ruthenium.	95
5.4.9	Synthesis No.15 - Palladium(II)dichlorocyclo octadiene.	96
5.4.10	Synthesis No.16 - Palladium(II)bis(trishydroxy methylphosphine)dichloride.	96



<u>Section Number</u>	<u>Title</u>	<u>Page Number</u>
5.4.11	Synthesis No.17 - Attempted Synthesis of Rutheniumpoly(trishydroxymethyl)dichloride.	97
5.4.12	Synthesis No.18 - Attempted Synthesis of dinitrosylbis(trishydroxymethylphosphine)ruthenium.	102
5.4.13	Synthesis No.19 - Potassiumtrisoxalato ruthenium(III).	103
5.4.14	Synthesis No.20 - Oxalatobis(ethylenediamine) ruthenium(III)bis(oxalato)ethylenediamine ruthenate(III).	104
5.4.15	Synthesis No.21 - Dichlorobis(ethylenediamine) ruthenium(III)chloridemonohydrate.	104
5.4.16	Synthesis No. 22 - <i>trans</i> -Carbonylchlorobis (triphenylphosphine)iridium (Vaska's Compound).	104
5.4.17	Synthesis No. 23 - Attempted Synthesis of Carbonylchlorobis(tris(hydroxymethyl)phosphine) iridium.	105
<b>Chapter 6</b>	<b>EXPERIMENTAL.</b>	<b>110</b>
6.1	Polymerisation of 7-Norbornene dicarboxylic acid using $\text{RuCl}_3 \cdot 3\text{H}_2\text{O}$ .	110
6.2	Dilatometry.	111
6.3	Interaction between 7-Oxanorbornene dicarboxylic acid and $\text{Ru}(\text{CO})\text{Cl}_2(\text{H}_2\text{O})$ .	116
6.4	Interaction between 7-Oxanorbornene dicarboxylic acid and $\text{Ru}(\text{CO})\text{Cl}_2(\text{H}_2\text{O})$ Monitored by UV Spectroscopy.	116

<u>Section Number</u>	<u>Title</u>	<u>Page Number</u>
6.5	Interaction between Bicyclic Monomers and a Ru-P(CH <sub>2</sub> OH) <sub>3</sub> Complex.	121
6.6	Initiation of Polymerisation using Ethyldiazoacetate.	124
6.7	Interaction between <i>cis</i> -[Ru(en) <sub>2</sub> (H <sub>2</sub> O) <sub>2</sub> ] <sup>2+</sup> and 7-Oxanorbornene dicarboxylic acid.	126
6.8	Interaction between [Ru(NH <sub>3</sub> ) <sub>5</sub> N <sub>2</sub> ] <sup>2+</sup> and 7-Oxanorbornene dicarboxylic acid.	126
<b>Chapter 7</b>	<b>RESULTS.</b>	<b>128</b>
7.1	Polymerisation of 7-Norbornene dicarboxylic acid using RuCl <sub>3</sub> .3H <sub>2</sub> O.	128
7.2	Dilatometry as a Method for Monitoring Aqueous ROMP.	128
7.3	The Interaction between 7-Oxanorbornene dicarboxylic acid and Ru(CO)Cl <sub>2</sub> (H <sub>2</sub> O) and its Monitoring by UV Spectroscopy.	138
7.4	The Interaction between 7-Oxanorbornene dicarboxylic acid and a Ru-P(CH <sub>2</sub> OH) <sub>3</sub> Complex.	147
7.5	The Interaction between 7-Oxanorbornene dicarboxylic acid and various Ru <sup>2+</sup> Complexes.	148
<b>Chapter 8</b>	<b>DISCUSSION AND CONCLUSIONS.</b>	<b>149</b>
8.1	The Synthesis of a Ruthenium Complex containing the Ligand P(CH <sub>2</sub> OH) <sub>3</sub> .	149
8.2	The Mechanism of Production of Fumaric acid.	157
8.3	The Interaction between 7-Oxanorbornene dicarboxylic acid and Ru(CO)Cl <sub>2</sub> (H <sub>2</sub> O) Monitored by UV Spectroscopy.	169

<u>Section Number</u>	<u>Title</u>	<u>Page Number</u>
8.4	Aqueous ROMP using Ruthenium Complex Catalysts - Conclusions.	176
	<b>References</b>	<b>178</b>
	<b>Appendix A - Data Tables.</b>	<b>187</b>
	<b>Appendix B - NMR and IR spectra.</b>	<b>199</b>

## List of Tables.

<u>Section Number</u>	<u>Title</u>	<u>Page Number</u>
<b>Chapter 1</b>		
<b>Section 1.4</b>		
Table 1.4.1	Comparison of experimental techniques for the polymerisation of oxanorbornene dicarboxylic acid. (100% aqueous solvent)	39
Table 1.4.2	ROMP of <i>exo, exo</i> -2,3-bis(methoxymethyl)-7-oxanorbornene catalysed by commercial RuCl <sub>3</sub> .	40
Table 1.4.3	ROMP of 7-oxanorbornene derivatives catalysed by RuCl <sub>3</sub> .	46
<b>Chapter 2</b>		
<b>Section 2.2.2</b>		
Table 2.2.2.1	Dilatometer dimensions.	49
<b>Chapter 3</b>		
<b>Section 3.1</b>		
Table 3.1.1	Monomers used in aqueous ROMP.	54
<b>Section 3.4</b>		
Table 3.4.1	<sup>13</sup> C NMR data for <i>exo</i> -oxabicyclo[2.2.1]hept-5-ene-2,3-dicarboxylic anhydride.	59
Table 3.4.2	<sup>1</sup> H NMR data for <i>exo</i> -oxabicyclo[2.2.1]hept-5-ene-2,3-dicarboxylic anhydride.	60

<u>Section Number</u>	<u>Title</u>	<u>Page Number</u>
<b>Section 3.7</b>		
Table 3.7.1	Chemical shifts in ppm from $^{13}\text{C}$ spectra of <i>endo</i> -adduct and <i>exo</i> -adduct of bicyclo[2.2.1]hept-5-ene dicarboxylic anhydride.	63
 <b>Chapter 4</b>		
<b>Section 4.1</b>		
Table 4.1.1	$^{31}\text{P}$ and $^{13}\text{C}$ NMR data for synthesised $\text{P}(\text{CH}_2\text{OH})_3$ .	66
Table 4.1.2	$^1\text{H}$ NMR data for synthesised $\text{P}(\text{CH}_2\text{OH})_3$ .	66
Table 4.1.3	Negative $^{31}\text{P}$ NMR data for phosphine mix.	68
<b>Section 4.2</b>		
Table 4.2.1	$^{31}\text{P}$ and $^{13}\text{C}$ NMR data for TPPTS, TPPTS-oxide and synthesised product.	71
 <b>Chapter 5</b>		
<b>Section 5.1</b>		
Table 5.1.1	Some physical properties of Ruthenium.	73
<b>Section 5.3.1</b>		
Table 5.3.1.1	Rate constants for the electron exchange reaction between various $\text{Ru}^{3+/2+}$ ammines at $25^\circ\text{C}$ .	86
<b>Section 5.3.2</b>		
Table 5.3.2.1	Rate and $\Delta V^\ddagger$ data for solvent exchange on Ru(III) and Ru(II).	89
Table 5.3.2.2	Radius, configuration and $\Delta V^\ddagger$ data for $\text{M}^{2+}$ .	90
<b>Section 5.4.1</b>		
Table 5.4.1.1	Infra-red data for hexammineruthenium(II)dichloride.	92

<u>Section Number</u>	<u>Title</u>	<u>Page Number</u>
<b>Section 5.4.3</b>		
Table 5.4.3.1	Infra-red data for pentamminechlororuthenium(III) dichloride.	93
<b>Section 5.4.11</b>		
Table 5.4.11.1	$^{31}\text{P}$ and $^{13}\text{C}$ NMR data for Ru-P(CH <sub>2</sub> OH) <sub>3</sub> complex from synthesis No.17.	100
Table 5.4.11.2	$^1\text{H}$ NMR spectral data for Ru-P(CH <sub>2</sub> OH) <sub>3</sub> complex from synthesis No.17.	101
Table 5.4.11.3	Elemental analysis of Ru-P(CH <sub>2</sub> OH) <sub>3</sub> complex from synthesis No.17.	102
<b>Section 5.4.17</b>		
Table 5.4.17.1	$^{31}\text{P}$ , $^1\text{H}$ and $^{13}\text{C}$ NMR data for products from synthesis No. 23.	107
 <b>Chapter 6</b>		
<b>Section 6.2</b>		
Table 6.2.1	Experimental details for Dil1.	111
Table 6.2.2	Experimental details for Dil2.	111
Table 6.2.3	Experimental details for Dil3.	112
Table 6.2.4	Experimental details for Dil4.	112
Table 6.2.5	Experimental details for Dil5.	113
Table 6.2.6	Experimental details for Dil6.	113
Table 6.2.7	Experimental details for Dil7.	114
Table 6.2.8	Experimental details for Dil8.	114
Table 6.2.9	Experimental details for Dil9.	115
Table 6.2.10	Experimental details for Dil10.	115

<u>Section Number</u>	<u>Title</u>	<u>Page Number</u>
<b>Section 6.3</b>		
Table 6.3.1	Experimental details for reaction between 7-oxanorbornene dicarboxylic acid and Ru(CO)Cl <sub>2</sub> (H <sub>2</sub> O).	116
<b>Section 6.4</b>		
Table 6.4.1	Experimental details for UV1.	118
Table 6.4.2	Experimental details for UV2.	119
Table 6.4.3	Experimental details for UV3.	119
Table 6.4.4	Experimental details for UV4.	119
Table 6.4.5	Experimental details for UV5.	119
<b>Section 6.5</b>		
Table 6.5.1	Experimental details for Set 6.5.1.	121
Table 6.5.2	Experimental details for Set 6.5.2.	122
Table 6.5.3	Precipitate yields for Set 6.5.2.	122
Table 6.5.4	Experimental details for Set 6.5.3.	123
Table 6.5.5	Precipitate yields for Set 6.5.3.	123
<b>Section 6.6</b>		
Table 6.6.1	Experimental details for Set 6.6.2.	124
Table 6.6.2	Experimental details for Set 6.6.3.	125
Table 6.6.3	Product yield for Set 6.6.3.	125
<b>Chapter 7</b>		
<b>Section 7.2</b>		
Table 7.2.1	Rates of change in meniscus height and best straight line fits for Dil1 and Dil2.	129
Table 7.2.2	Rates of change in meniscus height and best straight line fits for Dil3.	130

<u>Section Number</u>	<u>Title</u>	<u>Page Number</u>
Table 7.2.3	Rates of change in meniscus height and best straight line fits for Dil4 - Samples 3, 6 &7.	131
Table 7.2.4	Rates of change in meniscus height and best straight line fits for Dil5.	133
Table 7.2.5	Rates of change in meniscus height and best straight line fits for Dil6.	134
<b>Section 7.3</b>		
Table 7.3.1	$K_1$ , $k_1$ and $\beta[A]_0$ for early data ( $t < 180$ mins) from UV2 - UV5.	142
Table 7.3.2	$k_0$ , Z and Y for UV1- UV5.	145
Table 7.3.3	$^1\text{H}$ and $^{13}\text{C}$ NMR data for product from reaction between $\text{Ru}(\text{CO})\text{Cl}_2(\text{H}_2\text{O})$ and monomer.	146
<b>Section 7.4</b>		
Table 7.4.1	$^1\text{H}$ , $^{13}\text{C}$ and $^{31}\text{P}$ NMR data for product from the reaction between monomer and $\text{Ru}-\text{P}(\text{CH}_2\text{OH})_3$ complex.	148
<b>Chapter 8</b>		
<b>Section 8.1</b>		
Table 8.1.1	Synthesis of $\text{P}(\text{CH}_2\text{OH})_3$ complexes of Pt, Pd and Ni.	149
Table 8.1.2	Sum of orbital energies - $d^6$ and $d^8$ octahedral and square planar complexes.	154
Table 8.1.3	Cone angles for various triphosphines.	155
<b>Section 8.3</b>		
Table 8.3.1	Equation constants for solutions with constant $\text{Ru}(\text{CO})\text{Cl}_2(\text{H}_2\text{O})$ concentration. (0.025 M) ( $T=70^\circ\text{C}$ ).	170



<u>Section Number</u>	<u>Title</u>	<u>Page Number</u>
Table 8.3.2	Equation constants for solutions with constant monomer concentration. (0.01 M) (T=60°C).	170

**APPENDIX A.**

Table A1	List of chemicals and suppliers.	187
Table A2	Dilatometry data for DIL1.	188
Table A3	Dilatometry data for DIL2.	188
Table A4	Dilatometry data for DIL3.	189
Table A5	Dilatometry data for DIL4.	190
Table A6	Dilatometry data for DIL5.	190
Table A7	Dilatometry data for DIL6.	191
Table A8	Dilatometry data for DIL7.	191
Table A9	Dilatometry data for DIL8.	192
Table A10	Dilatometry data for DIL9.	192
Table A11	Dilatometry data for DIL10.	193
Table A12	Absorbance data for UV1.	193
Table A13	Absorbance data for UV2.	193
Table A14	Absorbance data for UV3.	195
Table A15	Absorbance data for UV4.	197
Table A16	Absorbance data for UV5.	198

## List of Figures

<u>Section Number</u>	<u>Title</u>	<u>Page Number</u>
<b>Chapter 1</b>		
<b>Section 1.1</b>		
Figure 1.1.1	Metathesis of linear olefins.	27
Figure 1.1.2	Ring-Opening Metathesis Polymerisation (ROMP) of a cyclic olefin.	27
Figure 1.1.3	ROMP of norbornene.	27
Figure 1.1.4	Metathesis of propene into ethene and 2-butene.	28
<b>Section 1.2</b>		
Figure 1.2.1	The general form of the pair-wise mechanism for metathesis.	28
Figure 1.2.2	The general form of the carbene mechanism for metathesis polymerisation.	29
Figure 1.2.3	A pair-wise reaction scheme for a co-metathesis reaction.	29
Figure 1.2.4	A carbene reaction scheme for a co-metathesis reaction.	30
Figure 1.2.5	Carbene formation from a transition metal and a metal alkyl.	31
Figure 1.2.6	Carbene formation from an O <sub>2</sub> mechanism.	31
<b>Section 1.3</b>		
Figure 1.3.1.1	Synthesis of an alkylidene complex of Niobium and Tantalum.	33
Figure 1.3.1.2	Synthesis of a unary metathesis catalyst of tungsten.	34
Figure 1.3.1.3	Synthesis of a stable ruthenium-carbene metathesis catalyst.	35
<b>Section 1.4</b>		
Figure 1.4.1	Aqueous ROMP of oxanorbornene derivatives.	36

<u>Section Number</u>	<u>Title</u>	<u>Page Number</u>
Figure 1.4.2	Mono-olefin adduct from polymerisation of (II) with Ru(H <sub>2</sub> O) <sub>6</sub> (tos) <sub>2</sub> .	37
Figure 1.4.3	Polymerisation of oxanorbornenedicarboxylic anhydride in 10% water in ethanol.	38
Figure 1.4.4	Plot of change in k <sub>obs</sub> vs concentration of RuCl <sub>3</sub> added, [C].	40
Figure 1.4.5	Proposed deactivation of the active centre by ruthenium species.	43
 <b>Chapter 3</b>		
<b>Section 3.2</b>		
Figure 3.2.1	The Diels-Alder reaction.	55
Figure 3.2.2	Orbital overlap for the Diels-Alder reaction of maleic anhydride with cyclopentadiene.	56
<b>Section 3.3</b>		
Figure 3.3.1	Synthesis of <i>exo, exo</i> -7-oxabicyclo[2.2.1]hept-5-ene-2,3-dimethanol.	57
<b>Section 3.4</b>		
Figure 3.4.1	Synthesis of <i>exo</i> -7-oxabicyclo[2.2.1]hept-5-ene-2,3-dicarboxylic anhydride.	58
Figure 3.4.2	Carbon numbering for <sup>13</sup> C NMR analysis.	59
Figure 3.4.3	Proton numbering for <sup>1</sup> H NMR analysis.	60
<b>Section 3.5</b>		
Figure 3.5.1	Synthesis of <i>endo, endo</i> -bicyclo[2.2.1]hept-5-ene-2,3-dicarboxylic acid.	61

<u>Section Number</u>	<u>Title</u>	<u>Page Number</u>
<b>Section 3.6</b>		
Figure 3.6.1	Synthesis of <i>exo</i> -bicyclo[2.2.1]hept-5-ene-dicarboxylic anhydride.	62
<b>Section 3.7</b>		
Figure 3.7.1	Carbon numbering for <sup>13</sup> C NMR analysis	63
<b>Chapter 4</b>		
<b>Section 4.1</b>		
Figure 4.1.1	Possible five membered ring structure in crude phosphine mixture.	67
Figure 4.1.2	Mechanism for the formation of a methyl phosphine species.	68
<b>Section 4.2</b>		
Figure 4.2.1	Carbon number assignments for <sup>13</sup> C NMR data.	70
Figure 4.2.2	Complex peak region of <sup>1</sup> H NMR spectrum of TPPTS/TPPTS-oxide mix	72
<b>Chapter 5</b>		
<b>Section 5.2</b>		
Figure 5.2.1	Alkene oxidation by RuO <sub>4</sub> .	74
Figure 5.2.2	The disproportionation of ruthenate(VI) in aqueous solution.	75
Figure 5.2.3	Proposed structure of ruthenium red.	77
Figure 5.2.4	Proposed structure of ruthenium brown.	77
Figure 5.2.5	Alkyne oxidation by aquapentachlororuthenate(III).	78
Figure 5.2.6	Mixed oxidation state complex - [Ru <sub>2</sub> Cl <sub>5</sub> (PBU <sub>3</sub> ) <sub>4</sub> ]	79
Figure 5.2.7	Alkene cleavage to produce carbenes.	80
Figure 5.2.8	A synthetic route to a ruthenium-carbene complex.	80

<u>Section Number</u>	<u>Title</u>	<u>Page Number</u>
Figure 5.2.9	ROMP using a diazoester initiated ruthenium complex.	80
Figure 5.2.10	Chlorocarbonylruthenium complex formation.	82
<b>Section 5.3.1</b>		
Figure 5.3.1.1	Bridge formation in an inner-sphere redox reaction.	83
Figure 5.3.1.2	Redox process proceeding by either an inner-sphere or outer-sphere mechanism.	85
Figure 5.3.1.3	Plot of logarithm of the observed exchange rate constant (log K) vs the reciprocal of the mean distance of closest approach of the ruthenium centres (1/r).	86
<b>Section 5.3.2</b>		
Figure 5.3.2.1	Schematic representation of the range of substitution mechanisms.	87
Figure 5.3.2.2	Rate constants ( $s^{-1}$ ) for water exchange of metal cations.	88
<b>Section 5.4</b>		
Figure 5.4.17.1	Possible structure of organic species in the precipitated product.	108
 <b>Chapter 6</b>		
<b>Section 6.4</b>		
Figure 6.4.1	Typical UV/Vis spectra for 7-oxanorbornene-2,3-dicarboxylic acid and $Ru(CO)Cl_2(H_2O)$ .	117
Figure 6.4.2	Typical change in UV/Vis spectra for monomer/catalyst solution over time at elevated temperature.	117
Figure 6.4.3	Plot of absorbance (323nm) vs time for UV2 - Samples 1 & 2.	120
Figure 6.4.4	Plot of absorbance vs time for UV4 - Sample 1.	120

<u>Section Number</u>	<u>Title</u>	<u>Page Number</u>
<b>Section 6.8</b>		
Figure 6.8.1	Synthesis of $[\text{Ru}(\text{NH}_3)_6]\text{Cl}_2$ .	126
Figure 6.8.2	Synthetic scheme for $[\text{Ru}(\text{NH}_3)_5\text{N}_2]^{2+}$ .	127
<b>Chapter 7</b>		
<b>Section 7.2</b>		
Figure 7.2.1	Plot of drop in meniscus height vs time for Dil1 and Dil2	129
Figure 7.2.2	Plot of corrected drop in meniscus height vs time for Dil3 - Samples 3 & 5.	130
Figure 7.2.3	Plot of corrected drop in meniscus height vs time for Dil4 - Samples 3, 6 & 7.	131
Figure 7.2.4	Plot of corrected drop in meniscus height vs time for Dil5 - Samples 6, 7 & 8.	132
Figure 7.2.5	Plot of corrected drop in meniscus height vs time for Dil6 - Samples 3, 4 & 5.	133
Figure 7.2.6	Plot of change in meniscus height vs time for Dil7 - Control 2 & Sample 3.	134
Figure 7.2.7	Plot of change in meniscus height vs time for Dil8 - Control 2 & Sample 3	135
Figure 7.2.8	Plot of rise in meniscus height vs time for Dil9 - Controls 1 & 2 & Sample 4.	136
Figure 7.2.9	Plot of change in meniscus height vs time for Dil10 - Samples 1 & 3.	137
<b>Section 7.3</b>		
Figure 7.3.1	Plot of absorbance vs time for UV1.	138
Figure 7.3.2	Plot of absorbance vs time for UV2.	138
Figure 7.3.3	Plot of absorbance vs time for UV3.	139

<u>Section Number</u>	<u>Title</u>	<u>Page Number</u>
Figure 7.3.4	Plot of absorbance vs time for UV4.	139
Figure 7.3.5	Plot of absorbance vs time for UV5.	140
Figure 7.3.6	Plot of absorbance vs time for UV3 - Sample 2.	143
Figure 7.3.7	Plot of absorbance vs time for UV4 - Sample 1.	145
 <b>Chapter 8</b>		
<b>Section 8.1</b>		
Figure 8.1.1	Aqueous solution equilibrium of $[\text{Pt}(\text{PCH}_2\text{OH})_3]_4 \cdot \text{H}_2\text{O}$ .	150
Figure 8.1.2	Co-ordination of the tetradentate ligand $\text{P}(\text{CH}_2\text{CH}_2\text{PPh}_3)_3$ .	150
Figure 8.1.3	Synthesis of water soluble gold(I) complexes containing a nucleoside ligand.	151
Figure 8.1.4	Products from the reaction of $[\text{PtCl}_2(\text{P}(\text{CH}_2\text{OH})_3)_2]$ and excess $\text{P}(\text{CH}_2\text{OH})_3$ .	152
Figure 8.1.5	Crystal field splitting for a $d^8$ ion.	154
Figure 8.1.6	Possible structures for a Ru- $\text{P}(\text{CH}_2\text{OH})_3$ complex.	155
Figure 8.1.7	Nitrosyl transfer reaction.	157
Figure 8.1.8	Modified nitrosyl transfer reaction.	157
<b>Section 8.2</b>		
Figure 8.2.1	Mechanism for the isomerisation of maleic acid to fumaric acid using KCNS.	158
Figure 8.2.2	Metal-hydride addition-elimination mechanism for olefin isomerisation.	160
Figure 8.2.3	$\Pi$ -allyl hydride mechanism for olefin isomerisation.	160
Figure 8.2.4	Hydrogen shifts by different isomerisation mechanisms.	161
Figure 8.2.5	Exclusive Markovnikov addition in isomerisation by a Ru(II) catalyst.	162

<u>Section Number</u>	<u>Title</u>	<u>Page Number</u>
Figure 8.2.6	Selective formation of <i>trans</i> - products due to bond rotation.	163
Figure 8.2.7	Ru(II)-2,5-dihydrofuran co-ordination complex.	164
Figure 8.2.8	Proposed initial Ru-monomer complex.	164
Figure 8.2.9	Proposed initial Ru-monomer complex - ChemX molecular modelling software.	165
Figure 8.2.10	Proposed mechanism for the isomerisation of a ruthenium methoxycarbonyl complex.	166
Figure 8.2.11	Bis-chelate complex $\text{Ru}(\text{H}_2\text{O})(\eta^1(\text{O}):\eta^2(\text{C},\text{C}')-\text{OCOCH}_2\text{CH}=\text{CHCH}_3)_2$ .	166
Figure 8.2.12	Bond breaking and rotation in Ru-monomer complex.	167
Figure 8.2.13	Proposed Ru-monomer chelate complex.	167
Figure 8.2.14	Proposed Ru-monomer chelate complex - ChemX molecular modelling software.	168
<b>Section 8.3</b>		
Figure 8.3.1	Variation of Z with change in $\text{Ru}(\text{CO})\text{Cl}_2(\text{H}_2\text{O})$ concentration.	171
Figure 8.3.2	Variation of Y with change in $\text{Ru}(\text{CO})\text{Cl}_2(\text{H}_2\text{O})$ concentration	171
Figure 8.3.3	Formation of a Ru-Monomer $\Pi$ -complex.	173
Figure 8.3.4	Partial degradation of ruthenium chelate complex.	174
Figure 8.3.5	Proposed isomerisation mechanism and associated kinetic scheme.	175
<b>Appendix</b>		
Figure B1	$^{13}\text{C}$ NMR of oxanorbornenedicarboxylic anhydride.	199
Figure B2	$^1\text{H}$ NMR of oxanorbornenedicarboxylic anhydride.	199



<u>Section Number</u>	<u>Title</u>	<u>Page Number</u>
Figure B3	$^{13}\text{C}$ NMR of <i>endo</i> -norbornenedicarboxylic anhydride.	200
Figure B4	$^{13}\text{C}$ NMR of <i>exo</i> -norbornenedicarboxylic anhydride.	201
Figure B5	$^{13}\text{C}$ NMR of THMP.	202
Figure B6	$^1\text{H}$ NMR of THMP.	202
Figure B7	$^{31}\text{P}$ NMR of THMP.	203
Figure B8	$^{13}\text{C}$ NMR of TPPTS.	203
Figure B9	$^{31}\text{P}$ NMR of TPPTS.	204
Figure B10	$^1\text{H}$ NMR of TPPTS.	204
Figure B11	FTIR of $\text{Ru}(\text{NH}_3)_6\text{Cl}_2$ .	205
Figure B12	FTIR of $[\text{Ru}(\text{NH}_3)_5\text{Cl}]\text{Cl}_2$ .	205
Figure B13	FTIR of $\text{Ru}(\text{CO})_2\text{Cl}_2$ - KBr disk.	206
Figure B14	FTIR of $\text{Ru}(\text{CO})_2\text{Cl}_2$ - Nujol Mull.	206
Figure B15	FTIR of $\text{Ru}(\text{CO})\text{Cl}_2(\text{H}_2\text{O})$ .	207
Figure B16	FTIR of $\text{Ru}(\text{NO})_2(\text{PPh}_3)_2$ .	207
Figure B17	$^{13}\text{C}$ NMR of $\text{Ru}-\text{P}(\text{CH}_2\text{OH})_3$ complex- Method 2.	208
Figure B18	$^1\text{H}$ NMR of $\text{Ru}-\text{P}(\text{CH}_2\text{OH})_3$ complex- Method 2.	208
Figure B19	$^{31}\text{P}$ NMR of $\text{Ru}-\text{P}(\text{CH}_2\text{OH})_3$ complex- Method 2.	209
Figure B20	$^{13}\text{C}$ NMR of $\text{Ru}-\text{P}(\text{CH}_2\text{OH})_3$ complex- Method 3.	209
Figure B21	$^1\text{H}$ NMR of $\text{Ru}-\text{P}(\text{CH}_2\text{OH})_3$ complex- Method 3.	210
Figure B22	$^{31}\text{P}$ NMR of $\text{Ru}-\text{P}(\text{CH}_2\text{OH})_3$ complex - Method 3.	210
Figure B23	FTIR of crystals from attempted synthesis of $\text{Ru}(\text{NO})_2(\text{P}(\text{CH}_2\text{OH})_3)_2$ .	211
Figure B24	FTIR of precipitate from attempted synthesis of $\text{Ru}(\text{NO})_2(\text{P}(\text{CH}_2\text{OH})_3)_2$ .	211
Figure B25	FTIR of Vaska's Compound	212
Figure B26	$^{13}\text{C}$ NMR of orange residue from $\text{Ir}-\text{P}(\text{CH}_2\text{OH})_3$ complex synthesis.	212

<u>Section Number</u>	<u>Title</u>	<u>Page Number</u>
Figure B27	$^1\text{H}$ NMR of orange residue from Ir-P(CH <sub>2</sub> OH) <sub>3</sub> complex synthesis.	213
Figure B28	$^{31}\text{P}$ NMR of orange residue from Ir-P(CH <sub>2</sub> OH) <sub>3</sub> complex synthesis.	213
Figure B29	$^{13}\text{C}$ NMR of precipitate from Ir-P(CH <sub>2</sub> OH) <sub>3</sub> complex synthesis.	214
Figure B30	$^1\text{H}$ NMR of precipitate from Ir-P(CH <sub>2</sub> OH) <sub>3</sub> complex synthesis.	214
Figure B31	$^{31}\text{P}$ NMR of precipitate from Ir-P(CH <sub>2</sub> OH) <sub>3</sub> complex synthesis.	215
Figure B32	$^{13}\text{C}$ NMR of precipitate from the reaction between Ru(CO)Cl <sub>2</sub> (H <sub>2</sub> O) and monomer - run 4.	215
Figure B33	$^{13}\text{C}$ NMR of precipitate from the reaction between Ru(CO)Cl <sub>2</sub> (H <sub>2</sub> O) and monomer - run 5.	216
Figure B34	$^1\text{H}$ NMR of precipitate from the reaction between Ru(CO)Cl <sub>2</sub> (H <sub>2</sub> O) and monomer - run 4.	216
Figure B35	$^1\text{H}$ NMR of precipitate from the reaction between Ru(CO)Cl <sub>2</sub> (H <sub>2</sub> O) and monomer - run 5.	217
Figure B36	$^{13}\text{C}$ NMR of residue from the reaction between Ru(CO)Cl <sub>2</sub> (H <sub>2</sub> O) and monomer - run 4.	217
Figure B37	$^{13}\text{C}$ NMR of residue from the reaction between Ru(CO)Cl <sub>2</sub> (H <sub>2</sub> O) and monomer - run 5.	218
Figure B38	$^1\text{H}$ NMR of residue from the reaction between Ru(CO)Cl <sub>2</sub> (H <sub>2</sub> O) and monomer - run 4.	218
Figure B39	$^1\text{H}$ NMR of residue from the reaction between Ru(CO)Cl <sub>2</sub> (H <sub>2</sub> O) and monomer - run 5.	219

<u>Section Number</u>	<u>Title</u>	<u>Page Number</u>
Figure B40	$^{13}\text{C}$ NMR of product of reaction between monomer and Ru-P(CH <sub>2</sub> OH) <sub>3</sub> complex.	219
Figure B41	$^1\text{H}$ NMR of product of reaction between monomer and Ru-P(CH <sub>2</sub> OH) <sub>3</sub> complex.	220

# CHAPTER 1

## INTRODUCTION.

### 1.1 - Background to Metathesis.<sup>1, 2</sup>

Metathesis is defined as a reaction in which an interchange of atoms or groups of atoms takes place between two molecules. In olefin chemistry, this specifically refers to the interchange of carbon atoms between a pair of multiple bonds. If the interchange occurs between linear olefins then the reaction results in the formation of one or two new alkene molecules (Fig 1.1.1). If the double bond is part of a cyclic structure then polymerisation occurs - this is known as Ring-Opening Metathesis Polymerisation (ROMP) (Fig 1.1.2).



**Fig 1.1.1 - Metathesis of linear olefins.**

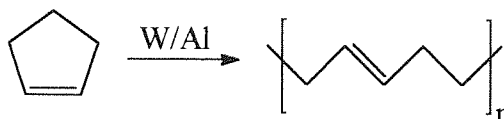


**Fig 1.1.2 - Ring-Opening Metathetical Polymerisation (ROMP) of a cyclic olefin.**

The first observation of the metathesis reaction was made in 1955 in the Du Pont laboratories and was the transition metal catalysed polymerisation of norbornene (Fig 1.1.3). Shortly after this observation was made, the metathesis reaction was recognised to be occurring between acyclic olefins e.g. the metathesis of propene into ethene and 2-butene (Fig 1.1.4)

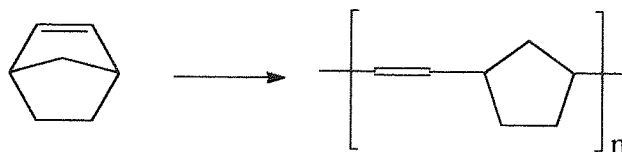


**Fig 1.1.3 - ROMP of norbornene.**

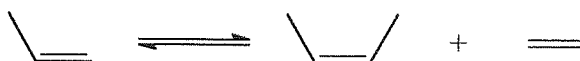


**Fig 1.1.4 - Metathesis of propene into ethene and 2-butene.**

However it was not until 1967 that the two reactions were proposed to proceed via the same pathway and it was Calderon who termed the phrase "olefin" or "alkene metathesis".

### 1.2 - The Mechanism of Metathesis.

Although the metal-carbene mechanism is now generally accepted for the metathesis reaction, it was initially thought that the reaction proceeded by a "pair-wise" mechanism. There were various different types of pair-wise mechanism proposed by different people, all of which involved two reactant molecules meeting at the active centre, reacting and then separating from the active centre leaving it free to complex with two more molecules. The general form of these proposals is summarised in Fig 1.2.1.

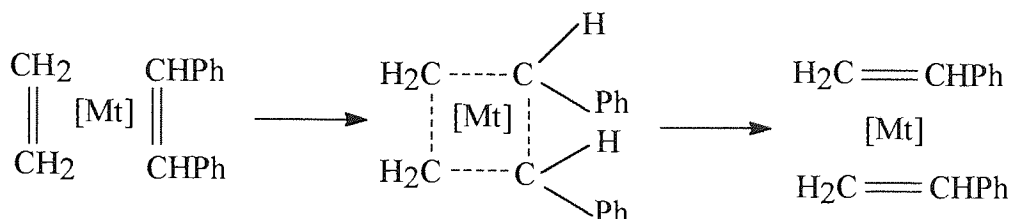


**Fig. 1.2.1 - The pair-wise mechanism for metathesis.**

The metal carbene chain mechanism proposed by Herisson and Chauvin<sup>3</sup> is different in that reactant molecules add individually to the active centre which, in the case of cyclic olefins, results in the stepwise growth of the polymer chain. The active centre is a metal carbene which must have a vacant site to allow the co-ordination of monomer. The mechanism is summarised for a cyclic olefin in Fig 1.2.2.

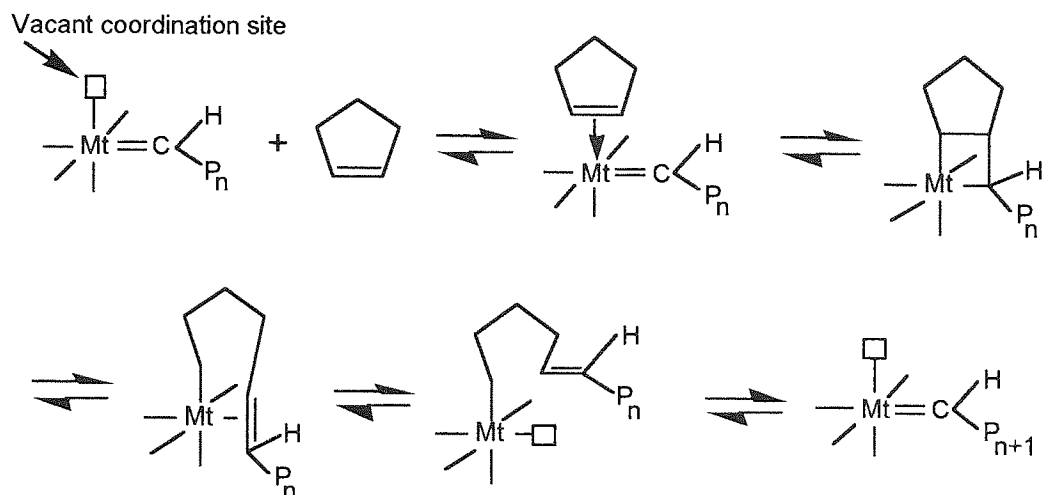


**Fig. 1.2.2 - The general form of the carbene mechanism for metathesis polymerisation.**

Evidence supporting the carbene mechanism was provided by two groups of workers headed by Katz<sup>4</sup> and Grubbs<sup>5</sup> respectively. Both groups made use of co-metathesis experiments and analysis of product ratios - the two different mechanisms producing distinctly different product ratios as can be seen by the general schemes shown below. As shown in Fig 1.2.3, in the co-metathesis of a cyclo-olefin with two symmetrical dienes, a pair-wise mechanism would result in the formation of the two symmetrical scission dienes (I and II) as the first major reaction products.

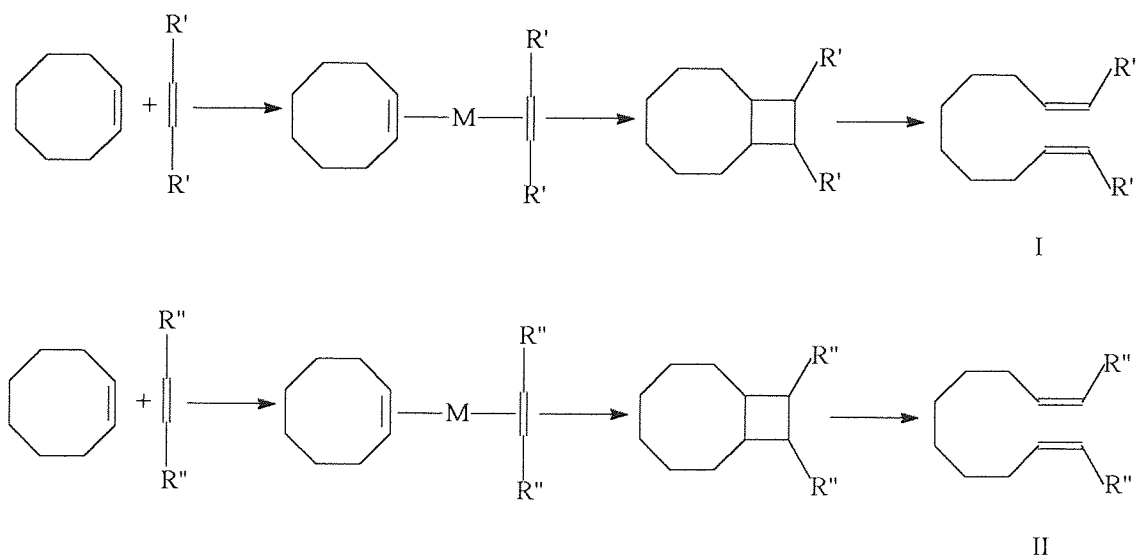


**Fig 1.2.3 - A pair-wise reaction scheme for a co-metathesis reaction.**

However, a carbene chain mechanism suggests a different product mix with the first major product being the unsymmetrical scission product of the cyclo-olefin, as shown in Fig 1.2.4.

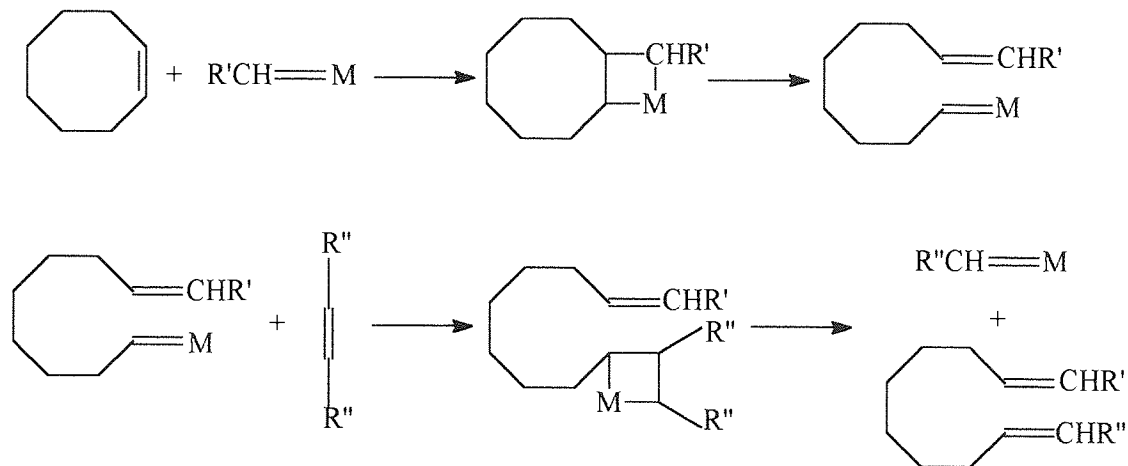


**Fig 1.2.4 - A carbene reaction scheme for a co-metathesis reaction.**

Analysis of product ratios and extrapolation of the results to time zero showed a greater than zero value for the unsymmetrical diene. Since the pair-wise mechanism excludes the early formation of this unsymmetrical diene, the reaction must proceed via a carbene mechanism.<sup>4</sup>

The mechanism by which the carbene is formed from the catalyst is not fully understood and a number of different mechanisms have been proposed. For catalytic systems containing a transition metal compound and a metal alkyl co-catalyst, it is generally accepted that a reaction between the two components produces a metal-carbene compound. A mechanism for such a reaction was proposed by Muetterties<sup>6</sup> who studied the interaction of tungsten(IV)chloride and dimethylzinc in benzene. The reaction produces methane which must come initially from the metal-alkyl as the methane produced contains no deuterium when the reaction is performed in deuterated solvent. The carbene is produced by  $\alpha$ -hydrogen elimination from the tungsten-methyl group by one of two mechanisms (A or B) shown in Fig 1.2.5.

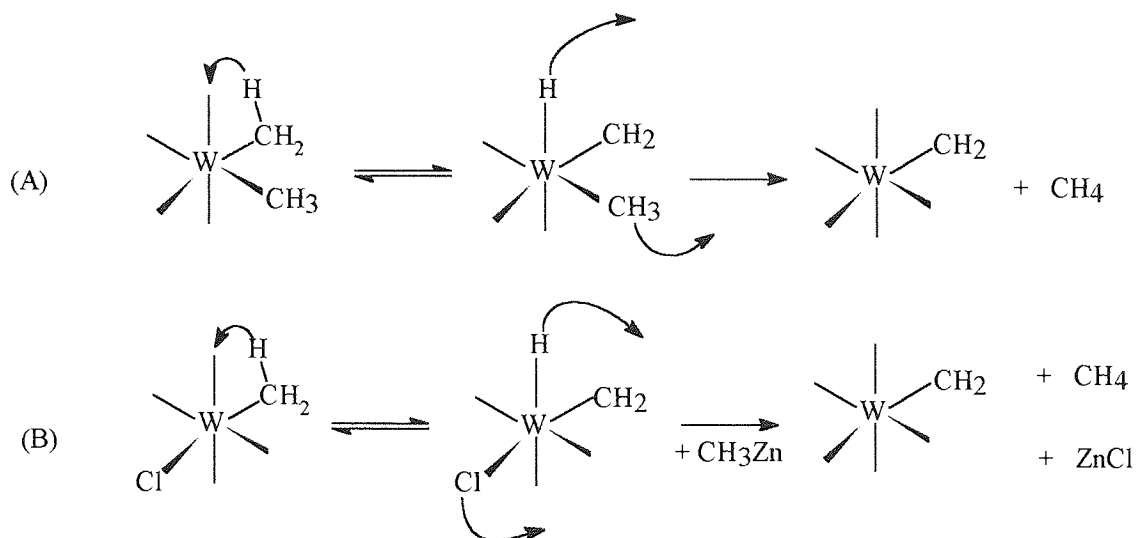


Fig 1.2.5 - Carbene formation from a transition metal and a metal alkyl.

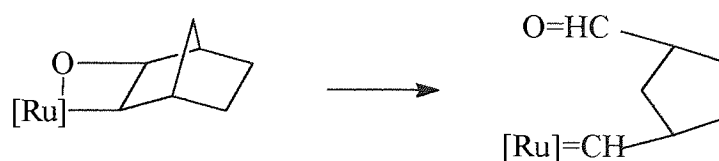
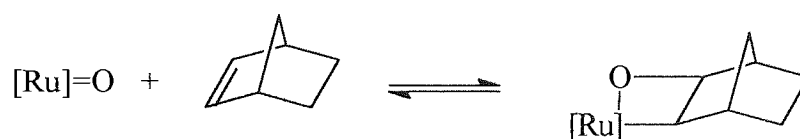
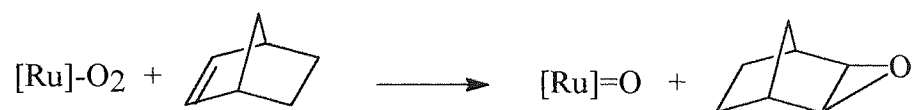


Fig 1.2.6 - Carbene formation from an O<sub>2</sub> mechanism.



However metathesis systems exist in which no co-catalyst is necessary so another carbene forming reaction must be considered in these cases. Lavery, Rooney & Stewart<sup>7</sup> have proposed a mechanism which allows for the formation of metal-carbenes via metal-hydride species with the metathesising olefin acting as the alkyl source. More significantly, Ivin, Reddy & Rooney<sup>8</sup> have proposed a mechanism whereby dioxygen facilitates the formation of a metal-carbene from the transition metal and the metathesising olefin. They found that by bubbling O<sub>2</sub> through solutions of norbornene in chlorobenzene containing RuCl<sub>2</sub>(PPh<sub>3</sub>)<sub>3</sub> or RuCl<sub>2</sub>(py)<sub>2</sub>(PPh<sub>3</sub>)<sub>2</sub>, the rate of ROMP increased by as much as 100-fold. Similar results were obtained when the Ru compounds were first separately oxidised by O<sub>2</sub> at 100°C in chlorobenzene solution and the isolated products used as catalysts. The mechanism proposed is shown in Fig 1.2.6. Interestingly, this effect was also seen using the catalyst precursor RuHCl(PPh<sub>3</sub>)<sub>3</sub>. However Lavery *et al.*<sup>7</sup> had previously proposed a hydride mechanism for polymerisation using RuCl<sub>3</sub>.3H<sub>2</sub>O and since the treatment with di-oxygen removes all the hydride ligand from RuHCl(PPh<sub>3</sub>)<sub>3</sub> (as evidenced by the disappearance of a distinctive hydride I.R band at 2035 cm<sup>-1</sup>) the authors have expressed some doubt about a mechanism solely concerning a metal-hydride in the case of RuCl<sub>3</sub>.3H<sub>2</sub>O.

### 1.3 - Metathesis Catalysts.

Numerous heterogeneous and homogeneous catalytic systems are known to initiate the metathesis reactions of olefins and the ROMP of cyclo-olefins. Heterogeneous catalysts are used largely for the metathesis of olefins and for the ROMP of cyclo-olefins to a much smaller extent. Such catalysts usually consist of a promoter (such as a metal oxide, carbonyl or sulphide or a transition metal salt) supported on a carrier (such as alumina, silica or a metal oxide or salt), but the reader may wish to refer to the general references quoted for a detailed description of heterogeneous metathesis catalysts.

Homogeneous catalytic systems can be conveniently split into three types;

- (I) One component (Unary).
- (II) Two component (Binary).
- (III) Three component (Ternary).

#### 1.3.1 - One Component (Unary) Catalytic Systems.

Unary systems consist of a transition metal compound without any co-catalyst e.g. toluenetricarbonyltungsten (CH<sub>3</sub>C<sub>6</sub>H<sub>4</sub>W(CO)<sub>3</sub>) which was observed to metathesise 4-

nonene in heptane solvent by Lewandos and Pettit<sup>9</sup> and, of course, the polymerisation of oxanorbornene derivatives using RuCl<sub>3</sub> in aqueous solvent<sup>10</sup>. However, one must be careful not to consider these as catalysts themselves but merely (and more accurately) as catalyst precursors. As has been previously discussed, a mechanism must be invoked whereby the precursor can be transformed into a metal-carbene species which is believed to be the catalytically active species in the metathesis reaction.

Significant work has been done in producing one component systems containing stable metal carbene species. The first such compound used for a metathesis reaction was diphenyl-pentacarbonyltungsten-carbene ((C<sub>6</sub>H<sub>5</sub>)<sub>2</sub>C=W(CO)<sub>5</sub>), which was used for the co-metathesis of 1-octene and 1-hexene by Katz and co-workers<sup>11</sup> who also studied other carbenic complexes of this type such as diphenyl-pentachlorotungsten-carbene ((C<sub>6</sub>H<sub>5</sub>)<sub>2</sub>C=WCl<sub>5</sub>) and phenyl-methoxy-pentacarbonyltungstencarbene (C<sub>6</sub>H<sub>5</sub>(CH<sub>3</sub>O)C=W(CO)<sub>5</sub>). Work on catalysts of this type has also been carried out by Casey and co-workers, who examined the catalytic activity of ditolylpentacarbonyltungsten-carbene, (CH<sub>3</sub>C<sub>6</sub>H<sub>4</sub>)<sub>2</sub>C=W(CO)<sub>5</sub>, and observed the transfer of the tolyl-carbenic ligand to the attendant alkene and also identified phenyl-methyl-pentacarbonyltungsten-carbene, (C<sub>6</sub>H<sub>5</sub>(CH<sub>3</sub>)C=W(CO)<sub>5</sub>), as an efficient catalyst for the cyclopropanation of styrene<sup>12</sup>.

Stable complexes of tantalum and niobium have been synthesised by Schrock<sup>13</sup> that are unusual in that they do not contain hetero-atoms to stabilise the carbene ligands. These alkylidene complexes are simply synthesised (Fig 1.3.1.1) and thermally stable but react violently on exposure to moisture.

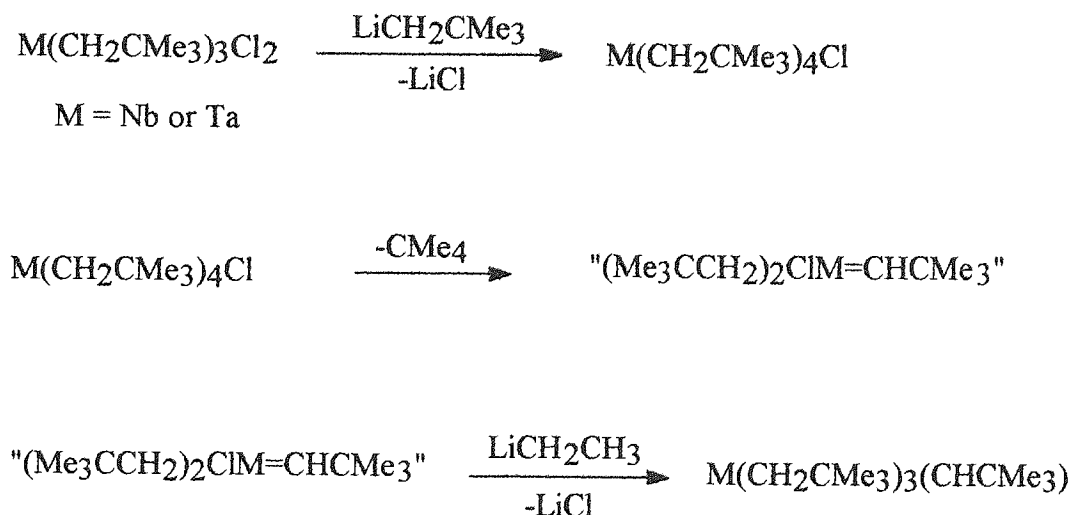


**Fig 1.3.1.1 - Synthesis of an alkylidene complex of Niobium or Tantalum**

In an attempt to prepare tungsten or molybdenum-alkylidene complexes which were isoelectronic to the previously mentioned Ta and Nb complexes, Schrock<sup>14</sup> successfully produced a tungsten complex which is an active catalyst for the metathesis of both terminal and internal olefins (Fig 1.3.1.2). The complex with two PEt<sub>3</sub> ligands (I) is an effective binary catalyst when combined with AlCl<sub>3</sub> whereas when one of the ligands is removed (II) the catalyst is effective in the absence of AlCl<sub>3</sub>. It is therefore plausible to propose that complex (II) is an intermediate in the system containing (I) plus AlCl<sub>3</sub>.

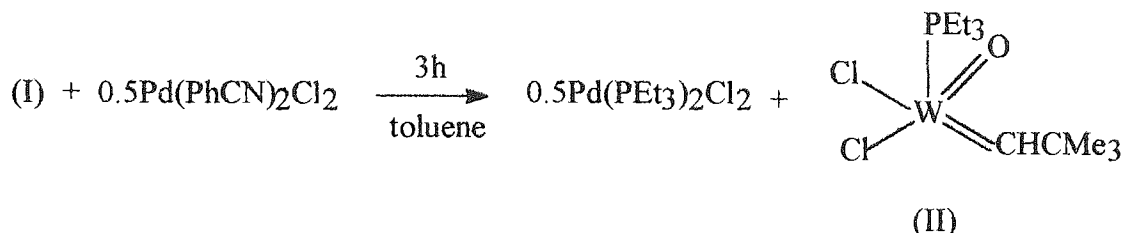
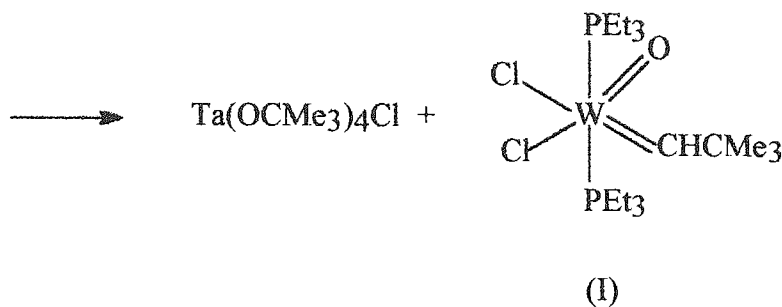
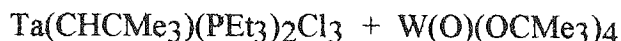


**Fig 1.3.1.2 - Synthesis of a unary metathesis catalyst of tungsten.**

More recently Grubbs and co-workers have synthesised a number of stable ruthenium-carbene complexes which show metathetical activity and are stable in protic media<sup>15</sup> (Fig 1.3.1.3). Complex (I) is able to catalyse the metathesis of norbornene and other highly strained cyclic-olefins such as *trans*-cyclooctene but is ineffective with less strained systems. However replacing the PPh<sub>3</sub> ligands with tricyclohexyl (PCy<sub>3</sub>) ligands enables the complex to catalyse the metathesis of *cis*-2-pentene and the ROMP of *cis*-cyclooctene<sup>16</sup>. (II) is also an effective catalyst for the ring *closing* metathesis of dienes.<sup>17</sup>

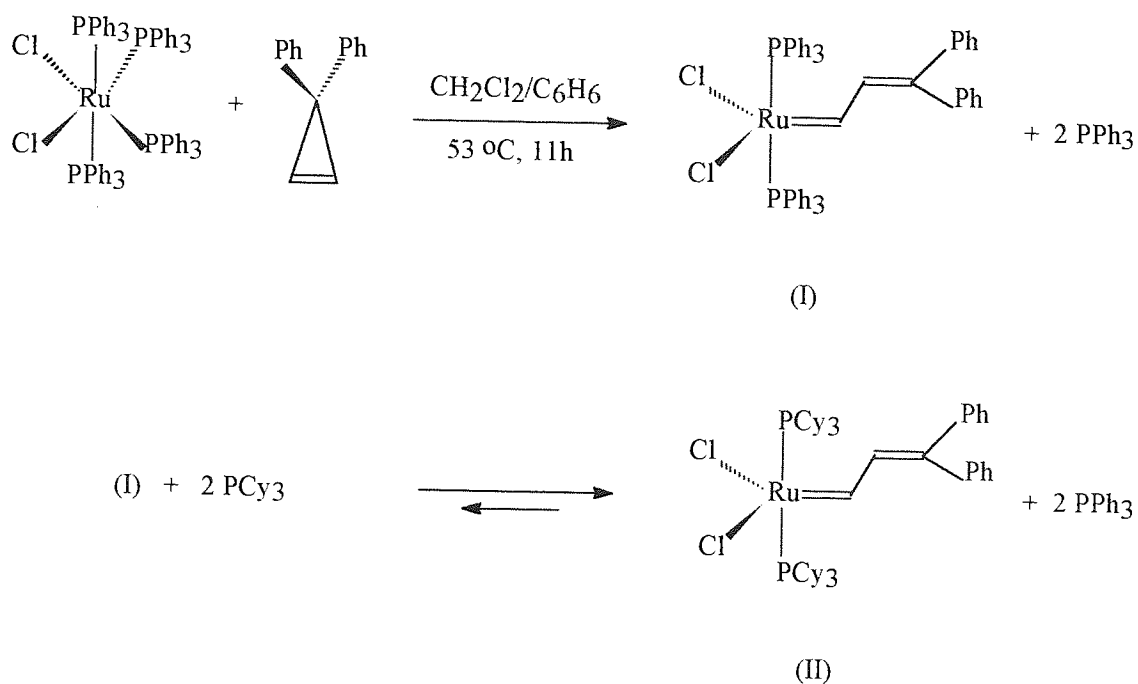


**Fig 1.3.1.3 - Synthesis of a stable ruthenium-carbene metathesis catalyst.**

### 1.3.2 - Two Component (Binary) Catalytic Systems.

Two component systems contain a salt of a transition metal and a co-catalyst. Depending on the nature of the co-catalyst the binary systems can be further divided into Ziegler-Natta- and Friedel-Crafts-type systems.

The Ziegler-Natta-type system, where the co-catalyst is an organo-metallic compound, is the most widely used binary system. One of the first studied was  $WCl_6 \cdot C_2H_5AlCl_2$  which was employed in the cross metathesis of 2-butene and 2-butene- $d_8$  by Calderon.<sup>18</sup> Numerous catalytic systems of this type are known where the tungsten halide is replaced by halides or other derivatives of various transition metals such as  $MoCl_5$  and  $ReCl_5$ . Wang and Menapace<sup>19</sup> changed the co-catalyst to butyl-lithium to give  $WCl_6 \cdot n-C_4H_9Li$  and this was found to be an effective catalyst for the metathesis of 2-pentene. Zeuch<sup>20</sup> employed a different type of system altogether using nitrosyl complexes of molybdenum or tungsten, instead of tungsten hexachloride, in the form  $L_2Cl_2(NO)_2M$  ( $M = Mo, W$ ;  $L = PPh_3, C_5H_5N, Ph_3PO$ ) and an organometallic compound as co-catalyst (e.g.  $C_2H_5AlCl_2, (C_2H_5)_2AlCl, (CH_3)_3AlCl_3, (C_2H_5)_3AlCl_3$ ). These systems afforded high yields in the metathesis of 2-pentene and the molybdenum systems were more active than those based on tungsten. The first ring-opening polymerisation of cyclo-olefins was also performed using a Ziegler-Natta type catalyst when Merckling and Anderson<sup>21</sup>

polymerised norbornene using a catalyst consisting of titanium tetrachloride ( $\text{TiCl}_4$ ) and tetraheptyllithium-aluminium  $(\text{C}_7\text{H}_{15})_4\text{AlLi}$ .

Friedel-Crafts-type two component systems contain a Lewis acid as co-catalyst. Dall'Asta and Carella<sup>22</sup> were the first to demonstrate the activity of such systems when they studied a system consisting of  $\text{WCl}_6$ ,  $\text{WOCl}_4$ ,  $\text{WCl}_2$  or  $\text{WBr}_2$  combined with  $\text{AlCl}_3$  or  $\text{AlBr}_5$ . The activity of these systems was increased over the activity of the transition metal salt alone. These systems were also effective in the polymerisation of cyclopentane and other cyclo-olefins

### 1.3.3 Three Component (Ternary) Catalytic Systems.

In many cases a third component is added to binary catalyst systems to act as either an activator, promoter, stabiliser or inhibitor of side reactions. The first ternary system consisted of  $\text{WCl}_6$ ,  $\text{C}_2\text{H}_5\text{OH}$  and  $\text{C}_2\text{H}_5\text{AlCl}_2$  and was employed by Calderon<sup>23</sup> initially in the polymerisation of 2-pentene and then with other acyclic and cyclic olefins. Many other systems have been produced with the exact nature of the components being tailored to increase the efficiency of specific metathesis reactions e.g. catalyst systems consisting of triphenylphosphine, transition metal salts and organoaluminium compounds have been found to be active in the metathesis of  $\beta$ -olefins.

### 1.4 - Aqueous ROMP.

Ring-opening metathesis polymerisation (ROMP) in aqueous solvent is a relatively new phenomenon first reported by Novak and Grubbs<sup>10</sup> in 1988. During investigations into the polymerisation of 7-oxanorbornene derivatives (Fig 1.4.1), they discovered that the rigorous exclusion of water unexpectedly increased the initiation time before polymerisation occurred.

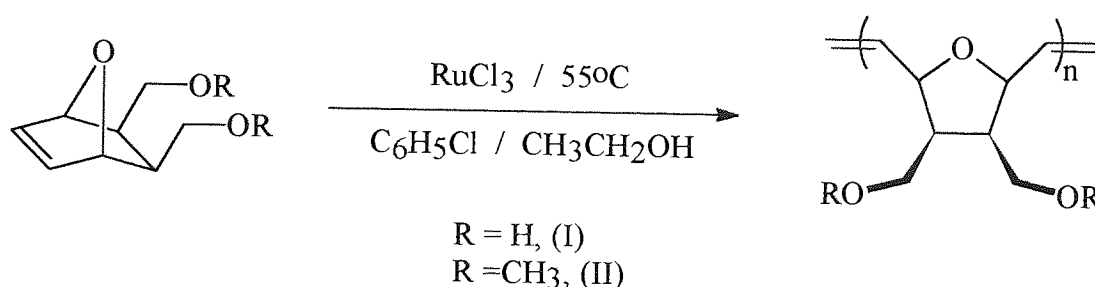
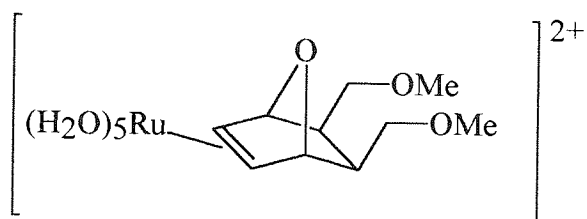


**Fig 1.4.1 - Aqueous ROMP of oxanorbornene derivatives.**

Rather than deactivating the catalyst as would be expected, the water seemed to act as a co-catalyst. Initiation times (time before the first appearance of polymer) decreased from 22-24 hours in organic solvents to 30-35 minutes in water alone. It was also found that the catalyst was not only recyclable but increased in activity on subsequent repetitive re-use. When aqueous ruthenium solutions from the polymerisation of (II) were recovered and re-used the initiation time dropped from 37.5 minutes to 10-12 seconds (after 2-3 polymerisation cycles) and the aqueous solutions were successfully recycled up to 14 times without any noticeable loss of activity.

Similar observations were made when (II) was polymerised by  $\text{Ru}(\text{H}_2\text{O})_6(\text{tos})_2$  (tos = *p*-toluenesulfonate) and the catalyst was observed by NMR to convert to the mono-olefin adduct (III) (Fig 1.4.2).



(III)

**Fig 1.4.2 - Mono-olefin adduct from polymerisation of (II) with  $\text{Ru}(\text{H}_2\text{O})_6(\text{tos})_2$**

Aqueous solutions of (III) were found to be highly active in subsequent polymerisations (showing the same limiting initiation times of 10-12 seconds as previously found) and it was therefore hypothesised that the increased catalytic activity of  $\text{Ru}^{3+}$  systems is due to the disproportionation of  $\text{Ru}^{3+}$  to  $\text{Ru}^{2+}$  and  $\text{Ru}^{4+}$  followed by formation of a  $\text{Ru}^{2+}$ -monomer complex which in turn initiates polymerisation.

The aqueous ROMP of *exo, exo*-oxanorbornenedicarboxylic acid using transition metal chlorides was investigated by Feast and Harrison<sup>24</sup> with particular attention paid to the effect on molecular weight of using chain transfer agents. They found that of the trichlorides, those of ruthenium and osmium were successful (producing polymers of molecular weight  $M_n > 10^5$ ) but those of iridium, rhodium and palladium did not initiate polymerisation. Of the chain transfer agents investigated the most successful was *cis*-but-2-ene-1, 4-diol which allowed control of the molecular weight over the range  $M_n = 10^5$  to  $7 \times 10^2$  (Molecular weights relative to poly(ethylene oxide) standards). This compound and its dimethyl ether were also found to be successful chain transfer agents for the bis-methoxymethyl derivative of oxanorbornene<sup>25</sup>. France, Grubbs, McGrath

and Paciello<sup>26</sup> have similarly shown that 3-buten-1-ol and methyl acrylate are useful chain transfer agents for the  $\text{Ru}(\text{H}_2\text{O})_6(\text{tos})_2$  catalysed aqueous ROMP of the bis-methoxymethyl derivative of oxanorbornene

The aqueous ROMP of *exo, exo*-oxanorbornenedicarboxylic anhydride was studied by another group (Lu, Quayle, Heatley, Booth, Yeates and Padget)<sup>27</sup> who found that polymerisation was most successful in a solvent of 10% water in ethanol and was accompanied by break-up of the bicyclic monomer and esterification of the resultant maleic acid (Fig 1.4.3.).

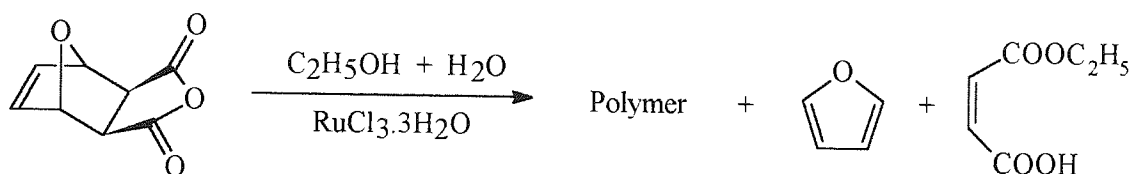


**Fig 1.4.3 - Polymerisation of oxanorbornenedicarboxylic anhydride in 10% water in ethanol.**

Polymerisation in water alone resulted in moderate yields of low molecular weight polymer ( $M_{pk} \sim 700$ ). The reason for the discrepancy between the two papers (24 and 27) is unclear although the two groups utilised different experimental, separation and characterisation techniques (Table 1.4.1.).

A range of other monomers (all disubstituted derivatives of oxanorbornene) have been polymerised using  $\text{RuCl}_3 \cdot 3\text{H}_2\text{O}$ <sup>28</sup>. However in all cases the solvent system used was a mix of various amounts of water in ethanol (usually 10% water in ethanol). Therefore it cannot be correctly termed aqueous ROMP but rather ROMP in a protic media. However, the most important aspect of studies of this type is that it further demonstrates the unusual tolerance of ruthenium catalysts to the presence of water during ROMP

**Table 1.4.1 - Comparison of experimental techniques for the polymerisation of oxanorbornenedicarboxylic acid. (100% aqueous solvent).**

	<b>Feast and Harrison<sup>24</sup></b>	<b>Lu <i>et al.</i><sup>27</sup></b>
<b>Experimental Procedure</b>	Mon. conc. = 0.84M Mon:Ru ratio = 20:1 Temp. = 55°C Time = 48 hr	Mon. conc. = 2M Mon:Ru ratio = 100:1 Temp. = 60°C Time = 48 hr
<b>Product separation</b>	Filtered Converted to disodium salt. Precipitated into methanol 3 times.	Reaction solution diluted with THF. Product precipitated with pentane.
<b>Characterisation</b>	GPC - Aqueous eluent.	GPC - THF eluent.
<b>Mol. Weight.</b>	$M_n = > 10^5$	$M_{pk} \sim 700$

*Molecular weights relative to poly(ethylene oxide) standards.*

Although there have been a number of papers published on aqueous ROMP concerning the yield, molecular weight and characterisation of the product polymers, there is a marked scarcity of papers dealing with the rate of reaction of aqueous ROMP. The first paper to be concerned with this aspect was published by Lu, Quayle, Heatly, Booth, Yeates and Padgett<sup>29</sup> in 1992. In this paper, *exo, exo*-bis(methoxymethyl)-7-oxanorbornene was polymerised using RuCl<sub>3</sub> in 10% water in ethanol as solvent. The reaction was followed by <sup>13</sup>C NMR by performing the reaction in a standard NMR tube in deuterated solvent and heating the probe to the required temperature. <sup>13</sup>C NMR spectra were recorded at regular intervals and the rate of monomer conversion calculated by monitoring the decrease in intensity of a specific peak (corresponding to the olefinic carbons of the monomer) between successive spectra. Some of the results are presented in Table 1.4.2.

The results show an initial slow period of conversion. The rate accelerates over the first few hours until it reaches a constant value covering the range from 10% to 90% conversion before levelling off as 100% conversion is approached. The final conversion varied between 81% and 95%. Varying the catalyst concentration produces surprising results in that the rate of polymerisation decreases as catalyst concentration increases (Fig 1.4.4 - The derivation of the best fit line will be explained further on in this section.)



Table 1.4.2 - ROMP of *exo, exo*-2,3-bis(methoxymethyl)-7-oxanorbornene catalysed by commercial RuCl<sub>3</sub>.

[C] <sub>0</sub> / mol dm <sup>-3</sup>	[Mon] / mol dm <sup>-3</sup>	k × 10 <sup>4b</sup> / dm <sup>3</sup> mol <sup>-1</sup> s <sup>-1</sup>	Slow period /hr	Slow period % conv.	Final % conv.	M <sub>nk</sub> / 10 <sup>5</sup> (GPC)
0.002	1.57	8.08	1	15	93.1	2.8
0.0051	1.57	5.31	1.5	14	95.2	1.6
0.01	1.57	3.33	2.5	16	89.6	1.5
0.017	2.5-0.4 <sup>a</sup>	1.81	4	20	94.4	2.5
0.029	1.57	0.8	5.5	16	88.5	1.8
0.053	1.6-0.7 <sup>a</sup>	0.6	6	36	81.7	2

Polymerisation conditions - 70°C; 10% water in ethanol.

a) Averages of several runs with different monomer concentrations.

b) Pseudo-second-order rate constant from the straight line portion of the 1/[M] versus time plot.

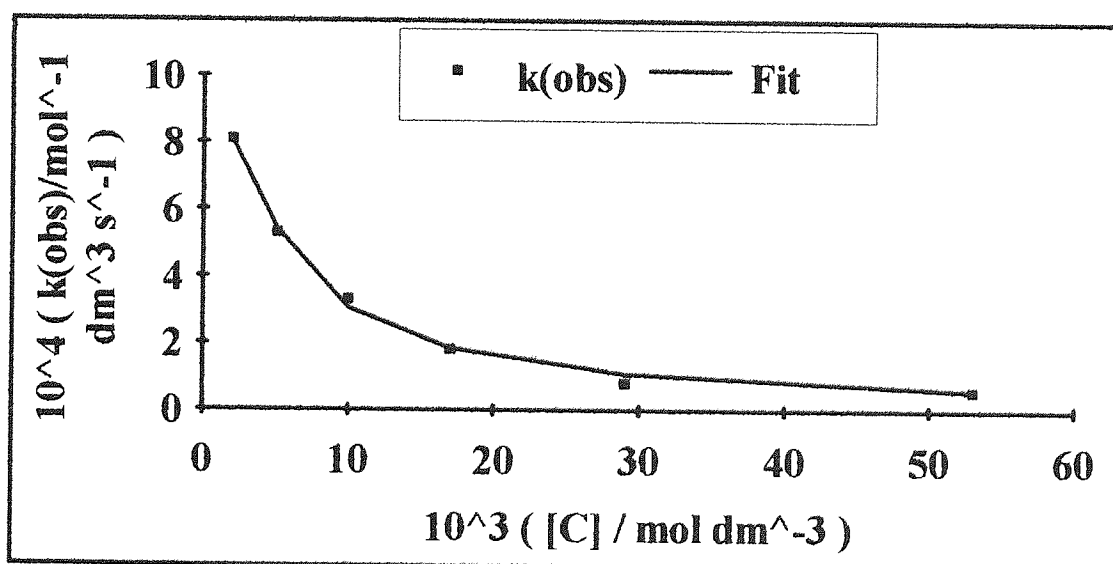
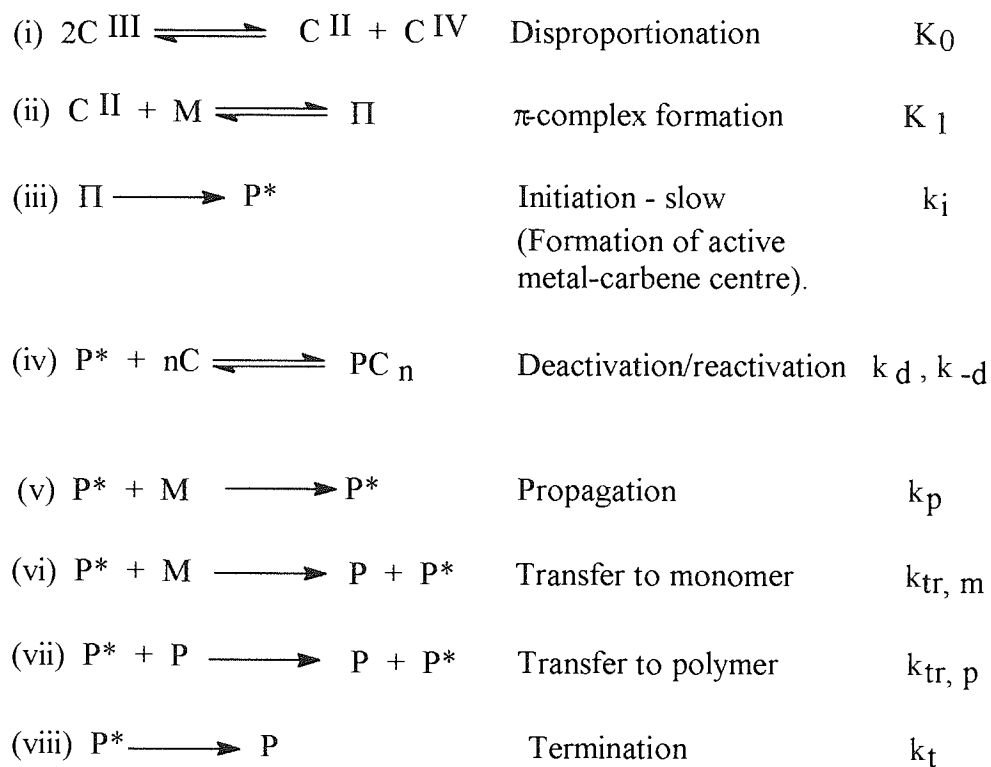


Fig 1.4.4 - Plot of change in k<sub>obs</sub> vs concentration of RuCl<sub>3</sub> added, [C].

The authors rationalise the results within a conventional polymerisation framework i.e. a chain reaction involving slow formation of an active species (initiation) and slow termination of the chain, giving rise to a steady-state concentration of active species and a rapid propagation reaction. However to explain the decrease in rate of reaction with increase in RuCl<sub>3</sub> added, the authors have proposed an equilibrium between the active centre, P\*, and a deactivated species consisting of the active centre combined with "n"

ruthenium species, which effectively removes the catalyst from the system. A schematic representation of the polymerisation proposed by the authors<sup>29</sup> is reproduced below.



$K_0$  and  $K_1$  are small so that C, which formally represents the  $Ru^{III}$  concentration in whatever form (possibly  $[RuCl_2(H_2O)_4]^+Cl^-$ )<sup>30</sup> is practically equivalent to the total Ru concentration. Combining equilibria (i) and (ii) gives :-

$$[C \text{ II}] = K_0^{1/2}[C]$$

$$[\Pi] = K_1 K_0^{1/2}[C][M]$$

therefore  $[\Pi] \propto [C][M]$

It is assumed that equilibrium (iv) is multistage e.g.



Therefore, the parameter n will have a value dependent on the position of the equilibria.

Application of the steady state principle to the active species P\* gives

$$d[P^*]/dt = 0 = k_i'[C][M] - k_d[P^*][C]^n + k_{-d}[PC_n] - k_t[P^*]$$

where  $k_i' = k_i K_1 K_0^{1/2}$ . If it is assumed that equilibrium (iv) lies well to the right (i.e. that  $k_d \gg k_{-d}$ ), then  $[PC_n] \sim [P^*]$  and

$$[P^*] \sim k_i'[C][M]/\{k_d[C]^n - k_{-d} + k_t\}$$

or with  $k_d \gg k_{-d}$

$$[P^*] \sim k_i'[M]/k_d[C]^{n-1}$$

Hence the rate of polymerisation is

$$R_p \sim k_p[P^*][M] \sim k'[M]^2[C]^{1-n}$$

where  $k' = k_i'k_p/k_d$ , or

$$R_p \sim k[M]^2$$

where  $k = k'[C]^{1-n}$ .

The early part of the scheme, (i) to (iii), is logical in that an Ru(II) species is the most likely active centre and the formation of a carbene (i.e. the active centre P\*) from a  $\Pi$  complex is the likely mode of action. However stage (iv), despite providing an algebraic explanation for the relationship between  $k_{obs}$  and  $[C]$ , does not seem plausible.

The authors plotted  $\log k$  against  $[C]$  - their data fitted a quadratic function such that:-

$$\log 10^4 k = -6.99 - 2.56 \log[C] - 0.41(\log[C])^2$$

and  $n = 3.56 + 0.82 \log[C]$

This allowed them to calculate  $n$  as a function of  $[C]$  giving  $n$  as 1 at very low catalyst concentrations, rapidly increasing to 2 or 3 at higher catalyst concentrations. This implies that the active species P\* is further co-ordinated by two or more Ru species. There is no evidence in the literature for a complex of one monomer co-ordinated to

three ruthenium atoms and it is unlikely to be correct e.g. a scheme of the type shown in Fig 1.4.5 is being proposed.

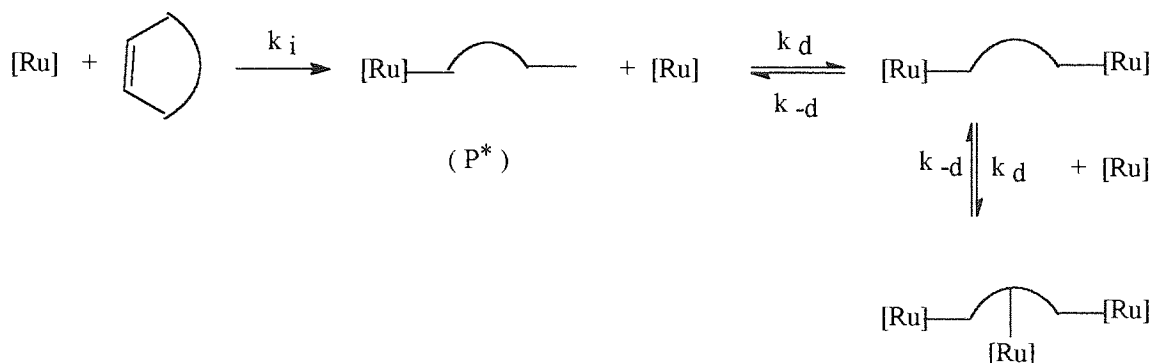


**Fig 1.4.5 - Proposed deactivation of the active centre by ruthenium species.**

However an alternative explanation can be proposed in which the active centre is not deactivated by ruthenium species but rather is prevented from forming by the coordination of  $\text{Cl}^-$ , which is present in abundance, to its ruthenium-containing precursor.

I accept the published suggestion that effectively all the ruthenium is in the form  $[\text{Ru}^{\text{III}}\text{Cl}_2]^+\text{Cl}^-$ .<sup>30</sup> Therefore:-

$$[\text{Cl}^-] = [\text{C}] = [\text{Ru}]_{\text{total}}$$

This point has been missed by the original authors. The amount of disproportionation to Ru(II) is very small such that:-

$$[\text{Ru}^{\text{II}}] = K_0^{1/2}[\text{C}]$$

However, an equilibrium can be envisaged where:-



Such that,  $[\text{Ru}^{\text{II}}\text{Cl}_2] = \beta_2[\text{Ru}^{\text{II}}][\text{Cl}^-]^2$

where  $\beta_2$  is the overall stability constant for the formation of the dichloride.

The concentration of Ru(II) which is available for complex formation with monomer is then given by :-

$$[\text{Ru}^{\text{II}}] = [\text{Ru}^{\text{II}}]_{\text{Total}} / (1 + \beta_2[\text{Cl}^-]^2)$$

but  $[\text{Cl}^-] = [\text{C}]$

and  $[\text{Ru}^{\text{II}}]_{\text{Total}} = K_o^{1/2}[\text{C}]$

$$\therefore [\text{Ru}^{\text{II}}] = K_o^{1/2}[\text{C}] / (1 + \beta_2[\text{C}]^2)$$

[In reality the co-ordination of  $\text{Cl}^-$  occurs in a stepwise fashion and some  $\text{RuCl}^+$  will be present. This should be included in the scheme above giving  $(1 + K_1[\text{C}] + \beta[\text{C}]^2)$ . However on fitting the final equation to the data, the resultant value for  $K_1$  was found to be negligibly small when compared to that of  $\beta_2$ .]

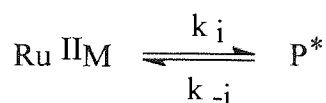
Compared to  $\text{Cl}^-$  the monomer, M, is a poor ligand, therefore the following equilibrium can be assumed to lie far to the left.



$$\therefore [\text{Ru}^{\text{II}}\text{M}] = K_3[\text{Ru}^{\text{II}}][\text{M}]$$

$$\therefore [\text{Ru}^{\text{II}}\text{M}] = K_3 K_o^{1/2}[\text{C}][\text{M}] / (1 + \beta_2[\text{C}]^2)$$

Once formed, the Ru-monomer species can then go on to form the active centre  $\text{P}^*$  as in the original mechanism.



Therefore, the scheme can be carried through as suggested by the authors through steps (v) to (viii). Applying the steady state hypothesis to  $[\text{P}^*]$  gives

$$-d[\text{P}^*]/dt = 0 = k_i[\text{Ru}^{\text{II}}\text{M}] - k_{-i}[\text{P}^*] - k_t[\text{P}^*]$$

$$\therefore [\text{P}^*] = k_i[\text{Ru}^{\text{II}}\text{M}] / (k_{-i} + k_t)$$

or  $[P^*] = k' [Ru^{II}M]$  where  $k' = k_i / (k_{-i} + k_t)$

Therefore for the monomer:-

$$-d[M]/dt = k_p [P^*][M]$$

$$\therefore -d[M]/dt = k_p k' [Ru^{II}M][M]$$

$$\therefore -d[M]/dt = k_p k_i K_3 K_O^{1/2} [C][M]^2 / (k_{-i} + k_t)(1 + \beta_2[C]^2)$$

or  $R_p = k'' [M]^2$

where  $k'' = k_p k_i K_3 K_O^{1/2} [C] / (k_{-i} + k_t)(1 + \beta_2[C]^2)$

This is a similar form to the equation quoted by the original authors. In order to observe the dependence of the rate on the catalyst concentration - or rather the concentration of  $RuCl_3$  added, the following equation can be used.

$$k_{obs} = k_p k_i K_3 K_O^{1/2} [C] / (k_{-i} + k_t)(1 + \beta_2[C]^2)$$

or  $k_{obs} = k'_{obs} [C] / (1 + \beta_2[C]^2)$

where  $k'_{obs} = k_p k_i K_3 K_O^{1/2} / (k_{-i} + k_t)$

Fitting this equation against the data given by the authors provides the excellent fit seen in Fig 1.4.4., giving values of:-

$$k'_{obs} = 0.82 \text{ M}^{-2} \text{ s}^{-1}$$

$$\beta_2 = 2.6 \times 10^5 \text{ M}^{-2}$$

with  $\beta_2$  being the stability constant for the formation of  $RuCl_2$  in 10% water in ethanol (no comparison values are available).

No experimental work has been done to check this theory but it is easy to envisage an experiment where a polymerisation system with low  $RuCl_3$  concentration is performed with added  $Cl^-$  (e.g. in the form of  $NaCl$ ). This should decrease the rate of polymerisation as  $[Cl^-]_{added}$  increases and competes with the monomer for  $Ru(II)$ . Despite the lack of experimental confirmation, I believe that a mechanism where  $Cl^-$  acts

to decrease the concentration of the active centre is more probable than one which requires the co-ordination of three ruthenium species per monomer.

The second order dependence of monomer concentration on the rate of polymerisation is confirmed by the results of polymerisations performed over a range of monomer concentrations (2.5 - 0.4 mol dm<sup>-3</sup>). Similar results were obtained by the same group<sup>27</sup> for the 2,3-dicarboxylic acid mono-methyl ester derivative with the following results obtained.

**Table 1.4.3 - ROMP of 7-oxanorbornene derivatives catalysed by RuCl<sub>3</sub>.**

Derivative	[M] <sub>0</sub> / mol dm <sup>-3</sup>	[C] <sub>0</sub> / mol dm <sup>-3</sup>	k x 10 <sup>4</sup> / dm <sup>3</sup> mol <sup>-1</sup> s <sup>-1</sup>	Slow Period	Final conv.
2,3 bis(methoxymethyl)	1.56	0.017	1.3	3 hr	94.4%
2,3-dicarboxylic acid mono-methyl ester	1.98	0.014	3.6	0.5 hr	96.6%
2,3-dicarboxylic acid mono-methyl ester	1.84	0.014	3.8	0.5 hr	93.9%

### **1.5 - Summary.**

I have tried to provide in this introduction an indication of the historical background of metathesis, a description of the process of thinking that lead earlier workers to distinguish between various mechanisms of reaction and catalyst formation and a brief review of the type of compounds used as metathesis catalysts. A more thorough and detailed review can be found in the cited references, particularly "Comprehensive Polymer Science- Vol. 4"<sup>2</sup> and "Olefin Metathesis and Ring-Opening Polymerisation of Cyclo-olefins"<sup>1</sup>. A review of the work which can be usefully classified as "Aqueous Metathesis" follows. This provides a direct backcloth for the studies contained within this thesis.

A full and complete survey of the area of metathesis is deemed unnecessary here but it is important that the reader should be able to appreciate the breadth of work that has been carried out in the past and that he or she should also be aware of the somewhat limited amount of work that has been undertaken on "Aqueous Ring-Opening Metathesis Polymerisation".

## CHAPTER 2

### MATERIALS AND METHODS

#### 2.1- Materials.

Within the appendix (Table A1) a list is provided containing all the solvents and chemicals used during this research and the suppliers who provided them. In all cases COSHH information was obtained from the suppliers or researched using BDH Hazard Data Sheets and/or the Aldrich catalogue. Solvents and chemicals were used as received and handled with care in all cases and with latex gloves and in a fume cupboard where appropriate.

#### 2.2- Methods.

##### 2.2.1- General Synthetic Methods.

All reactions were carried out using standard quick-fit laboratory glassware. Reflux and distillation apparatus were fitted with standard single condensers unless the reaction was to be left overnight, in which case a double coil condenser was used. Stirring and heating was achieved using a combined heating and stirring isomantle and a magnetic follower. When appropriate, reactions were performed in a fume cupboard. Vacuum filtrations were carried out using Buchner flasks attached to a standard water aspirator. Whatman No. 1 filter paper was used for all filtrations. Reactions under reduced pressure were performed using a Metrovac Rotary Vacuum Pump. Solvent removal and reduction was performed using a Buchi Rotavapor-R rotary evaporator. Water or air sensitive compounds were stored in a Miller-Howe dry box (oxygen removed using BASF-R311 catalyst and moisture removed using 3Å molecular sieves) or in a vacuum desiccator over P<sub>2</sub>O<sub>5</sub>.

##### 2.2.2 - Dilatometry.<sup>31</sup>

In the polymerisation of a known and fixed mass of monomer the resultant increase in density on polymerisation causes a directly proportional decrease in the volume of the reaction solution. The progress of the polymerisation can therefore be monitored in a dilatometer by measuring the change in height of a meniscus in a capillary caused by the contraction in volume of the reaction solution.



The decrease in height of the meniscus in the capillary,  $\Delta h$ , is related to the change in volume of the system,  $\Delta V$ , by the equation:-

$$(1) \quad \Delta V = \pi r^2 \Delta h \quad r = \text{radius of the capillary}$$

If  $m$  grams of monomer are converted to  $m$  grams of polymer, then the volume contraction can be expressed as:-

$$\Delta V = V_p - V_m \quad \begin{array}{l} V_p = \text{Volume of polymer} \\ V_m = \text{Volume of monomer} \end{array}$$

$$\therefore \quad \Delta V = m/\rho_p - m/\rho_m \quad \begin{array}{l} \rho_p = \text{Density of polymer} \\ \rho_m = \text{Density of monomer} \end{array}$$

$$\therefore \quad \Delta V = m(\rho_m - \rho_p / \rho_p \rho_m)$$

$$\therefore \quad (2) \quad m = \Delta V(\rho_p \rho_m / \rho_m - \rho_p)$$

If  $\Delta M$  is the number of moles polymerised, then:-

$$(3) \quad \Delta M = m/M_m \quad M_m = \text{relative molecular mass}$$

Substituting (2) into (3) :-

$$(4) \quad \Delta M = (-\Delta V/M_m)(\rho_p \rho_m / \rho_m - \rho_p)$$

Assuming the volume of the dilatometer,  $V$ , is much larger than the change in volume in the capillary, then the change in monomer concentration,  $\Delta[M]$ , can be expressed as :-

$$(5) \quad \Delta[M] = \Delta M/V$$

Substituting (4) into (5) :-

$$(6) \quad \Delta[M] = (1/V)(\Delta V/M_m)(\rho_p \rho_m / \rho_m - \rho_p)$$

Substituting (1) into (6) :-

$$(7) \quad \Delta[M] = (\pi r^2 \Delta h / VM_m)(\rho_p \rho_m / \rho_m - \rho_p)$$

$$\therefore \quad \Delta[M] = K \Delta h \quad \text{where } K = (\pi r^2 / VM_m)(\rho_p \rho_m / \rho_m - \rho_p)$$

K is constant for the system. To obtain absolute rates therefore, the densities of both the monomer and polymer must be known.

Monomer and catalyst solutions were prepared separately and immersed in a water bath to equilibrate at the reaction temperature. The solutions were mixed thoroughly and the time noted. The reaction solution was then injected into the dilatometer body using a long needled syringe. Injection of the solution had to be done slowly and with great care to avoid introducing bubbles into the capillary. The dilatometer was then allowed to settle at the reaction temperature so that the meniscus could rise to a suitable level, before the capillary was sealed and the dilatometer fully immersed. Sealing of the dilatometers was tried by a number of methods, the most effective of which was by fixing a glass plug into the neck of the capillary using quick setting glass adhesive. However it is not thought that the sealing method greatly affected the results obtained. Initial experiments were carried out in a single dilatometer but the majority of the experiments were performed in an array of eight identical dilatometers which allowed for up to six different reaction solutions and two controls at any one time. The dimensions of the dilatometers are given below in table 2.2.2.1 The dilatometers were immersed in a large glass sided constant temperature water bath for the duration of the experiment and height measurements were taken using a cathetometer fitted with a vernier scale Height measurements were taken relative to a fixed point on the dilatometer body marked by adhesive tape.

**Table 2.2.2.1 - Dilatometer Dimensions.**

	Body Height / mm	Body Diameter / mm	Body Volume / ml	Capillary Height / mm	Capillary Internal Diameter / mm
Single	80	18	~ 12	150	1.5
Array	130	15	~ 15	170	1.5

### **2.2.3- Ultra-Violet/Visible Spectroscopy.**

UV/Visible spectroscopy is a non-destructive analytical technique which relies on the absorption of light by a species in solution. The impinging light may cause an electronic transition to occur in the species in solution. For a transition metal the transition may be between *d*-orbitals in the metal and such d-d transitions are forbidden and therefore tend to be weak. Alternatively a transition can occur between a donor orbital in one part of

the complex to an acceptor orbital in another part. These charge-transfer transitions are allowed and therefore tend to have very large molar absorptivities.

The spectrometer measures the difference in light intensity between the incident light and the light passing through the sample. Therefore the optical density ( $d$ ) is measured as a function of wavelength as given by the equation below.

$$d = \log_{10}(I_0/I)$$

where  $I_0$  = intensity of impinging light, and  $I$  = intensity of emerging light. The optical density can be used to calculate the molar absorption coefficient (extinction coefficient),  $\epsilon$ , which is specific to the absorbing species at a given wavelength, via the equation below.

$$\epsilon = d/cl$$

where  $c$  = concentration of the absorbing species ( $\text{mol dm}^{-3}$ ), and  $l$  = path length of the impinging light through the absorbing species (cm). This equation is more usually rearranged to the form known as Beer's law, given below.

$$d = \epsilon cl$$

Routine UV/Vis spectra were obtained using a Pye-Unicam SP8-100 double beam spectrometer fitted with a deuterium lamp. In all cases, samples were analysed in quartz glass spectrometer cells with a path length of 1cm. Due to instrumental problems, studies into the interaction of  $\text{Ru}(\text{CO})\text{Cl}_2(\text{H}_2\text{O})$  with 7-oxanorbornenedicarboxylic acid were performed using three different data retrieval methods. Throughout this section, 'monomer' refers to 7-oxanorbornene-2,3-dicarboxylic acid and 'catalyst' refers to  $\text{Ru}(\text{CO})\text{Cl}_2(\text{H}_2\text{O})$ .

### **Method 1.**

This method utilised a Pye-Unicam SP8-100 UV spectrometer. Monomer and catalyst solutions were prepared and allowed to reach the reaction temperature in a constant temperature water bath before being mixed to give reaction solutions with concentrations as given in Table 6.4.1 (Section 6.4). At regular intervals, 0.4mls of each solution were removed and diluted to 10mls with distilled water to give a solution for analysis with concentration given in the table specified above. Samples were scanned from 600nm to

250nm and the absorbance at 323nm measured from the spectra obtained. The reaction solutions remained at the reaction temperature for the duration of the experiment.

### **Method 2.**

This method utilised a Pye-Unicam SP800 UV spectrometer fitted with a four cell carriage attached to a constant temperature water bath. This allowed water at elevated temperature to be circulated around the UV cells so that continuous absorbance readings could be taken at elevated temperature over an extended period of time. Monomer and catalyst solutions were prepared separately and allowed to reach reaction temperature before mixing to give reaction solutions of concentrations given in Table 6.4.2 (Section 6.4). The reaction solutions were poured into the UV cells without dilution and all four samples were then placed in the four cell, temperature adjusted carriage. The SP800 spectrometer was programmed to take an absorbance reading at 323 nm for each sample in rotation at regular intervals. For the early part of the experiment readings were taken every 10 minutes and for the latter part every 15 minutes. The cells were regularly checked for evaporation of the solution and if evaporation had occurred, the solution in the cell was replaced with excess reaction solution which had been held at the reaction temperature for the duration of the experiment.

### **Method 3.**

Attempts were made to proceed as described in Method 2 (above) but due to constant malfunctioning of the moveable four cell carriage this proved impossible.

This method utilised a Pye-Unicam SP8-100 UV spectrometer fitted with a four cell carriage attached to a constant temperature water bath. Monomer and catalyst solutions were prepared and allowed to reach reaction temperature before being mixed to give solutions with concentrations given in Tables 6.4.3 to 6.4.5 (Section 6.4). Samples were poured into UV cells and placed in the temperature adjusted carriage individually. The samples were then scanned at 323 nm for a period of time (usually 2-3 hours) at the reaction temperature. The samples were then removed from the spectrometer and returned to the bulk reaction solution which was constantly held at the reaction temperature. This procedure was then repeated for the next sample. In this way, the samples were scanned at the single wavelength for a few hours at a time, in rotation, for the duration of the experiment.

#### **2.2.4 - Infra-Red Spectroscopy.**

IR spectra were obtained using a Perkin-Elmer Paragon 1000 FT-IR spectrometer and prepared and analysed using GRAMS Analyst 1000 computer software.

#### **2.2.5- Nuclear Magnetic Resonance Spectroscopy.**

All NMR spectra were obtained using a Bruker AC-E 300MHz NMR Spectrometer by Dr. M. Perry and were prepared and analysed using Bruker 1D WinNMR computer software. In all cases the spectra were recorded in DMSO-d<sub>6</sub> and at the following frequencies; <sup>1</sup>H = 300 MHz, <sup>31</sup>P = 121.5 MHz, <sup>13</sup>C = 75.5 MHz. All <sup>13</sup>C spectra were proton de-coupled and acquired using a *J*-modulated spin-echo sequence (*J*-mod.). This acquisition sequence causes the inversion of -CH<sub>2</sub>- and -C- peaks (which appear as negative peaks) and leave -CH<sub>3</sub>- and -CH- peaks as positive. This aids in the interpretation of spectra.

#### **2.2.6- Size Exclusion Chromatography.**

Size Exclusion Chromatography (SEC) was performed using a Polymer Labs PLgel 10µm Mixed-B column. The column was calibrated using polystyrene narrow molecular weight standards. Samples were dissolved in HPLC grade THF (0.5% w/w) and pumped through the column using a Knauer HPLC Pump 64. Samples were identified by the difference in refractive index when compared to the eluent using a Knauer Differential Refractometer and the data collected using a PL DCU (Data collection unit) and analysed using PL Caliber computer software.

#### **2.2.7 - Elemental Analysis.**

Elemental analyses were carried out by MEDAC Limited, Department of Chemistry, Brunel University, Uxbridge, Middlesex, UB8 3PH.

#### **2.2.8 - Melting points.**

Melting points were determined, in duplicate, using Gallenkamp melting point apparatus and are uncorrected.

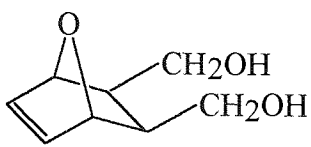
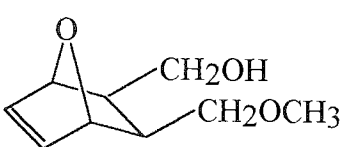
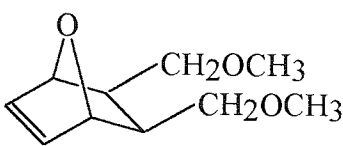
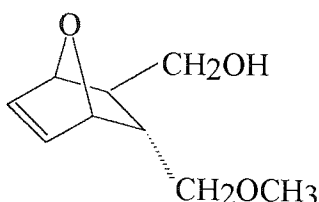
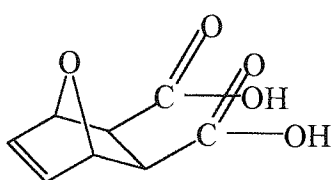
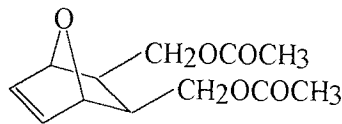
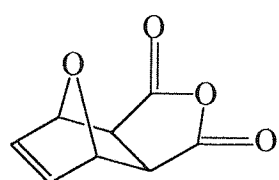
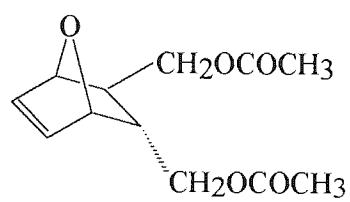
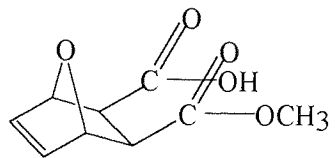
## CHAPTER 3

### SYNTHESIS OF BICYCLIC MONOMERS

#### 3.1 - Introduction

As discussed elsewhere in this thesis (Section 1.4), the first account of aqueous ROMP was published by Novak and Grubbs<sup>10</sup> in 1988. In this paper the polymerisation of two monomers using a ruthenium catalyst, namely the 2,3-dimethanol (I) and 2,3-dimethoxymethyl (II) derivatives of 7-oxanorbornene (See Table 3.1) is described. Other papers published on this topic likewise all concern themselves with the polymerisation of various derivatives of 7-oxanorbornene. Feast and Harrison<sup>24</sup> published a report on the polymerisation of 7-oxanorbornene-2,3-dicarboxylic acid (III) by  $\text{RuCl}_3 \cdot 3\text{H}_2\text{O}$  and presented a detailed NMR and GPC analyses of the reaction products, and in another paper<sup>25</sup> the same authors presented a study of the polymerisation of the 2,3-dimethoxymethyl derivative and the control of its molecular weight by the use of a chain transfer agent. It is interesting to note that Feast and Harrison describe this polymerisation as an aqueous **emulsion** polymerisation due to the monomer's insolubility in water whereas Novak and Grubbs<sup>10</sup> do not mention this point. France, Grubbs, McGrath and Paciello have also published a paper on the polymerisation of this monomer and the effect of chain transfer agents on molecular weight<sup>26</sup> and again describe it as an aqueous polymerisation rather than aqueous emulsion polymerisation. Lu, Quayle, Heatley, Booth, Yeates and Padget published the first detailed rate measurements of "aqueous" metathesis polymerisation when they described the polymerisation of the 2,3-dimethoxymethyl derivative using  $\text{RuCl}_3 \cdot 3\text{H}_2\text{O}$  in aqueous ethanol<sup>29</sup>. The amount of water present was usually 10% but on some runs up to 50% water was present in the solvent system. As they mention, the reason for the mixed water/alcohol solvent is to ensure complete solubility of both monomer and catalyst; at solvent mixtures of <50% ethanol, the polymerisation system was inhomogeneous. The polymerisation of the dicarboxylic anhydride derivative (IV) in 10% water in ethanol as solvent and the polymerisation of the 2,3-dicarboxylic acid mono-methyl ester derivative (V) in the same solvent and in 10% ethanol in water is reported by the same authors<sup>27</sup>. The most recent paper published by this group (accompanied by Amass, Majid, Glennon and Byerly)<sup>28</sup> discusses the polymerisation of a range of 2,3 -di-substituted derivatives of 7-oxanorbornene most commonly in 10% water in ethanol as solvent. A list of all the derivatives is given in Table 3.1.1.

**Table 3.1.1- Monomers used in aqueous ROMP.**

Monomer	Refs.	Monomer	Refs.
(I) 	10 28	(VI) 	28
(II) 	10 25 26 28 29	(VII) 	28
(III) 	24	(VIII) 	28
(IV) 	27 28	(IX) 	28
(V) 	27 28		

For the purposes of my research, it was desirable to synthesise a minimum number of monomers as the main aim of the work was to concentrate on the affect of catalyst structure on ROMP. Therefore the factors governing choice of monomer were:-

- 1/ Solubility - the monomer must be readily water soluble.
- 2/ Presence of functional groups.
- 3/ Ability to synthesise the monomer easily in bulk - to minimise the number of synthetic experiments needed during the period of research.

The first choice for monomer is that first used by Grubbs in the literature<sup>10</sup>, namely the dimethoxymethyl derivative of oxanorbornene, which has been shown to be polymerisable using water-soluble ruthenium complexes. However considerable problems were encountered in this synthesis, especially during separation and purification ( see synthesis No. 1).

The next choice for monomer was the dicarboxylic acid derivative of oxanorbornene which has also been shown in the literature to be polymerisable<sup>24</sup>.

The dicarboxylic acid derivative of norbornene was also synthesised in both its *endo* and *exo* forms<sup>32</sup>.

### 3.2 - The Diels-Alder reaction.

All the monomer syntheses carried out involved the use of the Diels-Alder reaction. This reaction is a pericyclic cycloaddition reaction between a diene and a dienophile.

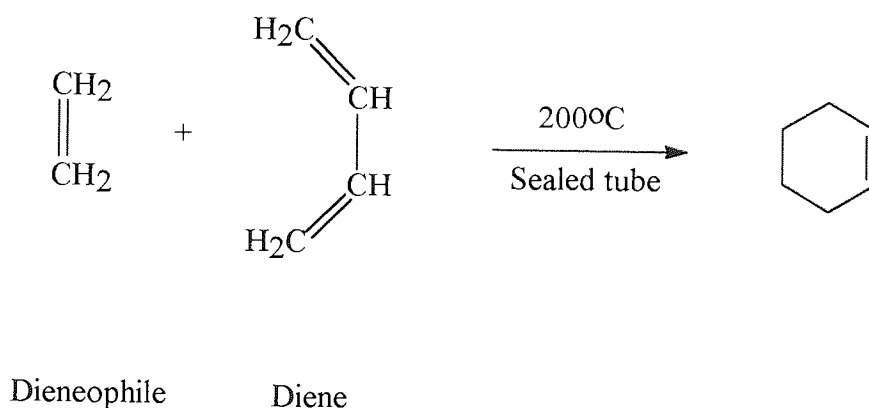


**Fig 3.2.1 - The Diels Alder reaction**

Pericyclic reactions involve a concerted bond rearrangement in which the essential bond changes occur within a cyclic array. The reactions are highly stereo specific due to the symmetry requirements of the reactant and product orbitals. A pericyclic reaction can only occur if the symmetry of all the reactant molecular orbitals is the same as the symmetry of the product molecular orbital. The lobes of the reactant orbitals must be of the correct sign for bonding overlap to occur in the transition state leading to the product. For example, in the case of one of the monomer syntheses discussed here (Synthesis No. 3), the reaction between cyclopentadiene and maleic anhydride, orbital overlap occurs between the LUMO of the diene and the HOMO of the dienophile (see Fig 3.2.2). It can clearly be seen that two structural isomers can be produced. For my



monomer, the *endo* form is normally produced at room temperature due to the enhanced overlap of orbitals between the diene and dienophile. However by performing the reaction at higher temperature (i.e. in a high boiling solvent), the thermodynamically more stable *exo* adduct can be produced.

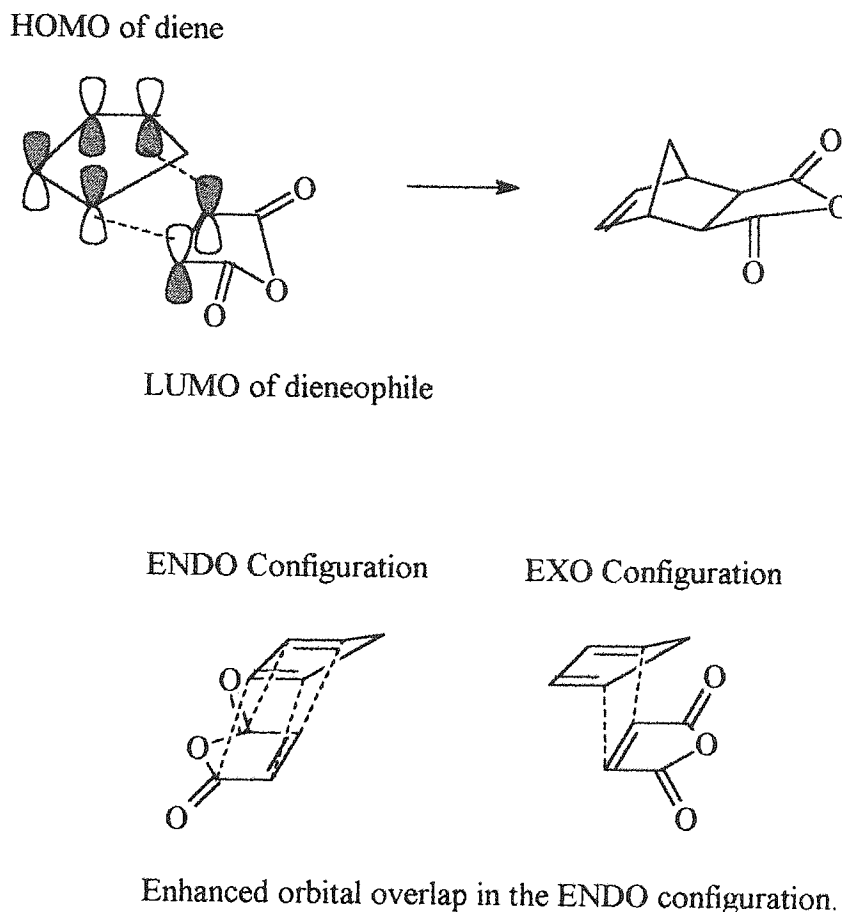


**Fig. 3.2.2 - Orbital overlap for the Diels-Alder reaction of maleic anhydride with cyclopentadiene.**

### 3.3 - Synthesis No.1 - Exo, exo-7-oxabicyclo[2.2.1]hept-5-ene-2,3-dimethanol.<sup>33</sup>

Maleic anhydride (9.8g, 0.1 moles) dissolved in dry THF (70 ml) was added dropwise to furan (6.8g, 0.1 moles) and stirred for 2 hours at room temperature. This formed the dicarboxylic anhydride. This product was added dropwise from a pressure equalised dropping funnel to a stirred suspension of lithium aluminium hydride (1.9g, 0.05 moles) in THF (30 ml) under an N<sub>2</sub> blanket. The addition was done slowly and over an ice bath because of the large exotherm produced by the reaction. The mixture was left stirring for 3 hours over ice and then left stirring overnight to allow a rise to room temperature.

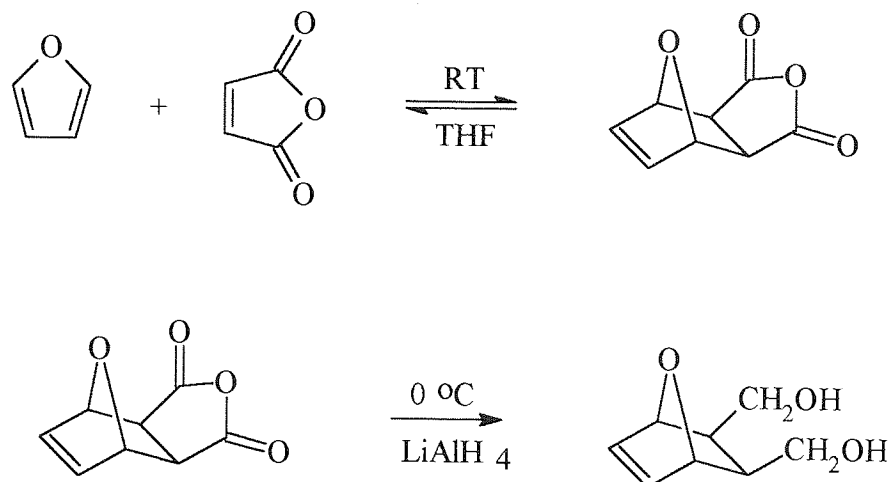


**Fig 3.3.1 - Synthesis of *exo, exo*-7-oxabicyclo[2.2.1]hept-5-ene-2,3-dimethanol**

Excess LiAlH<sub>4</sub> was removed by addition of water saturated with sodium sulphate. Anhydrous magnesium sulphate was added and the mixture was filtered leaving a reddish filtrate and an orange residue. The residue was washed thoroughly with dichloromethane and 10% acetonitrile in ethyl acetate. Problems were encountered in the washing as the residue was completely immiscible with both the eluents. The combined filtrate was concentrated and left to stand for 2 weeks. After this period, excess sodium sulphate had crystallised out and was filtered off. An attempt to purify the filtrate by flash chromatography was then made. Vacuum concentration of each eluent produced no product residue. In an attempt to remove any product still absorbed on the silica gel from the flash chromatography, the silica gel was subjected to a soxhlet extraction, first with hexane and then with ethyl acetate. Neither extraction produced any product.

### Conclusions.

Since the product should be a viscous oil, it seems likely that it was contained in the original reaction residue and could not be washed out. It is also thought that the grade of silica gel used for the flash chromatography, although chromatographic grade, was too coarse for effective separation. No further attempts were made to synthesise this monomer.

**3.4 - Synthesis No. 2 - *exo*-oxabicyclo[2.2.1]hept-5-ene-2,3-dicarboxylic anhydride.**<sup>24, 34</sup>

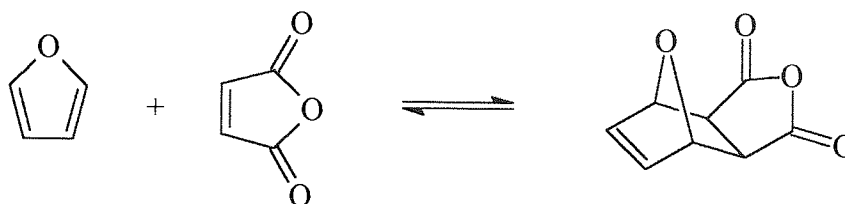


**Fig 3.4.1 - Synthesis of *exo*-oxabicyclo[2.2.1]hept-5-ene-2,3-dicarboxylic anhydride.**

This synthesis was attempted on a number of occasions using water (to produce the diacid), THF and excess furan as solvents. The most successful experiment using furan as solvent is described below.

Maleic anhydride (49g, 0.5 moles) was dissolved with stirring in furan (150 mls,  $\approx 1.5$  moles) over an ice bath. The mixture was stirred over ice for 3 hours and then left to rise to room temperature overnight. A large amount of brilliant white crystals precipitated from the solution overnight and these were separated by filtration and dried under vacuum over  $P_2O_5$ . Yield = 76.5g (92% based on maleic anhydride). Melting Point = 117-118°C (Lit. Value. - Aldrich = 118°C).

Yields from this procedure were very variable but the following conditions tended to increase the quantity and purity of the crude yield.

- 1/ Excess furan was the most reliable of the solvents tried. However too large an excess i.e.  $>3:1$  leads to a reduced yield due to the increased amount of product remaining in solution.
- 2/ The reaction solution should be held at  $\approx 0^\circ\text{C}$  for the stated time and then allowed to reach room temperature slowly as this increases the product purity.
- 3/ Once filtered, the mother liquor can be left, or slightly reduced, to yield a second crop of crystals. However the second crop is always of much lower purity containing significant amounts of maleic anhydride. This is shown by a reduced melting point ( $\approx 110^\circ\text{C}$ ) and characteristic NMR resonances (see below). Impure crops can be purified by recrystallisation from iso-propanol. However as stated in the literature<sup>34</sup> this

drastically reduces the yield due to the instability of the product in boiling solutions. In my experience a large (> 80 %) impure yield would be reduced to a very small (< 10 %) pure yield. As this may require two or three recrystallisations the time taken to produce a large amount of pure product from an initially impure crop makes the use of recrystallisation impractical for the synthesis of this monomer.

### Product analysis by NMR.

The product was characterised by  $^{13}\text{C}$  and  $^1\text{H}$  NMR (See Appendix B - Fig B1 and Fig B2 respectively). Presence of maleic anhydride impurity can be easily seen in the  $^1\text{H}$  spectrum making NMR spectroscopy a good indicator of monomer purity.

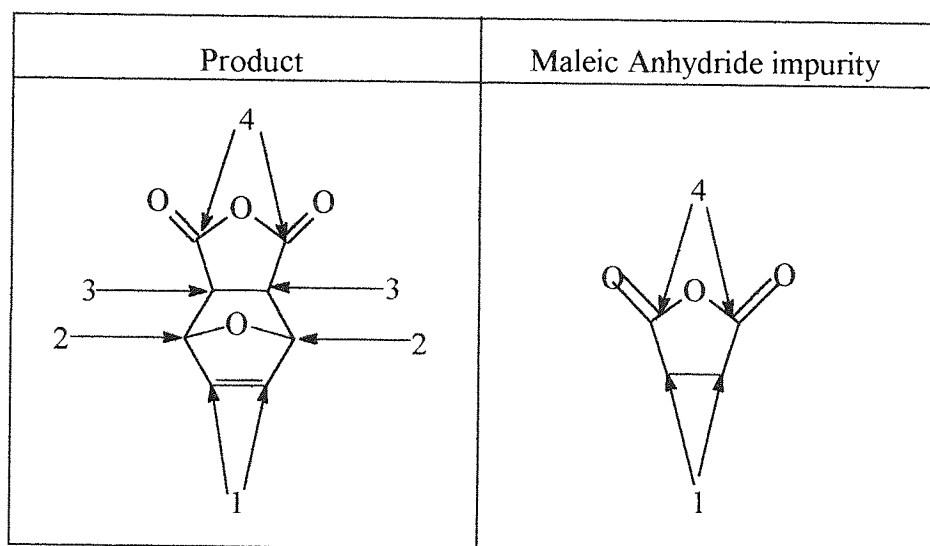


Fig 3.4.2 - Carbon numbering for  $^{13}\text{C}$  NMR analysis.

Table 3.4.1 -  $^{13}\text{C}$  NMR data for *exo*-oxabicyclo[2.2.1]hept-5-ene-2,3-dicarboxylic anhydride.

Carbon Number.	$\delta$ /ppm for product. (Appendix B - Fig B1)	$\delta$ / ppm for maleic anhydride.
1	135.6	136
2	80.9	-----
3	47.6	-----
4	169.0	164

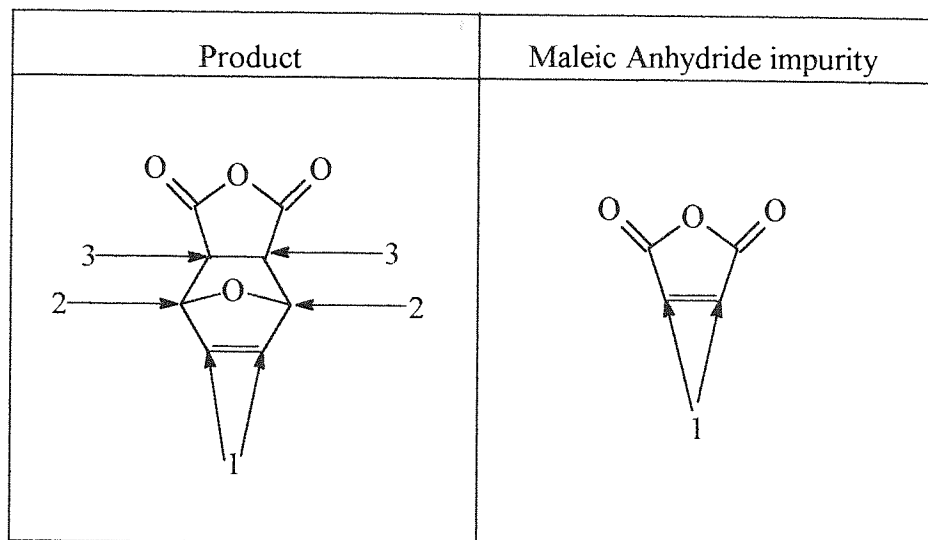


Fig 3.4.3 - Proton numbering for  $^1\text{H}$  NMR analysis.

Table 3.4.2 -  $^1\text{H}$  NMR data for *exo*-oxabicyclo[2.2.1]hept-5-ene-2,3-dicarboxylic anhydride.

Proton Number	$\delta$ / ppm for product.	$\delta$ / ppm for maleic anhydride.
1	6.5	7.1
2	5.3	-----
3	3.2	-----

The presence of two peaks in the general region of 6.5 ppm to 7 ppm signifies the presence of maleic anhydride impurity. The integral ratio of the two peaks gives the ratio of product to impurity, as long as the correct NMR acquisition procedures have been followed i.e. a time equivalent to  $5T_1$  has been allowed to lapse between each acquisition pulse.

#### Hydrolysis of the anhydride derivative to the dicarboxylic acid derivative.

The anhydride derivative can be hydrolysed by dissolving in hot water. However attempts to recrystallise the dicarboxylic anhydride from boiling water produced high amounts of maleic acid impurity. Therefore the monomer was used in later aqueous polymerisation experiments as the anhydride derivative and the dicarboxylic acid derivative produced *in situ*.

### 3.5- Synthesis No. 3 - *endo, endo*-bicyclo[2.2.1]hept-5-ene-2,3-dicarboxylic acid<sup>32</sup>

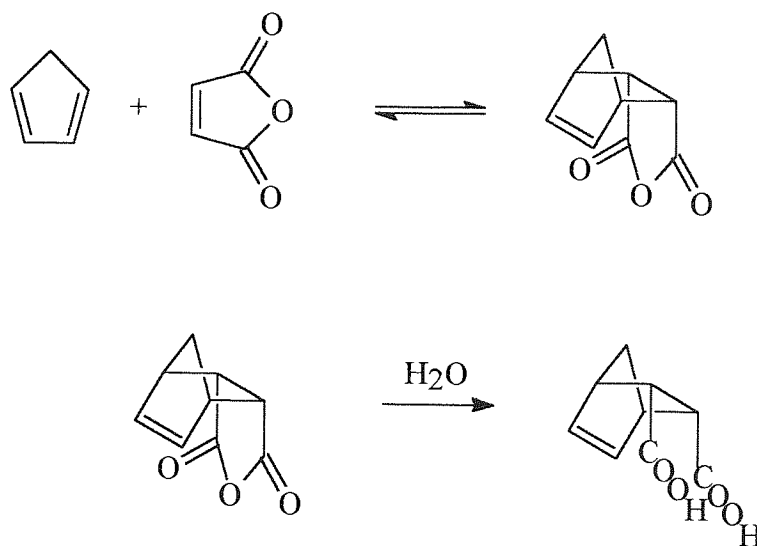


**Fig 3.5.1 - Synthesis of *endo, endo* bicyclo[2.2.1]hept-5-ene-2,3-dicarboxylic acid**

Approximately 30 ml of cyclopentadiene was freshly cracked from dicyclopentadiene for this experiment.

Crushed maleic anhydride (12g, 0.122 moles) was dissolved in ethyl acetate (40 ml) and gently warmed until dissolution was complete. 60/40 Pet ether (40 ml) was slowly added and the solution cooled by swirling in an ice bath. Cyclopentadiene (12 ml, 0.146 moles) was carefully added and the flask continually swirled to dissipate the exothermic heat of reaction. Upon cooling, product crystals came out of solution. These were re dissolved in the reaction solvent by gentle warming and then the solution was left to cool slowly to allow product recrystallisation. The reaction was performed twice yielding 16.2g(81%) and 17.4g(87%) of glistening white crystals, with melting point 163-165°C (Lit value = 164-165°C for the unhydrolysed adduct)<sup>32</sup>.

The product from the first experiment was hydrolysed by refluxing it in water until complete dissolution occurred (approximately 1/2 hour) and then leaving to cool and recrystallise. The product was filtered off and dried over P<sub>2</sub>O<sub>5</sub> in a vacuum desiccator. The overall yield of the di-acid based on 0.122 moles of maleic anhydride was 75%

### 3.6 - Synthesis No. 4 - *exo*-bicyclo[2.2.1]hept-5-enedicarboxylic anhydride.<sup>35</sup>

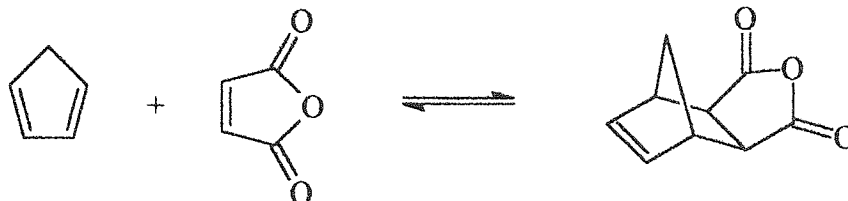


**Fig 3.6.1 - Synthesis of *exo*-bicyclo[2.2.1]hept-5-enedicarboxylic anhydride.**

Maleic anhydride (19.6g, 0.2 moles) was dissolved in *o*-dichlorobenzene (100 ml) and heated to 173°C. Dicyclopentadiene (15 ml, 0.112 moles - slight excess) was added and heating continued until reflux was maintained at 183°C. After 90 minutes, heating was stopped and the reaction allowed to cool to room temperature overnight. The mother liquor was slightly reduced under vacuum to facilitate recrystallisation. The crystalline product was recrystallised twice from chlorobenzene at room temperature.

The total yield was 6.3g (19.2%) of white crystals with melting point 142-143°C. This melting point agrees with that quoted in the literature<sup>35</sup>.

### 3.7 - Comparison of *endo*- and *exo*-bicyclo[2.2.1]hept-5-ene dicarboxylic anhydride.

Samples of both the *endo*- and *exo*- adduct were analysed by <sup>13</sup>C NMR spectroscopy. (Appendix B - Figs B3 and B4). Carbon numbering assignments are given in Fig 3.7.1 and chemical shift data in Table 3.7.1.

As expected the peak due to the quaternary carbon has not changed position on going from the *endo* adduct to the *exo* adduct. Peaks numbered 1,2 & 4 all show a slight down field shift in position between the *endo* and *exo* adduct. However, the bridging methylene carbon No.3 undergoes an up field shift (9 ppm) on going from the *endo* form to the *exo* form. These changes are due to the change in position of the anhydride group in relation to the carbon atoms. For the methylene carbon No.3, this change in environment is the most dramatic. In the *endo* form, this carbon was on the opposite side of the molecule to the anhydride group. In the *exo* adduct however, it is in an adjacent plane on the same side of the molecule. The greater proximity of the electron rich oxygens on the anhydride group increase the shielding (through space interaction)

on the methylene carbon and the chemical shift moves up field in relation to the endo form.

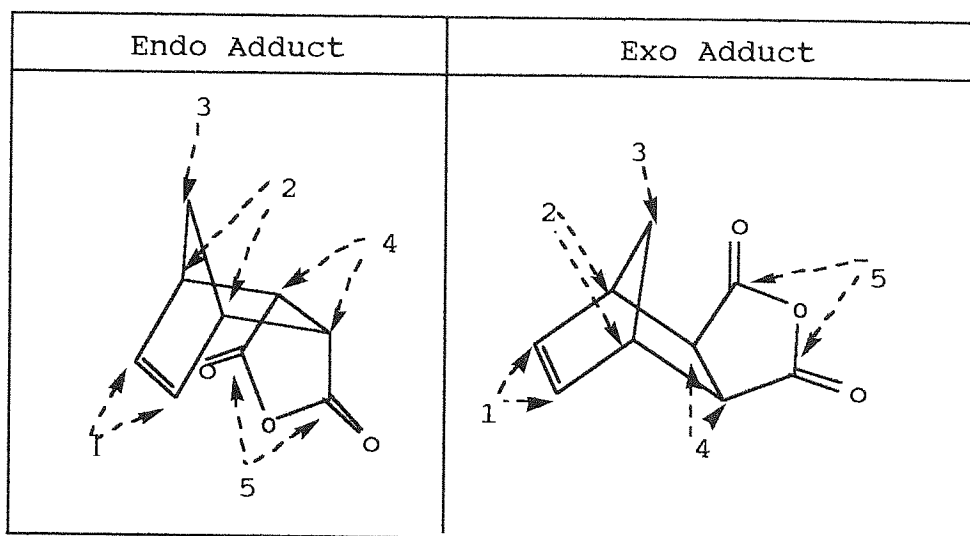


Fig 3.7.1 - Carbon numbering for NMR analysis.

Table 3.7.1 - Chemical shifts in ppm from  $^{13}\text{C}$  spectra of *endo*-adduct and *exo*-adduct (Appendix B - Figs B3 and B4 respectively).

Carbon Number	$\delta$ / ppm <i>Endo</i> - spectrum	$\delta$ / ppm <i>Exo</i> - spectrum
1	132.5	137.8
2	47.1	48.9
3	52.5	43.7
4	45.4	46.1
5	172.5	172.5



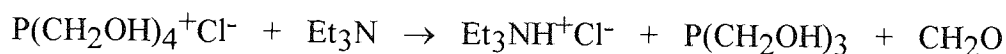
## CHAPTER 4

### SYNTHESIS OF WATER SOLUBLE PHOSPHINE COMPOUNDS

One route to producing water soluble ruthenium complexes is to modify the ligands of complexes which are known to show catalytic activity in non-aqueous systems. One such complex is  $\text{Ru}(\text{PPh}_3)_3\text{Cl}_2$  which when combined with an initiator has been shown to form ruthenium carbene species which will polymerise norbornene in protic media<sup>15</sup> (See 1.3). The synthesis of two water soluble phosphines is described.

#### 4.1 - Synthesis No. 5 - Tris(hydroxymethyl)phosphine (THMP).<sup>40</sup>

Tris(hydroxymethyl)phosphine has been shown to form water soluble complexes with a number of metals such as platinum, palladium, nickel, rhodium and gold<sup>36, 37, 38</sup>. The existence of the corresponding ruthenium complex has been alluded to in the literature<sup>39</sup> but no details have been published. The ligand can be prepared directly from gaseous  $\text{PH}_3$  but the somewhat safer route via  $[\text{P}(\text{CH}_2\text{OH})_4]^+\text{Cl}^-$  has been used in this thesis.



$[\text{P}(\text{CH}_2\text{OH})_4]^+\text{Cl}^-$  is supplied by Albright and Wilson Ltd. as an 80% wt/wt aqueous solution and the water must be completely removed before reaction with triethylamine. This is done by first removing as much water as possible on a rotary evaporator. The remaining water is removed by azeotropic distillation with toluene. Anhydrous tetrakis(hydroxymethyl)phosphonium chloride (THPC) is recrystallised from two weight equivalents of propan-2-ol giving a white, highly hygroscopic powder. For my purposes it was convenient to prepare a large quantity of THPC in advance and store this in a dry box for future use. The following synthesis is representative of the scale of reaction usually carried out.

$\text{P}(\text{CH}_2\text{OH})_4\text{Cl}$  (6.35g, 0.03 moles) was charged to a 3-neck flask under an argon atmosphere. Dry triethylamine (100 ml) was added with stirring. The mixture was heated to 60°C and held for 1 hour with continuous stirring. If the temperature goes above 65°C the solid sticks together resulting in inefficient mixing. After 1 hour the solution was cooled and the precipitated triethylaminehydrochloride by-product was removed by filtration. The excess triethylamine was removed by distillation (some of the formaldehyde by-product sublimes out during the distillation) leaving the crude product as a viscous oil. Care must be taken when removing the last few mls of triethylamine not

to overheat the crude product as this can lead to product decomposition. The formaldehyde by-product reacts with tris(hydroxymethyl)phosphine in a reversible side reaction to form mono, di and tri hemiacetals.



The formaldehyde can be removed by heating the crude product to 90°C on an oil bath under vacuum under a slow flow of argon. Care must be taken to ensure the temperature does not rise above 90°C as the product can undergo an exothermic disproportionation generating phosphine gas above 130°C. The literature recommends monitoring the course of the purification by NMR via the characteristic <sup>31</sup>P resonances of the hemiacetal impurities. However this form of monitoring was not available to me, so heating was maintained for 5 hours as suggested in the literature. It was observed that formaldehyde stopped subliming after approximately 3 hours of heating, so for subsequent syntheses only 3 hours heating was performed. This yielded a viscous oil product as described in the literature.

Recrystallisation from methanol at -20°C was attempted but proved very difficult. When crystals were retrieved from solution, filtration under argon proved unsuccessful as the damp crystals adhered to the filter paper and could not be removed. As it was convenient to immediately react the phosphine compound with ruthenium complexes (See 5.4.11) recrystallisation was deemed unnecessary and no further attempts were made. The literature reports essentially quantitative yields for the product from recrystallised THPC and although no recrystallised product yields can be quoted here, I have no reason to suspect that my yields are substantially less than quantitative.

### Product analysis by NMR.

$^{13}\text{C}$ ,  $^1\text{H}$  and  $^{31}\text{P}$  NMR spectra (Appendix B - Figs B5 to B7 respectively) of the unrecrystallised phosphine were acquired and the results compared to literature data<sup>40</sup>.

Table 4.1.1 -  $^{31}\text{P}$  and  $^{13}\text{C}$  NMR data for synthesised  $\text{P}(\text{CH}_2\text{OH})_3$ .

$^{31}\text{P}$	$^{13}\text{C}^a$	
$\delta / \text{ppm}$	$\delta / \text{ppm}$	Type & J/Hz
-37.76	9.24 (+)	d / 117.7
-29.92	54.61 (-)	d / 75.2
-29.74	56.11 (-)	d / 8.7
-25.29	57.18 (-)	d / 79.6
29.17	58.93 (-)	d / 9.8
33.34	61.83 (-)	d / 6.5
44.05	66.66 (-)	d / 122
45.33		
49.84		

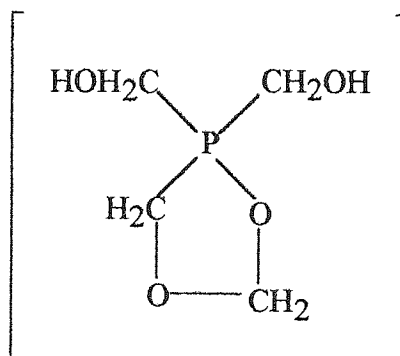
a) Spectra recorded using PENDANT pulse sequence. C &  $\text{CH}_2$  annotated (-), CH &  $\text{CH}_3$  annotated (+).

Table 4.1.2 -  $^1\text{H}$  NMR data for synthesised  $\text{P}(\text{CH}_2\text{OH})_3$ .

$\delta / \text{ppm}$	Type	J / Hz	R.I
0.87	Doublet	2.64	90
0.92	Triplet	7.08	100
1.31	Doublet	12.88	1023
1.37	Singlet	-	77
3.65	Doublet	4.11	15
3.69	Doublet	3.96	426
3.72	Doublet	3.78	543
3.79	Doublet	3.3	1930
3.83	Doublet	5.6	9562
4.83	Broad	-	5503

### Interpretation of $^{13}\text{C}$ NMR data (Appendix B - Fig B5).

The three doublets at  $\delta = 56.1, 58.9, 61.8$  with coupling constants of around 10 Hz can be assigned to carbons attached to phosphorus in a three co-ordinate compound (c.f.  $\text{PCH}_3$ ,  $J(\text{PC}) = 12.1 \text{ Hz}$ )<sup>85</sup>. These resonances can be assigned to the methylene carbon in tris(hydroxymethyl)phosphine and the methylene carbons in the mono-hemiacetal i.e.  $\text{P}(\underline{\text{CH}_2\text{OH}})_3$  and  $\text{P}(\underline{\text{CH}_2\text{OH}})_2(\underline{\text{CH}_2\text{OCH}_2\text{OH}})$ . The other carbon in the mono-hemiacetal should show a resonance significantly downfield in relation to the other three resonances and with a reduced coupling constant but no obviously attributable resonance can be seen. Although the di- and tri-hemiacetals are present, (see interpretation of  $^{31}\text{P}$  spectrum) the concentrations are probably too low for their resonances to be visible. The two doublets at  $\delta = 54.6, 57.2 \text{ ppm}$  are significant for their large coupling constants which suggests a four co-ordinate phosphorous compound ( $\text{CF} [\text{PCH}_4]^+\text{Cl}^-$   $J(\text{PC}) = 56.25 \text{ Hz}$ )<sup>85</sup>. One possible explanation for the existence of a four co-ordinate species is a 5 membered ring structure of the type shown below, in which the hemiacetal ligand loses a proton and "backbites" the phosphorus centre.



**Fig 4.1.1 - Possible five membered ring structure in crude phosphine mixture.**

In this instance the two distinct types of directly attached carbons would provide the two doublets observed. The third carbon between the two oxygens should show a resonance downfield of the other two with a reduced coupling constant. No resonance for this carbon can be assigned. The doublet at  $\delta = 9.2 \text{ ppm}$  is characteristic of a methyl carbon and the large coupling constant ( $J(\text{PC}) = 117.7 \text{ Hz}$ ) suggests a four co-ordinate rather than a three co-ordinate species. The five membered ring provides a route for the formation of such a species (See Fig 4.1.2). This type of structure agrees very well with data for similar structures e.g.  $(\text{CH}_3)_2(\text{HO})\text{P}=\text{O}$ ,  $\delta = 16.5 \text{ ppm}$ ,  $J(\text{PC}) = 95.25 \text{ Hz}$ <sup>85</sup>. This structure would also require a doublet with similar coupling constant and downfield for the hydroxymethyl ligands. The doublet at  $\delta = 66.7 \text{ ppm}$  can be assigned to these groups.

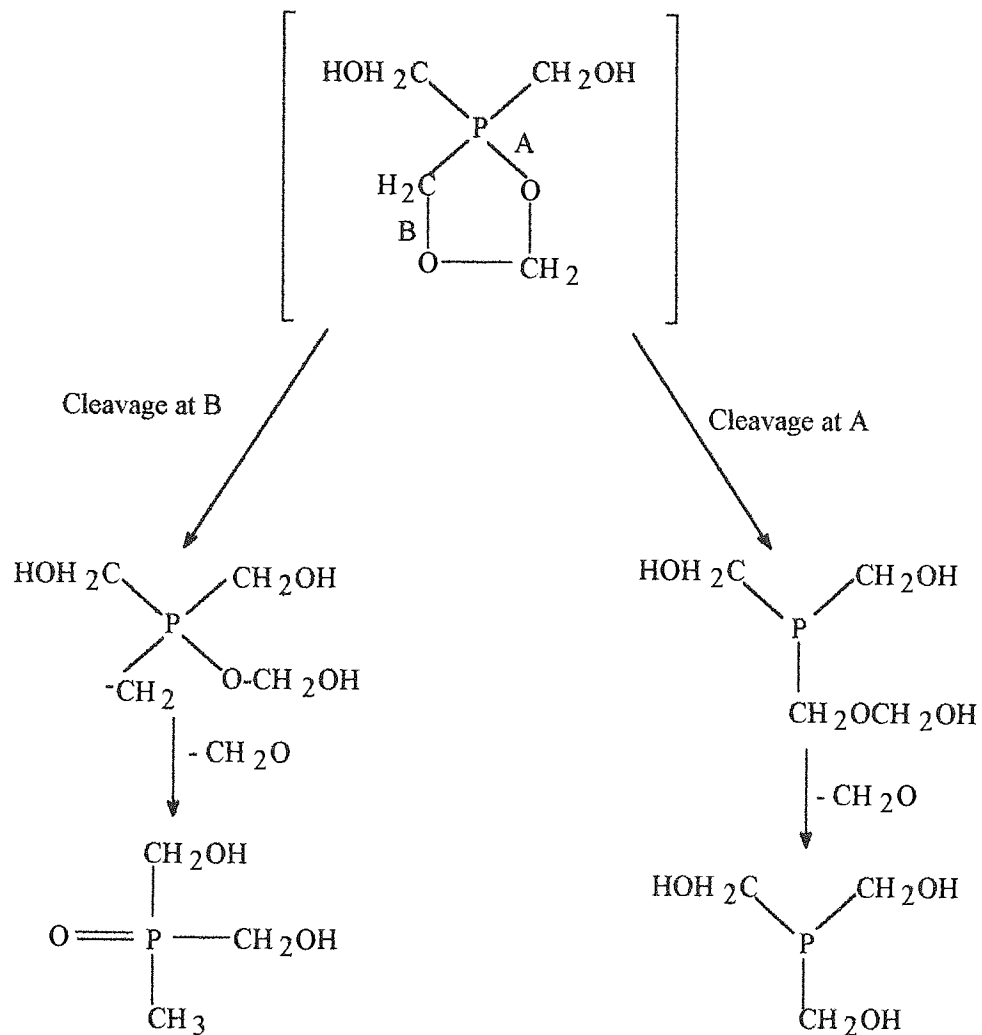


**Fig 4.1.2 - Mechanism for the formation of a methyl phosphine species.**

**Interpretation of  $^{31}\text{P}$  NMR data (Appendix B - Fig B7).**

The four peaks at negative ppm can be directly assigned to the desired product and to hemiacetal impurities.

**Table 4.1.3 - Negative  $^{31}\text{P}$  NMR Data for Phosphine mix.**

Structure	$\delta / \text{ppm} - ^{31}\text{P}$	$\delta / \text{ppm} - ^{31}\text{P}$ Lit <sup>40</sup>
$\text{P}(\text{CH}_2\text{OH})_3$	-25.9	-24.5
$\text{P}(\text{CH}_2\text{OH})_2(\text{CH}_2\text{OCH}_2\text{OH})$	-29.74	-28.9
$\text{P}(\text{CH}_2\text{OH})(\text{CH}_2\text{OCH}_2\text{OH})_2$	-29.92	-33.0
$\text{P}(\text{CH}_2\text{OCH}_2\text{OH})_3$	-37.76	-37.5

The peaks at 29 ppm and 50 ppm must therefore be explained in terms of the four co-ordinate species for which there is evidence in the  $^{13}\text{C}$  spectrum. Although there are only two four co-ordinate species suspected, both contain two  $\text{CH}_2\text{OH}$  ligands which could in turn exist as hemiacetals, therefore there could be up to six different four co-ordinate species with distinct phosphorus environments. Direct assignments cannot be made for these peaks but it is reasonable to attribute them to four co-ordinate species in general.

### **Interpretation of $^1\text{H}$ NMR data (Appendix B - Fig B6)**

The four co-ordinate phosphine oxide species requires an absorbance for three methyl protons split into a doublet. This is clearly seen at  $\delta = 1.3$  ppm,  $J = 12.9$  Hz and agrees well with literature data e.g.  $(\text{CH}_3)_2(\text{OH})\text{P}=\text{O}$ ,  $\delta \sim 1.5$ ,  $J = 15$  Hz.<sup>85</sup> The protons in the hydroxymethyl ligand for the desired product  $\text{P}(\text{CH}_2\text{OH})_3$  are probably represented by the large doublet at  $\delta = 3.8$  ppm,  $J = 5.6$  Hz. The R.I values suggest a  $\text{P}(\text{CH}_2\text{OH})_3:\text{P}(\text{CH}_2\text{OH})_2(\text{CH}_3)(\text{O})$  ratio of 14:1. The four doublets at  $\delta = 3.8, 3.7, 3.7$  and  $3.7$  ppm are probably due to  $\text{CH}_2\text{OH}$  ligands in hemiacetal contaminated phosphines but a more accurate assignment cannot be made. Protons within hemiacetal ligands will show resonances within the same region or slightly down field but due to low concentrations these peaks cannot be seen with any certainty - some very small resonances which could be doublets can be seen between 3.8 and 4.8 ppm and these could be due to these protons.

### **Summary**

The NMR data shows the crude product mix to be substantially more complex than suggested in the product-information literature. This is due to inefficient formaldehyde removal and non-recrystallisation. The product as used is mainly the desired product but with hemiacetal and four co-ordinate phosphine impurities.

### **4.2 - Synthesis No 6 - Trisodium salt of tri(*m* - sulfophenyl)phosphine (TPPTS)<sup>41,42</sup>**

The trisodium salt of tri(*m* - sulfophenyl)phosphine (TPPTS) is a very highly water-soluble phosphine which finds industrial use in the hydroformylation of propene when combined with rhodium<sup>43</sup>. A number of ruthenium-TPPTS complexes have been described in the literature<sup>44</sup> and their use as catalysts for the hydrogenation of propionaldehyde investigated.<sup>45</sup>

Initial attempts to synthesise this ligand were based on the French Patent<sup>41</sup> of Emile Kuntz without the work-up with butyl phosphate. These attempts were largely unsuccessful for reasons which will be discussed at the end of this section. Later attempts were based on an improved work-up procedure published by Bartik, Bartik, Hanson, Glass and Bebout<sup>42</sup>. This procedure will be described.

Triphenylphosphine (10g, 0.038 moles) was slowly added to fuming sulphuric acid (100 ml) in a round bottomed flask which was maintained at 0°C on an ice bath. The mixture was slowly allowed to reach room temperature and left stirring at room temperature for approximately 170 hours (one week). In the literature it is suggested that the reaction is best monitored by NMR spectroscopy, however this option was not available so trust was placed in the recommended time scale for complete reaction of 150 hours. After this time the reaction mixture was carefully neutralised at 0°C with 20% aqueous NaOH. The volume was reduced to 200 ml by distillation producing an amount of white precipitate. This was removed by filtration and refluxed in methanol (1 L) for approximately 1 hour. The mixture was filtered whilst hot and the white solid further extracted with boiling methanol (500 ml) and again filtered hot. The combined methanol portions were reduced to 200 ml in volume and acetone (800 ml) added to precipitate the sulphonated products. Yield = 1.95g  $\equiv$  9% (based on triphenylphosphine). The literature suggests that this product is 75%-85% TPPTS and 25%-15% TPPTS oxide and recommends a purification process involving a twice repeated extraction with 300 ml of an acetone/methanol/water (10:5:1) and reprecipitation in order to reduce the oxide content to <5%. However due to the small amount of product initially retrieved this procedure was thought unwise.

#### Product analysis by NMR.

<sup>31</sup>P, <sup>1</sup>H and <sup>13</sup>C NMR spectra were recorded (Appendix B - Fig B8 to B10) and compared to data published in the literature<sup>42</sup>. Data from <sup>13</sup>C and <sup>31</sup>P NMR spectra are in table 4.2.1.

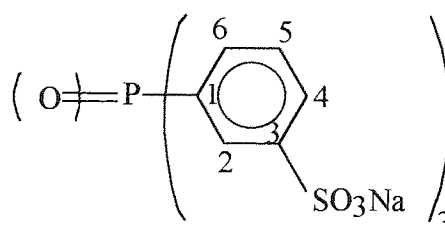


**Fig 4.2.1- Carbon number assignments for <sup>13</sup>C NMR data.**

**Table 4.2.1 -  $^{31}\text{P}$  and  $^{13}\text{C}$  NMR data for TPPTS, TPPTS-oxide and synthesised product.**

	TPPTS $\delta$ / ppm	TPPTS-oxide $\delta$ / ppm	Product <sup>c</sup> $\delta$ / ppm	Product Assign.
<b><math>^{31}\text{P}</math></b>	$\sim -3.7a$ $-5.1b$	$\sim 30.5a$ $35.2b$	$-4.0$ $27.1$	P in TPPTS P in oxide
<b><math>^{13}\text{C}d</math></b>	129.4 (s)-C4	128.8 (d, J(PC)=12.27)-C5	126.5 (s)	C4 - TPPTS
	132.5 (d, J(PC)=6.13)-C5	130.3 (d, J(PC)=12.97)-C6	128.5 (s)	
	133.1 (d, J(PC)=23.64)-C6	130.6 (d, J(PC)=2.3)-C4	128.7 (s)	
	139.2 (d, J(PC)=16)-C2	135.0 (d, J(PC)=10.66)-C2	129.4 (s)	C4 - oxide
	139.4 (d, J(PC)=8.45)-C1	143.7 (d, J(PC)=12.97)-C1	130.6 (d, J(PC)=25.07)	C6 - TPPTS
	145.8 (d, J(PC)=10.6)-C3	143.8 (d, J(PC)=12.97)-C3	(-) 131.3 (s)	
			131.8 (d, J(PC)=10.9)	C2 -oxide
			(-) 132.7 (s)	
			133.5 (d, J(PC)=16.35)	C2 - TPPTS
			(-) 136.0	C1 - oxide
			(d, J(PC)=11.99)	
			(-) 148.1	C1 - TPPTS
			(d, J(PC)=7.63)	
			(-) 148.3 (s)	

a) Spectra recorded at 81 MHz in methanol- $d_4$ :THF- $d_8$ : $\text{D}_2\text{O}$  5:3:2 solvent.

b) Spectra recorded at 81 MHz in  $\text{D}_2\text{O}$ .

c)  $^{13}\text{C}$  spectra acquired with pendant pulse sequence with C &  $\text{CH}_2$  negative and CH &  $\text{CH}_3$  positive. Negative peaks denoted (-) in table.

d) Literature  $^{13}\text{C}$  spectra recorded at 100.6 MHz in  $\text{D}_2\text{O}$ .



### Interpretation of NMR data.

Both the  $^{13}\text{C}$  and  $^{31}\text{P}$  spectra show resonances consistent with a mixture of TPPTS and TPPTS-oxide, although a complete assignment of  $^{13}\text{C}$  resonances is not possible. The  $^1\text{H}$  spectrum exhibits a complex series of overlapping doublets, triplets and multiplets between 7.1 ppm and 8 ppm (Fig 4.2.2). Although a direct correlation with the literature data is not possible due to solvent differences, the overall pattern of peaks is sufficiently similar to that shown in the literature for a product mix of 76% TPPTS and 24% TPPTS-oxide to be certain that the product isolated from my synthesis is a mix of TPPTS and TPPTS-oxide.

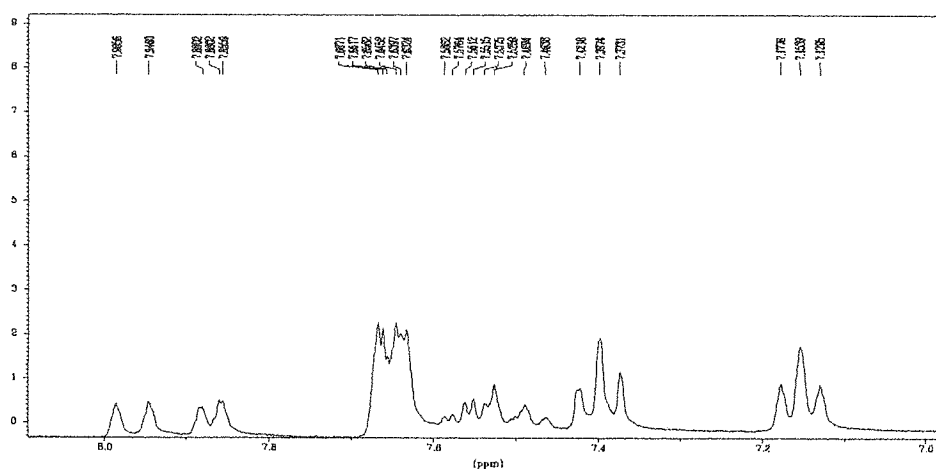


**Fig 4.2.2 - Complex peak region for  $^1\text{H}$  NMR spectrum of TPPTS/TPPTS-oxide mix.**

### Product separation.

Initial attempts at the synthesis of TPPTS relied on the precipitation of the crude product mix from the neutralised reaction solution followed by aqueous extraction of the soluble part. However all the attempts to isolate the product this way failed, probably due the required pH levels not being achieved. In an attempt to retrieve the product by alternative means, excess  $\text{BaCl}_2$  was added to the neutralised solution to precipitate all the sulphate groups as barium salts. The white precipitate formed was separated by centrifuge and then subjected to extended (approximately 1 week) soxhlet extraction with water in the hope that even though the barium salt would be insoluble in cold water it may be soluble enough in hot water to be separated by this method from the bulk  $\text{BaSO}_4$ . Soxhlet extraction did yield a quantity of white solid when the solvent was reduced to dryness, but when analysed by NMR this proved to be TPPTS-oxide as evidenced by the NMR spectra ( $\delta(^{31}\text{P})=26.9$  ppm cf  $\delta(^{31}\text{P})=30.5$ ).<sup>42</sup>

## CHAPTER 5

### RUTHENIUM COMPLEXES AND THEIR SYNTHESSES.

#### 5.1- The Element<sup>46, 30</sup>

In 1826 Gottfried Wilhelm Osann with the help of Berzelius examined a sample of the residue produced by the treatment of crude platinum from the Urals with aqua regia and announced the discovery of three new elements which he called Pluranium, Ruthenium and Polonium although Berzelius himself did not accept these findings and refused to be associated with the announcement. It was not until 1844 when the work was taken up by Karl Karlovitch Klaus that the discovery of Ruthenium was accepted and this time by Berzelius also. Klaus isolated the metal by taking the insoluble residues from the aqua regia treatment of platinum concentrates and ignited them with a potassium nitrate - potash mixture in a silver crucible. The melt was dissolved in water and then distilled with aqua regia which removed osmium as the tetroxide. On mixing the residue with ammonium chloride and heating the resulting ammonium hexachlororuthenate(IV) in an inert atmosphere the metal was isolated.

The metal is present in the earth's crust in very small amounts ( $\approx 4 \times 10^{-4}$  ppm), the major deposits being within nickel-copper sulphide ores in South Africa, Sudbury (Canada) and within the river sands of the Ural mountains in Russia.

**Table 5.1.1- Some physical properties of Ruthenium.**

<b>Atomic Number</b>	44	<b>Density / gcm<sup>-3</sup> (20°)</b>	12.41
<b>Atomic Weight</b>	101.07 ± 0.03	<b>Electron Config.</b>	[Kr] 4d <sup>7</sup> 5s <sup>1</sup>
<b>M.P / °C</b>	2282 (±20)	<b>Electronegativity</b>	2.2
<b>B.P / °C</b>	extrap. 4050 (± 100)		

#### 5.2 - The Complex Chemistry of Ruthenium.

Ruthenium exhibits complex formation in oxidation states (VIII) to (0) inclusive. However the greatest diversity of complexes is for Ru(III) which exists in a stable low spin d<sup>5</sup> electron configuration with one unpaired electron. The higher oxidation states (VIII) to (IV) are found in association with small electronegative ligands which are capable of forming short strong bonds, such as fluoride and oxide. In the case of the

oxide ligand this may be associated with its strong  $\Pi$ -donor properties. Conversely, efficient  $\Pi$ -acceptor ligands such as cyanide carbon monoxide and phosphines can stabilise the lower oxidation states, Ru(II), (I) & (0). Ligands which are good  $\sigma$ -donors but have no marked  $\Pi$ -donor or  $\Pi$ -acceptor properties, such as water, ammonia and ethylenediamine are often associated with the most common oxidation state Ru(II). The great majority of ruthenium complexes are six co-ordinate with an octahedral or approximately octahedral stereochemistry around the metal atom.

A comprehensive review of the myriad complexes formed by ruthenium would require a separate volume for itself. See for example the books written by W. P. Griffith<sup>46</sup> and E. A. & K. R. Seddon<sup>30</sup> for a more complete review. The following sections serve to give a brief glimpse of some of the more relevant ruthenium complexes and their properties in order of metal oxidation state.

### Ru(VIII)

The only established Ru(VIII) compound is the tetrahedral  $\text{RuO}_4$  (volatile and extremely toxic) which is a powerful oxidising agent and has been effectively employed as an oxidant in organic chemistry i.e. in the oxidation of alkenes to carbonyls.

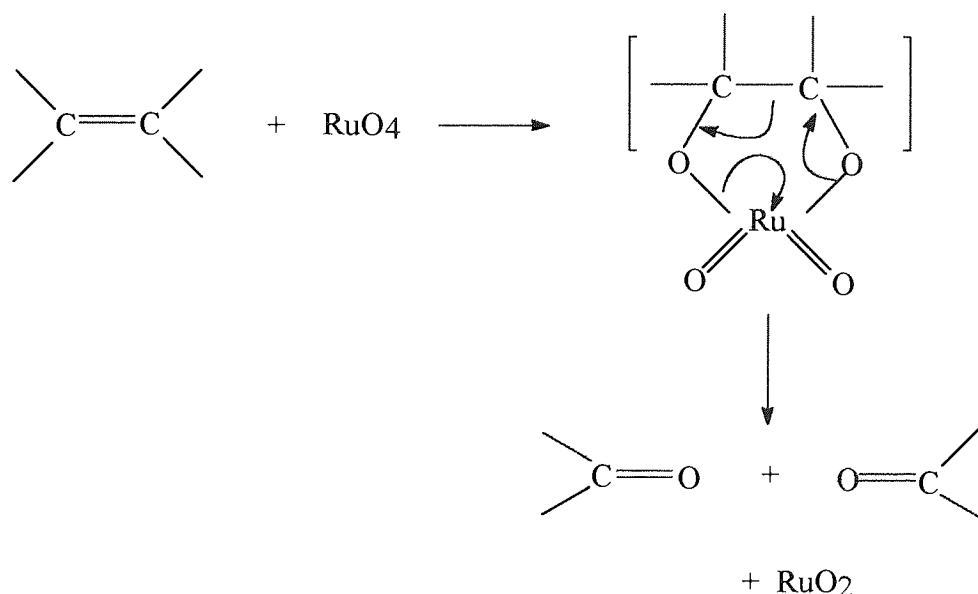


**Fig 5.2.1 - Alkene oxidation by  $\text{RuO}_4$ .**

## Ru(VII)

This oxidation state of ruthenium is represented exclusively by  $\text{K}[\text{RuO}_4]$  which is prepared either by passing chlorine into an aqueous solution of potassium ruthenate(VI) ( $\text{K}_2[\text{RuO}_4]$ ) or by fusing ruthenium with potassium nitrate and potassium hydroxide. In aqueous solution, the black complex is unstable and decomposes to  $\text{K}_2[\text{RuO}_4]$ .

## Ru(VI)

Complexes with this oxidation state are more numerous than is the case for the two higher states. The only single-ligand halide in this oxidation state is the hexafluoride,  $\text{RuF}_6$ , which can be made by direct fluorination of the metal to produce the product as black crystals. However, mixed ligand halides are known such as the oxotetrafluoride,  $\text{RuOF}_4$ , which can be made by the action of a mixture of bromine trifluoride and bromine on the metal and the dioxotetrachloride salts,  $\text{Rb}_2[\text{RuO}_2\text{Cl}_4]$  and  $\text{Cs}_2[\text{RuO}_2\text{Cl}_4]$ . The dioxo-species are thought to be analogous to osmium dioxo-species and hence the oxo- groups are postulated to be in a trans position relative to each other. Treatment of  $[\text{RuO}_2\text{X}_4]^{2-}$  in aqueous  $\text{HX}$  ( $\text{X}=\text{Cl}, \text{Br}$ ) at  $0^\circ\text{C}$  followed by addition of  $\text{CsX}$  forms the nitride complex  $\text{Cs}_2[\text{RuNX}_5]$ . The  $[\text{AsPh}_4]^+$  and  $[\text{NBu}_4]^+$  salts can be similarly formed.

Of the other  $\text{Ru(VI)}$  complexes, the most interesting is probably potassium ruthenate(VI),  $\text{K}_2[\text{RuO}_4]$ . This is made by the fusion of the metal with potassium nitrate and potassium hydroxide producing black green crystals with a metallic lustre which are however orange in aqueous solution and readily disproportionate to perruthenate and ruthenium dioxide (See below)

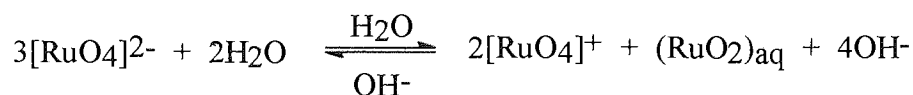


**Fig 5.2.2 - The disproportionation of ruthenate(VI) in aqueous solution.**

## Ru(V)

Complexes in this oxidation state are represented almost exclusively by fluoride complexes.  $[\text{RuF}_5]_4$  is made by the reaction between the metal and bromine trifluoride which gives  $\text{RuBrF}_8$  which is decomposed *in vacuo* to give the pentafluoride, or by direct fluorination of the metal. The structure of the dark green crystals has been

determined by X-ray methods and the molecule is seen to be tetrameric with the four ruthenium atoms at the corners of a rhombus and a bridging fluorine atom between each pair of metal atoms.

A further example of the domination of this oxidation state by the fluorides is  $\text{K}[\text{RuF}_6]$  which can be made by the action of bromine trifluoride and bromine on ruthenium tetrabromide in the presence of potassium bromide; the colour of the product varying from blue to pink depending on the exact conditions of preparation. The Li, Na, Rb, Cs, Ca, Sr, Ba, Ag and Th salts are also known. Other fluoride complexes of ruthenium in this oxidation state include various addition compounds such as  $\text{SeF}_4 \cdot \text{RuF}_5$  and xenon compounds such as  $[\text{XeF}][\text{RuF}_6]$ .

The only exceptions to the monopoly of fluorine in this oxidation state are a few oxide and oxy complexes such as  $\text{Ru}_2\text{O}_5$  and  $\text{Ru}_4\text{O}_9$ .

### Ru(IV)

Ru (IV) halides are represented by  $\text{RuF}_4$  and  $\text{RuCl}_4$  ( although the chloride only exists in the vapour phase at  $>750^\circ\text{C}$ ). Attempts to synthesise the bromide and iodide result in the formation of the trihalides. However, the hexahaloruthenates,  $[\text{RuX}_6]^{2-}$ , are known for fluorine, chlorine and bromine.  $\text{K}_2[\text{RuCl}_6]$  can be made by passing chlorine through a solution of  $\text{K}_2[\text{RuCl}_5(\text{H}_2\text{O})]$  or by fusing potassium chlorate with ruthenium metal. Rubidium, caesium and ammonium salts have also been made for the hexachloride and hexabromide.

A number of Ru(IV) complexes with oxygen ligands are known. Ruthenium dioxide,  $\text{RuO}_2$ , can be made by heating the metal or the trichloride in a stream of oxygen at  $1000^\circ\text{C}$  or by reduction of ruthenium (VI) complexes and is stable in cold acid but is reduced to the metal when heated with hydrogen or carbon monoxide. Mixed ligand oxo-halo complexes are well known such as  $\text{Ru}_2\text{OCl}_6$  and  $\text{K}_4[\text{Ru}_2\text{OCl}_{10}] \cdot \text{H}_2\text{O}$ . The latter complex has a linear Ru-O-Ru backbone with short Ru-O bonds i.e. with a high degree of  $\Pi$ -bond character, which is rationalised by considering the complex to exist as  $[\text{Cl}_5\text{Ru}=\text{O}=\text{RuCl}_5]^{4-}$ . Another type of Ru(IV)-oxygen compound is the metal ruthenium trioxides e.g.  $\text{CaRuO}_3$  which exist in a number of different multi-layer structures.

One of the more curious complexes of ruthenium is the descriptively named "ruthenium red". This intensely red species can be made in a number of ways, the commonest being

the aerial oxidation of  $[\text{Ru}(\text{NH}_3)_6]\text{Cl}_3$ . The complex has been isolated and analysed as  $[\text{Ru}_3\text{O}_2(\text{NH}_3)_{14}]\text{Cl}_6 \cdot 4\text{H}_2\text{O}$  and its structure is thought to be a trimer with a linear Ru-O-Ru system. (Fig 5.2.3).

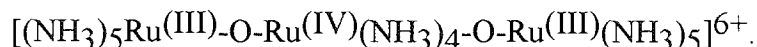


**Fig 5.2.3 - Proposed structure of Ruthenium Red.**

Aerial oxidation in hydrochloric acid solution, or oxidation by nitric acid or cerium(IV) in sulfuric acid creates a further mixed oxidation state complex known as "ruthenium brown" which analyses as  $[\text{Ru}_3\text{O}_2(\text{NH}_3)_{14}][\text{NO}_3]7 \cdot 5\text{H}_2\text{O}$  (for the nitric acid oxidation). The proposed structure (Fig 5.2.4) shows an inversion of the mixed oxidation states from (III)-(IV)-(III) to (IV)-(III)-(IV).



**Fig 5.2.4 - Proposed structure for Ruthenium Brown.**

### Ru(III)

As mentioned earlier, this oxidation state is by far the most "popular" oxidation state for ruthenium.

Probably the most important ruthenium complex from the synthetic point of view is the trichloride,  $\text{RuCl}_3$ , the commonest complex of ruthenium and the starting point for all the ruthenium complex syntheses within this thesis. It exists in both water soluble and insoluble forms. The soluble form is obtained from the prolonged action of HCl on ruthenium tetroxide and is usually characterised (wrongly) as the trihydrate,  $\text{RuCl}_3 \cdot 3\text{H}_2\text{O}$ . However, commercial ruthenium trichloride contains a mixture of polynuclear ruthenium(IV) oxy and hydroxy chloro species. "Activation" of ruthenium trichloride is achieved by refluxing the commercial source in HCl to produce the  $\text{Ru}^{3+}$  species in solution. The trifluoride and triiodide are also known. Other halo species are known such as  $[\text{RuCl}_6]^{3+}$ ,  $[\text{RuCl}_5]^{2+}$  and  $[\text{RuCl}_7]^{4+}$  which commonly exist as their potassium salts.

Ru(III) halo complexes also exist in mixed ligand form. The aquapentahaloruthenates(III),  $\text{A}_2[\text{RuCl}_5(\text{H}_2\text{O})]$  (A=K, Rb, Cs or  $\text{NH}_4$ ), are prepared by heating solutions of  $[\text{RuO}_4]$  or  $\text{K}_4[\text{Ru}_2\text{OCl}_{10}]$  in hydrochloric acid in the presence of

ethanol and the requisite cation, and oxidation of this anion in HCl/HClO<sub>4</sub> solutions produces products believed to be dimeric oxo-bridged ruthenium(IV) species (See earlier). The di-, tri-, tetra- and penta- aquahaloruthenates(III) are also known. The aquahaloruthenate(III) anions exhibit catalytic activity in the oxidation of some alkynes (Fig 5.2.5), the catalytic activity depending on the combined concentrations of [RuCl<sub>4</sub>(H<sub>2</sub>O)<sub>2</sub>]<sup>-</sup> and [RuCl<sub>5</sub>(H<sub>2</sub>O)]<sup>2-</sup>.

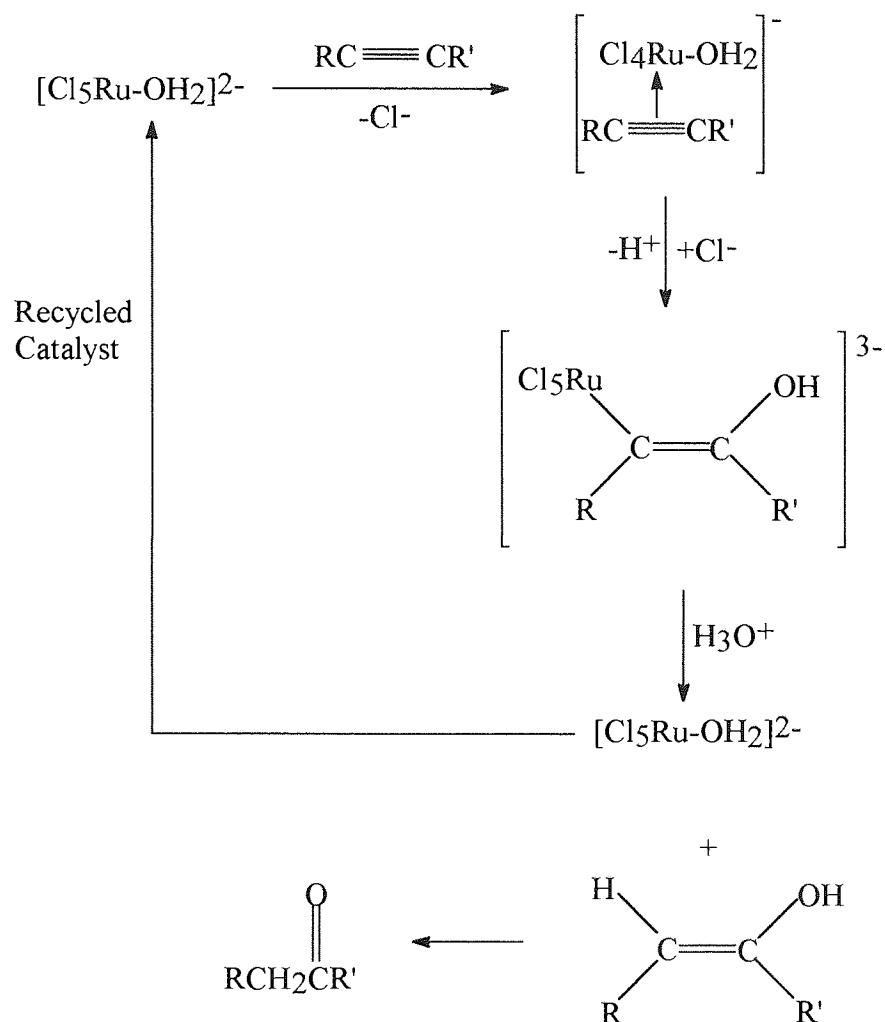


**Fig 5.2.5 - Alkyne oxidation by aquapentachlororuthenate(III).**

Ruthenium(III) ammines constitute a large and interesting group of ruthenium complexes. The hexammine salts, [Ru(NH<sub>3</sub>)<sub>6</sub>]<sup>3+</sup>, are most easily prepared by the treatment of hexammine ruthenium(II) with chlorine. Most of the salts are very stable, even in the presence of acids and are synthetically useful as starting materials. Alkaline solutions of [Ru(NH<sub>3</sub>)<sub>6</sub>]<sup>3+</sup> however are readily oxidised by oxygen to give "ruthenium red" (see earlier). Of the many known substituted ruthenium(III) ammines the most

important are the halo- and aquo-pentammines.  $[\text{Ru}(\text{NH}_3)_5\text{Cl}]\text{Cl}_2$  can be made by the prolonged action of chlorine on  $[\text{Ru}(\text{NH}_3)_6]\text{Cl}_2$  or from  $[\text{Ru}(\text{NH}_3)_6]\text{Cl}_3$  and hydrochloric acid. The chloro- ligand is easily substituted by a number of groups i.e.  $\text{H}_2\text{O}$ ,  $-\text{N}_3^-$ ,  $-\text{SCN}^-$ ,  $-\text{OH}^-$ , to produce an array of different ruthenium(III)pentaammines. The aquo complex  $[\text{Ru}(\text{NH}_3)_5(\text{H}_2\text{O})]^{3+}$  can be produced by both acid and base hydrolysis; base hydrolysis being much the faster. The di- and tri-haloruthenium(III)ammines are also known. Ru(III) forms many other complexes with nitrogen ligands for example Ru(III) pyridine complexes which all have a pyridine:metal ratio of less than 4:1 e.g.  $\text{Rupy}_3\text{Cl}_3$ . A wide range of complexes with the chelate ligand 2,2'-bipyridyl (bipy) are known such as  $[\text{Ru}(\text{bipy})_3][\text{PF}_6].n\text{H}_2\text{O}$  as well as mixed ligand complexes such as  $[\text{Rupy}_2(\text{bipy})(\text{ox})]\text{Cl}$  (ox = oxalate) and similarly the chelate ligand ethylenediamine (en) also forms Ru(III) complexes e.g. *cis*- $[\text{Ru}(\text{en})_2\text{X}_2]^+$  (X=Cl, Br, I).

A large number of Ru(III) phosphine and arsine complexes exist ranging from simple two ligand systems i.e.  $\text{RuX}_3\text{L}_2$  (X=Cl, Br, I; L= phosphine or arsine ligands), to more complex mixed adducts i.e.  $\text{RuX}_3\text{L}_2\text{L}'$  (X=Cl, Br; L= $\text{PPh}_3$ ,  $\text{AsPh}_3$ ; L'= oxygen ligands - THF, sulphur ligands -  $\text{SMe}_2$ ). Ru(III) also maintains its willingness to form complexes with nitrogen ligands within such mixed adducts e.g.  $[\text{RuCl}_3(\text{AsPh}_3)(\text{bipy})]$ . Phosphine and arsine complexes can also be anionic e.g.  $[\text{AsPh}_4][\text{RuCl}_4(\text{PMe}_2\text{Ph})_2]$  or cationic e.g.  $[\text{Ru}(\text{diars})_2\text{Cl}_2]\text{Cl}$  (diars=1,2-bis(dimethylarsino)benzene).

Similarly to Ru(IV), Ru(III) also forms mixed oxidation state complexes. When a concentrated ethanolic solution of commercial  $\text{RuCl}_3 \cdot 3\text{H}_2\text{O}$  and tributylphosphine (mole ratio 1:2.2) is allowed to stand at  $20^\circ\text{C}$  under nitrogen for three days, dark red crystals of  $[\{\text{RuCl}_3(\text{PBu}_3)_2\}_2]$  are formed. These are filtered in air and the mother liquor left to stand for a further 24 hours after which time dark red crystals of the mixed oxidation state complex  $[\text{Ru}_2\text{Cl}_5(\text{PBu}_3)_4]$  are deposited. The complex structure contains three bridging chlorine atoms.

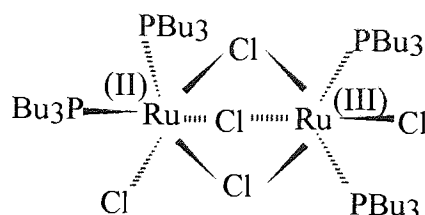


**Fig 5.2.6 - Mixed oxidation state complex -  $[\text{Ru}_2\text{Cl}_5(\text{PBu}_3)_4]$**



## Ru(II)

Some of the more interesting Ru(II) complexes are the ruthenium-carbenes (the importance of carbene complexes to the metathesis reaction is discussed in Section 1.2). Ruthenium-carbene chemistry is relatively new and the synthesis of such complexes is achieved via a variety of precursors. One route is via electron rich alkenes which cleave to generate carbenes.

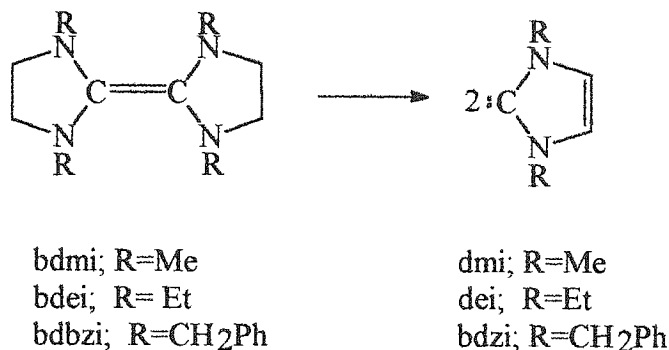


Fig 5.2.7 - Alkene cleavage to produce carbenes.

Reaction of any of the above precursors with [Ru(PPh<sub>3</sub>)<sub>3</sub>Cl<sub>2</sub>] will produce a ruthenium-carbene.

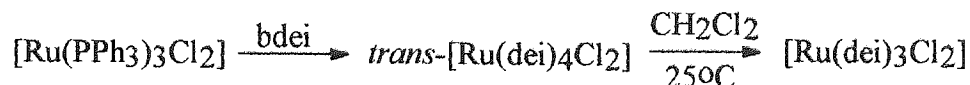


Fig 5.2.8 - A synthetic route to a ruthenium-carbene complex.

As well as Grubbs *et al*<sup>15</sup> who have produced ruthenium carbenes which show ring-opening metathetical activity (section 1.3.1), Demonceau, Noels, Saive and Hubert<sup>47</sup> have produced similar complexes using alkyl diazoesters as carbene precursors and reacting them with various ruthenium complexes to form *in situ* ruthenium-carbenes for the polymerisation of cyclic olefins.

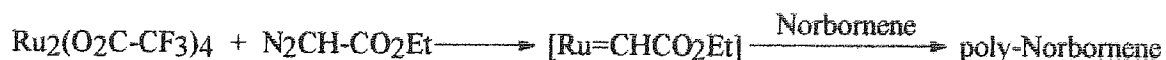


Fig 5.2.9- ROMP using a diazoester initiated ruthenium complex.

Ru(II) ammines can be made by the action of zinc dust with ammonia and ammonium chloride on ruthenium trichloride solution. The resulting  $[\text{Ru}(\text{NH}_3)_6]\text{Cl}_2$  is very sensitive to aerial oxidation.  $[\text{Ru}(\text{NH}_3)_5]^{2+}$  or  $[\text{Ru}(\text{NH}_3)_5(\text{H}_2\text{O})]^{2+}$  can be formed by reduction of Ru(III) pentammine species with chromous ion. The pentammine derivative  $[\text{Ru}(\text{NH}_3)_5\text{N}_2]^{2+}$  prepared from the reduction of aqueous  $\text{RuCl}_3$  with  $\text{N}_2\text{H}_4$  was the first dinitrogen complex of a transition metal to be produced. The dinuclear derivative  $[(\text{NH}_3)_5\text{Ru}-\text{N}-\text{N}-\text{Ru}(\text{NH}_3)_5]^{4+}$  is also known.

One of the most important groups of Ru(II) complexes are the ruthenium(II)nitrosyls and ruthenium forms more nitrosyl complexes than any other element. The nitrosyl complex  $[\text{Ru}(\text{NH}_3)_5\text{NO}]^{3+}$  obtained by the action of  $\text{HNO}_2$  on  $[\text{Ru}(\text{NH}_3)_6]^{2+}$  is typical of all the Ru(II) nitrosyls. The NO group in these species is extraordinarily stable and the Ru-NO bond is difficult to break by any normal chemical substitution or oxidation-reduction methods. The ligand also exerts a strong trans effect, labilising the opposite ligand to substitution. The nitrosyl halides  $[\text{Ru}(\text{NO})\text{X}_3]_n(\text{aq})$  are all hydrated to some degree and the pentahalide potassium salts,  $\text{K}_2[\text{Ru}(\text{NO})\text{X}_5]$  can be made from the trihalide and the appropriate potassium halides. One example of a Ru(II) nitrosyl complex exhibiting catalytic properties is  $[\text{Ru}(\text{salen})(\text{NO})(\text{H}_2\text{O})]\text{SbF}_6$  (salen = N,N'-bis(salicylidene)ethylenediamine dianion) which is an effective catalyst for the Diels-Alder reaction<sup>48</sup>. Other Ru(II) nitrosyls are too numerous to mention but all are mixed ligand complexes.

A range of carbonyl halides can be made either by the action of carbon monoxide at 200°C on the trihalide or by refluxing the trihalide with a 1:1 v/v mixture of formic acid and hydrochloric acid. The product obtained depends on the time of reflux and method of product isolation as shown below for the chloride (see Fig 5.2.10).<sup>54</sup> The carbonyls also form mixed ligand complexes with phosphines of the type  $\text{RuX}_2(\text{CO})_2(\text{PR}_3)_2$ .

In a similar fashion to Ru(III), Ru(II) forms a large range of phosphine, arsine and stibine complexes, the main types being of the form  $\text{RuX}_2(\text{LR}_3)_4$  (X=Cl, Br ; L=P, As),  $\text{RuX}_2(\text{LR}_3)_3$  (X=Cl, Br ; L=P, Sb) and the binuclear species  $[\text{Ru}_2\text{Cl}_3(\text{PR}_3)_6]\text{Cl}$ .  $\text{RuCl}_2(\text{PPh}_3)_3$  is prepared by the action of excess triphenylphosphine on ruthenium trichloride and exists in a distorted octahedral shape with a proton from one of the phenyl groups occupying the space left by the vacant co-ordination site. A wide range of nitrosyl phosphine complexes also exist with the general form  $\text{Ru}(\text{NO})\text{Cl}_3\text{L}_2$  (L=phosphines, arsines or stibines).

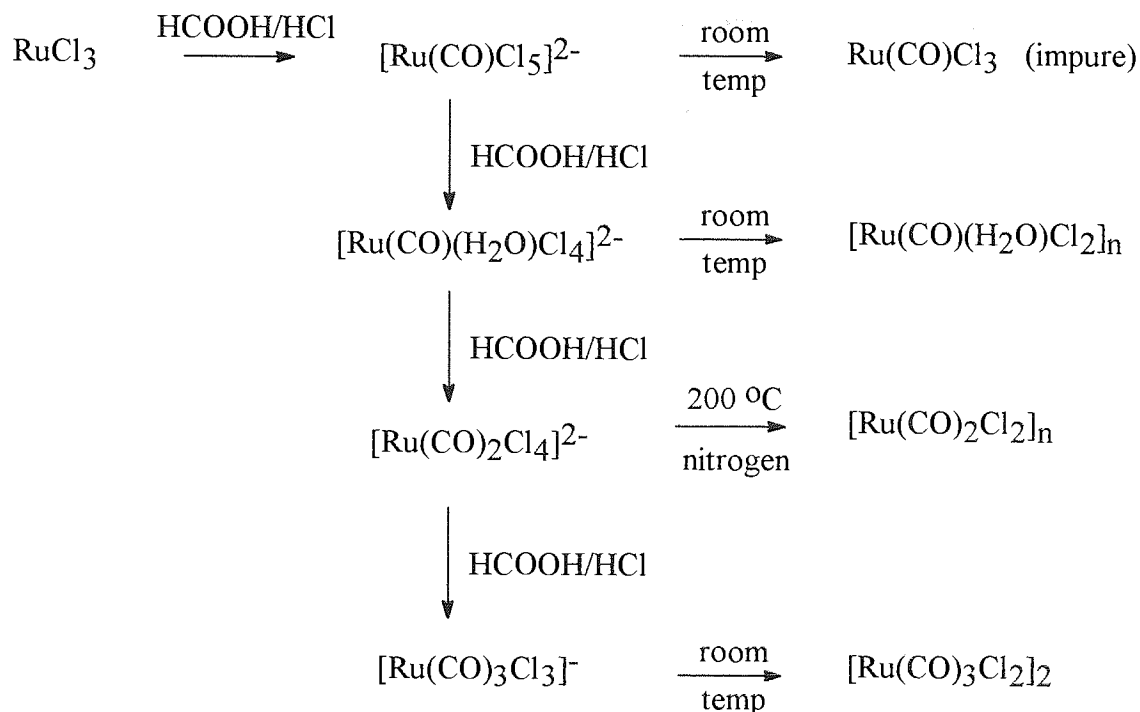


**Fig 5.2.10 - Chlorocarbonyl Ruthenium complex formation.**

As would be expected Ru(II) also forms cyanide complexes.  $\text{K}_4[\text{Ru}(\text{CN})_6]$  can be made by the action of potassium cyanide on potassium ruthenate or by the treatment of a boiling solution of  $\text{RuCl}_3$  with an excess of potassium cyanide. The sodium, copper and silver salts are also known as is the anhydrous free acid  $\text{H}_4[\text{Ru}(\text{CN})_6]$  which is prepared by addition of hydrochloric acid and ether to the potassium salt.  $\text{K}_2[\text{Ru}(\text{NO})(\text{CN})_5]$  is the only fully established nitrosyl cyanide complex of the platinum metals. In this case the nitrosyl ligand is deemed to be  $(\text{NO})^+$ .

One other Ru(II) complex of note is the sandwich ruthenocene complex,  $\text{RuCp}_2$  ( $\text{Cp}=\text{C}_5\text{H}_5$ ), which is directly analogous to ferrocene.

### Ru(I) and (0)

Complexes of ruthenium in its two lowest oxidation states are very few in number.  $[\text{Ru}^{\text{(I)}}(\text{NO})\text{X}_2]_n$  ( $\text{X}=\text{Br}, \text{I}$ ) can be made by the action of nitric acid at  $230\text{ }^\circ\text{C}$  on  $[\text{RuX}_2(\text{CO})_2]_n$  and the iodo complex reacts with ligands such as pyridine to give  $[\text{Ru}(\text{NO})\text{I}_2\text{py}_2]_2$ . As before, in these complexes the nitrosyl ligand is deemed to be  $(\text{NO})^+$ .  $[\text{Ru}(\text{CO})\text{Br}]_n$  is made from the tribromide and carbon monoxide at  $180^\circ\text{C}$  and 350 atmospheres pressure.

The most common complexes of Ru(O) are carbonyl cluster complexes such as Ru(CO)<sub>5</sub> and Ru<sub>3</sub>(CO)<sub>12</sub>. Ru<sub>3</sub>(CO)<sub>12</sub> will react with dienes (such as C<sub>6</sub>H<sub>9</sub>) to give [Ru(CO)<sub>3</sub>(diene)], trienes (such as C<sub>7</sub>H<sub>8</sub>) to give [Ru(CO)<sub>3</sub>(triene)] and tetraenes (such as C<sub>8</sub>H<sub>8</sub>) to give [Ru(CO)<sub>3</sub>(tetraene)]. This carbonyl is also a precursor to bisarene complexes of the type [Ru(C<sub>6</sub>H<sub>6</sub>)<sub>2</sub>]

Mixed ligand carbonyl phosphine complexes can be synthesised either by the reduction of RuCl<sub>2</sub>(CO)<sub>2</sub>(PPh<sub>3</sub>)<sub>2</sub> with zinc in DMF under 4 atmospheres pressure of carbon monoxide to give Ru(CO)<sub>3</sub>(PPh<sub>3</sub>)<sub>2</sub> or by reaction of Ru<sub>3</sub>(CO)<sub>12</sub> with triphenyl phosphine to give Ru<sub>3</sub>(CO)<sub>9</sub>(PPh<sub>3</sub>)<sub>3</sub>. Ru(O) also forms single ligand phosphine species the most notable being [Ru(PF<sub>3</sub>)<sub>5</sub>] formed from the reaction of Ru<sub>3</sub>(CO)<sub>12</sub> or RuCl<sub>3</sub>.3H<sub>2</sub>O with excess PF<sub>3</sub> at high pressure and temperature.

### 5.3 - Some Kinetic Aspects of Ruthenium Chemistry<sup>49</sup>.

#### 5.3.1- Reduction-Oxidation (Redox) Reactions.

##### Theory.

Redox reactions occur between two reactant molecules and involve the transfer of one or more electrons between the reactants. They can occur via one of two possible mechanisms which are denoted either inner-sphere or outer-sphere mechanisms.

In an inner-sphere mechanism, part of one of the reactants penetrates the inner coordination shell of the other reactant. Bonds are formed between the two reactants to produce a bridge and one or more electrons pass along the bridge from oxidant to reductant. The bridge can be mono- or poly-atomic as long as the two reactants can communicate electronically across the bridge.

In some cases the bridged intermediate is stable enough to be isolated and characterised and ruthenium chemistry provides one such example.

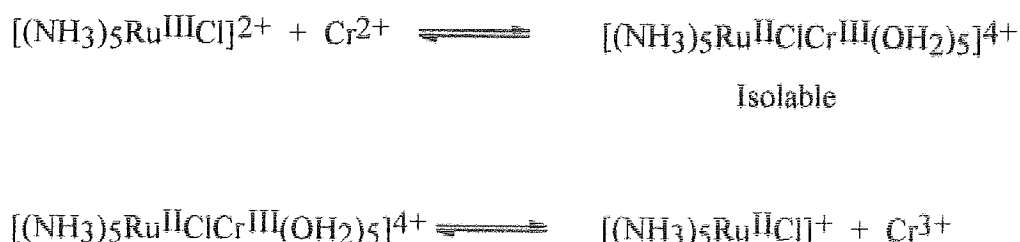


Fig 5.3.1.1 - Bridge formation in an inner-sphere redox reaction.

In this example it is found that the electron has already been transferred from ruthenium to chromium in the isolated intermediate.

In an outer-sphere mechanism, the two reactants approach close enough to each other to allow overlap of their outer co-ordination shells but no actual bonds or bridges are formed between the reactants. The rate of an outer-sphere mechanism is determined by one of three aspects of the reaction.

1/ The two reactants must approach each other so that their outer co-ordination shells can overlap. The energy required to achieve this is determined by such factors as the viscosity of the solution and relative charges of the reactants.

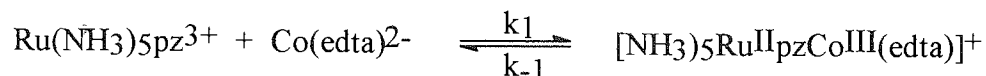
2/ Before electron transfer can occur it may be necessary for either or both of the reactants to rearrange. Since this involves atomic motion, the Frank Condon Principle holds i.e. the more atomic motion required the more slowly the reaction will proceed.

3/ As the two reactants are close but not electronically connected via a bridged intermediate, the electron must traverse a high energy barrier to be transferred. Since the electron does not possess enough classical energy, in order to be transferred the electron must employ quantum mechanical tunnelling i.e. the electron has a finite possibility at any given time of possessing the required amount of energy. The higher the energy barrier, the lower the probability of an electron being able to traverse it. Therefore the probability of more than one electron possessing enough energy to do this is vanishingly small. Subsequently, the outer-sphere mechanism applies only to one-electron processes.

### **Examples.**<sup>49</sup>

Although the large majority of redox reactions involving ruthenium are outer sphere processes (see later) some inner sphere examples exist such as the process producing the bridged intermediate in Fig 5.3.1.1 and interestingly an example of a reaction that proceeds via both inner and outer sphere mechanisms exists within ruthenium chemistry. The reaction pathways of this reaction are summarised in Fig 5.3.1.2.

**Inner sphere** -  $k_1 = 2.5 \times 10^3 \text{ M}^{-1}\text{s}^{-1}$ ,  $k_{-1} = 16.9 \text{ s}^{-1}$



**Outer Sphere** -  $k_2 = 1.0 \times 10^3 \text{ M}^{-1}\text{s}^{-1}$ ,  $k_{-2} = 3.2 \text{ M}^{-1}\text{s}^{-1}$

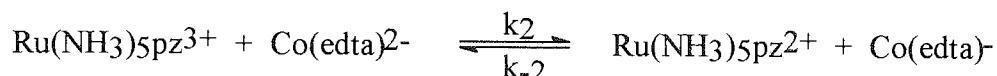


**Fig 5.3.1.2 - Redox process proceeding by either an inner sphere or outer sphere mechanism.**

The outer sphere pathway produces the products directly. This process is identified by a rapid increase in absorbance at 474 nm which is a maximum for  $\text{Ru}(\text{NH}_3)_5\text{pz}^{2+}$ . Simultaneously the binuclear complex is formed by a rapid inner sphere process. This undergoes a back electron transfer to the starting complexes ( $k_{-1}$ ) which then undergo the outer sphere redox process

Apart from a few interesting oddities, some of which have been mentioned above, the relative inertness of  $\text{Ru}^{3+}$  and  $\text{Ru}^{2+}$  to substitution (See 5.3.2) means redox reactions involving ruthenium in these oxidation states are virtually all outer shell processes.

The observed rate for the reaction between the ion pair  $\text{Ru}(\text{H}_2\text{O})_6^{3+/2+}$  is  $20 \text{ M}^{-1}\text{s}^{-1}$  at  $25^\circ\text{C}$  in 2.5 M acid. This is noticeably slower than for the ion pair  $\text{Ru}(\text{NH}_3)_6^{3+/2+}$  ( $3.2 \times 10^3 \text{ M}^{-1}\text{s}^{-1}$  at  $25^\circ\text{C}$ ). In terms of the factors affecting the rate of outer shell processes this can be attributed to the greater degree of reorganisation needed by the hexaquo ion when compared to the hexaammine.

A large amount of experimental data has been published<sup>50, 51</sup> concerning the rate of reduction/oxidation for the electron exchange reactions between various  $\text{Ru}^{3+}/\text{Ru}^{2+}$  amines, some of which is presented in Table 5.3.1.1.

**Table 5.3.1.1 - Rate constants for the electron exchange reaction between various Ru<sup>3+/2+</sup> amines at 25°C.**

	$k / \text{M}^{-1}\text{s}^{-1}$	Mean radius <sup>c</sup> / pm
$\text{Ru}(\text{NH}_3)_6^{3+/2+ a}$	$3.2 \times 10^3$	330
$\text{Ru}(\text{NH}_3)_5(\text{py})^{3+/2+ a}$	$1.1 \times 10^5$	380
$\text{Ru}(\text{NH}_3)_4(\text{bpy})^{3+/2+ a}$	$7.7 \times 10^5$	440
$\text{Ru}(\text{NH}_3)_2(\text{bpy})_2^{3+/2+ b}$	$8.4 \times 10^7$	560
$\text{Ru}(\text{bpy})_3^{3+/2+ b}$	$4.2 \times 10^8$	680

*a/ Data recorded in 0.1M CF<sub>3</sub>SO<sub>3</sub>H. b/ Data recorded in 0.1M HClO<sub>4</sub>. c/ Due to lack of symmetry within the complexes, mean radius was calculated as  $a = 1/2(d_1d_2d_3)^{1/3}$ .*

This data shows a strong correlation between complex size and rate of electron exchange. This can be even more clearly seen when log k is plotted against the reciprocal of the mean distance of closest approach of the ruthenium centres.

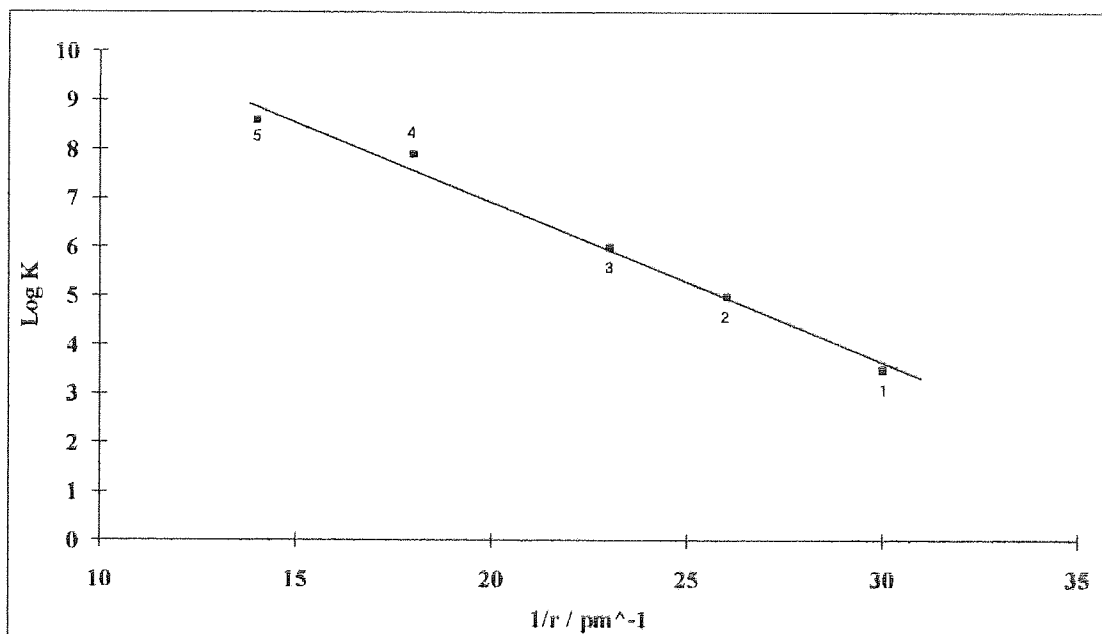


**Fig 5.3.1.3 - Plot of logarithm of the observed exchange rate constant (Log K) vs the reciprocal of the mean distance of closest approach of the ruthenium centres (1/r).**

**1=Ru(NH<sub>3</sub>)<sub>6</sub><sup>3+/2+</sup>; 2=Ru(NH<sub>3</sub>)<sub>5</sub>(py)<sup>3+/2+</sup>; 3=Ru(NH<sub>3</sub>)<sub>4</sub>(bpy)<sup>3+/2+</sup>;  
4=Ru(NH<sub>3</sub>)<sub>2</sub>(bpy)<sub>2</sub><sup>3+/2+</sup>; 5=Ru(bpy)<sub>3</sub><sup>3+/2+</sup>**

These results imply that for these complexes the major contributory factor to the activation energy of reaction and hence the rate constant is the amount of solvent reorganisation required.

### 5.3.2 - Substitution Reactions.

#### Background.

A substitution reaction involves the replacement of a ligand co-ordinated to a metal by a free ligand in solution. The mechanism of substitution can vary between two extremes. If the new ligand enters the co-ordination sphere of the metal and forms a bond with the metal before the leaving ligand has broken its bond (i.e. the metal undergoes an increase in co-ordination number) then the mechanism is said to be associative (A). At the other extreme, if the leaving ligand has broken its bond to the metal and left the co-ordination sphere before the new ligand has entered (i.e. the metal undergoes a decrease in co-ordination number) then the mechanism is said to be dissociative (D). Exactly half way between the two extremes when there is partial and equal association and dissociation of both the entering and leaving groups then the mechanism is said to be an interchange mechanism (I). In practice, most individual reactions will not fall exactly on any of these calibration points, but rather somewhere in-between. Such mechanisms are denoted  $I_a$  or  $I_d$ . A schematic representation of the range of mechanisms is given in Fig 5.3.2.1. (The light circle represents the metal co-ordination sphere, the bold circle on the right represents the entering group and on the left, the leaving group.)

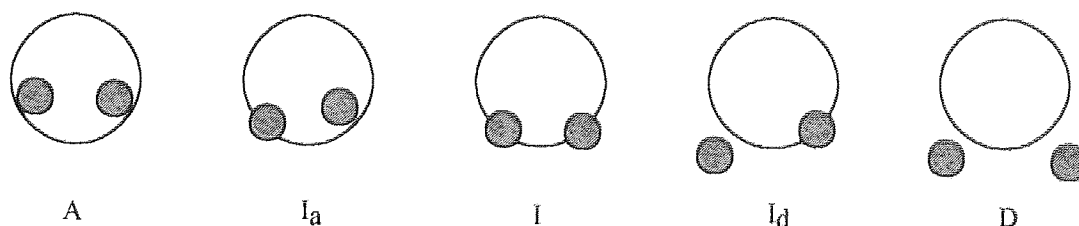


**Fig 5.3.2.1 - Schematic representation of the range of substitution mechanisms.**

One method for determining the nature of a substitution mechanism is by observing the effect of pressure on the rate of reaction. In a dissociative mechanism, as the leaving group leaves the co-ordination shell, the volume of the system increases i.e.  $\Delta V^\ddagger$  is positive (the limit of the increase being the molar volume of the leaving group). Increasing the pressure would work against this volume increase and lead to a decrease in the rate of substitution. For an associative mechanism the inverse would be true and



therefore  $\Delta V^\ddagger$  would be negative and an increase in pressure would increase the rate of substitution. For an interchange mechanism there is no net change in  $\Delta V^\ddagger$  and subsequently a change in pressure will not affect the rate of substitution.

### Examples<sup>49, 52</sup>

The large majority of studies of ruthenium substitution reactions have concerned themselves with Ru(III) and Ru(II). Some aspects of these studies will be discussed.

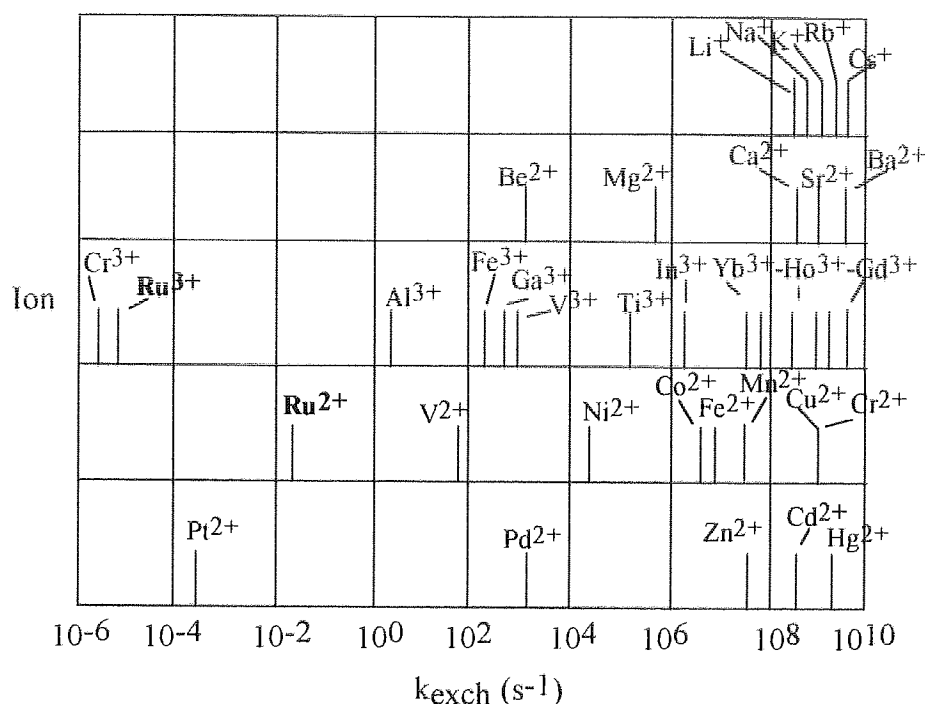


**Fig 5.3.2.2 - Rate Constants ( $\text{s}^{-1}$ ) for water exchange of metal cations.<sup>49</sup>**

The relative substitution rates of the transition metals can be clearly seen from the above diagram and the slow nature of Ru(III) and Ru(II) substitution is evident from even a cursory glance. The most overriding reason for this is the very stable electron configurations of octahedral Ru(III) and Ru(II) complexes. Ru(III) has a low spin  $d^5$  configuration and Ru(II) low spin  $d^6$ , both of which confer a great deal of CFSE (Crystal Field Stabilisation Energy). Although ground state electron configuration is not the only factor governing relative substitution rates, a high CFSE means that Ru(III) and Ru(II) start out from an initial position of stability before other factors are considered.

There is evidence for differing substitution mechanisms between Ru(III) and Ru(II). In the substitution of Ru(edta)H<sub>2</sub>O, the rate was found to be strongly dependant on the nature of the incoming group. Also, in the aquation and anation of [Ru(NH<sub>3</sub>)Cl]<sup>2+</sup>, large negative  $\Delta V^\ddagger$  values were found. Both these findings are consistent with a mechanism at the associative end of the scale. For Ru(II), in the substitution of *cis*-[Ru(phen)<sub>2</sub>(py)<sub>2</sub>]<sup>2+</sup> by X<sup>-</sup> (X<sup>-</sup>=Cl<sup>-</sup>, Br<sup>-</sup>, I<sup>-</sup>, NCS<sup>-</sup>, N<sub>3</sub><sup>-</sup>, NO<sub>2</sub><sup>-</sup>), the rate of substitution was found to be independent of the nature of X<sup>-</sup>. This is opposite to that found by Ru(III). Similarly, for the substitution of H<sub>2</sub>O by Cl<sup>-</sup>, Br<sup>-</sup> & I<sup>-</sup> in [Ru(H<sub>2</sub>O)<sub>6</sub>]<sup>2+</sup>, the rates and activation enthalpies are very similar indicating that the activation state is identical in each case i.e. dissociation of H<sub>2</sub>O. This evidence points towards a dissociative mechanism for Ru(II).

When examining the substitution rates and assigned substitution mechanisms for solvent exchange (i.e. replacement of a solvent ligand for another identical one from the bulk solvent) the following conclusions can be made.

**Table 5.3.2.1 - Rate and  $\Delta V^\ddagger$  data for solvent exchange on Ru(III) and Ru(II)**<sup>52</sup>

	[Ru(H <sub>2</sub> O) <sub>6</sub> ] <sup>3+</sup>	[Ru(H <sub>2</sub> O) <sub>5</sub> OH] <sup>2+</sup>	[Ru(H <sub>2</sub> O) <sub>6</sub> ] <sup>2+</sup>	[Ru(CH <sub>3</sub> CN) <sub>6</sub> ] <sup>2+</sup>
k <sup>298</sup> / s <sup>-1</sup>	(3.5 ± 0.3) × 10 <sup>-6</sup>	(1.1 ± 0.2) × 10 <sup>-6</sup>	(1.8 ± 0.2) × 10 <sup>-2</sup>	(8.9 ± 2) × 10 <sup>-11</sup>
$\Delta V^\ddagger$ / cm <sup>-1</sup> mol <sup>-1</sup>	-8.3 ± 2.1	-2.1 ± 1.4	-0.4 ± 0.7	+0.4 ± 0.6
Assigned Mechanism	I <sub>a</sub>	I	I	I

For Ru(II), in both water and acetonitrile, solvent exchange occurs by an interchange mechanism (i.e.  $\Delta V^\ddagger=0$  within experimental error). Two factors must be considered when explaining the reason for an interchange mechanism -

- 1/ The ionic radius of the metal.
- 2/ The electron configuration of the ion.

Table 5.3.2.2 - Radius, configuration and  $\Delta V^\ddagger$  data for  $M^{2+}$

	Ionic Radius / pm	Electron Configuration	$\Delta V^\ddagger$ / $\text{cm}^{-1}\text{mol}^{-1}$ ( $\text{H}_2\text{O}$ exchange)	Substitution Mechanism
Ru(II)	73	Low spin $d^6$ ( $t_{2g}^6$ )	$-0.4 \pm 0.7$	Increased dissociative nature ↓
Fe(II)	78	High spin $d^6$ ( $t_{2g}^4 e_g^2$ )	+3.8	
Co(II)	74	High spin $d^7$ ( $t_{2g}^5 e_g^2$ )	+6.1	
Ni(II)	69	$d^8$ ( $t_{2g}^6 e_g^2$ )	+7.2	

As the ionic radius increases, it would be reasonable to assume that the associative nature of the substitution should increase as the metal ion becomes more able to accommodate a seven co-ordinate intermediate. This is not observed. However as the number of electrons in the  $e_g$  orbital increase, then the dissociative nature should increase (because the  $e_g$  orbital is a  $\sigma$ -antibonding orbital). This fits the experimental data, so for this series of  $M^{2+}$  ions the electron configuration is the predominant factor affecting substitution mechanism. The large difference in substitution rates between water and acetonitrile exchange (a difference of  $10^8 \text{ s}^{-1}$ ) is due to the high thermodynamic stability of the acetonitrile complex.

For Ru(III) the  $\Delta V^\ddagger$  is strongly negative so it is seen as an  $A$  or  $I_a$  mechanism. Since the  $\Delta V^\ddagger$  value is much less than the most negative experimental value ( $\text{Ti}^{3+}$ ,  $\Delta V^\ddagger = -12.1$ ) then it is reasonable to assign an  $I_a$  mechanism. For  $[\text{Ru}(\text{H}_2\text{O})_6]^{3+}$  in water, hydrolysis is kinetically important and the conjugate base  $[\text{Ru}(\text{H}_2\text{O})_5\text{OH}]^{2+}$  is in equilibrium with the hexaquo ion. For Ru(III) the change from hexaquo to monohydropentaaquo sees an increase in rate of substitution and an increase in dissociative nature (i.e.  $\Delta V^\ddagger$  becomes less negative). These observations can be explained in terms of the bonding and electron donating ability of the  $\text{OH}^-$  ligand. The strong  $\text{M}-\text{OH}^-$  bond weakens the remaining  $\text{M}-\text{H}_2\text{O}$  bonds (particularly the trans bond) and the associated increase in lability increases the dissociative nature of the substitution. This effect is seen most markedly for the analogous Fe(III) which is  $I_a$  for  $[\text{Fe}(\text{H}_2\text{O})_6]^{3+}$  but  $I_d$  for  $[\text{Fe}(\text{H}_2\text{O})_5\text{OH}]^{2+}$ .

#### 5.4 - Complex Synthesis

The choice of the ruthenium complexes synthesised was determined by the aims of the research, namely that the complex should be water soluble and be of such a structure that monomer co-ordination and carbene formation are feasible.

Syntheses 7 to 9 describe the initial steps in an attempt to synthesise  $[\text{Ru}(\text{NH}_3)_5(\text{N}_2)]\text{Cl}_2$  via a non - hydrazine route. The first step is the synthesis of  $[\text{Ru}(\text{NH}_3)_6]\text{Cl}_2$  followed by the synthesis of  $[\text{Ru}(\text{NH}_3)_5\text{Cl}]\text{Cl}_2$ . *In situ* synthesis of  $[\text{Ru}(\text{NH}_3)_5(\text{N}_2)]^{2+}$  and its reaction with bicyclic monomer was attempted by Allen and Senhoff's hydrazine route<sup>53</sup> and will be described in section 6.8.

Syntheses 10 and 11 describe the preparation of two of the carbonyl halide products described by Colton and Farthing<sup>54</sup>. The product obtained from the reaction of  $\text{RuCl}_3$  with an excess of a formic acid/HCl mixture depends on the time of reaction and method of isolation as described in section 5.2.

Syntheses 12 to 18 are compounds relating to the production of transition metal complexes containing water soluble phosphine ligands. The synthesis of the ligands is described in Chapter 4.

Syntheses 19 to 21 relate to the synthesis of  $[\text{Ru}(\text{en})_2\text{Cl}_2]\text{Cl}\cdot\text{H}_2\text{O}$  and syntheses 22 and 23 relate to the synthesis of Vaska's compound and a  $\text{P}(\text{CH}_2\text{OH})_3$  containing analogue.

##### 5.4.1 - Synthesis No.7 - Hexammineruthenium (II) Chloride - $[\text{Ru}(\text{NH}_3)_6]\text{Cl}_2$ .<sup>55</sup>



$\text{RuCl}_3\cdot 3\text{H}_2\text{O}$  (1g,  $3.8 \times 10^{-3}$  moles) was activated by dissolving and refluxing in conc. HCl (3.3 ml) for 1 hour. This was then slowly added dropwise to a stirred solution of 0.880 ammonia (10 ml) containing  $\text{NH}_4\text{Cl}$  (0.3g,  $5.6 \times 10^{-3}$  moles). The mixture was gently boiled and zinc dust (0.5g) was added in small portions. The mixture changed colour from black through brown to a green/yellow colour. The solution was then filtered to remove excess zinc dust and  $\text{NH}_4\text{Cl}$  (2.6g,  $4.9 \times 10^{-2}$  moles) was dissolved in the filtrate with minimum heating and then left to cool. Hexammineruthenium dichloride crystallised as glistening yellow crystals. These were filtered off and dried in a vacuum desiccator over  $\text{P}_2\text{O}_5$ . Yield = 0.172g (16.5% based on  $\text{RuCl}_3\cdot 3\text{H}_2\text{O}$ )

### Analysis (Appendix B - Fig B11)

An infrared spectrum was obtained and compared with literature data.<sup>56, 53, 57</sup>

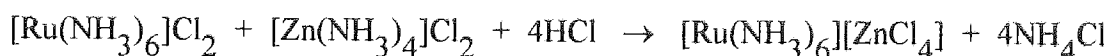
**Table 5.4.1.1 - Infra-red data for hexammineruthenium(II)dichloride.**

All values in cm <sup>-1</sup>	Product absorbances	Values from source 56	Values from source 53	Values from source 57 - for NH <sub>4</sub> Cl
N-H str	3322 & 3252	3300 & 3195	-	3138 & 3041
N-H d-def	1622	1610	1607	1710
N-H s-def	1403 & 1248	1220	1217	1403
NH <sub>3</sub> rocking	753	769	765	-
Ru-N str	Too much noise in spectrum.	437	-	-

The data agree well with the expected product containing some NH<sub>4</sub>Cl impurity. An attempt was made to purify the product by subliming out the NH<sub>4</sub>Cl on a cold finger. NH<sub>4</sub>Cl was seen to sublime out during the process but the heat applied decomposed the product to a blue black solid. This was discarded.

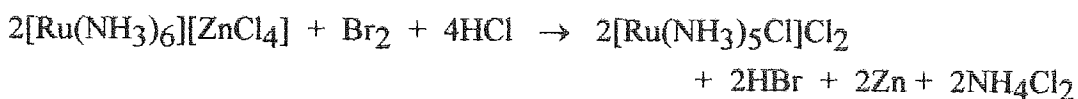
### 5.4.2 - Synthesis No.8 - Hexammineruthenium(II)tetrachlorozincate

#### [Ru(NH<sub>3</sub>)<sub>6</sub>][ZnCl<sub>4</sub>].<sup>55</sup>



The filtrate from the synthesis of hexammineruthenium(II)dichloride was just acidified with conc. HCl and left (two weeks) to allow the hexammineruthenium(II) tetrachlorozincate to crystallise out. After this time a small amount of yellow/orange crystals were retrieved from solution. These were retrieved by filtration and dried over P<sub>2</sub>O<sub>5</sub>. No analysis was performed due to the small quantity of product.

**5.4.3 - Synthesis No.9 -- Pentamminechlororuthenium(III)dichloride --  
[Ru(NH<sub>3</sub>)<sub>5</sub>Cl]Cl<sub>2</sub><sup>58</sup>**



This synthesis was performed on the assumption that the product from synthesis No.8 was [Ru(NH<sub>3</sub>)<sub>6</sub>][ZnCl<sub>4</sub>].

[Ru(NH<sub>3</sub>)<sub>6</sub>][ZnCl<sub>4</sub>] (0.08g, 1.9 x 10<sup>-4</sup> moles) was dissolved in 0.6 ml of distilled water. A few drops of bromine water were added until the solution became just orange. 0.6 ml of conc. HCl was then added and the mixture refluxed for 2 hours. The yellow/orange crystals that precipitated were filtered of and dried over P<sub>2</sub>O<sub>5</sub>.

Yield = 0.026g ( 44.4% based on [Ru(NH<sub>3</sub>)<sub>6</sub>][ZnCl<sub>4</sub>] ).

**Analysis (Appendix B - Fig B12).**

An infrared spectrum was obtained and the absorbances compared to literature data<sup>53</sup>.

**Table 5.4.3.1 - Infra-red data for pentamminechlororuthenium(III)dichloride.**

All values in cm <sup>-1</sup>	Product spectrum	Reference 53
NH str	Broad absorbance	3279 cm <sup>-1</sup> - broad
NH <sub>3</sub> s-def	1614 cm <sup>-1</sup>	1604 cm <sup>-1</sup>
NH <sub>3</sub> d-def	1300 cm <sup>-1</sup> with shoulder	1297 & 1254 cm <sup>-1</sup>
NH <sub>3</sub> rocking	802 cm <sup>-1</sup>	801 cm <sup>-1</sup>
Ru - N str	488 & 463 cm <sup>-1</sup>	485 & 466 cm <sup>-1</sup>

**Conclusions.**

This synthesis becomes difficult due to the need for scaling down the quantities of RuCl<sub>3</sub>.H<sub>2</sub>O used - the literature procedure uses 15g of ruthenium. The recrystallisation relies on the differences in solubility between the product and NH<sub>4</sub>Cl at the specified pH. Since such a small amount of acid (3.3 ml) is required in the scaled down experiment, any small change in the applied amount due to human error can have a dramatic effect on the recrystallisation of product, hence the very low yield.

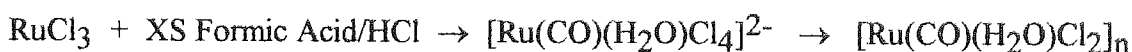
On leaving the filtrate from synthesis No. 1 standing in the fridge, small amounts of orange crystals were seen. Since the  $[\text{Ru}(\text{NH}_3)_6]^{2+}$  ion is prone to aerial oxidation in solution, it is reasonable to assume that these crystals are  $[\text{Ru}(\text{NH}_3)_6]\text{Cl}_3$ .

#### 5.4.4 - Synthesis No.10- Dichlorodicarbonylruthenium(II) -- $\text{Ru}(\text{CO})_2(\text{Cl})_2$ .<sup>59</sup>



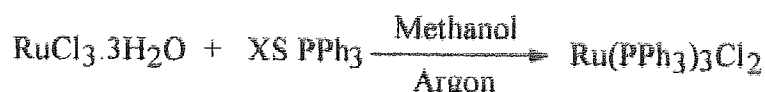
$\text{RuCl}_3 \cdot 3\text{H}_2\text{O}$  (1g,  $3.8 \times 10^{-3}$  moles) was refluxed for 10 hours in a HCl/Formic acid (50/50 v/v) mixture (40 ml) and then left to stand overnight leaving a bright orange solution. This was reduced to a small volume and then dried under vacuum at  $150^\circ\text{C}$ , yielding a fine orange yellow powder. Yield = 0.668g (77% based on  $\text{RuCl}_3 \cdot 3\text{H}_2\text{O}$ ). Elemental analysis gives C = 11.25%, Cl = 26.44%.  $\text{RuC}_2\text{O}_2\text{Cl}_2$  requires C = 10.54%, Cl = 26.44%. Appendix B - Figs B13 & B14 -  $\nu_{\text{CO}} = 2145, 2080, 2025 \text{ cm}^{-1}$  (KBr disc),  $\nu_{\text{CO}} = 2144, 2080, 2026 \text{ cm}^{-1}$  (Nujol mull) cf. Lit values<sup>59</sup>  $\nu_{\text{CO}} = 2150, 2070, 2030 \text{ cm}^{-1}$  (Nujol mull).

#### 5.4.5 - Synthesis No. 11 - Dichloroaquocarbonylruthenium(II) - $\text{Ru}(\text{CO})(\text{H}_2\text{O})\text{Cl}_2$ <sup>60</sup>



$\text{RuCl}_3 \cdot 3\text{H}_2\text{O}$  (0.5g,  $1.9 \times 10^{-3}$  moles) was refluxed for 5 hours in a HCl / Formic acid (50/50 - v/v) mixture (20 ml). The reaction is characterised by a colour change from dark brown to bright green. The solution was cooled and evaporated to dryness at room temperature in a vacuum desiccator over  $\text{P}_2\text{O}_5$  leaving shining dark green crystals in quantitative yield. Elemental analysis gives C = 6.68%, H = 1.37%, Cl = 30.62%.  $\text{RuCH}_2\text{O}_2\text{Cl}_2$  requires C = 5.51%, H = 0.92%, Cl = 32.53%. Appendix B - Fig B15 -  $\nu_{\text{CO}} = 2018, 2085 \text{ cm}^{-1}$  cf. Lit<sup>54</sup>  $\nu_{\text{CO}} = 2025, 2085 \text{ cm}^{-1}$ .

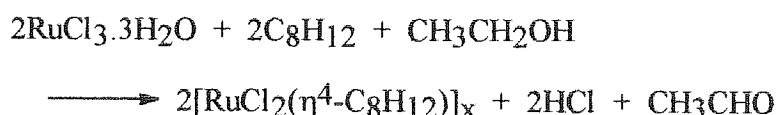
#### 5.4.6 - Synthesis No. 12 - Ruthenium(II)tris(triphenylphosphine)dichloride - $\text{Ru}(\text{PPh}_3)_3\text{Cl}_2$ .<sup>61</sup>



$\text{RuCl}_3 \cdot 3\text{H}_2\text{O}$  (3g,  $1.14 \times 10^{-2}$  moles) was dissolved in methanol (500 ml) and refluxed under argon for 5 minutes. The solution was then cooled and triphenylphosphine (18g,

$6.87 \times 10^{-2}$  moles) added with stirring. The mixture was then refluxed for 3 hours under argon. (The time of reaction alters the product retrieved in that refluxing for 4 hours produces glistening dark brown crystals indicative of  $\text{Ru}(\text{PPh}_3)_4\text{Cl}_2$  instead of the desired product.) The black glistening product crystals were filtered under argon, washed with ether and dried in a vacuum dessicator. Yield = 9.87g  $\cong$  90% (based on  $\text{RuCl}_3 \cdot 3\text{H}_2\text{O}$ ). (Elemental analysis C = 67.37%, H = 4.75%.  $\text{RuCl}_2\text{PC}_{54}\text{H}_{45}$  requires C = 67.65%, H = 4.7%.)

#### 5.4.7 - Synthesis No. 13 - Ruthenium(II)cyclooctadienedichloride - $\text{Ru}(\text{COD})\text{Cl}_2$ .<sup>62</sup>



$\text{RuCl}_3 \cdot 3\text{H}_2\text{O}$  (1g,  $3.8 \times 10^{-3}$  moles) and cyclooctadiene (1 ml,  $8 \times 10^{-3}$  moles) were refluxed in ethanol (15 ml) for 24 hours. The initial dark brown colour changed first to a deep blue/green before returning to dark brown as the solid product precipitated out. The precipitate was filtered from the solution and washed with diethyl ether.

Yield = 0.98g  $\cong$  92% (based on  $\text{RuCl}_3 \cdot 3\text{H}_2\text{O}$ ). Elemental analysis gives C = 34.02%, H = 4.41%, Cl = 24.94%.  $\text{RuC}_8\text{H}_{12}\text{Cl}_2$  requires C = 34.3%, H = 4.32%, Cl = 25.31%.

#### 5.4.8 Synthesis No.14 - Dinitrosylbis(triphenylphosphine)ruthenium - $\text{Ru}(\text{NO})_2(\text{PPh}_3)_2$ .<sup>63</sup>

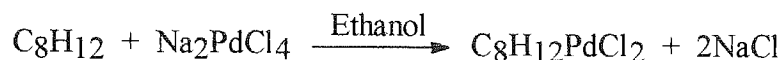


MNTS = *N*-Methyl-*N*-nitrosotoluene-*p*-sulphonamide (Diazald).<sup>TM</sup>

$\text{RuCl}_3 \cdot 3\text{H}_2\text{O}$  (0.13g,  $5 \times 10^{-4}$  moles) in ethanol (10 ml) was rapidly added to a stirred solution of  $\text{PPh}_3$  (0.79g,  $3 \times 10^{-3}$  moles) in boiling ethanol (40 ml).  $\text{NaBH}_4$  (0.1g,  $2.6 \times 10^{-3}$  moles) in ethanol (10 ml) was then added dropwise until a deep purple colour developed. *N*-Methyl-*N*-nitrosotoluene-*p*-sulphonamide (0.21g,  $8.7 \times 10^{-4}$  moles) in ethanol (10 ml) and the remaining  $\text{NaBH}_4$  solution were added rapidly. Heating was continued for 5 minutes and the solution was then cooled. The resultant dark red precipitate was removed by filtration, washed with ethanol, water and ethanol again and then dried in a vacuum dessicator. Yield = 0.233g  $\cong$  68% (based on  $\text{RuCl}_3 \cdot 3\text{H}_2\text{O}$ ). Elemental analysis gives C = 60.75%, H = 4.43%, N = 2.08%.  $\text{RuC}_{36}\text{H}_{30}\text{P}_2\text{N}_2\text{O}_2$  requires C = 63.06%, H = 4.41%, N = 4.09%. Appendix B - Fig B16 -  $\nu_{\text{NO}} = 1646$  &  $1613 \text{ cm}^{-1}$  (KBr disk),  $\text{Li}^{63} \nu_{\text{NO}} = 1665$  &  $1619 \text{ cm}^{-1}$  ( $\text{CH}_2\text{Cl}_2$  solution).



#### 5.4.9 - Synthesis No 15- Palladiumdichlorocyclooctadiene - PdCl<sub>2</sub>(COD).<sup>64, 65</sup>

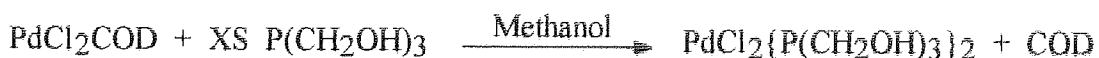


Due to solubility problems encountered with my starting palladium salt, a combination of the techniques described in the literature were employed.

Potassiumtetrachloropallidate(II) (0.5g,  $1.53 \times 10^{-3}$  moles) was dissolved in methanol (30 ml). Even with gentle heating, complete dissolution of the palladium salt did not occur and the insoluble portion was removed by filtration. Cyclooctadiene (0.5 ml,  $4 \times 10^{-3}$  moles) was added to the orange solution which on rapid swirling changed colour to bright yellow. Slight reduction of the solution by evaporation and cooling resulted in the deposition of yellow micro-crystals which were recovered by filtration and dried in a vacuum dessicator.

The insoluble portion of the palladium salt was dissolved in warm conc. HCl (10 ml) and a small portion (5-10 ml - the addition of too large an amount of alcohol can cause all the dissolved palladium salt to reprecipitate) of ethanol or methanol added. Any solid remaining was removed by filtration and cyclooctadiene (0.5 ml,  $4 \times 10^{-3}$  moles) added to the orange solution. Swirling produced the same colour change as observed above and yellow micro-crystals were recovered in the manner previously described. This process was repeated until all the original palladium salt had been dissolved and reacted. Yield = 0.25g  $\equiv$  60% (based on K<sub>2</sub>PdCl<sub>4</sub>). Elemental analysis gives C = 26.42%, H = 3.38%. PdC<sub>8</sub>H<sub>12</sub>Cl<sub>2</sub> requires C = 33.65%, H = 4.24%.

#### 5.4.10 - Synthesis No.16 - Palladium(II)bis(trishydroxymethylphosphine)dichloride - PdCl<sub>2</sub>{P(CH<sub>2</sub>OH)<sub>3</sub>}<sub>2</sub>.<sup>66</sup>



PdCl<sub>2</sub>(COD) (0.1g,  $3.5 \times 10^{-4}$  moles) was suspended in methanol (5 ml) and added to a methanolic solution of P(CH<sub>2</sub>OH)<sub>3</sub> (5.25 ml, 0.14 M). Complete dissolution of the palladium complex occurred after a few minutes vigorous shaking, giving the solution a

yellow colour. The solution was reduced to 1-2 ml on a rotary evaporator and the product precipitated by addition of dichloromethane (20 mls). The product was retrieved by filtration and dried in a vacuum desiccator over  $P_2O_5$ . Yield = 0.046g  $\equiv$  31% (based on  $PdCl_2(COD)$ ).

#### 5.4.11 - Synthesis No.17- Attempted synthesis of ruthenium poly(trishydroxymethyl)dichloride - $RuCl_2\{P(CH_2OH)_3\}_x$ .

There is no published synthesis for the ruthenium analogue of the palladium, platinum and nickel tris(hydroxymethyl)phosphine complexes. A number of different methods were employed in attempt to synthesise this product. One example of each method is given below.

n.b/ In all cases  $P(CH_2OH)_3$  was freshly prepared and unrecrystallised for reasons explained in section 4.1.

##### Method 1

$RuCl_2(COD)$  (0.1g,  $3.6 \times 10^{-4}$  moles) was suspended in methanol (5 ml) and added to a methanolic solution of  $P(CH_2OH)_3$  (5.25 ml, 0.14 M). Even with extended vigorous shaking and gentle heating,  $RuCl_2(COD)$  would not dissolve in the methanol. The high insolubility is due to this compounds polymeric chloro-bridged structure. However after having been left standing for a considerable time (a number of weeks) a colour change from colourless to light orange was noticeable in the methanol. This is good evidence that a small amount of the Ru complex had gone into solution and co-ordinated with the ligand (see later methods) although the majority of the  $RuCl_2(COD)$  remained undissolved.

##### Method 2

$Ru(PPh_3)Cl_2$  (2.5g,  $2.6 \times 10^{-3}$  moles) was dissolved in dichloromethane (60 ml).  $P(CH_2OH)_3$  (1.24g,  $1 \times 10^{-2}$  moles) was dissolved in water (50 ml) and added to the organic ruthenium solution to produce a biphasic mixture. This mixture was vigorously stirred for 3 hours during which time an orange colour appeared in the aqueous layer. The two layers were separated in a separating funnel and the organic layer discarded. The aqueous layer was reduced on a rotary evaporator to give a deep red oil/tar like substance. This was cleaned by refluxing twice in toluene (100 ml) for 3 hours. This produced a very sticky, bright orange product which was isolated by decanting of the

toluene. Reduction to dryness of the toluene produced 0.19g of off-white waxy solid - probably excess  $P(CH_2OH)$ . The orange product was removed from the flask by taking up in the minimum amount of water and then drying first on a rotary evaporator and finally by drying in a vacuum oven at  $110^\circ C$  for 4 hours. Yield = 0.953g. The final product is a bright orange, sticky, glass like solid which is very hygroscopic - on leaving open to the air the product becomes increasingly sticky taking on a "toffee" like consistency after a day or two. The original product consistency can be recovered by reheating in a vacuum oven and storing in a dry box.

Similar results are obtained when  $RuCl_3 \cdot 3H_2O$  or  $Ru(PPh_3)_3Cl_2$  are reacted with the ligand in methanol solution alone.

### Method 3

$P(CH_2OH)_3$  (3.29g,  $1.7 \times 10^{-2}$  moles) was dissolved in toluene (100 ml).  $RuCl_3 \cdot 3H_2O$  (0.75g,  $2.9 \times 10^{-3}$  moles) was added and the mixture refluxed for 3 hours. Due to the insolubility of  $RuCl_3$  in toluene it remains as a suspension during the reaction. As soon as some reaction between the ruthenium and ligand had occurred small globules of sticky orange product appeared in the mixture to the surface of which the suspended  $RuCl_3$  tended to stick. A good indicator of completion of reaction was when no more  $RuCl_3$  could be seen adhered to the domains of orange product. The toluene was removed by decantation (reducing to dryness yielded 0.35g of off white waxy residue) and the orange product removed from the flask by freezing the flask and its contents by cooling externally with liquid nitrogen and chipping the product from the inside surface of the vessel. The product was dried in the vacuum oven, leaving an orange product as described above. Yield = 2.72g.

Similar results were obtained when  $Ru(PPh_3)Cl_2$  was used instead of  $RuCl_3 \cdot 3H_2O$ . As it was thought that the product consistency could be due to entrapped solvent in the product matrix, the reaction was also performed in mesitylene (3,5-dimethyltoluene) solvent in the hope that the solvents size would prevent it from being incorporated into the product. However the immiscibility and insolubility of the ligand in the solvent led to incomplete reaction.

### Summary

Reactions performed in both biphasic methanol/organic mixtures and in monophasic methanol solution produce a deep red tar-like substance. The product is retrieved by

extracting excess reactants and by-products with toluene. Reactions in toluene produce the orange product without the need for further work-up procedures.

### NMR Analysis.

$^{31}\text{P}$ ,  $^{13}\text{C}$  and  $^1\text{H}$  spectra (Appendix B - Figs B17 to B22) were acquired for representative samples of the orange "toffee" products synthesised by both method 2 and method 3. The data are presented in tables 5.4.11.1 and 5.4.11.2.

Spectra of both samples are very similar despite the different synthesis conditions and more importantly, different work up procedures. This indicates that whatever by-products and unreacted starting products which are present in the crude oil/tar from method 2 are removed by refluxing in toluene, producing exactly the same product as produced by method 3.

### Interpretation of $^{31}\text{P}$ NMR data (Appendix B - Figs B19 and B22).

The  $^{31}\text{P}$  spectra show two different features. The broad resonance at 68-72 ppm is indicative of phosphorous nuclei within an indiscrete environment. This suggests the presence of unreacted ligand/phosphorus species within the product matrix, which presumably are not removed by refluxing in toluene.

The other region of interest in the  $^{31}\text{P}$  spectra is between 43 and 46 ppm where three discrete resonances can be seen. The major peaks at  $\delta = 43.7$  ppm (Method 2) and 44.3 ppm (Method 3) relate reasonably well to the corresponding resonances in the analogous palladium complex ( $\delta = 34.4$  ppm<sup>66</sup>) although there is a large variation in chemical shift for this resonance among the transition metals (For the platinum complex  $\delta = 9.5$  ppm<sup>66</sup>). The smaller peaks in the same region are probably due to co-ordinated phosphorus ligands containing hemiacetal groups.

Table 5.4.11.1 -  $^{31}\text{P}$  and  $^{13}\text{C}$  NMR data for Ru-P(CH<sub>2</sub>OH)<sub>3</sub> complex from synthesis No. 17.

Nucleus	Method 2 - Methanol solvent $\delta$ / ppm	Method 3 - Toluene solvent $\delta$ / ppm
$^{31}\text{P}$	68 - 72 broad	68 - 72 broad
	44.86	45.61
	43.71	44.33
	43.28	43.05
$^{13}\text{C}^a$	8.91 (+)	8.77 (+) Doublet J(PC) = 30.5 Hz
	37.75 (+)	37.82 (+)
	45.42 (-)	45.52 (-)
	49.26 (-)	49.35 (-)
	54.56 (-) Doublet J(PC) = 74 Hz	54.61 (-) Doublet J(PC) = 74 Hz

a) Spectra acquired with PENDANT pulse sequence. C & CH<sub>2</sub> resonances annotated (-), CH & CH<sub>3</sub> annotated (+).

#### Interpretation of $^{13}\text{C}$ NMR data (Appendix B - Figs B17 and B20).

The lack of doublets in the  $^{13}\text{C}$  spectra indicates that the strength of the sigma interaction between phosphorus and carbon has been reduced by the bonding between ruthenium and phosphorus to such an extent that the coupling constant is too small to be resolved by the spectrometer. Therefore the doublet at  $d = 54.56$  ppm probably corresponds to a phosphine compound which is uncoordinated to ruthenium and the size of the coupling constant ( $J = 74$  Hz) suggests that the compound is four co-ordinate. The doublet at  $d = 8.77$  ppm (Method 3)  $J = 30.5$  Hz (unresolved in Method 2) must be due to a methyl group although the reduction in coupling constant from the crude phosphine mix is unusual. The large peak at  $d = 45.42$  ppm (Method 2) and 45.52 ppm (Method 3) could be due to co-ordinated P(CH<sub>2</sub>OH)<sub>3</sub> and the other singlets due to any remaining methylene groups in hemiacetal containing ligands. The peak at  $d = 37.75$  ppm (Method 2) and 37.82 ppm (Method 3) is unexpected and could be due to either a CH or CH<sub>3</sub> group which wasn't originally present in the crude phosphine mix.

### Interpretation of $^1\text{H}$ NMR data (Appendix B - Figs B18 and B21).

The reduction in number of doublets in the proton spectra when compared to the phosphine spectra again suggests a reduction in sigma interaction due to the formation of P-Ru bonds. The doublet at  $\delta = 3.79$  ppm (Method 2 & 3 - unresolved singlet in 3),  $J = 2.85$  Hz and the broad signal at  $\delta = 4.23$  ppm (Method 2) and  $\delta = 4.19$  ppm (Method 3) is comparable to the pair of doublets at  $\delta = 3.79$  ppm and  $\delta = 3.83$  ppm in the phosphine spectrum and are therefore attributable to protons in  $\text{CH}_2\text{OH}$  and hemiacetal ligands. Overall the  $^1\text{H}$  spectra are not as clean as the ligand spectra which is consistent with a moiety where unreacted ligand species are trapped within a more discrete product matrix.

**Table 5.4.11.2 -  $^1\text{H}$  NMR data for Ru-P( $\text{CH}_2\text{OH}$ ) $_3$  complex from synthesis No. 17.**

$\delta$ / ppm	Method 2 Methanol solvent Type and J / Hz	R.I	$\delta$ / ppm	Method 3 Toluene solvent. Type and J / Hz	R.I
0.87	Triplet - J = 7.26	1.55	0.87	Unresolved multiplet	-
1.17	Unresolved multiplet	12.4	1.17	Triplet - J = 7.04	21.5
1.8	Broad	7.64	1.77	Broad	8.98
2.49	Singlet	0.82	2.49	Singlet	↓
-	-	-	2.56	Singlet	1.55
2.63	Doublet - J = 4.05	2.02	2.64	Singlet	↑
3.03	Unresolved multiplet	4.9	3.03	Doublet - J = 3.84	13.6
3.58	Doublet - J = 5.7	-	3.56	Singlet	-
3.79	Doublet - J = 2.85	3.64	3.79	Singlet	13.6
4.23	Broad	25.7	4.19	Broad	48.1
10.33	Broad	1	10.08	Broad	1

*n.b/ R.I values are not comparable between separate spectra.*

### Elemental analysis.

A sample of the product from method 3 was sent for elemental analysis and the following results obtained. C = 23.26%, H = 5.44%, Cl = 11.87%, P = 17.81%, Ru = 16.61%.

### Interpretation of Elemental Analysis.

**Table 5.4.11.3 - Elemental analysis of Ru-P(CH<sub>2</sub>OH) complex from synthesis No. 17.**

Element	Ru	P	C	H	O	Cl
Percentage	16.61	17.81	23.26	5.44	25.01 <sup>E</sup>	11.87
Ratio	1	3.6	12.1	34	9.8	2

*E = Estimated percentage*

The ligand P(CH<sub>2</sub>OH)<sub>3</sub> has a composition of 1P:3C:9H:3O. The elemental analysis is slightly higher but in agreement with this figure and suggests a ratio of 1P:3.4C:9.4H:3.3O for this product. The ratio of phosphorus to ruthenium is 1Ru:3.6P which is in very good agreement with an expected product composition of between three and four phosphorus ligands per ruthenium. The two chlorines per ruthenium is again in good agreement with analogous transition metal compounds.

### Summary.

The orange product seems to consist of a discrete Ru-Phosphine matrix in which unreacted ligand impurities are enclosed as suggested by NMR analysis. The elemental analysis suggests a Ru:P ratio of 1:3.6. This is consistent with three or four phosphorus ligands per ruthenium.

### 5.4.12 - Synthesis No 18- Attempted synthesis of dinitrosylbis(trishydroxymethylphosphine)ruthenium - Ru(NO)<sub>2</sub>{P(CH<sub>2</sub>OH)<sub>3</sub>}<sub>2</sub>.

Direct ligand substitution between Ru(NO)<sub>2</sub>(PPh<sub>3</sub>)<sub>2</sub> and P(CH<sub>2</sub>OH)<sub>3</sub> in methanolic solution was unsuccessful due to the insolubility of the Ru complex in methanol. An attempt was made to synthesise the desired product using the same method as for Ru(NO)<sub>2</sub>(PPh<sub>3</sub>)<sub>2</sub> but substituting P(CH<sub>2</sub>OH)<sub>3</sub> for PPh<sub>3</sub>.

P(CH<sub>2</sub>OH)<sub>3</sub> (1.736g, 1.4 x 10<sup>-2</sup> moles) was dissolved in ethanol (50 ml) and heated to reflux. RuCl<sub>3</sub>.3H<sub>2</sub>O (0.612g, 2.35 x 10<sup>-3</sup> moles) in ethanol (30 ml) was added rapidly to this solution followed by the portion wise addition of NaBH<sub>4</sub> (0.47g, 1.24 x 10<sup>-2</sup> moles) in ethanol (30 ml). A colour change from dark brown to light brown/olive green was observed. At this point *N*-Methyl-*N*-nitrosotoluene-*p*-sulphonamide (1.13g, 4.68 x 10<sup>-3</sup> moles) in ethanol (30 ml) and the remaining NaBH<sub>4</sub> solution were rapidly added,

which caused the solution to effervesce vigorously. The solution was refluxed for a further 5 minutes during which time the colour lightened. The solution was cooled and the light brown precipitate filtered off, washed with ethanol and dried under vacuum over  $P_2O_5$  to give a light brown product, yield = 1.58g. Elemental analysis gives C = 17.5%, H = 4.45%, N = 1.39%, P = 13.27%. The deep red filtrate was slightly reduced and then cooled producing a slightly darker brown precipitate, yield = 0.7g. Elemental analysis gives C = 16.43%, H = 3.72%, N = 1.33%, P = 7.88%. ( $Ru(NO)_2(P(CH_2OH)_3)_2$  requires C = 18%, H = 4%, N = 7%, P = 15%)

Both products were soluble in water and sparingly soluble in methanol only. Attempts to obtain NMR spectra in  $D_2O$  proved unsuccessful. IR spectra were obtained, Appendix B - Figs B23 and B24,  $\nu_{NO} = 1653\text{ cm}^{-1}$  (1<sup>st</sup> precipitate) and  $1669\text{ cm}^{-1}$  (2<sup>nd</sup> precipitate) cf Lit.<sup>63</sup>  $\nu_{NO} = 1665\text{ cm}^{-1}$  and  $1619\text{ cm}^{-1}$ .

#### 5.4.13 - Synthesis No. 19- Potassiumtrioxalatoruthenium(III) - $K_3(RuOx_3)4H_2O$ .<sup>67</sup>

The reference uses  $Ru(H_2O)Cl_5K_2$  as a  $Ru^{3+}$  source. In my synthesis I have substituted activated  $RuCl_3.3H_2O$ .

$RuCl_3.3H_2O$  (1.307g,  $5 \times 10^{-3}$  moles), was dissolved in water (10 ml), a few drops of conc. HCl added and the solution refluxed for 15 minutes. The solution was cooled and potassium oxalate (2.76g,  $1.5 \times 10^{-2}$  moles) in water (10 ml) added and the solution returned to reflux. Over the first few hours a subtle colour change could be seen from initially dark brown through red/brown until it achieved a green/yellow/brown colour which it retained during reflux overnight. The solution was then cooled and repeated reduction in volume and cooling resulted in the retrieval of orange plate like crystals. Yield = 0.66g. Elemental analysis gives C = 10.84%, H = 0.63%.

The literature procedure requires the reaction to be carried out in an autoclave at  $130^\circ C$  leading to the isolation of large green crystals. However when the orange crystals from my synthesis were used in the synthesis of  $[RuOx_2][RuOx_2].2H_2O$  as if they were  $K_3(RuOx_3)4H_2O$  then the desired product was achieved. This suggested the possibility of continuing the chain of reactions to  $[RuCl_2en_2]Cl.H_2O$  without first isolating  $K_3(RuOx_3)4H_2O$ .



**5.4.14- Synthesis No.20 - Oxalatobis(ethylenediamine)ruthenium(III)Bis(oxalato)-ethylenediamineruthenate(III) [Ruoxen<sub>2</sub>][Ruox<sub>2</sub>en].2H<sub>2</sub>O.**<sup>68</sup>

RuCl<sub>3</sub>.3H<sub>2</sub>O (1.307g, 5 x 10<sup>-3</sup> moles) was dissolved in water (10 ml), a few drops of conc. HCl added and the solution refluxed for 15 minutes. The solution was cooled and potassium oxalate (2.76g, 1.5 x 10<sup>-2</sup> moles) in water (10 ml) added. The solution was refluxed for 6 hours and the expected colour change from dark brown to green/yellow/brown was observed. The solution was left to cool overnight. Ethylenediammonium oxalate (22.2 ml of a 0.9 M solution  $\equiv$  0.02 moles) was added and the solution refluxed for 20 minutes during which time a yellow precipitate appeared. The solution was filtered whilst hot isolating orange/yellow crystals. Yield = 1.16g  $\equiv$  34% (based on RuCl<sub>3</sub>.3H<sub>2</sub>O). Elemental analysis gives C = 21.37%, H = 4.13%, N = 11.89%. Ru<sub>2</sub>C<sub>12</sub>H<sub>28</sub>N<sub>6</sub>O<sub>14</sub> requires C = 21.12%, H = 4.13%, N = 12.31%.

The solution was refiltered once and cooled isolating 1.03g of glistening white crystals (a mixture of potassium and ethylenediammonium oxalates). Reduction in volume and cooling of the filtrate led to the recovery of more white crystals and 0.1g of an olive green powder. It is expected that the yield could be substantially improved by adding ethylenediammonium oxalate as a solid instead of in solution and thus reducing the reaction volume and encouraging a greater precipitation of the desired product.

**5.4.15 - Synthesis No. 21 - Dichlorobis(ethylenediamine)ruthenium(III)chloride monohydrate - cis-(RuCl<sub>2</sub>en<sub>2</sub>)Cl.H<sub>2</sub>O.**<sup>68</sup>

[Ruoxen<sub>2</sub>][Ruox<sub>2</sub>en].2H<sub>2</sub>O (1g, 1.5 x 10<sup>-3</sup> moles) was dissolved in conc. HCl (4.3 ml) and left to stand overnight. This produced an amount of brown solid and red solution. The solid was removed by filtration through a sinter funnel and washed with ethanol and acetone. The brown solid was then dissolved in warm 1M HCl (9 ml). No crystals formed on cooling but a slight reduction in volume and further cooling resulted in the formation of bright orange crystals. Initial yield = 0.11g  $\equiv$  21% (based on [Ruoxen<sub>2</sub>][Ruox<sub>2</sub>en].2H<sub>2</sub>O). Elemental analysis gives C = 13.91%, H = 5.28%, N = 15.99%. RuC<sub>4</sub>H<sub>18</sub>N<sub>4</sub>OCl<sub>3</sub> requires C = 13.90%, H = 5.25%, N = 16.21%.

**5.4.16 - Synthesis No. 22 - trans-Carbonylchlorobis(triphenylphosphine)iridium (Vaska's Compound) - IrCl(CO)(Ph<sub>3</sub>P)<sub>2</sub>.**<sup>69</sup>

KIrCl<sub>4</sub> (1g, 3 x 10<sup>-3</sup> moles), triphenylphosphine (3.7g, 0.015 moles) and aniline (1.5ml) were vigorously refluxed in dimethylformamide (50ml) overnight. The resultant red

brown solution was filtered whilst hot and then warm methanol (100ml) was added rapidly with stirring. The mixture was cooled with an ice bath and the characteristic bright yellow crystals produced were collected by filtration and washed with methanol and diethyl ether. Yield = 6.7g  $\equiv$  76 %.

**5.4.17 - Synthesis No. 23 - Attempted synthesis of Carbonylchlorobis(tris(hydroxymethyl)phosphine)iridium -  $\text{IrCl}(\text{CO})(\text{P}(\text{CH}_2\text{OH})_3)_2$ .**

This synthesis was attempted using the method described for Vaska's compound (above) but substituting tris(hydroxymethyl)phosphine for triphenylphosphine. An earlier attempt to substitute triphenylphosphine with tris(hydroxymethyl)phosphine using the biphasic substitution method described earlier (Section 5.4.11 method 2 - Vaska's compound in the organic phase) proved unsuccessful.

$\text{P}(\text{CH}_2\text{OH})_3$  (6.2g, 0.05 moles) was freshly prepared from  $\text{P}(\text{CH}_2\text{OH})_4\text{Cl}$  (9.5g, 0.05 moles). To this was added  $\text{KIrCl}_4$  (3.59g, 0.01 moles), aniline (4ml) and dimethylformamide (150ml) and the mixture vigorously refluxed. After 1 hour a large amount of pale brown precipitate was seen to come out of solution. The mixture was left refluxing overnight. On returning the mixture was cooled and the precipitate separated by centrifuge. This produced 2.8g of brown/white powder. The remaining DMF solution was reduced on a rotary evaporator in an attempt to induce crystallisation. This was not successful so it was decided to remove any alcohol soluble product.

**Product separation.**

The DMF residue (a red/brown sticky solid) and the pale brown precipitate were recombined and refluxed for two hours in two 100ml portions of propan-2-ol. This produced a orange/red propanol solution and a large amount of the pale brown precipitate which was removed by filtration (final yield = 4.8g Mt. Pt. =  $>300^\circ\text{C}$ ). The propanol solution was reduced and cooled again in attempt to induce recrystallisation. This proved unsuccessful but it was observed that on further reduction, the 'toffee' like residue (remarkably similar in appearance and consistency to the ruthenium- $\text{P}(\text{CH}_2\text{OH})_3$  product) seemed to consist of two distinct phases; a transparent orange/red 'toffee' like phase and a more opaque phase. The opaque phase was identified as containing some of the pale brown precipitate isolated earlier in the experiment, which was apparently sparingly soluble in propanol and was only being fully released from solution at these small volumes. After further reducing the residue by drying in a vac oven at  $70^\circ\text{C}$  for

two hours, the extreme hygroscopicity of the product was employed to separate the two phases. On leaving the residue exposed to the atmosphere for only a few minutes, the orange/red transparent phase became liquid enough to pour off from the less mobile opaque phase. The product was then returned to a vacuum desiccator in an attempt to remove the absorbed water. This produced a soft, sticky orange/red residue. It is readily apparent that this product is considerably more hygroscopic than its ruthenium analogue.

### NMR Analysis.

$^{31}\text{P}$ ,  $^1\text{H}$  and  $^{13}\text{C}$  NMR spectra (Appendix B - Figs B26 - B31) were obtained for the pale brown precipitate and the orange residue. Results are given in Fig 5.4.17.1.

### NMR Analysis - Precipitate.

The single resonance at 0 ppm in the  $^{31}\text{P}$  spectrum (B31) of the precipitate is indicative of phosphoric acid. This suggests two things. Firstly, that the phosphine ligand has decomposed during the reaction. Secondly, that the precipitated product is an inorganic phosphate of some kind (the precipitate has a high melting point which also suggests an ionic compound). As the ligand appears to have decomposed, we also need to consider possible product compositions containing ligand fragments rather than  $\text{P}(\text{CH}_2\text{OH})_3$ . The lack of doublets could indicate reduced coupling due to Ir-P co-ordination but the presence of phosphate, indicating ligand decomposition, would suggest none of the carbon fragments present in the product are attached to a phosphorus atom.

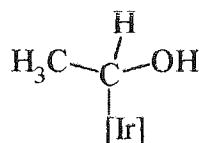
The single peak at 25.7 ppm in the  $^{13}\text{C}$  spectrum (B29) is in the correct region for a methyl group. Its lack of splitting suggests that it is not attached to phosphorus but its position rules out a direct bond to iridium (chemical shifts for Ir- $\text{CH}_3$  groups tend to lie between -9 ppm and -13 ppm)<sup>70</sup>. The low field resonance at 129 ppm is in the correct region for an organic carbonyl and its positive displacement suggests a -CH group i.e. an aldehyde, although for an aldehydic resonance, this seems somewhat up-field (normal resonance position for aldehyde groups = 190-210 ppm). However, as was shown for the methyl group, co-ordination to iridium causes an up-field shift in the resonant position (Ir-CO = 174-158 ppm but no data for Ir-CHO available<sup>70</sup>) so it is not unfeasible for this to be caused by an aldehydic group attached directly to iridium. The resonance at 32.6 ppm (negative displacement) might indicate an Ir- $\text{CH}_2$ - group but literature sources suggest that it occurs at too low a field (Ir- $\text{CH}_2$ -R = 1-10 ppm<sup>70</sup>) to be reliable.

Table 5.4.17.1 -  $^{31}\text{P}$ ,  $^1\text{H}$  and  $^{13}\text{C}$  NMR data for products of Synthesis No. 23.

	$^{31}\text{P}$ $\delta$ / ppm	$^1\text{H}$ $\delta$ / ppm	$^1\text{H}$ Relative intensities	$^{13}\text{C}$ $\delta$ / ppm
Pale Brown Precipitate (Figs B24 - B31 )	-0.18	1.03 (d,J=6.15 Hz)	74.5	25.71 (+ive)
		1.23 (s)	1.5	32.6 (-ive)
		2.08 (s)	1.5	62.2 (+ive)
		2.49 (s)	6	129 (+ive)
		2.8 (d,J=47.5 Hz)	1	
		3.5 (Broad)	4	
		3.77 (Mult.)	22	
		7.07 (V. broad)	1	
Orange Residue (Major peaks) (Fig B26 - B28)	0.209	2.05	11	34.06(+ive)
	16.78	2.49	145	112.56(+ive)
	17.83	2.72	7	117.6(+ive)
	20.62	6.91(d,J=7.38)	8	119.18(+ive)
	24.99	7.04(q,J=7.38)	39	123.62(+ive)
	29.66	7.11(d,J=5.25)	6	128.88(+ive)
	32.6	7.15(d,J=7.38)	10	129.43(+ive)
	41.27	7.29(t,J=7.86)	68	138.4(-ive)
	42.78	7.62(d,J=7.62)	41	159.67(+ive)
	45.19	8.27(d,J=1.89)	40	162.6(+ive)
46.77	8.78(d,J=11.19)	9		
	9.06(broad)	9		
	10.23(d,J=10.71)	1		
Ligand (analogous resonances) (Figs B5 - B7)	29.17	0.87(d,J=2.64)		9.24(+ive)(d,J=117.7)
	33.34	0.92(t,J=7.08)		54.61(-ive)(d,J=75.2)
	44.05	1.31(d,J=12.88)		56.11(-ive)(d,J=8.7)
	45.33	1.37(s)		57.18(-ive)(d,J=79.6)
	49.84	3.65(d,J=4.11)		58.93(-ive)(d,J=9.8)
		3.69(d,J=3.96)		61.83(-ive)(d,J=6.5)
		3.72(d,J=3.78)		66.66(-ive)(d,J=122)
		3.79(d,J=3.3)		
		3.83(d,J=5.6)		
	4.83(broad)			

However if the R group is -OH it is possible that the associated de-shielding could account for the down-field shift. The remaining peak at 62 ppm is at the low-field end of the range associated with a tertiary CH group but it is difficult to assign this resonance with any certainty.

The major methyl peak in the  $^1\text{H}$  spectrum (B30) is a doublet with  $J=6.15$  Hz, suggesting the methyl group is next to a CH group. The only multiplet observed in the spectrum is at 3.7 ppm, which would correspond to a -CH-O- group. The relative intensities are consistent with a one to one ratio of  $\text{CH}_3$  to CH therefore confirming the hypothesis that the major species present takes the general form  $\text{CH}_3\text{-CH-O-}$ . One candidate for this species is acetaldehyde,  $\text{CH}_3\text{CH=O}$ , but the resonances do not match with literature sources for this molecule. It is not unreasonable to suggest that the oxygen could itself be co-ordinated to iridium, but this leaves the problem of what other group is attached to the -CH. The only other possible structure is for the CH carbon to be co-ordinated iridium and the oxygen to exist as a hydroxyl -OH (Fig 5.4.17.1) although this seems highly unlikely. No relevant NMR resonances from similar or analogous complexes can be found in the literature.



**Fig. 5.4.17.1 - Possible structure of organic species in the precipitated product.**

The broad resonances at 3.5 ppm and 7 ppm are associated with hydrogen bonded protons, but in neither case does the relative intensity meet the requirements of the species (the R.I's of 4 and 1 respectively are far short of the 22 which would be anticipated by the proposed structure).

The relative intensities of the proton resonances associated with the  $\text{CH}_3$  and CH groups suggest that the other resonances observed are associated with minor by-products and it is assumed that the two ambiguous  $^{13}\text{C}$  resonances (32.6 ppm and 62.2 ppm) can be assigned likewise.

#### NMR Analysis - Orange Residue (Appendix B - Figs B26 - B28).

Apart from the single resonance at 0.2 ppm, all the other resonances in the  $^{31}\text{P}$  spectrum are in the same region observed for the various ligand moieties. The complexity of the

$^{13}\text{C}$  and  $^1\text{H}$  spectra when compared to the precipitate spectra coupled with the probable phosphine decomposition, make it likely that the residue is a mixture of reaction by-products and ligand decomposition products.

### Summary.

The phosphine decomposition has highly complicated the analysis procedure. The lack of splitting in the  $^{13}\text{C}$  spectrum and the single resonance at 0 ppm in the  $^{31}\text{P}$  spectrum indicates that any co-ordination to iridium is via ligand fragments rather than the ligand, but the resonant positions do not match known Ir-C shift patterns. It is therefore impossible to do any more than suggest a possible structure for the major species observed.

## CHAPTER 6

### EXPERIMENTAL

#### 6.1 Polymerisation of 7-norbornene dicarboxylic acid using $\text{RuCl}_3 \cdot 3\text{H}_2\text{O}$ .

Initial experiments were performed to examine the polymerisation of norbornene dicarboxylic acid using  $\text{RuCl}_3 \cdot 3\text{H}_2\text{O}$  as a catalyst. These experiments were performed to compare with the results obtained by Feast and Harrison for the polymerisation of 7-oxanorbornene dicarboxylic acid<sup>24</sup>.

##### Experiment 6.1.1.

A norbornene dicarboxylic acid solution (450 ml, 0.01 M) was warmed and held at 55°C and a  $\text{RuCl}_3 \cdot 3\text{H}_2\text{O}$  solution (50ml,  $6.25 \times 10^{-4}$  M) was warmed similarly. After 1 hour at this temperature, the two solutions were mixed and charged to the reaction vessel. The reaction vessel was a double jacketed glass reactor fitted with a mechanical stirrer. Temperature controlled water at 55°C was circulated through the glass jacket. After approximately 2 days, an amount of fine, brown precipitate came out of solution. Attempts to retrieve the precipitate by normal filtration methods proved unsuccessful due to the adhesive nature of the product which could not be removed from the filter paper or sinter so separation was performed by centrifugation and decantion. Even so, due to the exceptionally fine nature of the precipitate, it proved impossible to completely separate it from all the solution, so the final amount of liquid was removed by evaporation. Therefore no meaningful yield can be quoted.

##### Experiment 6.1.2.

During initial attempts at characterisation, it was found that the precipitate would only dissolve in dilute base. Therefore it was decided to attempt a polymerisation in basic solution to delay the onset of precipitation and hopefully increase the molecular weight. The same experiment as previously described was repeated but solutions were made up in 0.02M KOH. After 2 days no precipitate was noticed so the experiment was stopped. The solution was diluted with THF and product precipitated by addition of hexane. This process was repeated a number of times as on leaving the solution overnight more product was found to have precipitated out. However, as explained previously, no meaningful yield can be quoted due to filtration problems. In total only 0.03g was successfully retrieved for analysis.

On leaving the solution from 6.1.1 standing over an extended period of time (weeks) it was observed that small amounts of opaque polymer had been formed in solution. The characteristics of this and all other products from these experiments can be found described in Section 7.1.

## **6.2 - Dilatometry**

A number of experiments were performed in an attempt to measure the rate of polymerisation of a bicyclic monomer using a ruthenium complex catalyst by dilatometry. Procedural details are given in Section 2.2.2. Experimental details are given below in Tables 6.2.1 to 6.2.10. Previous experiments using both  $\text{RuCl}_3 \cdot 3\text{H}_2\text{O}$  and  $\text{Ru}(\text{CO})\text{Cl}_2(\text{H}_2\text{O})$  had produced varying amounts of precipitate during reaction and as precipitation would not be conducive to measuring rates by dilatometry, it was decided that experiments should be performed in basic KOH solutions. This successfully prevented (or delayed the onset of) precipitation.

**Table 6.2.1 - Experimental details for Dil1**

Monomer <sup>a</sup> Concentration <sup>c</sup> / mol l <sup>-1</sup>	Catalyst <sup>b</sup> Concentration <sup>c</sup> / mol l <sup>-1</sup>	Temperature / °C	Duration / hours
0.06	0.00375	70	144

*a) Monomer = norbornene dicarboxylic acid.*

*b) Catalyst =  $\text{RuCl}_3 \cdot 3\text{H}_2\text{O}$ .*

*c) Solutions made up in 0.12M KOH*

**Table 6.2.2 - Experimental details for Dil2**

Monomer <sup>a</sup> Concentration <sup>c</sup> / mol l <sup>-1</sup>	Catalyst <sup>b</sup> Concentration <sup>c</sup> / mol l <sup>-1</sup>	Temperature / °C	Duration / hours
0.06	0.00375	70	97

*a) Monomer = norbornene dicarboxylic acid.*

*b) Catalyst =  $\text{Ru}(\text{CO})\text{Cl}_2(\text{H}_2\text{O})$*

*c) Solutions made up in 0.12M KOH*



**Table 6.2.3 - Experimental details for Dil3**

	Monomer <sup>a</sup> Concentration <sup>e</sup> / mol l <sup>-1</sup>	Catalyst Concentration <sup>e</sup> / mol l <sup>-1</sup>	Temperature / °C	Duration / hours
Sample 1 <sup>b</sup>	-	-	60	98
Sample 2 <sup>b</sup>	-	-	60	98
Sample 3 <sup>c</sup>	0.1	0.003	60	98
Sample 4 <sup>c</sup>	0.1	0.003	60	98
Sample 5 <sup>c</sup>	0.1	0.003	60	98
Sample 6 <sup>d</sup>	0.1	0.003	60	98
Sample 7 <sup>d</sup>	0.1	0.003	60	98
Sample 8 <sup>d</sup>	0.1	0.003	60	98

a) Monomer = norbornenedicarboxylic acid.

b) Control dilatometers containing water only.

c) Catalyst = RuCl<sub>3</sub>.3H<sub>2</sub>O.

d) Catalyst = Ru(CO)Cl<sub>2</sub>(H<sub>2</sub>O).

e) Solutions made up in 0.2M KOH.

**Table 6.2.4 - Experimental details for Dil4.**

	Monomer <sup>a</sup> Concentration <sup>e</sup> / mol l <sup>-1</sup>	Catalyst Concentration <sup>e</sup> / mol l <sup>-1</sup>	Temperature / °C	Duration / hours
Sample 1 <sup>b</sup>	-	-	70	102
Sample 2 <sup>b</sup>	-	-	70	102
Sample 3 <sup>c</sup>	0.1	0.003	70	102
Sample 4 <sup>c</sup>	0.1	0.006	70	102
Sample 5 <sup>c</sup>	0.1	0.013	70	102
Sample 6 <sup>d</sup>	0.1	0.003	70	102
Sample 7 <sup>d</sup>	0.1	0.006	70	102

a) Monomer = norbornenedicarboxylic acid.

b) Control dilatometers containing water only.

c) Catalyst = RuCl<sub>3</sub>.3H<sub>2</sub>O.

d) Catalyst = Ru(CO)Cl<sub>2</sub>(H<sub>2</sub>O).

e) Solutions made up in 0.2M KOH.

**Table 6.2.5 - Experimental details for Dil5**

	Monomer <sup>a</sup> Concentration <sup>e</sup> / mol l <sup>-1</sup>	Catalyst Concentration <sup>e</sup> / mol l <sup>-1</sup>	Temperature / °C	Duration / hours
Sample 1 <sup>b</sup>	-	0.003	70	572
Sample 2 <sup>b</sup>	0.1	-	70	572
Sample 3 <sup>c</sup>	0.1	0.003	70	572
Sample 4 <sup>c</sup>	0.05	0.003	70	572
Sample 5 <sup>c</sup>	0.025	0.003	70	572
Sample 6 <sup>d</sup>	0.1	0.005	70	572
Sample 7 <sup>d</sup>	0.1	0.01	70	572
Sample 8 <sup>d</sup>	0.1	0.02	70	572

a) Monomer = norbornenedicarboxylic acid.

b) Control dilatometers containing monomer or catalyst solutions only.

c) Catalyst = RuCl<sub>3</sub>·3H<sub>2</sub>O.

d) Catalyst = Ru(CO)Cl<sub>2</sub>(H<sub>2</sub>O).

e) Solutions made up in KOH solution (2M KOH per 1M monomer).

**Table 6.2.6 - Experimental details for Dil6**

	Monomer <sup>a</sup> Concentration / mol l <sup>-1</sup>	Catalyst <sup>e</sup> Concentration / mol l <sup>-1</sup>	Temperature / °C	Duration / hours
Sample 1 <sup>b</sup>	-	0.003	85	96
Sample 2 <sup>b</sup>	0.1	-	85	96
Sample 3 <sup>c</sup>	0.1	0.003	85	96
Sample 4 <sup>c</sup>	0.05	0.003	85	96
Sample 5 <sup>c</sup>	0.025	0.003	85	96
Sample 6 <sup>d</sup>	0.1	0.003	85	96
Sample 7 <sup>d</sup>	0.05	0.003	85	96
Sample 8 <sup>d</sup>	0.025	0.003	85	96

a) Monomer = norbornenedicarboxylic acid.

b) Control dilatometers containing monomer or catalyst solutions only.

c) Solutions made in 0.2M KOH.

d) Solutions made up in 0.4M KOH solution.

e) Catalyst = RuCl<sub>3</sub>·3H<sub>2</sub>O

**Table 6.2.7 - Experimental details for Dil7**

	Monomer <sup>a</sup> Conc. / mol l <sup>-1</sup>	Catalyst <sup>b</sup> Conc. / mol l <sup>-1</sup>	KOH Conc. / mol l <sup>-1</sup>	Temp. / °C	Duration. / hours
Sample 1 <sup>c</sup>	-	0.003	-	50	228
Sample 2 <sup>c</sup>	0.1	-	0.2	50	228
Sample 3	0.1	0.003	0.2	50	228
Sample 4	0.1	0.003	0.25	50	228
Sample 5	0.1	0.003	0.3	50	228
Sample 6	0.1	0.003	0.35	50	228
Sample 7	0.1	0.003	0.4	50	228
Sample 8	0.1	0.003	0.45	50	228

a) Monomer = norbornenedicarboxylic acid.

b) Catalyst = RuCl<sub>3</sub>.3H<sub>2</sub>O.

c) Controls containing monomer or catalyst solutions only.

**Table 6.2.8 - Experimental details for Dil8.**

	Monomer <sup>a</sup> Conc. / mol l <sup>-1</sup>	Catalyst <sup>b</sup> Conc. / mol l <sup>-1</sup>	KOH Conc. / mol l <sup>-1</sup>	Temp. / °C	Duration. / hours
Sample 1 <sup>c</sup>	-	0.003	-	50	218
Sample 2 <sup>d</sup>	0.1	-	0.2	50	218
Sample 3	0.1	0.003	0	50	218
Sample 4	0.1	0.003	0.05	50	218
Sample 5	0.1	0.003	0.1	50	218
Sample 6	0.1	0.003	0.15	50	218
Sample 7	0.1	0.003	0.2	50	218
Sample 8	0.1	0.003	0.4	50	218

a) Monomer = oxanorbornenedicarboxylic acid.

b) Catalyst = RuCl<sub>3</sub>.3H<sub>2</sub>O.

c) Catalyst control.

d) Catalyst control containing norbornenedicarboxylic acid.

**Table 6.2.9 - Experimental details for Dil9.**

	Monomer <sup>a</sup> Conc. / mol l <sup>-1</sup>	Catalyst <sup>b</sup> Conc. / mol l <sup>-1</sup>	KOH Conc. / mol l <sup>-1</sup>	Temp. / °C	Duration. / hours
Sample 1 <sup>c</sup>	-	0.0167	-	60	1.5
Sample 2 <sup>d</sup>	0.5	-	-	60	1.5
Sample 3	0.5	0.0167	-	60	1.5
Sample 4	0.5	0.0167	-	60	1.5
Sample 5	0.5	0.0167	0.1	60	1.5
Sample 6	0.5	0.0167	0.1	60	1.5

*a) Monomer = oxanorbornenedicarboxylic acid.*

*b) Catalyst = RuCl<sub>3</sub>·3H<sub>2</sub>O.*

*c) Catalyst control.*

*d) Monomer control containing oxanorbornenedicarboxylic acid.*

**Table 6.2.10 - Experimental details for Dil10.**

	Monomer <sup>a</sup> Concentration. / mol l <sup>-1</sup>	KOH Concentration. / mol l <sup>-1</sup>	Temperature. / °C	Duration. / hours
Sample 1 <sup>b</sup>	0.5	-	50	27
Sample 2 <sup>c</sup>	0.5	-	50	27
Sample 3 <sup>c</sup>	0.5	1	50	27
Sample 4 <sup>d</sup>	-	-	50	27

*a) Monomer = oxanorbornenedicarboxylic acid.*

*b) Monomer solution prepared and held at 50°C for 24 hours before introducing to the dilatometer.*

*c) Monomer solution freshly prepared.*

*d) Control containing water only.*

Tables of data are included in Appendix A - Tables A2 to A11, and the results are discussed in section 7.2.

### 6.3 - Interaction between 7-Oxanorbornene dicarboxylic acid and Ru(CO)Cl<sub>2</sub>(H<sub>2</sub>O).

Reaction solutions were prepared at various stages during the period of research with various monomer/catalyst ratios and held at elevated temperature. In all cases, the colour of solution changed from light yellow to deep amber over a period of seven days. Accompanying the colour change was the appearance of precipitate starting after approximately 2 days. Time before first appearance of precipitate decreased as catalyst concentration increased. The same precipitate was recovered when reaction was performed in either an argon or normal atmosphere. After a given amount of time, reaction was stopped and the precipitate collected by filtration. The solute was then reduced to dryness and the residue recovered. The physical properties and analysis of the products appears in Section 7.3. Table 6.3.1 gives experimental details of the reaction solutions prepared.

**Table 6.3.1 - Experimental details for reaction between 7-oxanorbornene dicarboxylic acid and Ru(CO)Cl<sub>2</sub>(H<sub>2</sub>O).**

	Monomer <sup>a</sup> Conc. / mol l <sup>-1</sup>	Catalyst <sup>b</sup> Conc. / mol l <sup>-1</sup>	Ratio (effective ratio in parentheses.)	Time of reaction / hours	Temp. / °C	Precipitate yield / %
Run 1	0.25	0.025	200:20 (10:1)	200	60	17
Run 2	0.25	0.01875	200:13 (15:1)	200	60	17
Run 3	0.03	3 x 10 <sup>-4</sup>	24:0.24 (100:1)	125	70	25
Run 4	0.00125	1.25 x 10 <sup>-5</sup>	1:0.01 (100:1)	5	100	10
Run 5 <sup>c</sup>	0.00125	1.25 x 10 <sup>-5</sup>	1:0.01 (100:1)	5	100	10

a) Monomer = 7-oxanorbornene dicarboxylic acid.

b) Catalyst = Ru(CO)Cl<sub>2</sub>(H<sub>2</sub>O).

c) Experiment performed under argon atmosphere.

### 6.4 - Interaction between 7-oxanorbornene dicarboxylic acid and Ru(CO)Cl<sub>2</sub>(H<sub>2</sub>O) monitored by UV Spectroscopy.

A number of experiments were performed to monitor the reaction between 7-oxanorbornene-2,3-dicarboxylic acid and Ru(CO)Cl<sub>2</sub>(H<sub>2</sub>O) at elevated temperature. Throughout this section, 'monomer' refers to 7-oxanorbornene-2,3-dicarboxylic acid and 'catalyst' refers to Ru(CO)Cl<sub>2</sub>(H<sub>2</sub>O).

Initial experiments were performed to measure the UV/Vis spectra of monomer, catalyst and monomer/catalyst solutions and their variation over time at elevated temperature was monitored. These experiments showed that monomer and catalyst spectra did not vary over time (See Fig 6.4.1) but the spectrum from the monomer/catalyst solution varied in the manner shown (See Fig 6.4.2). A local minimum at 323 nm was identified and this wavelength was used for continuous monitoring in further experiments.

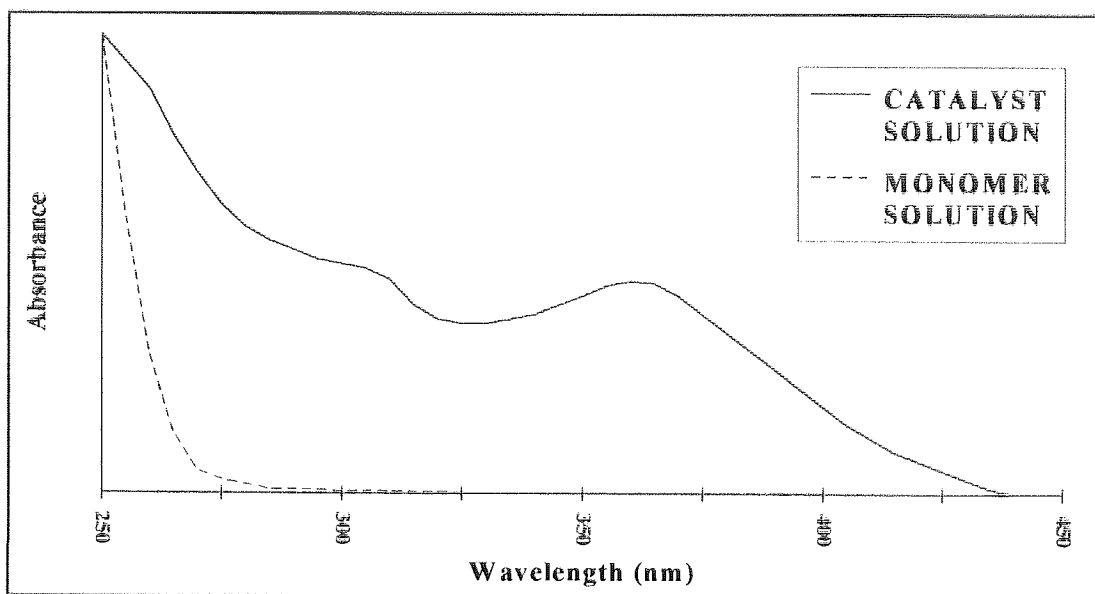


Fig 6.4.1 - Typical UV/Vis spectra for 7-oxanorbornene-2,3-dicarboxylic acid and  $\text{Ru}(\text{CO})\text{Cl}_2(\text{H}_2\text{O})$  solutions.

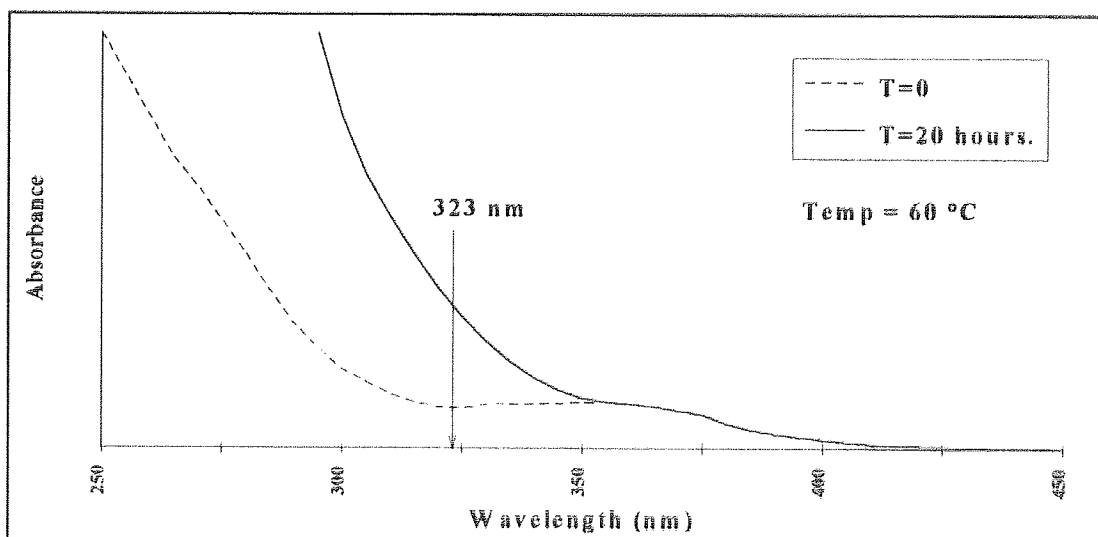


Fig 6.4.2 - Typical change in UV/Vis spectrum for monomer/catalyst solution over time at elevated temperature.

Five groups of experiments (UV1-UV5) were performed with variations in time-scale and reactant concentrations. Unfortunately, due to instrumentation problems, various spectrometers and subsequently data collection methods were used. As a result, experimental procedure varies between some of the groups of experiments but is consistent within individual groups. Procedural details are given in section 2.2.5. Experimental details for all the groups of experiments are given in Tables 6.4.1 to 6.4.5.

**Table 6.4.1 - Experimental details for UV1**

UV1	Monomer Conc. / mol l <sup>-1</sup> Reaction solution.	Catalyst Conc. / mol l <sup>-1</sup> Reaction solution.	Experiment Duration / hours	Temp. / °C	Experimental Procedure
Sample 1	0.25	0.025	184	60	1
Sample 2	0.25	0.01875	184	60	1
Sample 3	0.25	0.0125	184	60	1
Sample 4	0.25	0.00625	184	60	1
	Monomer Conc. / mol l <sup>-1</sup> Analysis solution,	Catalyst Conc. / mol l <sup>-1</sup> Analysis solution.			
Sample 1	0.01	0.001	184	60	1
Sample 2	0.01	0.00075	184	60	1
Sample 3	0.01	0.0005	184	60	1
Sample 4	0.01	0.00025	184	60	1

**Table 6.4.2 - Experimental details for UV2**

UV2	Monomer Conc. / mol l <sup>-1</sup>	Catalyst Conc. / mol l <sup>-1</sup>	Experiment Duration / hours	Temp. / °C	Experimental Procedure
Sample 1	0.01	0.001	36	60	2
Sample 2	0.01	0.0005	36	60	2
Sample 3	0.01	0.0002	36	60	2

**Table 6.4.3 - Experimental details for UV3**

UV3	Monomer Conc. / mol l <sup>-1</sup>	Catalyst Conc. / mol l <sup>-1</sup>	Experiment Duration / hours	Temp. / °C	Experimental Procedure
Sample 1	0.25	0.025	3.5	70	3
Sample 2	0.2	0.025	3.5	70	3
Sample 3	0.15	0.025	3.5	70	3
Sample 4	0.1	0.025	3.5	70	3

**Table 6.4.4 - Experimental details for UV4.**

UV4	Monomer Conc. / mol l <sup>-1</sup>	Catalyst Conc. / mol l <sup>-1</sup>	Experiment Duration / hours	Temp. / °C	Experimental Procedure
Sample 1	0.4	0.025	143	70	3
Sample 2	0.35	0.025	143	70	3
Sample 3	0.3	0.025	143	70	3

**Table 6.4.5 - Experimental details for UV5**

UV5	Monomer Conc. / mol l <sup>-1</sup>	Catalyst Conc. / mol l <sup>-1</sup>	Experiment Duration / hours	Temp. / °C	Experimental Procedure
Sample 1	0.01	0.001	70	70	3
Sample 2	0.16	0.0016	70	70	3
Sample 3	0.25	0.00025	70	70	3



Data tables are included in Appendix A - Tables A12 to A16 and plots of results in section 7.3. Below are two examples of typical plots. Fig 6.4.3 shows the rise in absorbance over the initial period of reaction and Fig 6.4.4 shows a complete plot over the full time scale of an extended reaction.

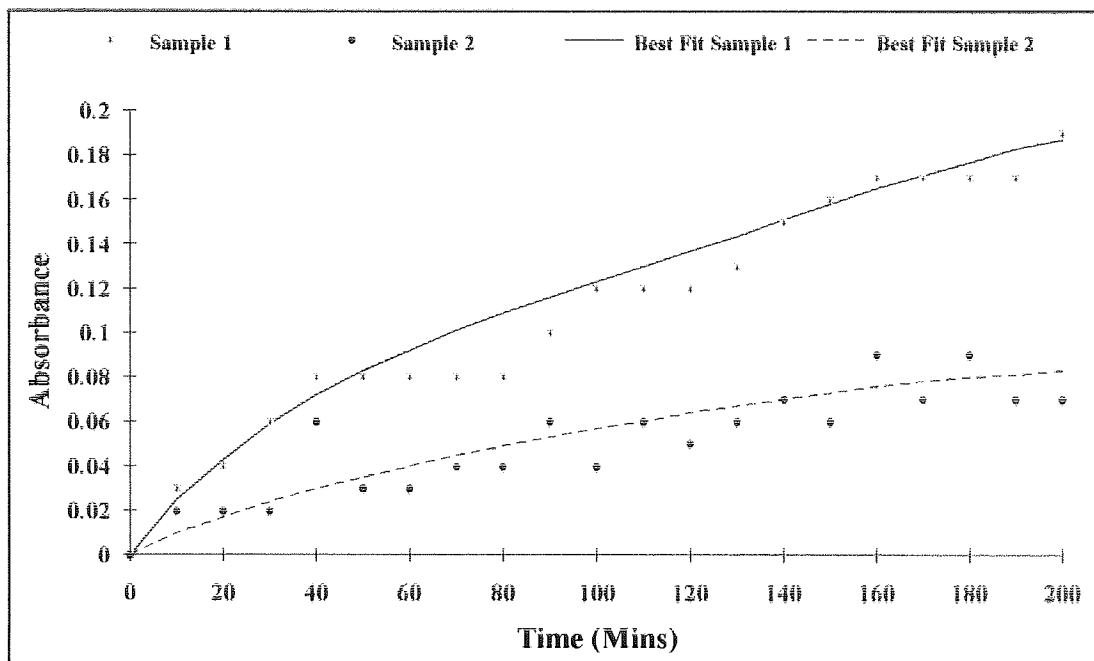


Fig 6.4.3 - Plot of Absorbance (323 nm) vs Time for UV2 - samples 1 and 2.

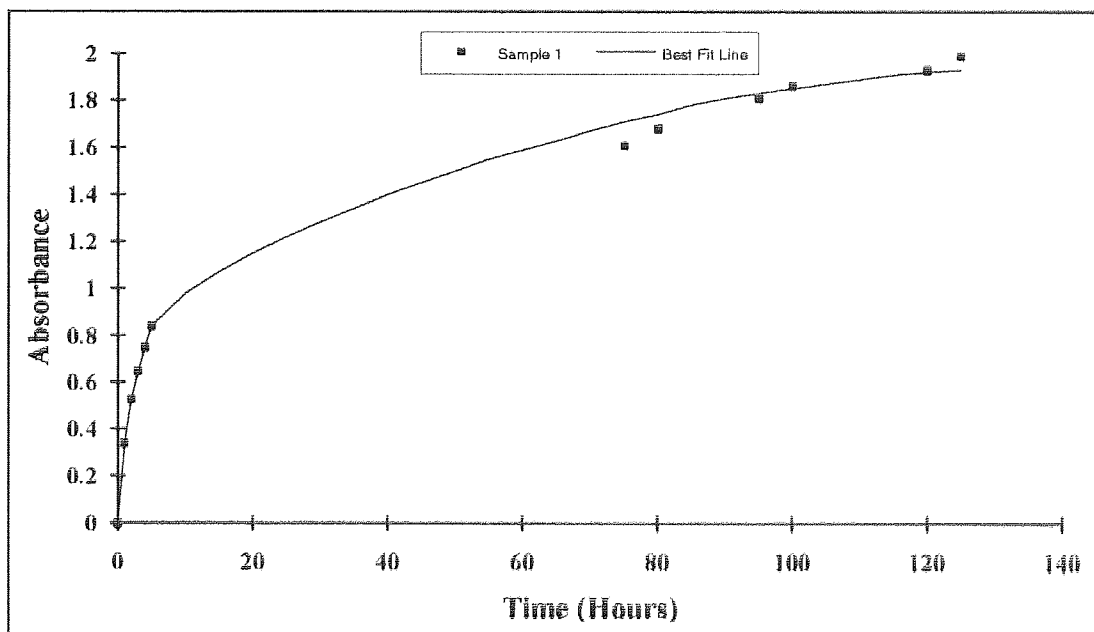


Fig 6.4.4 - Plot of Absorbance (323nm) vs time for UV4 - sample 1.

### 6.5 - Interaction between Bicyclic Monomers and a Ru-P(CH<sub>2</sub>OH)<sub>3</sub> Complex.

The interaction between bicyclic monomers (usually 7-oxanorbornene dicarboxylic acid) and the orange 'toffee' product from the reaction between ruthenium compounds and P(CH<sub>2</sub>OH)<sub>3</sub> was studied on a number of occasions throughout the course of the research. In all cases the 'toffee' product was deemed to be Ru(P(CH<sub>2</sub>OH)<sub>3</sub>)<sub>3</sub>Cl<sub>2</sub> for the purpose of calculating appropriate monomer:catalyst ratios. The experiments performed can be usefully arranged into 3 sets (6.5.1, 6.5.2 and 6.5.3) which are presented below in chronological order. In all cases, catalyst refers to the orange toffee product from the reaction between ruthenium compounds and P(CH<sub>2</sub>OH)<sub>3</sub>.

#### Experimental Set 6.5.1.

Table 6.5.1- Experimental details for Set 6.5.1.

	Monomer <sup>a</sup> Conc. / mol l <sup>-1</sup>	Catalyst Conc. / mol l <sup>-1</sup>	Monomer:Cat ratio.	Duration of experiment. / days	Temp. / °C
Sample 1	0.1	0.002	100:2	4	70
Sample 2	0.1	0.001	100:1	4	70

*a) Monomer = 7-oxanorbornene dicarboxylic acid.*

This set of experiments was performed in sealed flasks suspended in a constant temperature water bath. After the completion of the experiment, sample 1 was cooled, reduced to dryness and the residue recovered for analysis. Sample 2 produced a quantity of deep red precipitate after approximately 24 hours. This was recovered by decanting the hot solution, leaving 0.28g of a brown/red solid. The solution was then cooled, producing a small quantity (0.9g) of off-white solid which was recovered by filtration. The remaining solution was reduced to dryness and the residue recovered for analysis.

### Experimental Set 6.5.2.

**Table 6.5.2- Experimental details for Set 6.5.2.**

	Monomer <sup>a</sup> Conc. / mol l <sup>-1</sup>	Catalyst Conc. / mol l <sup>-1</sup>	Monomer:Cat ratio.	Duration of experiment. / days	Temp. / °C
Sample 1	1	0.03	100:3	8	70
Sample 2	1	0.02	100:2	8	70
Sample 3	1	0.01	100:1	8	70
Sample 4	1	0.005	100:0.5	8	70
Sample 5	1	0.003	100:0.33	8	70

*a) Monomer = 7-oxanorbornene dicarboxylic acid.*

This set of experiments was performed in sealed test tubes inserted into a multi test-tube heater. After approximately 16 hours a darkening of the solutions from an initial light yellow or colourless (depending on the concentration of the catalyst) was noticed until the solutions reached a deep amber colour at the end of the experiment. Deposition of a red/brown precipitate was noticed in all the samples with samples 1 and 2 depositing precipitate first, after approximately 16 hours. The precipitate initially appeared as a red oil on the surface of the reaction vessels but as the amount increased, it could be clearly seen floating in solution. The precipitate was not dense enough to sink to the bottom of the vessel until the last couple of days of the experiment. This suggests that the precipitate was either increasing in density during the course of the reaction or precipitate particles were adhering together. At the end of the experiment, the solutions were filtered through a sinter funnel and the precipitate recovered by taking up in THF and then reducing to dryness under vacuum. The remaining solutions were reduced to dryness and the residues recovered for analysis. Table 6.5.3 gives the yields of precipitate for each sample.

**Table 6.5.3 - Precipitate yields for Set 6.5.2**

	Mass of Precipitate / g	Percentage yield / %
Sample 1	0.014	1.3
Sample 2	0.019	1.8
Sample 3	0.036	3.6
Sample 4	0.026	2.7
Sample 5	0.024	2.5

### Experimental Set 6.5.3

This experimental set was performed using the multi test-tube heater as for Set 6.5.2.

**Table 6.5.4 - Experimental details for Set 6.5.3**

	Monomer Conc. / mol l <sup>-1</sup>	Catalyst Conc. / mol l <sup>-1</sup>	Monomer:Cat ratio.	Duration of experiment. / days	Temp. / °C
Sample 1 <sup>a</sup>	1	0.01	100:1	7	70
Sample 2 <sup>a</sup>	1	0.002	500:1	7	70
Sample 3 <sup>a</sup>	1	0.001	1000:1	7	70
Sample 4 <sup>b</sup>	1	0.01	100:1	7	70
Sample 5 <sup>c</sup>	0.1	0.001	100:1	7	70

*a) Monomer = 7-oxanorbornene dicarboxylic acid.*

*b) Monomer = Maleic acid.*

*c) Monomer = 7-norbornene dicarboxylic acid.*

The appearance of precipitate and the colour change as described in Set 6.5.2 occurred in the same fashion in Set 3 with the exception that for samples 4 and 5, no colour change occurred and no precipitate was produced. For samples 1, 2 and 3, the precipitate was retrieved by centrifugation and decantion to avoid any contact with THF. However due to the nature of the precipitate, it was impossible to retrieve the product completely free from the mother liquor, therefore the remaining drops of solution had to be removed by evaporation. The products were stored in a vacuum dessicator over P<sub>2</sub>O<sub>5</sub> as they were found to be highly hygroscopic.

**Table 6.5.5 - Precipitate yields for Set 6.5.3.**

	Mass of precipitate / g	Percentage Yield / %
Sample 1	0.108	6.5
Sample 2	0.153	9.2
Sample 3	0.052	3.1

## 6.6 - Initiation of polymerisation using ethyl diazoacetate.<sup>47</sup>

A number of experiments were performed to investigate the use of ethyl diazoacetate as an initiator for the polymerisation of 7-oxanorbornene dicarboxylic acid by ruthenium complexes. The experiments can usefully be arranged into 3 sets (6.6.1, 6.6.2 and 6.6.3.) which are described in chronological order.

### Experimental Set 6.6.1.

This experiment used the orange 'toffee' product as the ruthenium catalyst. This was assumed to be  $\text{Ru}(\text{P}(\text{CH}_2\text{OH})_3)_3\text{Cl}_2$  for calculation purposes.

$\text{Ru}(\text{P}(\text{CH}_2\text{OH})_3)_3\text{Cl}_2$  (0.0643g,  $1.2 \times 10^{-4}$  moles) was dissolved in water (5mls). Ethyl diazoacetate (0.0135g,  $1.2 \times 10^{-4}$  moles) was added carefully dropwise via a microsyringe attached to a micrometer screw attachment. The mixture was shaken thoroughly for a few minutes before adding to a pre-warmed ( $70^\circ\text{C}$ ) 7-oxanorbornene dicarboxylic acid solution (1.97g in 7mls water). This gave a final solution with a monomer:catalyst ratio of 100:1. The mixture was held for 4 days at  $70^\circ\text{C}$  during which time a darkening in colour was noticed from light to deep yellow/orange, with a dark oil deposited on the surface of the vessel. The solution was decanted off and the oil taken up in THF, then dried yielding 0.145g of a sticky black solid. This represents a 6.6% yield based on monomer. The remaining solution was reduced to dryness and the residue recovered for analysis.

### Experimental Set 6.6.2.

This experiment used  $\text{Ru}(\text{CO})\text{Cl}_2(\text{H}_2\text{O})$  as the ruthenium catalyst. The same procedure as for 6.6.1 was followed but strong effervescence was noticed on addition of ethyl diazoacetate to the  $\text{Ru}(\text{CO})\text{Cl}_2(\text{H}_2\text{O})$  solution.

**Table 6.6.1 - Experimental details for Set 6.6.2.**

	Monomer Conc. / mol l <sup>-1</sup>	Catalyst Conc. / mol l <sup>-1</sup>	Monomer:Cat ratio.	Duration of experiment. / days	Temp. / °C
Sample 1	1	0.01	100:1	4	70
Sample 2	1	0.003	300:1	4	70

Darkening of the reaction solutions was noticed as for 6.6.1 but no oily product was deposited on the surfaces of the vessel. The solutions were cooled, reduced to dryness and the residue recovered for analysis.

### **Experimental Set 6.6.3**

This set of experiments was performed to check whether the order of addition of diazoester altered the results obtained. The orange 'toffee' product was used as the ruthenium catalyst. As before this was assumed to be  $\text{Ru}(\text{P}(\text{CH}_2\text{OH})_3)_3\text{Cl}_2$  for calculation purposes.

**Table 6.6.2 - Experimental details for Set 6.6.3.**

	Monomer Conc. / mol l <sup>-1</sup>	Catalyst Conc. / mol l <sup>-1</sup>	Monomer:Cat ratio.	Duration of experiment. / days	Temp. / °C
Sample 1 <sup>a</sup>	1	0.01	100:1	4	70
Sample 2 <sup>b</sup>	1	0.01	100:1	4	70
Sample 3 <sup>c</sup>	1	0.01	100:1	4	70

*a) Monomer and catalyst only.*

*b) Catalyst dissolved in 2 mls of water and ethyl diazoacetate added. Added to monomer solution after shaking.*

*c) Catalyst dissolved in monomer solution and shaken before ethyl diazoacetate added.*

Samples 2 and 3 showed signs of deposition of a dark oil on the surface of the vessels. All three solutions were cooled, filtered through a sinter funnel and the residue taken up in THF before drying and retaining for analysis.

**Table 6.6.3- Product yield for 6.6.3.**

	Mass of precipitate / g	Percentage Yield / %
Sample 1	0.125	2.3
Sample 2	0.1	3.0
Sample 3	0.124	2.7

6.7 - Interaction between  $cis-[Ru(en)_2(H_2O)_2]^{2+}$  and 7-oxanorbornene dicarboxylic acid.<sup>71</sup>

$[Ru(en)_2Cl_2]Cl$  (0.03g,  $9 \times 10^{-5}$  moles) was dissolved in 0.1M  $H_2SO_4$  (100 ml) and stirred overnight over fresh zinc amalgam (20 mls) under argon. 10ml samples were removed at regular intervals and analysed by UV/Visible spectroscopy. The reduction from Ru(III) to Ru(II) is accompanied by the appearance of a peak in the UV/Vis spectrum at 300 nm.

20 mls of the  $cis-[Ru(en)_2(H_2O)_2]^{2+}$  solution was removed and added to 20 mls of a 0.1M 7-oxanorbornene dicarboxylic acid solution. This gave a reaction solution with a monomer:catalyst ratio of 100:1. The solution was refluxed overnight and no colour change or appearance of precipitate noticed. The solution was then cooled, reduced and the residue recovered.

6.8 - Interaction between  $[Ru(NH_3)_5N_2]^{2+}$  and 7-oxanorbornene dicarboxylic acid.

Initial attempts to synthesise  $[Ru(NH_3)_5N_2]^{2+}$  via  $[Ru(NH_3)_5Cl]Cl_2$  failed due to scaling down problems (See Sections 5.4.1 to 5.4.3). It was therefore decided to synthesise the  $Ru^{2+}$  ion *in situ* via Allen and Senhoff's route<sup>53</sup> and based on the observations of Bottomley.<sup>72</sup>

The reaction between  $RuCl_3 \cdot 3H_2O$  and hydrazine monohydrate leads to the isolation of  $[Ru(NH_3)_6]Cl_2$  via the scheme given in Fig 6.8.1.

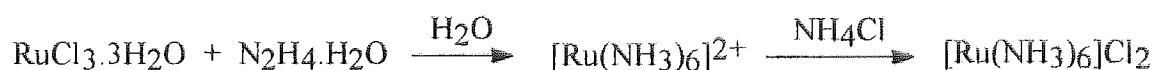


Fig 6.8.1 - Synthesis of  $[Ru(NH_3)_6]Cl_2$ .<sup>53</sup>

However, if excess hydrazine is used, then a sequence of reactions occurs which eventually leads to the production of  $[Ru(NH_3)_5N_2]^{2+}$ , (Fig 6.8.2).<sup>72</sup> The various intermediates can be identified by UV/Vis spectroscopy and the relevant wavelengths are given in the scheme.

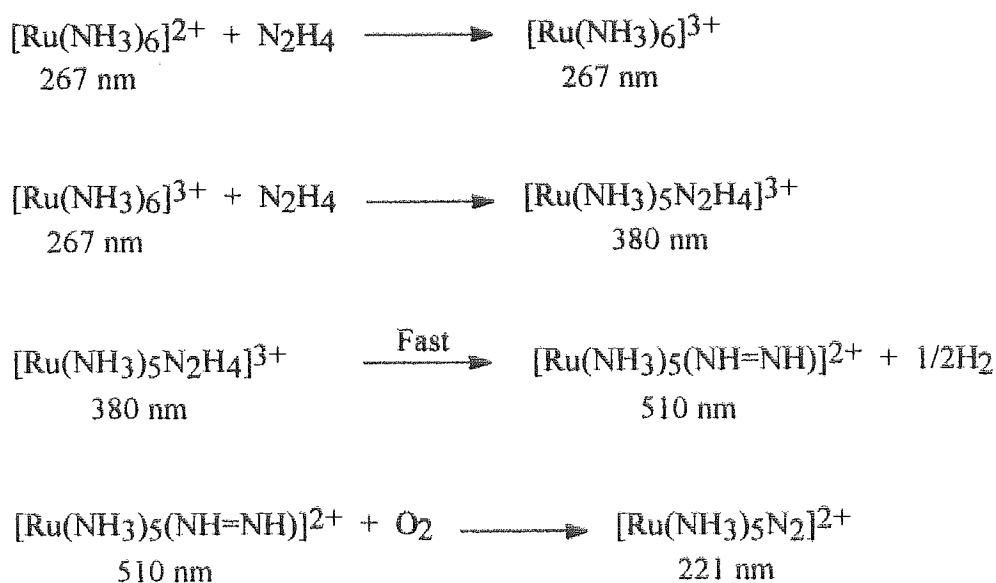


Fig 6.8.2 - Synthetic scheme for  $[\text{Ru}(\text{NH}_3)_5\text{N}_2]^{2+}$ .

$\text{RuCl}_3 \cdot 3\text{H}_2\text{O}$  (0.65g,  $2.5 \times 10^{-3}$  moles) was dissolved in water (20mls) and argon gently bubbled through the solution.  $\text{N}_2\text{H}_4 \cdot \text{H}_2\text{O}$  (10mls) was slowly added (portion wise to control the effervescence) and then the solution was gently refluxed. During the course of the reaction, the solution changed colour from brown/black through red/purple to yellow. After one hour the solution was cooled and a further 10mls of  $\text{N}_2\text{H}_4 \cdot \text{H}_2\text{O}$  added slowly and the solution refluxed again. After approximately 20 minutes, the yellow solution became red in colour and this corresponded to the appearance in the UV/Vis spectrum of a peak at 515 nm. This absorbance can be attributed to the formation of  $[\text{Ru}(\text{NH}_3)_5(\text{NH}=\text{NH})]^{2+}$ . The exclusion of oxygen throughout the experiment prevents the reaction from proceeding to the formation of the dinitrogen species  $[\text{Ru}(\text{NH}_3)_5\text{N}_2]^{2+}$ .

1ml of the  $[\text{Ru}(\text{NH}_3)_5(\text{NH}=\text{NH})]^{2+}$  solution was removed and added to 6ml of a 1M 7-oxanorborene dicarboxylic acid solution, and the mixture was held at  $70^\circ\text{C}$  for 4 days under a normal atmosphere. Initially, when heat was applied, the solution changed colour from red to yellow which is consistent with the formation of  $[\text{Ru}(\text{NH}_3)_5\text{N}_2]^{2+}$  on heating in the presence of oxygen but after a short time the solution changed colour to a deep red/purple and this colour remained for the duration of the experiment. The deep red/purple colour corresponds to a broad absorbance with a maximum at 520 nm. No precipitate was formed either during the reaction or on cooling so the solution was reduced and the residue recovered.



## CHAPTER 7

### RESULTS.

#### 7.1 - Polymerisation of norbornene dicarboxylic acid using $\text{RuCl}_3 \cdot 3\text{H}_2\text{O}$ .

Polymerisation experiments previously described in section 6.1 produced small amounts of a black, low density product. Quantitative isolation of this product proved impossible due to its adherence to filter paper and glass sinters. An attempt to analyse small amounts of isolated product by S.E.C proved unsuccessful due to its insolubility in THF which is the standard S.E.C eluent. Polymerisation solutions which were left standing over a period of time produced small sheets of translucent white/grey product suspended in the mother liquor. This product could be removed using tweezers but when placed into THF it hardened into a solid translucent polymeric material. Re-placing the hard polymer into aqueous solution returned the product into its original form and consistency. The products retrieved from these experiments are consistent with the products retrieved by Feast and Harrison during the polymerisation of 7-oxanorbornene dicarboxylic acid<sup>24</sup>. Unfortunately, molecular weight analysis could not be undertaken due to instrumentation restrictions. However the retrieval of an obviously polymeric material on leaving the reaction solution to stand is a good indication that polymerisation has occurred.

#### 7.2 - Dilatometry as a method for monitoring aqueous ROMP.

Experiments Dil1 and Dil2 were carried out as preliminary experiments using norbornene dicarboxylic acid as monomer and  $\text{RuCl}_3 \cdot 3\text{H}_2\text{O}$  and  $\text{Ru}(\text{CO})\text{Cl}_2(\text{H}_2\text{O})$  respectively as catalysts. The dilatometer in both experiments protruded above the water level in the water bath but the meniscus level was always below the level of the water. The open top of the dilatometer was sealed by placing a suba-seal over the end.

As can be seen in Fig 7.2.1 a drop in meniscus height is seen for both experiments although the overall rate of decrease is not matched by the rate of decrease in height on any given day. The rates of decrease in height (overall and daily) were calculated using Cricket Graph software, using a least squares fit method. The fit is given as  $r^2$  rounded to two decimal places.

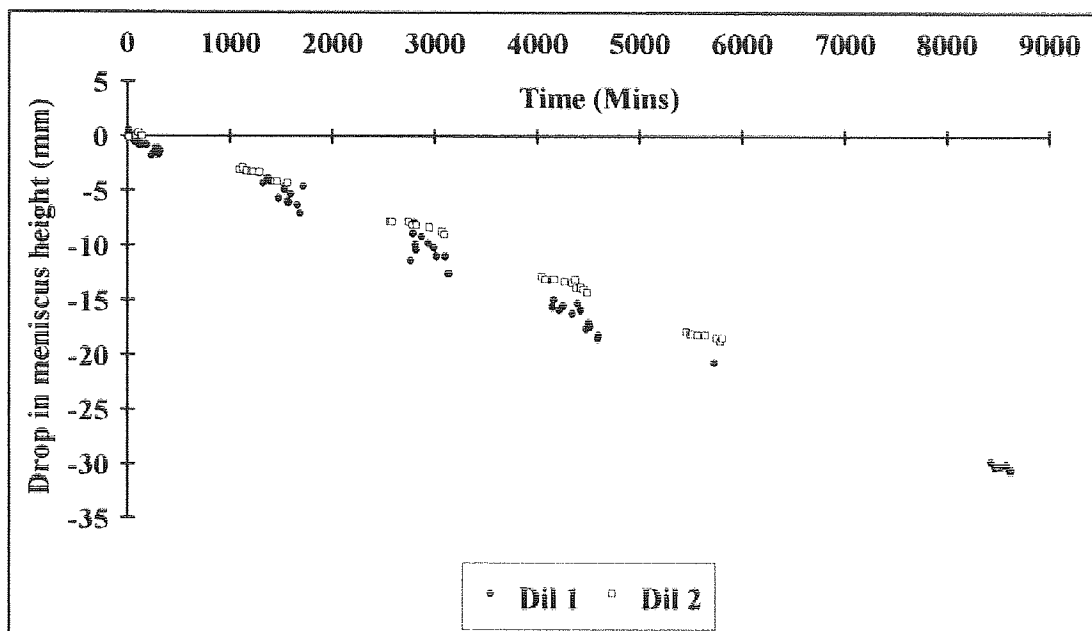


Fig 7.2.1 - Plot of drop in meniscus height vs time for Dil1 and Dil2.

Table 7.2.1 - Rates of change in meniscus height and best straight line fits for Dil1 and Dil2.

	Day 1		Day 2		Day 3		Day 4		Over all	
	Rate	Fit	Rate	Fit	Rate	Fit	Rate	Fit	Rate	Fit
Dil1	-5.7	0.82	-7.8	0.88	-6.9	0.73	-6.5	0.75	-3.6	0.99
Dil2	-3.8	0.93	-2	0.83	-2.8	0.88	-1.9	0.86	-3.3	0.99

$10^4 \times \text{rate} / \text{mm min}^{-1}$

As can be seen both experiments give good best straight line fits over the course of five days (Table 7.2.1). However over the duration of any one day the results obtained are more scattered and the overall profile is very irregular.

Experiment Dil3 was the first experiment performed using an array of 8 identical dilatometers (See 6.2). As with Dil1 and Dil2 the dilatometers were sealed by using suba-seals to cover the top of the dilatometers. The results from Samples 2 and 4 were unusable due to bubble formation in the capillary. The change in height in the control dilatometer (Sample 1) was used to correct the readings from the other dilatometers, and the corrected results plotted. Fig. 7.2.2 shows the plots for samples 3 and 5.

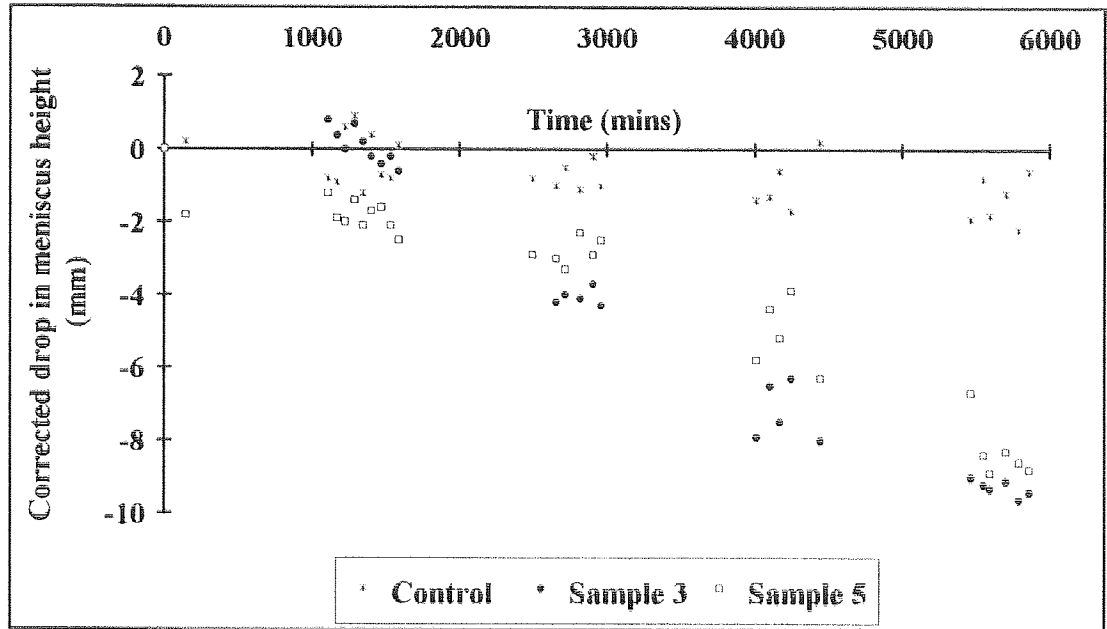


Fig 7.2.2 - Plot of corrected drop in meniscus height vs time for Dil3  
- Samples 3 & 5.

Table 7.2.2 - Rates of change in meniscus height and  
best straight line fits for Dil3.

Sample No.	Day 1		Day 2		Day 3		Day 4		Over all	
	Rate	Fit	Rate	Fit	Rate	Fit	Rate	Fit	Rate	Fit
3	-2.5	0.73	0.23	0.02	-0.75	0.02	-1	0.54	-2.2	0.97
5	-1.5	0.36	0.97	0.08	-1.6	0.07	-3.5	0.44	-1.4	0.9
6	-1.7	0.37	0.86	0.08	-1.2	0.03	-1.8	0.27	-1.9	0.97
7	-1.3	0.16	0.15	0.001	-3.3	0.24	-1.1	0.06	-1.4	0.94
8	-3.8	0.59	0.59	0.02	-3.7	0.35	-0.22	0.003	-2.1	0.96

$10^3 \times \text{rate} / \text{mm min}^{-1}$ .

Although the overall plot seems to indicate that a measurable drop in meniscus height is occurring the large scatter and negligible change in meniscus position during a day of readings suggests that the change in height is not being caused by a change in density within the dilatometer but is being caused by an external influence which appears to vary over the course of the day. It is thought that the cause of this drop in height is a combination of inefficient sealing, allowing evaporation from the dilatometer, and a rise in temperature overnight due to a drop in water level in the water bath and faulty heating control.

For Dil4 the dilatometers were reduced in height so that the top of the capillary was below the level of the water. The capillary head was again covered using a suba-seal. Samples 4 and 5 both became unreadable after one day due to froth formation at the meniscus, which is thought to be due to the higher  $\text{RuCl}_3 \cdot 3\text{H}_2\text{O}$  concentrations in these dilatometers. Plots of change in meniscus height vs time (Fig 7.2.3) and the rates and best straight line fits (Table 7.2.3) for the remaining samples are given below

**Table 7.2.3 - Rates of change in meniscus height and best straight line fits for Dil4  
- Samples 3, 6 & 7**

Sample No.	Day 1		Day 2		Day 3		Day 4		Over all	
	Rate	Fit	Rate	Fit	Rate	Fit	Rate	Fit	Rate	Fit
3	0.85	0.02	-3.3	0.39	-1.8	0.99	3.6	0.57	-2.3	0.97
6	4.0	0.37	-4.0	0.75	2.7	0.96	-0.83	0.01	-3.5	0.95
7	2.1	0.25	-4.8	0.47	1.2	0.26	-4.0	0.6	-3.5	0.98

$10^3 \times \text{rate} / \text{mm min}^{-1}$ .

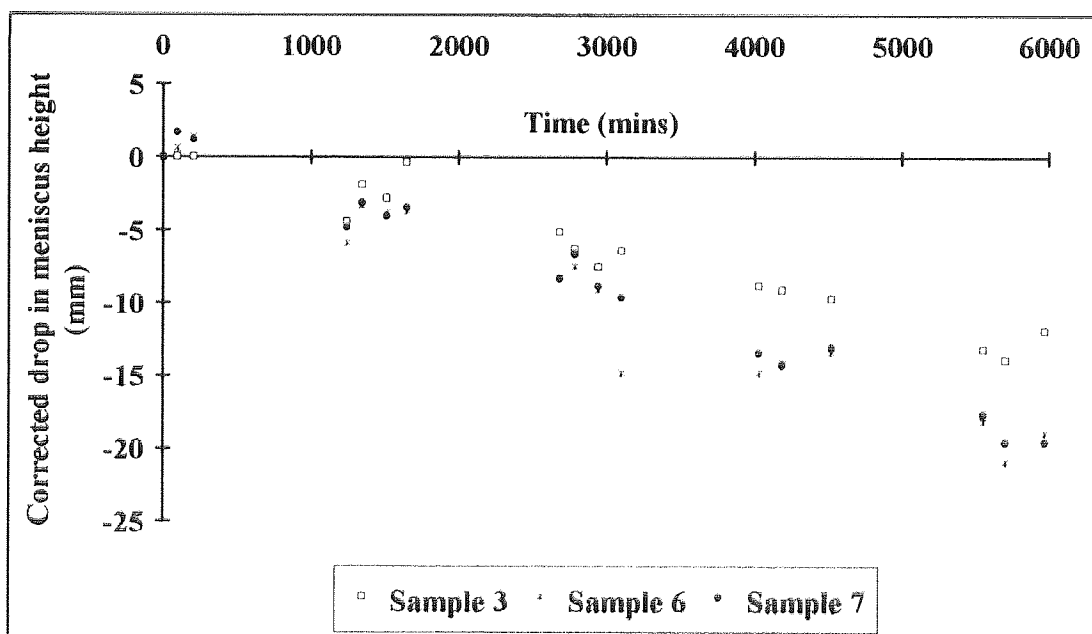


**Fig 7.2.3 - Plot of corrected drop in meniscus height vs time for Dil4  
- Sample 3, 6 & 7**

As for Dil3, the rate of drop in meniscus height for the whole reaction is not matched by the rate of change in height on any given day. There is no obvious reason for this discrepancy since the suspected problem of overnight evaporation has been negated by

lowering the level of the capillary top. However it was still suspected that an increase in temperature overnight (due to a drop in water level coupled with faulty heating) may be to blame

For Dil5 the water bath was modified so as to allow the water level to be topped up should excessive evaporation occur overnight. The dilatometers were sealed differently in this experiment by sticking glass cover slips over the top of the capillaries using Araldite Rapid adhesive. In some cases the cover slips became dislodged but the capillary remained sealed due to a plug of adhesive in the top of the capillary.

Fig. 7.2.4 shows the plots for samples 6, 7 and 8. As readings were taken over a longer time period and at greater time intervals, it is not possible to compare readings in daily groups, but weekly groups of results can be compared in the same way (Table 7.2.4).

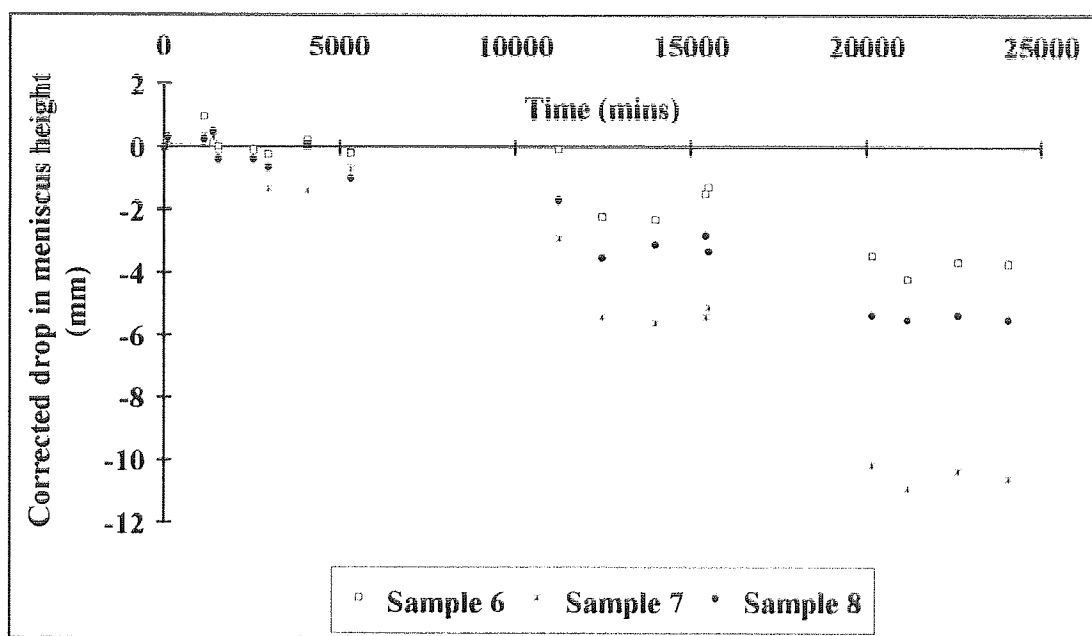


Fig 7.2.4 - Plot of corrected drop in meniscus height vs time for Dil5  
- Samples 6, 7 & 8.

Although over the course of the three weeks the results show a definite decrease in meniscus height the best straight line fit is poor when compared to previous experiments. Most surprisingly however is the lack of any straight line fit during the course of a week for any of the samples. In most cases readings over a week show little or no decrease whatsoever with random scatter as shown by the very low  $r^2$  values (Table 7.2.4). It is possible that the problem of accelerated overnight drops in meniscus height observed in

earlier experiments has been solved but that this problem is still occurring over the weekend.

**Table 7.2.4 - Rates of change in meniscus height and best straight line fits for Dil5.**

Sample No.	Week 1		Week 2		Week 3		Over all	
	$10^4$ Rate / mm min <sup>-1</sup>	Fit / r <sup>2</sup>	$10^4$ Rate / mm min <sup>-1</sup>	Fit / r <sup>2</sup>	$10^4$ Rate / mm min <sup>-1</sup>	Fit / r <sup>2</sup>	$10^4$ Rate / mm min <sup>-1</sup>	Fit / r <sup>2</sup>
3	0.6	0.04	-2.7	0.84	-0.33	0.02	-2.6	0.86
4	-0.08	0	-3.1	0.30	1.8	0.43	-2.6	0.79
5	-0.31	0.01	-2.5	0.30	0.64	0.47	-2.7	0.83
6	-1.3	0.26	-1.8	0.14	-0.02	0	-1.8	0.87
7	-3.2	0.5	-4.1	0.47	-0.5	0.07	-4.8	0.95
8	-2.2	0.40	-2	0.29	-0.2	0.17	-2.6	0.95

Dil6 was set up at a higher temperature and carried out over the course of one week in order to try and avoid the problem of the falling water level over a weekend. Samples 5,6 and 7, which contained twice the level of KOH as the other samples but all three formed precipitate within 90 mins of being in the water bath so no results could be retrieved from these samples.

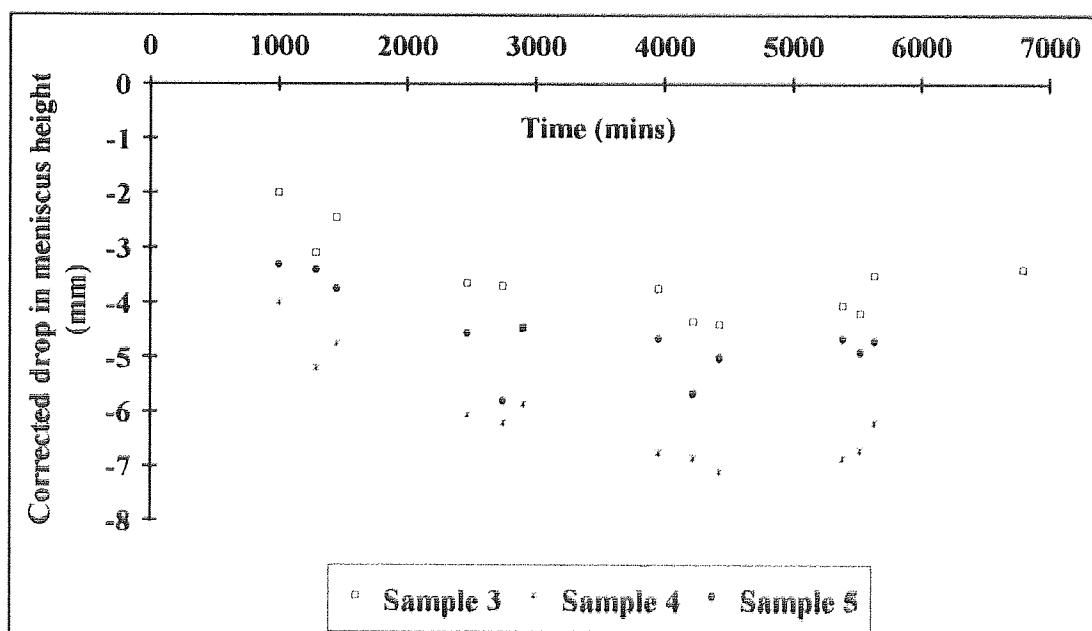


**Fig 7.2.5 - Plot of corrected drop in meniscus height vs time for Dil6 - Samples 3,4 &5**

The plot (Fig 7.2.5) shows very little drop in meniscus height and poor straight line fits for all three samples over the week.

**Table 7.2.5 - Rates of change in meniscus height and best straight line fits for Dil6.**

Sample no.	$10^4$ Rate / mm min <sup>-1</sup>	Fit - $r^2$
3	-2.2	0.31
4	-4.7	0.69
5	-2.9	0.38

As was hoped there was no accelerated drop in meniscus height overnight in any of the samples. However the total drop observed was considerably lower than for previous experiments. This suggests that little if any of the drop observed in earlier experiments is due to polymerisation.

Dil7 was run over ten days at a lower temperature (50°C) to completely negate the problem of falling water levels. The six experimental dilatometers contained increasing levels of KOH and samples 6,7 and 8 all produced precipitate after about 1 hour.

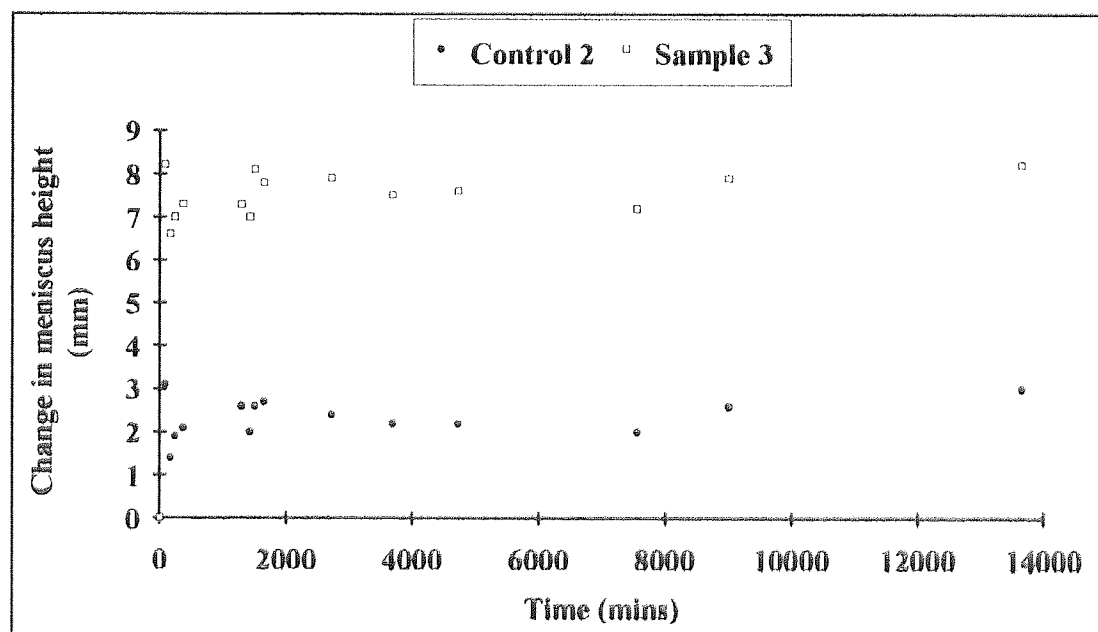


**Fig 7.2.6 - Plot of change in meniscus height vs time for Dil7 - Control 2 and Sample 3.**

The plots from Dil7 clearly showed that, after an initial rise, no drop in meniscus height occurred for any of the samples over the ten day period of observations. The experimental dilatometers behaved almost identically to the control dilatometers and this can be clearly seen when plotting the change in meniscus height for sample 3 and control 2 on the same graph (Fig 7.2.6).

Dil8 was run to see if changing the monomer to oxanorbornene dicarboxylic acid would produce a measurable dilatometric change. The six dilatometers contained varying KOH levels and the two controls contained  $\text{RuCl}_3 \cdot 3\text{H}_2\text{O}$  and norbornene dicarboxylic acid. Samples 4 and 5 produced no results due to bubble formation and sample 8 produced precipitate after approximately 2 hours. The other three samples all clearly showed a dramatic increase in meniscus height over time whilst the controls remained steady. The increase in samples 6 and 7 was large enough to require a re-setting of the liquid level in the capillary. The rise in meniscus height can be clearly seen when the plot of Sample 3 is compared to control 2, which contained norbornene dicarboxylic acid (Fig 7.2.7).

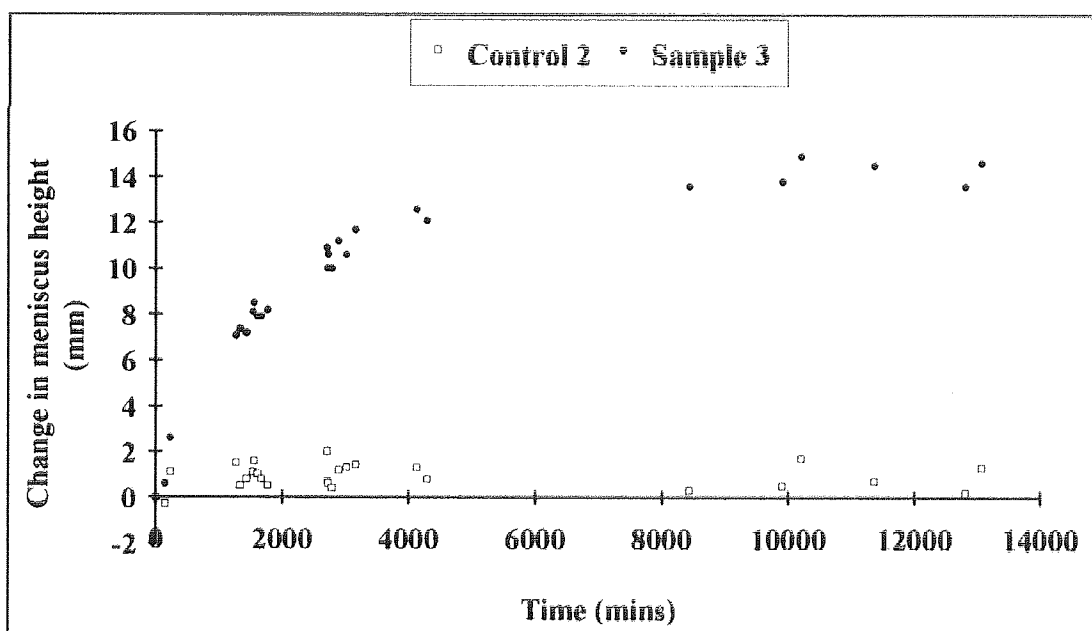


**Fig 7.2.7 - Plot of change in meniscus height vs time for Dil8  
- Control 2 and Sample 3.**

To check these results the experiment was repeated but control 2 was re-filled with oxanorbornene dicarboxylic acid.

The results from Dil9 clearly show that the increase in height is not a function of any polymerisation but is due to the monomer alone. Control 1 containing  $\text{RuCl}_3 \cdot 3\text{H}_2\text{O}$



remains steady whereas control 2 containing oxanorbornene dicarboxylic acid rises at a greater rate than the other four experimental dilatometers (Fig 7.2.8). This suggests that with catalyst present the dilatometers exhibit a net rise in the meniscus even though the polymerisation may be causing a decrease. It is probable that the rise in the monomer solutions alone is due to a reverse Diels-Alder reaction with the monomer decomposing into furan and maleic acid and the resultant drop in density is causing a rise in the meniscus level in the dilatometer.

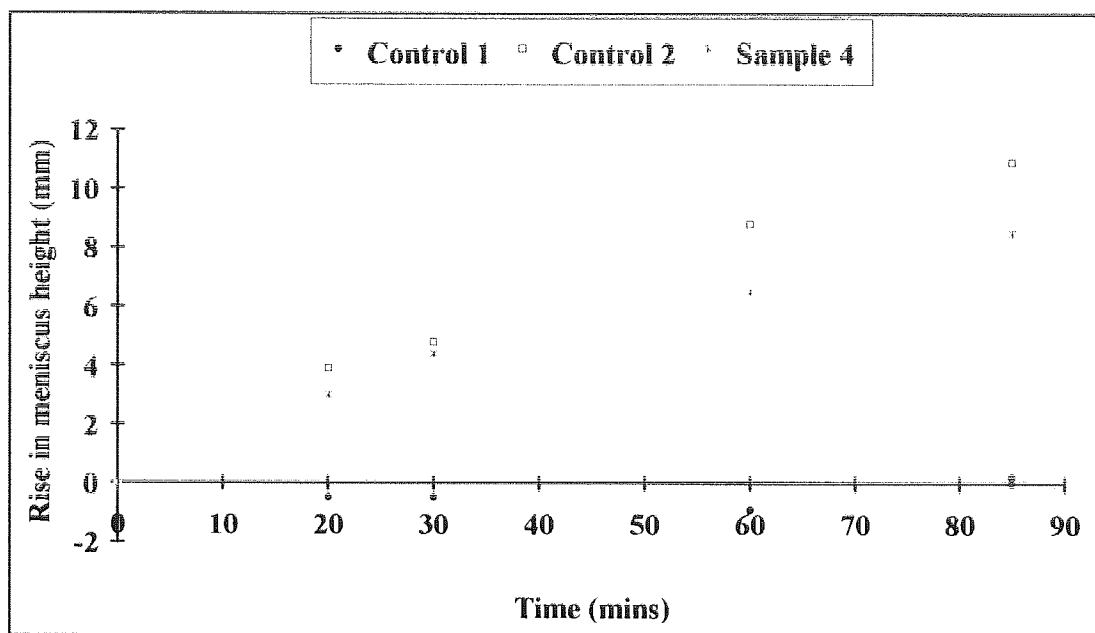


**Fig 7.2.8 - Plot of rise in meniscus height vs time for Dil9  
- Controls 1 & 2 and Sample 4.**

If the rise in the dilatometer is due to a reverse Diels-Alder process then this should level off when an equilibrium is reached between monomer and maleic acid. Dil10 was set up to investigate this.

Sample 2 produced no results due to bubble formation, but samples 1 and 3 produced the expected results. Sample 1 which had been previously held at 50°C for 1 day to establish an equilibrium showed only a very slight rise in meniscus height whereas sample 3 which was freshly prepared showed a rapid rise due to the system reaching equilibrium before levelling off after approximately 8 hours and then rising at a similar rate to sample 1. the continued rise in both the samples is probably due to loss of furan from the system which shifts the position of the equilibrium. These results can be seen in Fig. 7.2.9.

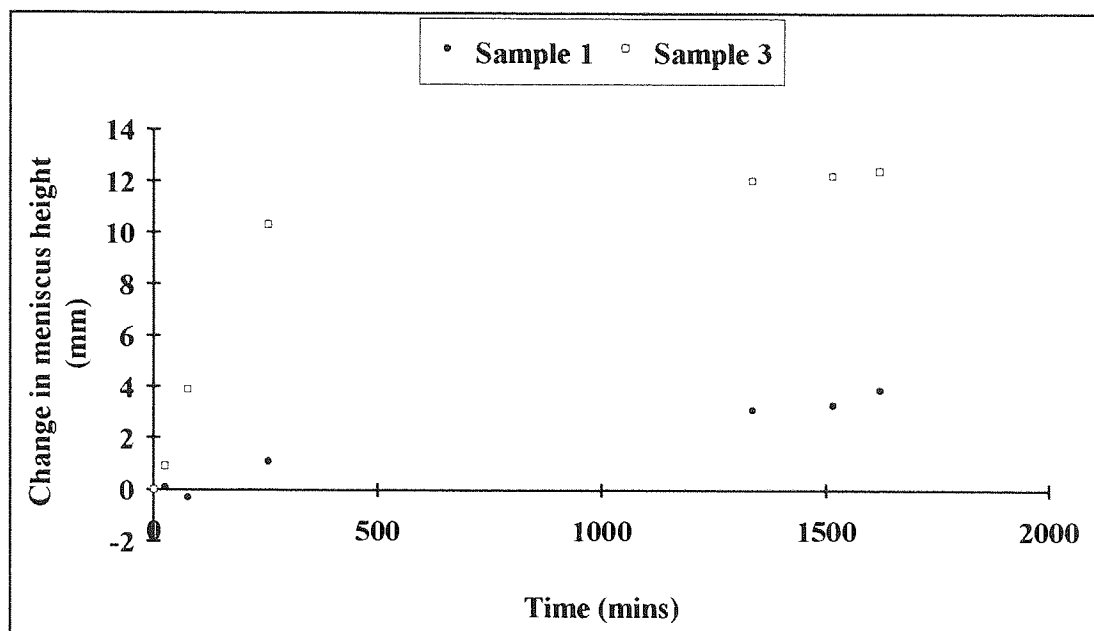


Fig 7.2.9 - Plot of change in meniscus height vs time for Dil10  
- Samples 1 and 3.

### Summary.

Dil1 and 2 both showed a measurable drop in meniscus height over time. However extended reaction runs at different temperatures and comparison with control dilatometers suggested that this drop in meniscus height was not due to polymerisation but to procedural anomalies and equipment malfunction. When the procedure was modified in a number of stages, Dil7 showed no change in meniscus height which could be attributed to polymerisation. Changing the monomer to oxanorbornene dicarboxylic acid unexpectedly caused an increase in the meniscus level over time. Dil9 and Dil10 proved this to be due to monomer decomposition. This was not observed for norbornene dicarboxylic acid due to this monomer's greater stability.

The time taken to progress through the experiments as described above, from the initial single dilatometer experiments to the final investigation of monomer decomposition, was considerable. Although further investigations may have eventually resulted in the development of a dilatometric procedure for measuring the rate of such aqueous metathesis reactions (either by further equipment modification or by the use of different reactants) it was felt that the remaining time available could be more profitably spent investigating other areas.

**7.3 - The interaction between 7-oxanorbornene dicarboxylic acid and Ru(CO)Cl<sub>2</sub>(H<sub>2</sub>O) and its monitoring by UV spectroscopy.**

Figs 7.3.1 to 7.3.5 show data plots for UV1 to UV5. In all cases the data has been zeroed so that the increase of absorbance from time zero can be plotted against time. Data tables containing the raw data can be found in Appendix A - Tables A12 to A16.

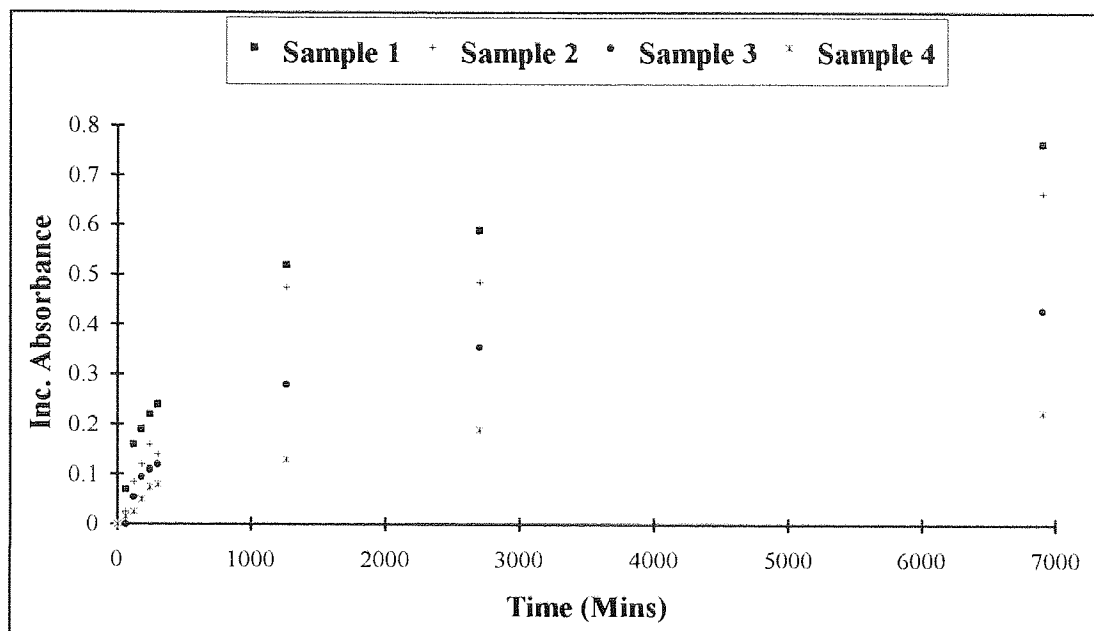


**Fig 7.3.1 - Plot of Absorbance vs Time for UV1**

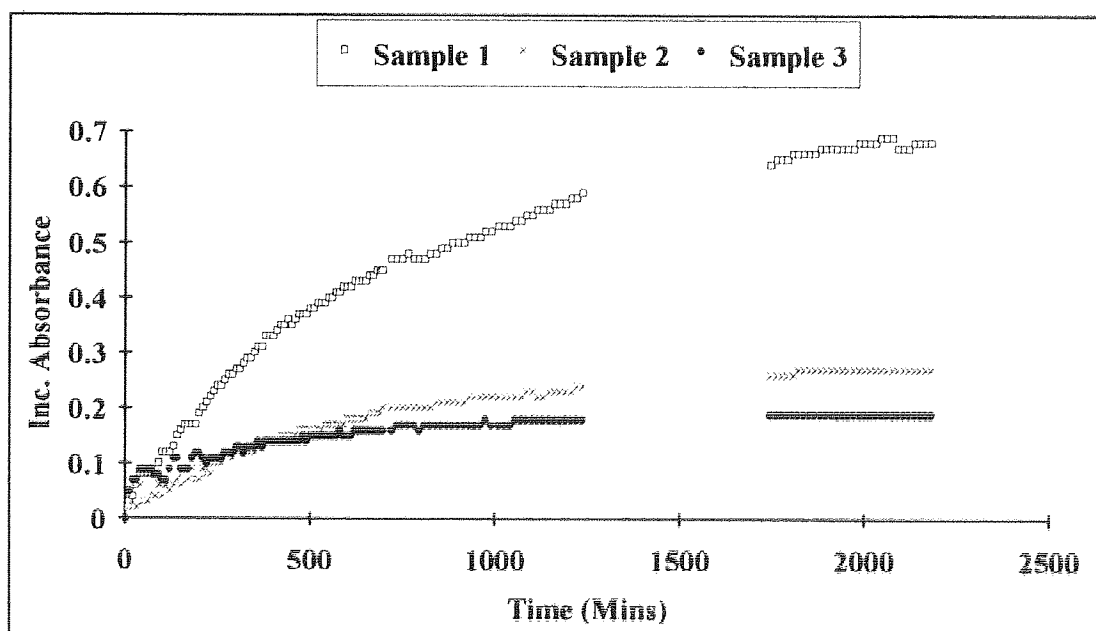


**Fig 7.3.2 - Plot of Absorbance vs Time for UV2**

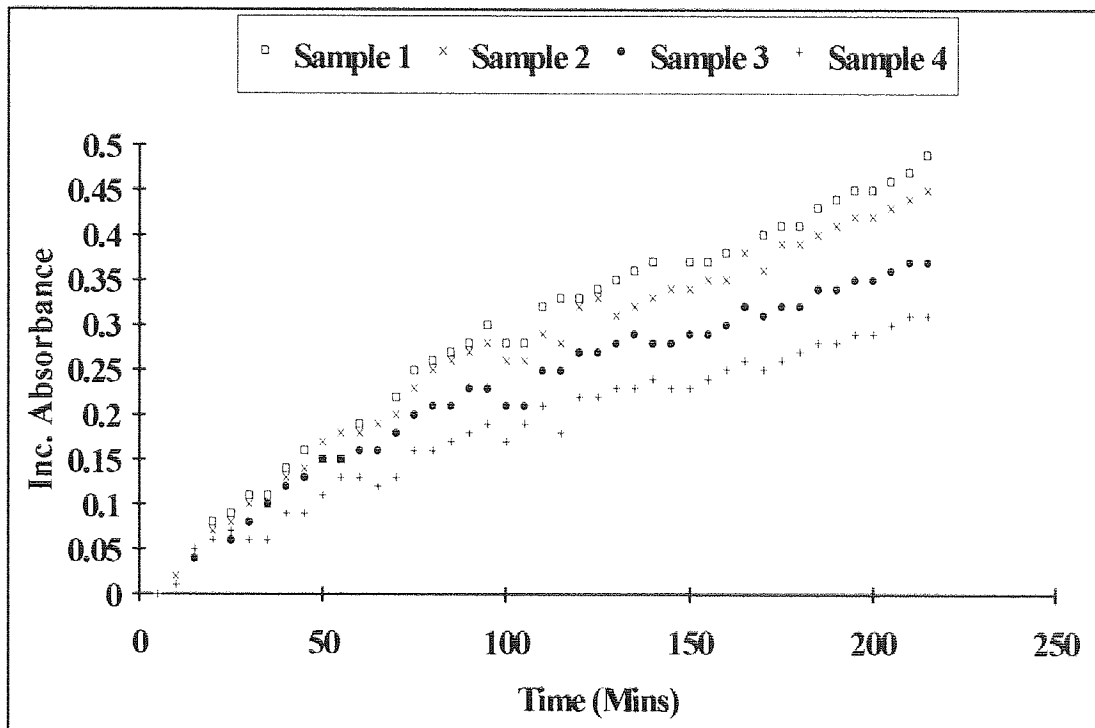


Fig 7.3.3 - Plot of Absorbance vs Time for UV3

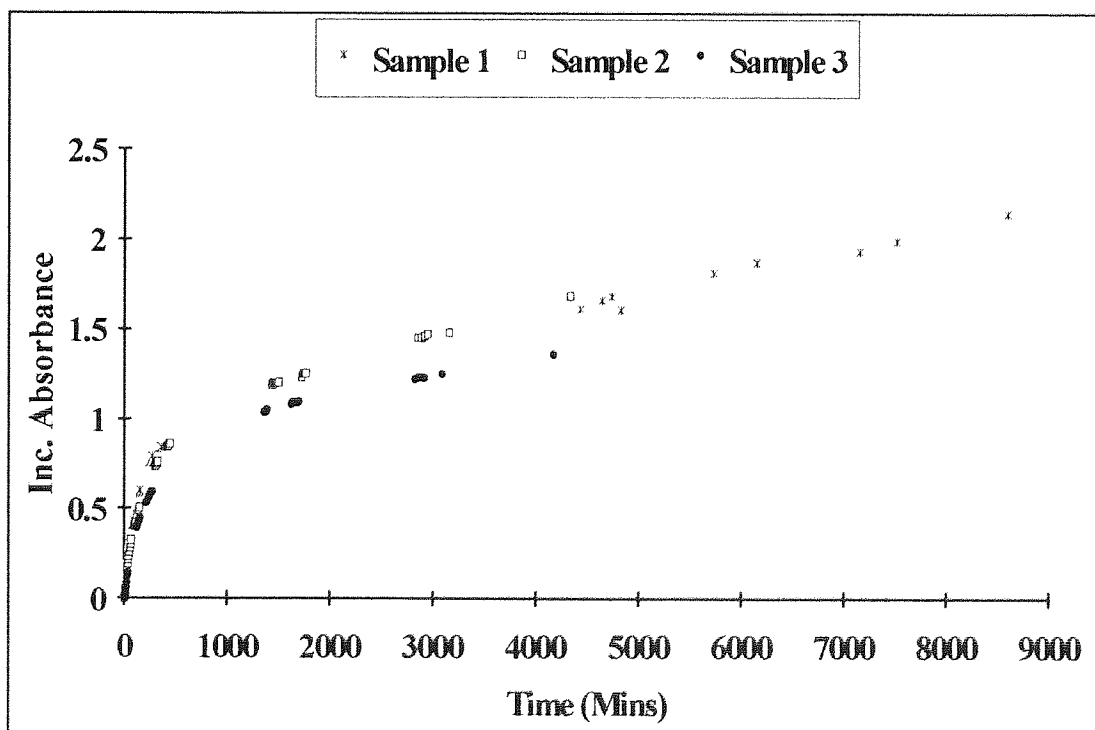


Fig 7.3.4 - Plot of Absorbance vs Time for UV4

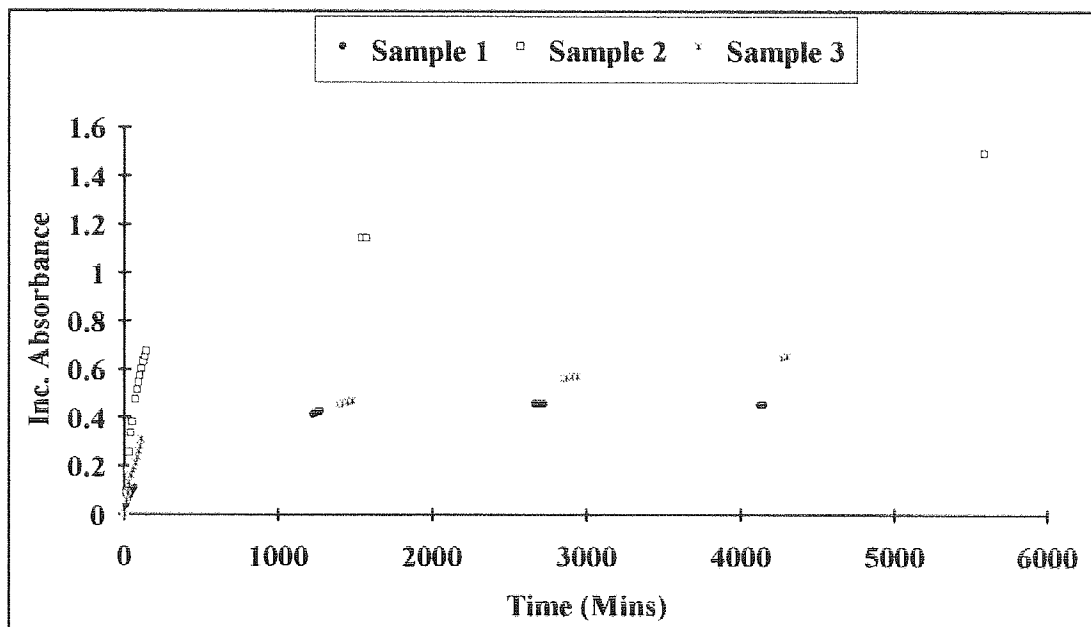
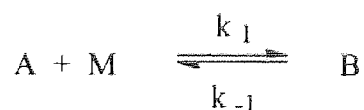


Fig 7.3.5 - Plot of Absorbance vs Time for UV5

Examining the data reveals that the reaction appears to consist of two separate stages. The first few hours seem to follow a simple 1<sup>st</sup> order curve. But instead of flattening of, the curve carries on linearly. Analysing the data is most easily done by considering it in two separate stages corresponding to the two separate curve shapes observed.

#### Initial Period of reaction.

The first stage can be considered as the setting up of an equilibrium.



$$d[B]/dt = k_1[A][M] - k_{-1}[B] \quad (1)$$

$$[A]_0 = [A] + [B] \quad (2)$$

Substituting (2) into (1)

$$d[B]/dt = k_1[A]_0[M] - [B]\{k_{-1} + k_1[M]\}$$

At equilibrium when  $t=t_{\infty}$  then

$$d[B]/dt = 0$$

$$\therefore d[B]/dt = k_{\text{obs}}([B]_e - [B]) \quad (3)$$

where  $k_{\text{obs}} = k_{-1} + k_1[M]$   
 $\therefore k_{\text{obs}} = k_{-1}\{1 + k_1/k_{-1}[M]\}$   
 $\therefore k_{\text{obs}} = k_{-1}\{1 + K_1[M]\}$

But  $-d([B]_e - [B]) = d[B]$  (4)

Substituting (4) into (3) gives

$$-d([B]_e - [B])/dt = k_{\text{obs}}([B]_e - [B]) \quad (5)$$

Integrating (5) gives

$$[B] = [B]_e(1 - e^{-k_{\text{obs}}t}) \quad (6)$$

Where  $[A]_0 = [A]_e + [B]_e$   
 but  $K_1 = [B]_e/[A]_e[M]$   
 $\therefore [A]_e = [B]_e/K_1[M]$   
 $\therefore [A]_0 = [B]_e/K_1[M] + [B]_e$   
 $\therefore K_1[M][A]_0 = [B]_e + [B]_eK_1[M]$   
 $\therefore K_1[M][A]_0 = [B]_e(1 + K_1[M])$   
 $\therefore [B]_e = K_1[M][A]_0/(1 + K_1[M])$

The early data (<180 mins) can be fitted to a pre-equilibrium equation:-

$$\text{Abs}[B] = \text{Abs}[B]_e(1 - e^{-k_{\text{obs}}t})$$

$$\therefore \text{Abs}[B] = \epsilon_B[A]_0K_1[M]\{1 - e^{-(k_{-1}(1 + K_1[M])t)}\}/(1 + K_1[M]) \quad (7)$$

The early data from UV2 - UV5 was fitted to equation (7) using Sigma Plot computer software (UV1 contained too few data points to give a valid fit). The results obtained are given in Table 7.3.1.

**Table 7.3.1 -  $K_1$ ,  $k_{-1}$  and  $\epsilon_B[A]_0$  for early data ( $t < 180$  mins) from UV2 - UV5**

UV2	$K_1$	$10^4 k_{-1} / \text{min}^{-1}$	$\epsilon_B[A]_0 / \text{mol}^{-1}\text{dm}^3$
Sample 1	12.3	60	2.19
Sample 2	7.5	80	1.26
Sample 3	7.8	700 (?)	1.23
UV3	$K_1$	$10^4 k_1 / \text{min}^{-1}$	$\epsilon_B[A]_0 / \text{mol}^{-1}\text{dm}^3$
Sample 1	6.5	22	1.07
Sample 2	6.8	26	1.03
Sample 3	6.7	33	0.94
Sample 4	7.0	33	1.03
UV4	$K_1$	$10^4 k_1 / \text{min}^{-1}$	$\epsilon_B[A]_0 / \text{mol}^{-1}\text{dm}^3$
Sample 1	7.5	26	0.99
Sample 2	7.2	27	0.89
Sample 3	6.3	12	1.67
UV5	$K_1$	$10^4 k_1 / \text{min}^{-1}$	$\epsilon_B[A]_0 / \text{mol}^{-1}\text{dm}^3$
Sample 1	-	-	-
Sample 2	16.4	35	1.11
Sample 3	6.6	9	2.32

An example of the fit obtained is given in Fig 7.3.6.

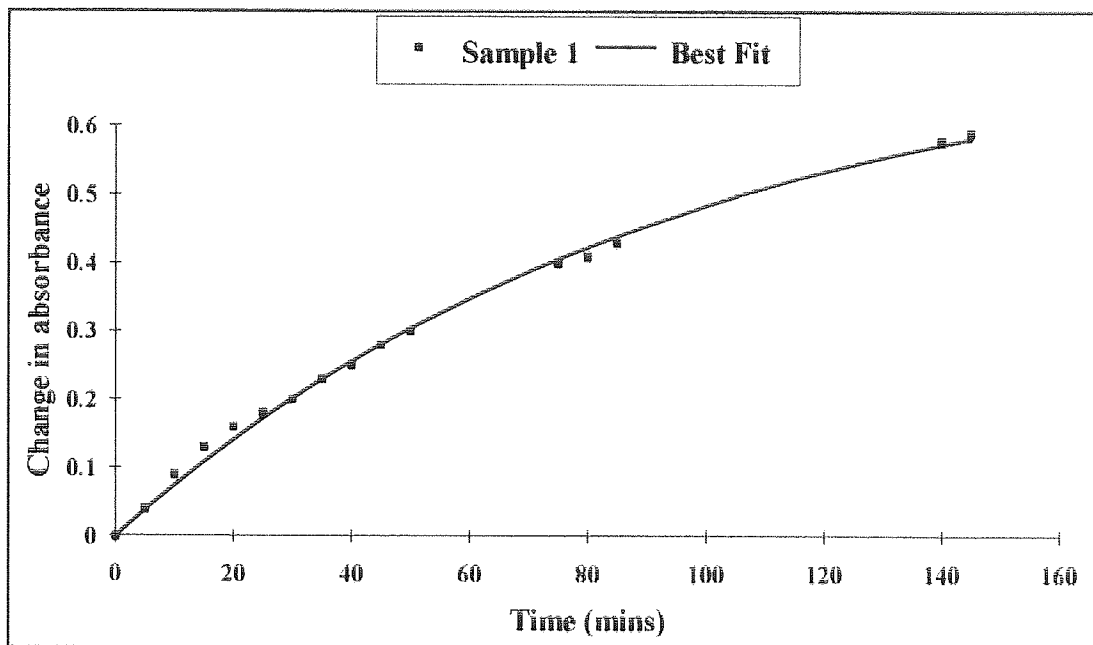
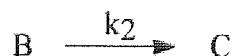


Fig 7.3.6 - Change in absorbance vs time for UV4 - Sample 1 (early data).  
Best fit equation 7.

### Complete Reaction.

After the initial period of reaction the experimental data deviates markedly from simple 1<sup>st</sup> order behaviour, with the absorbance increasing for longer and continuing in a linear fashion. This behaviour can be explained by considering a very slow second stage i.e. only a very small percentage of the reaction has occurred over the period of monitoring, but where the absorbance due to C is large i.e.  $\epsilon_C$  is very large.



where both B and C absorb at 323 nm - the monitored wavelength.

$$\therefore \quad d[C]/dt = k_2[B] \quad (8)$$

Substituting (6) into (8) gives

$$d[C]/dt = k_2[B]_e(1 - e^{k_{obs}t}) \quad (9)$$



Integrating (9) gives

$$[C] = k_2[B]_e \left\{ t - (1/k_{\text{obs}})(1 - e^{-k_{\text{obs}}t}) \right\} \quad (10)$$

For the complete reaction, the absorption is given by

$$\text{Abs} = \epsilon_B[B] + \epsilon_C[C] \quad (11)$$

Substituting (6) and (10) into (11) gives

$$\text{Abs} = \epsilon_B[B]_e(1 - e^{-k_{\text{obs}}t}) + \epsilon_C k_2 [B]_e \left\{ t - (1/k_{\text{obs}})(1 - e^{-k_{\text{obs}}t}) \right\}$$

$$\therefore \text{Abs} = \epsilon_B[B]_e(1 - e^{-k_{\text{obs}}t}) - \epsilon_C(k_2/k_{\text{obs}})[B]_e(1 - e^{-k_{\text{obs}}t}) + \epsilon_C k_2 [B]_e t$$

$$\therefore \text{Abs} = [B]_e(1 - e^{-k_{\text{obs}}t}) \{ \epsilon_B - \epsilon_C(k_2/k_{\text{obs}}) \} + \epsilon_C k_2 [B]_e t$$

$$\therefore \text{Abs} = Z(1 - e^{-k_{\text{obs}}t}) + Yt \quad (12)$$

where  $Z = [B]_e \{ \epsilon_B - \epsilon_C(k_2/k_{\text{obs}}) \}$

$$\therefore Z = [A]_0 K_1 [M] \{ \epsilon_B - \epsilon_C k_2 / k_{-1} (1 + K_1 [M]) \} / (1 + k_1 [M])$$

and  $Y = \epsilon_C k_2 [B]_e$

$$\therefore Y = \epsilon_C [A]_0 K_1 [M] k_2 / (1 + k_1 [M])$$

The data from UV1 - UV5 (except UV3 which only ran for 210 mins) was fitted to equation (12) using Sigma Plot computer software. The results obtained are given in Table 7.3.2.

Table 7.3.2 -  $k_{\text{obs}}$ , Z and Y for UV1 - UV5.

UV1	$10^4 k_{\text{obs}} / \text{min}^{-1}$	Z / mol dm <sup>-3</sup>	$10^5 Y / \text{min}^{-1}$
Sample 1	26	0.46	4.9
Sample 2	19	0.40	4.4
Sample 3	19	0.27	2.7
Sample 4	24	0.14	1.3
UV2	$10^4 k_{\text{obs}} / \text{min}^{-1}$	Z / mol dm <sup>-3</sup>	$10^5 Y / \text{min}^{-1}$
Sample 1	23	0.47	10.3
Sample 2	24	0.21	3.3
Sample 3	80	0.14	2.7
UV4	$10^4 k_{\text{obs}} / \text{min}^{-1}$	Z / mol dm <sup>-3</sup>	$10^5 Y / \text{min}^{-1}$
Sample 1	73	0.88	15.4
Sample 2	49	0.90	19.0
Sample 3	40	0.89	11.6
UV5	$10^4 k_{\text{obs}} / \text{min}^{-1}$	Z / mol dm <sup>-3</sup>	$10^5 Y / \text{min}^{-1}$
Sample 1	60	0.41	1.5
Sample 2	87	1.00	9.2
Sample 3	126	0.43	4.7

An example of the fit obtained is given in Fig 7.3.7.

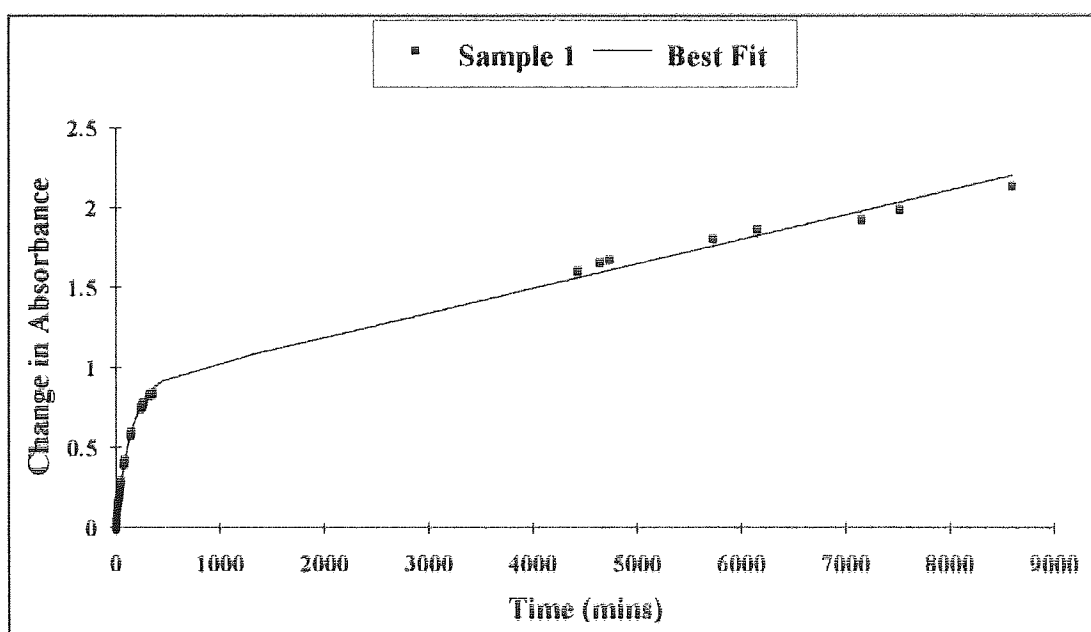


Fig 7.3.7- Change in absorbance vs time for UV4 - Sample 1. Best fit equation (12).

### Product analysis.

Section 6.3 describes the isolation of precipitates from bulk reaction mixtures of  $\text{Ru}(\text{CO})\text{Cl}_2(\text{H}_2\text{O})$  and 7-oxanorbornene-2,3-dicarboxylic acid. These products were analysed using SEC and runs 4 and 5 using NMR spectroscopy.

### SEC Analysis.

In all cases, the SEC traces obtained for these products were similar in appearance to standard traces of unreacted monomer, showing low molecular weight material only and no evidence of polymerisation.

### NMR Analysis.

$^{13}\text{C}$  and  $^1\text{H}$  NMR spectra were obtained for the precipitates and residues from runs 4 & 5 (Appendix B - Figs B32 to B35). The spectra obtained were identical between runs, indicating that the exclusion of oxygen by performing the reaction under argon has no effect on the products obtained.

**Table 7.3.3 - NMR data for the product from reaction between  $\text{Ru}(\text{CO})\text{Cl}_2(\text{H}_2\text{O})$  and monomer.**

	$\delta$ / ppm	
	$^{13}\text{C}$	$^1\text{H}$
Precipitate	134.2 (+ive) 166.2 (-ive)	6.6 13.1 (broad)
Residue	130.3 (+ive) 134.2 (+ive) 166.9 (-ive) 166.2 (-ive)	6.25 6.6 11.9 (broad)
Fumaric Acid Analogous Resonances.	133.96 (+ive) 166.1 (-ive)	6.69 12.9 (broad)
Maleic Acid Analogous resonances.	130.04 (+ive) 166.68 (-ive)	6.21 12.6 (broad)

The resonances for the precipitate clearly show that the precipitated product is fumaric acid and the residue from the reaction solution is a mixture of maleic and fumaric acid. These results are confirmed by the results from the melting point analysis

#### **Melting Point Analysis.**

Samples retrieved from runs 4 and 5 had melting point analyses performed in duplicate. Results were identical for both runs. No distinct melting point was observed for either the precipitate or the residue. The precipitate exhibited sublimation starting at approximately 150°C and the subliming solid eventually built up to form a solid plug blocking the melting point tube. This sublimation continued until 300°C where the small remaining amount of solid melted. This behaviour is consistent with fumaric acid. The residue behaved in a similar manner but with less distinct transitions. Before the onset of sublimation, at 110°C-120°C small droplets of water were formed higher up the melting point tube. This is probably due to dehydration of the sample. This behaviour and the appearance of the sample suggests the sample is a mixture containing fumaric acid.

#### **7.4 - The interaction between 7-oxanorbornene dicarboxylic acid and a Ru-P(CH<sub>2</sub>OH)<sub>3</sub> complex.**

Section 6.5 describes the procedure followed for the reaction of 7-oxanorbornene dicarboxylic acid and a Ru-P(CH<sub>2</sub>OH)<sub>3</sub> complex. The product obtained from experimental set 6.5.3 was retrieved as described and analysed by NMR spectroscopy (Appendix B - Figs B40 to B41). The NMR data are given in Table 7.4.1.

The most significant of the spectra obtained is the <sup>13</sup>C spectrum. The three resonances observed correspond to a mixture of maleic acid and fumaric acid (the carbonyl carbon resonance of fumaric acid is missing due to its much lower concentration and proximity to the carbonyl resonance of maleic acid). Similarly, the <sup>1</sup>H spectrum shows the expected resonances for the vinylic protons. (The identity of the resonances between 2 ppm and 4.3 ppm is unclear especially as there are no corresponding resonances in the <sup>13</sup>C spectrum.) The <sup>31</sup>P NMR spectrum surprisingly showed only one weak resonance at 0.0 ppm corresponding to phosphoric acid. This suggests some ligand degradation and its presence in the NMR spectrum of the precipitated product must be explained by the retrieval process. As was explained in the experimental procedure (Section 6.5.3) the retrieval of the product necessitated the evaporation of the last portion of mother liquor and this explains the large maleic acid resonances (maleic acid will have been precipitated from the solution on evaporation). The presence of fumaric acid agrees with the results

obtained from the reaction between  $\text{Ru}(\text{CO})\text{Cl}_2(\text{H}_2\text{O})$  and 7-oxanorbornene dicarboxylic acid.

**Table 7.4.1 - NMR data for the product of the reaction between monomer and a  $\text{Ru}-\text{P}(\text{CH}_2\text{OH})_3$  complex.**

	$\delta$ / ppm	
	$^{13}\text{C}$	$^1\text{H}$
Product	130.2 (+ive)	2.07 (singlet)
	134.1 (+ive)	2.49 (singlet)
	166.6 (-ive)	2.53 (singlet)
		4.2721
		4.2563
		4.2472
		4.2295
		6.26 (singlet)
	6.62 (singlet)	
Fumaric Acid	133.96 (+ive)	6.69 (singlet)
	166.1 (-ive)	
Maleic Acid	130.04 (+ive)	6.21 (singlet)
	166.68 (-ive)	

### 7.5 - The interaction between 7-oxanorbornene dicarboxylic acid and various $\text{Ru}^{2+}$ complexes.

Sections 6.7 and 6.8 describe the procedures followed for the reaction of 7-oxanorbornene dicarboxylic acid with  $\text{cis}[\text{Ru}(\text{en})_2(\text{H}_2\text{O})_2]^{2+}$  and  $[\text{Ru}(\text{NH}_3)_5\text{N}_2]^{2+}$  respectively. Section 6.6 describes the reaction between the above monomer with  $\text{Ru}(\text{CO})\text{Cl}_2(\text{H}_2\text{O})$  and a  $\text{Ru}-\text{P}(\text{CH}_2\text{OH})_3$  complex and the diazoester initiator ethyl diazoacetate. In all three cases the solutions were reduced and the products retrieved were analysed by SEC in order to detect any evidence of polymerisation.

For all three experiments no evidence of polymerisation was observed and the SEC traces obtained were in all cases similar in appearance to standard traces obtained for unreacted monomer. The lack of precipitation during reaction indicates that unlike the reaction of 7-oxanorbornene dicarboxylic acid with  $\text{Ru}(\text{CO})\text{Cl}_2(\text{H}_2\text{O})$  and a  $\text{Ru}-\text{P}(\text{CH}_2\text{OH})_3$  no fumaric acid has been produced.

## CHAPTER 8

### DISCUSSION AND CONCLUSIONS.

#### 8.1 - The Synthesis of a Ruthenium Complex containing the Ligand P(CH<sub>2</sub>OH)<sub>3</sub>.

Transition metal compounds containing the water soluble ligand P(CH<sub>2</sub>OH)<sub>3</sub> have been described in a number of recent papers. The most extensive body of work concerns the synthesis and characterisation of the zero-valent platinum, palladium and nickel complexes all of which are air-stable, water soluble solids.<sup>36, 66</sup>

The synthesis of all three complexes is achieved by simple substitution reactions involving no demanding conditions. The range of syntheses described is summarised in table 8.1.1.

**Table 8.1.1 - Synthesis of P(CH<sub>2</sub>OH)<sub>3</sub> complexes of Pt, Pd and Ni.<sup>66</sup>**

Transition Metal starting compound and solvent	Ligand solvent	Product
<p><b>[MX<sub>2</sub>(COD)]</b>                      M = Pt, Pd                      X = Cl, Br, I                      COD = Cyclooctadiene                      Solvent = methanol</p>	Methanol	$\begin{array}{ccc} \text{(HOCH}_2\text{)}_3\text{P} & \diagdown & \text{X} \\ & \text{M} & \\ \text{(HOCH}_2\text{)}_3\text{P} & \diagup & \text{X} \end{array} \quad \text{and} \quad \begin{array}{ccc} \text{(HOCH}_2\text{)}_3\text{P} & \diagdown & \text{X} \\ & \text{M} & \\ \text{X} & \diagup & \text{P(CH}_2\text{OH)}_3 \end{array}$ <p style="text-align: center;">Tendency for <i>trans</i>- Pd&gt;Pt I&gt;Br&gt;Cl</p>
<p><b>[PtCl(CH<sub>3</sub>)(COD)]</b>                      Solvent=methanol</p>	Methanol	$\begin{array}{ccc} \text{(HOCH}_2\text{)}_3\text{P} & \diagdown & \text{Me} \\ & \text{M} & \\ \text{(HOCH}_2\text{)}_3\text{P} & \diagup & \text{Cl} \end{array} \quad \text{and} \quad \begin{array}{ccc} \text{(HOCH}_2\text{)}_3\text{P} & \diagdown & \text{X} \\ & \text{M} & \\ \text{Me} & \diagup & \text{P(CH}_2\text{OH)}_3 \end{array}$ <p style="text-align: center;">X=Cl, Br, I</p>
<p><b>[Pt(CH<sub>3</sub>)<sub>2</sub>(COD)]</b>                      Solvent=DMSO-D<sub>6</sub></p>	DMSO-D <sub>6</sub>	<p>[Pt(CH<sub>3</sub>)<sub>2</sub>(P(CH<sub>2</sub>OH)<sub>3</sub>)<sub>2</sub>]                      Not isolated from solution.</p>
<p><b>[Ni(COD)<sub>2</sub>]</b>                      Solvent=toluene</p>	Methanol	[Ni(P(CH <sub>2</sub> OH) <sub>3</sub> ) <sub>4</sub> ]
<p><b>[Pd(dibenzylideneacetone)<sub>2</sub>]</b>                      Solvent=toluene</p>	Methanol	[Pd(P(CH <sub>2</sub> OH) <sub>3</sub> ) <sub>4</sub> ]
<p><b>[Pd(PPh<sub>3</sub>)<sub>4</sub>]</b>                      Solvent=CH<sub>2</sub>Cl<sub>2</sub></p>	Water	[Pd(P(CH <sub>2</sub> OH) <sub>3</sub> ) <sub>4</sub> ]
<p><b>[Pt(COD)<sub>2</sub>] or [Pt(PPh<sub>3</sub>)<sub>4</sub>]</b>                      Solvent=methanol</p>	Methanol	[Pt(P(CH <sub>2</sub> OH) <sub>3</sub> ) <sub>4</sub> ].H <sub>2</sub> O

Deep yellow crystals of  $[\text{Pd}(\text{P}(\text{CH}_2\text{OH})_3)_4]\cdot\text{MeOH}$  were obtained from a methanol/diethyl ether solution and crystal structure determination revealed the expected tetrahedral co-ordination around the platinum (0) centre. The crystal structure also revealed both intramolecular and intermolecular hydrogen bonding. There are two types of intermolecular hydrogen bond present. Firstly, hydrogen bonds linking the molecules into a two dimensional layer network and secondly, hydrogen bonds linking these two dimensional layers together. This extensive hydrogen bonding is implied as the reason for the unusual stability of these complexes when compared to other phosphine complexes i.e.  $\text{PMe}_3$  and  $\text{PEt}_3$  which are extremely air sensitive. The intramolecular hydrogen bonding links the four ligands in such a way that they can be considered as a single tetra-dentate ligand. Therefore the multiple chelate effect of such a ligand can be seen as providing extra stability when compared to non-hydrogen bonding ligands.

The platinum complex  $[\text{Pt}(\text{P}(\text{CH}_2\text{OH})_3)_4]\cdot\text{H}_2\text{O}$  in aqueous solution exists as an equilibrium mixture of the tetrahedral platinum (0) complex and a trigonal-bipyramidal hydridoplatinum(II) complex as shown in Fig. 8.1.1.

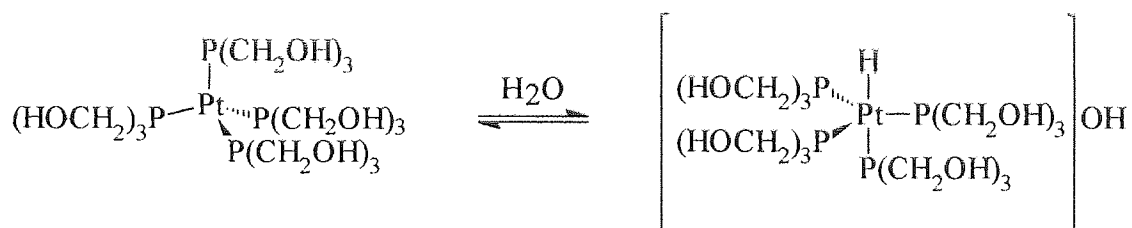


Fig 8.1.1 - Aqueous solution equilibrium of  $[\text{Pt}(\text{P}(\text{CH}_2\text{OH})_3)_4]\cdot\text{H}_2\text{O}$

The ligands in this case can be considered to be analogous to the tripodal tetra-dentate ligand  $\text{P}(\text{CH}_2\text{CH}_2\text{PPh}_3)_3$  which has been shown to confer stability to platinum geometry's of this sort.<sup>66</sup> (Fig 8.1.2).

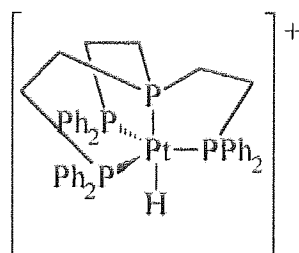
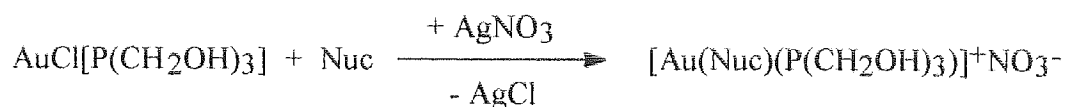


Fig 8.1.2 - Co-ordination of the tetradentate ligand  $\text{P}(\text{CH}_2\text{CH}_2\text{PPh}_3)_3$

Synthesis of the gold analogue is also simply achieved from the substitution reaction between the ligand and [AuCl(COD)]. This complex has been used as an intermediate in the synthesis of water soluble gold complexes containing a nucleoside ligand for the investigation of novel metal containing anti-tumour drugs.<sup>38</sup> (Fig 8.1.3).



Nuc = Guanosine, adenosine, cytidine

**Fig 8.1.3 - Synthesis of water-soluble gold (I) complexes containing a nucleoside ligand.**

The synthesis of water soluble ruthenium and rhodium complexes containing phosphine ligands is described by another group of workers.<sup>37</sup> Most interestingly, although both ruthenium and rhodium were studied, only a Rh-(P(CH<sub>2</sub>OH)<sub>3</sub>)<sub>3</sub> complex is described, suggesting that some problem was encountered in the synthesis of the ruthenium analogue. As for all the previous compounds, the rhodium complex is synthesised by a simple substitution reaction between Rh<sub>2</sub>Cl<sub>2</sub>(CO)<sub>4</sub> and the ligand in ethanolic solution giving [RhCl(CO)(P(CH<sub>2</sub>OH)<sub>3</sub>)<sub>2</sub>] which has a *trans*- square planar geometry.

The absence of published accounts of the synthesis of the ruthenium analogue is of interest in itself. The existence of the ruthenium complex is alluded to in the literature<sup>39</sup> but conversation with the author revealed that this complex was synthesised as part of an undergraduate project and not enough data was recovered for publication in the literature. The fact that neither this group nor the group responsible for the publication of information on the rhodium analogue<sup>37</sup> have published data for the ruthenium complex strongly suggests that either its synthesis or its isolation and characterisation is problematical. This inference is in agreement with the problems encountered in this study. (See section 5.5.11)

As described previously the product obtained from the attempted synthesis of the ruthenium analogue seems to consist of a discrete Ru-Phosphine matrix in which unreacted ligand impurities are enclosed, as suggested by NMR analysis. The elemental analysis indicates a Ru:P ratio of 1:3.6.



The NMR spectra suggest the presence of unreacted ligand moieties. Throughout this work, un-recrystallised ligand was used in the various syntheses due to the difficulty in obtaining recrystallised ligand in appropriate yield. It is possible that product purity could be improved by the use of a purer ligand source. NMR spectra of this ligand source showed the presence of hemiacetal and cyclic phosphine impurities. However the NMR spectra of recrystallised ligand produced in very small yield during an undergraduate research project, show these impurities still to be present. It is therefore unlikely that the use of recrystallised ligand for these syntheses would have produced product of a different consistency or of appreciably higher purity. The hydrophosphination of formaldehyde is catalysed by  $[\text{PtCl}_2(\text{P}(\text{CH}_2\text{OH})_3)_2]$  and this reaction lead Pringle *et al.* to investigate the addition of the catalyst to excess ligand<sup>73</sup>. They found that a number of products were formed. The stoichiometry of the reaction is shown below and the structure of the products is shown in Fig 8.1.4.

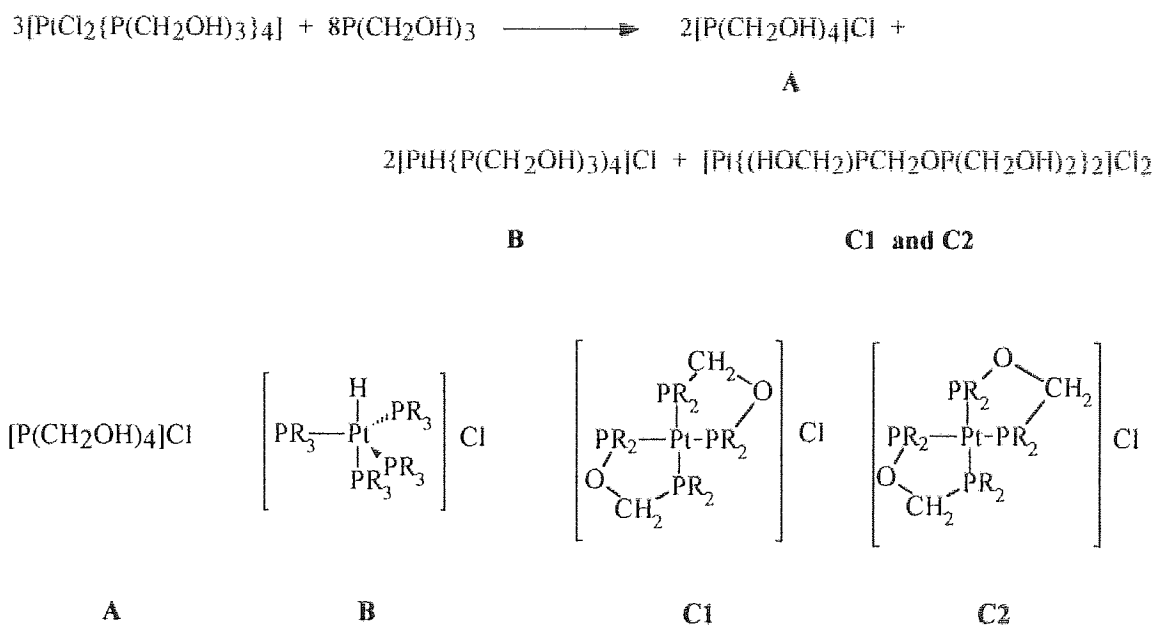


**Fig 8.1.4 - Products from the reaction of  $[\text{PtCl}_2(\text{P}(\text{CH}_2\text{OH})_3)_2]$  and excess  $\text{P}(\text{CH}_2\text{OH})_3$ . ( $\text{R} = \text{P}(\text{CH}_2\text{OH})_3$ ).**

Since the Ru- $\text{P}(\text{CH}_2\text{OH})_3$  complex is formed in conditions of refluxing in excess ligand, it is not unreasonable to assume that similar bis-chelate complexes could be formed during this synthesis and this may account for the complex NMR spectra (particularly the broad unresolved resonance between 68 and 72 ppm). It is possible that such products are formed in the synthesis of the analogous platinum and palladium complexes but as these are crystallised from solution, they are not observed in those syntheses.

The ligand is hygroscopic and therefore the observed hygroscopicity of the product obtained is not unexpected - such hygroscopicity in the gold analogue is commented upon in the literature<sup>38</sup>. The consistency of the product is therefore dependant on its storage and handling. When produced, prolonged heating in a vacuum oven is required to transform the product from a soft, malleable toffee to a hard, glassy product. However leaving the glassy product exposed to the air for any appreciable length of time allows it to completely revert to its original consistency. Although it may take weeks for the product to revert to its original state, a change in consistency, mainly in the form of an increase in tackiness, is observed after about one day.

All the transition metal -  $P(CH_2OH)_3$  complexes described in the literature are soluble only in water, methanol, ethanol and DMSO but are highly insoluble in common organic solvents. The ruthenium product obtained is similarly highly soluble in water, methanol and DMSO but only soluble in hot ethanol and completely insoluble in other organic solvents. Once in solution, the product can only be retrieved by vacuum removal of the solvent. The inability to recrystallise a product even from very concentrated solutions can be attributed to the extreme ability of the large number of  $P(CH_2OH)_3$  ligands to hydrogen bond strongly to the protic solvents in which the product is soluble. In contrast, the Pt, Pd, Ni and Rh complexes can be precipitated as discrete crystalline products by the addition of organic solvent to concentrated alcoholic solutions of the product. This method was unsuccessful for the precipitation of the ruthenium analogue. Application of this technique resulted in the orange toffee product's being separated from the solvent mixture.

Platinum(II) and palladium(II) are well known for forming square planar complexes. LFSE is maximised for a  $d^8$  atom in a square planar geometry as shown in Fig 8.1.5. The sum of the orbital energies for octahedral and square planar  $d^6$  and  $d^8$  ions is given in table 8.1.2.

For a  $d^8$  ion such as Pt(II) or Pd(II) an electrostatic LFSE increase of  $-1.26 \Delta$  is gained by forming a square planar geometry. Therefore, as long as this energy gain is greater than the energy required to pair the two otherwise unpaired electrons, then a square planar complex will be formed. For a  $d^6$  ion such as Ru(II), the octahedral geometry provides the lowest possible LFSE so no advantage is gained in a square planar geometry.

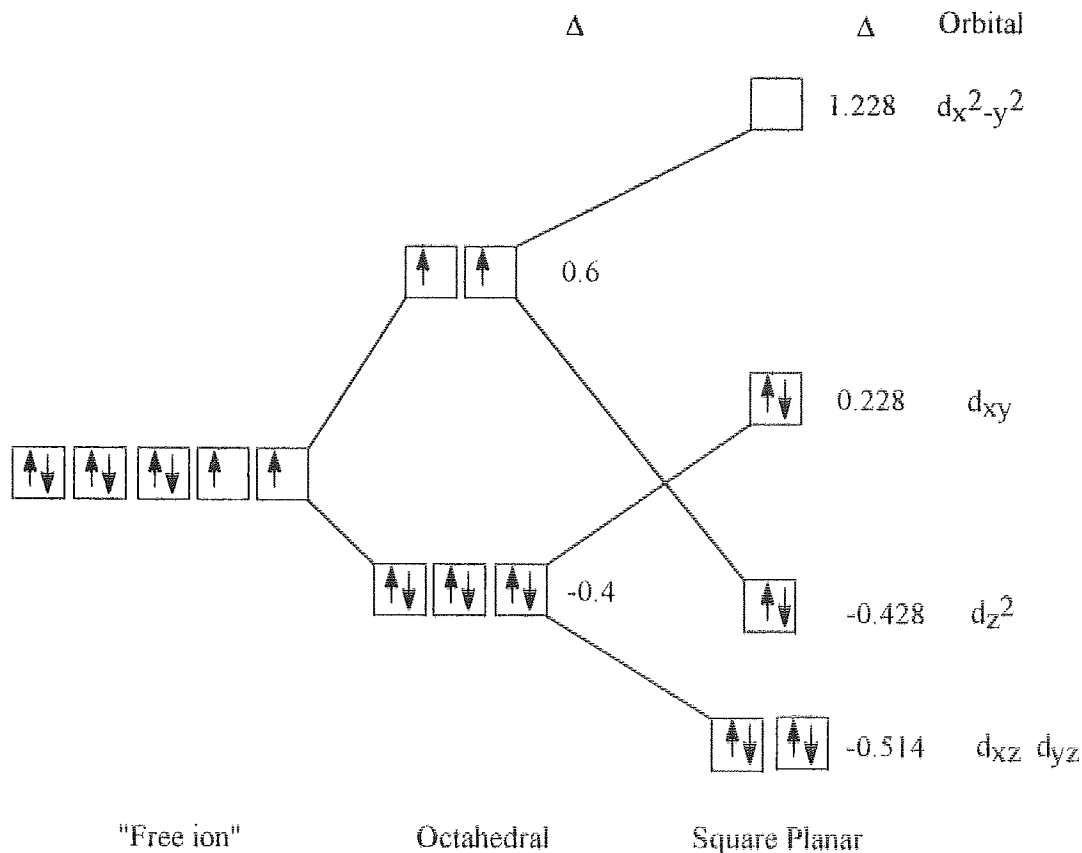


**Fig 8.1.5 - Ligand field splitting for a  $d^8$  ion.**

**Table 8.1.2 - Sum of orbital energies -  $d^6$  and  $d^8$  octahedral and square planar complexes.**

	Octahedral	Square Planar
$d^6$ - Ru(II)	$-2.4 \Delta$	$-1.6 \Delta$
$d^8$ - Pt(II), Pd(II) and Rh(I)	$-1.2 \Delta$	$-2.456 \Delta$

Similarly rhodium(I) -  $d^8$  predominantly forms square planar complexes (the majority of Rh(I) complexes contain phosphine ligands as a strong  $\Pi$ -acceptor ligand is required to stabilise this low oxidation state).

Ruthenium(II) exhibits only octahedral geometry's with the exception of the triphosphine complexes. This is due to the large cone angle of the co-ordinated phosphines causing the blocking of one of the co-ordination sites. The cone angles of a variety of triphosphines are given in table 8.1.3.

Table 8.1.3 - Cone angles for various triphosphines.

$P(CH_2)_6N_3$	$PMe_3$	$P(CH_2CH_2CN)_3$	$PEt_3$	$PPh_3$
102°	118°	132°	132°	145°

The  $P(CH_2OH)_3$  ligand probably has a cone angle of approximately 132°.<sup>37</sup> Both  $RuCl_2(PPh_3)_3$  and  $RuCl_2(P(CH_2CH_2CN)_3)$  exist in pseudo-octahedral geometry's and for  $RuCl_2(PPh_3)_3$  the space of the empty co-ordination site is occupied by a proton from an adjacent  $PPh_3$  ligand. However ruthenium can form a tetra- co-ordinated tris(triphenyl)phosphine complex,  $RuCl_2(PPh_3)_4$ , under the right conditions despite the steric hindrance associated with the large cone angle. In solution  $RuCl_2(PPh_3)_4$  exists in equilibrium with  $RuCl_2(PPh_3)_3$  and  $PPh_3$ . Due to the similarity in cone angles, it is reasonable therefore to predict a similar geometry and co-ordination number for a ruthenium- $P(CH_2OH)_3$  complex. Therefore the ratio 1Ru:2Cl:3.6 P found from elemental analysis of the product suggests a product mixture of  $RuCl_2(P(CH_2OH)_3)_3$  and  $RuCl_2(P(CH_2OH)_3)_4$

In  $RuCl_2(P(CH_2OH)_3)_3$ , for steric reasons, the three phosphine ligands do not all occur in a *cis*- configuration to each other despite this being the most favourable electronically. ( $PR_3$  is higher in the *trans*-effect series than Cl. That is, it labilises the ligand in the *trans*- position). The two  $Cl^-$  ligands therefore are *trans*- to each other. We would therefore expect one of the structures of the type given in Fig 8.1.6 for a complex of this stoichiometry. It is unknown whether a octahedral or trigonal bipyramidal structure predominates.

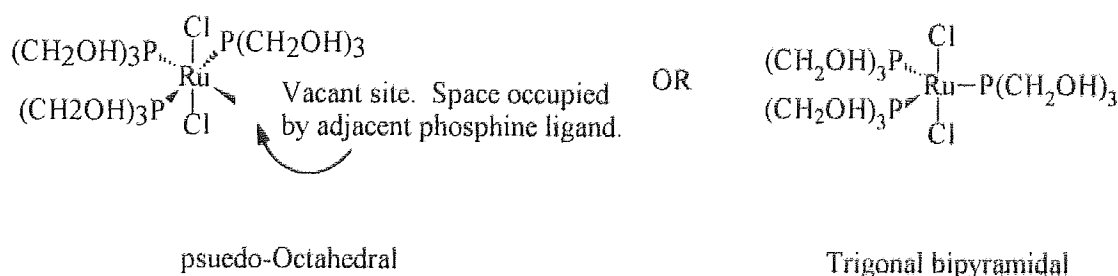


Fig 8.1.6 - Possible structures for a  $Ru-P(CH_2OH)_3$  complex.

The failure of this compound to produce discrete crystals can be explained in terms of extensive intermolecular hydrogen bonding. Although the platinum and palladium complexes can exist in both *trans*- and *cis*- forms, the *cis*- forms are highly dominant because of the *trans* effect as explained earlier - for platinum only  $[PtCl_2(P(CH_2OH)_3)_2]$

exists as the *trans*- form in appreciable amounts - 66% *trans*- in freshly prepared solutions, isomerising to only 9% after 4 hours.<sup>66</sup> In these *cis*- complexes hydrogen bonding will be mostly intramolecular in character due to the proximity of the two phosphine ligands to each other. However in a *trans*- complex the ligands will be able to extensively hydrogen bond intermolecularly as is shown by the crystal structure of the tetrahedral  $[\text{Pd}(\text{P}(\text{CH}_2\text{OH})_3)_4]\cdot\text{MeOH}$ , discussed earlier. The *trans*- location of the coordinated ligands and possibly some bis-chelate complexes and uncoordinated ligand moieties (as evidenced by the NMR spectra) could therefore provide the correct environment for a high degree of intermolecular hydrogen bonding, to such an extent that the complex would exist in a three dimensional polymeric matrix. Such a matrix would be able to trap and retain protic solvent molecules unless removed by heating in a vacuum oven, and therefore preventing recrystallisation. The reason for the non-crystallisation of  $\text{RuCl}_2(\text{P}(\text{CH}_2\text{OH})_3)_3$  when compared to the equally hydrogen bonded  $[\text{Pd}(\text{P}(\text{CH}_2\text{OH})_3)_4]\cdot\text{MeOH}$  could be the existence of the vacant site caused by the steric hindrance of the phosphine. Tetrahedral  $[\text{Pd}(\text{P}(\text{CH}_2\text{OH})_3)_4]\cdot\text{MeOH}$  effectively exists as spherical hydrogen-bonding ball. The palladium centre is sheathed within twelve equidistant  $-\text{CH}_2\text{OH}$  groups. The  $\text{RuCl}_2(\text{P}(\text{CH}_2\text{OH})_3)_3$  complex however has less evenly distributed  $-\text{CH}_2\text{OH}$  groups which, although allowing for extensive intermolecular hydrogen bonding, provide adequate spaces for solvent molecules to become entrapped in hydrogen bonded  $\text{RuCl}_2(\text{P}(\text{CH}_2\text{OH})_3)_3$  cages. Such a process could interfere sufficiently with the recrystallisation of the product to produce the results seen.

These arguments would suggest that a bisphosphine square-planar Ru(II) complex might be crystalline in nature due to the reduction in intermolecular hydrogen bonding. An attempt was made to synthesise a complex of this type -  $\text{Ru}(\text{NO})_2(\text{P}(\text{CH}_2\text{OH})_3)_2$  (See section 5.5.12). (The complex  $\text{Ru}(\text{NO})_2(\text{PPh}_3)_2$  is actually a highly distorted tetrahedron which has the effect of placing the phosphine ligands in a *trans*- relationship<sup>74</sup>). This synthesis produced a light brown precipitate which was only soluble in water and methanol. Attempts to retrieve NMR spectra of this product proved unsuccessful due to its insolubility. Elemental analysis of the precipitate is a reasonably good fit to the expected results for carbon, hydrogen and phosphorus, but the determined nitrogen content was found to be low. Without NMR spectra, it is impossible to say with any certainty that the product obtained is  $\text{Ru}(\text{NO})_2(\text{P}(\text{CH}_2\text{OH})_3)_2$  although the retrieval of a highly water soluble product in a reasonable yield is encouraging. The yield obtained suggests that high levels of impurity and/or by-products must be present.

A route to another similar "square planar" complex may be possible via a modification of the synthesis in (Fig 8.1.7)<sup>74</sup>.

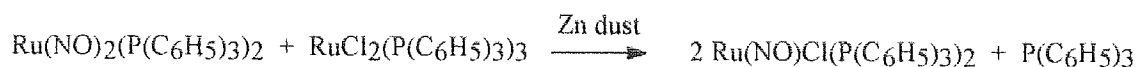


**Fig 8.1.7 - Nitrosyl transfer reaction.**

I have synthesised  $\text{Ru(NO)}_2(\text{PPh}_3)_2$  as part of this study (see section 5.5.8) and this complex provides a convenient route to the *trans*- geometry required. Simple substitution of its triphenylphosphine with  $\text{P}(\text{CH}_2\text{OH})_3$  proved unsuccessful (see 5.5.12) but a modification of the above reaction, replacing  $\text{RuCl}_2(\text{PPh}_3)_3$  with  $\text{RuCl}_2(\text{P}(\text{CH}_2\text{OH})_3)_3$ , might be successful in producing a product with the desired properties. (Fig 8.1.8)

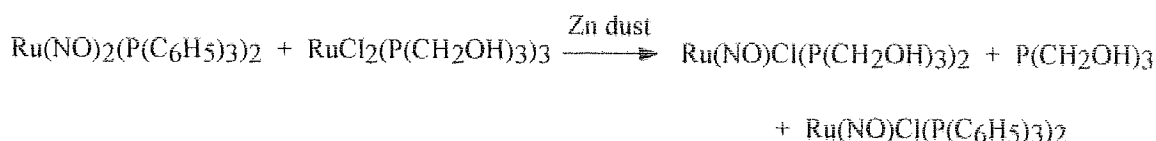


**Fig 8.1.8 - Modified nitrosyl transfer reaction**

## **8.2 - The mechanism of production of fumaric acid.**

The isomerisation of maleic acid to fumaric acid is a well known reaction whose rate and mechanism has been thoroughly studied. This isomerisation is known to be catalysed by inorganic acids and salts and the mechanism was elucidated by Nozaki and Ogg<sup>75</sup> who recognised that the nature of the anion had an effect on the rate of isomerisation. The mechanism proposed by them is given in Fig 8.2.1

Steps (iii) and (iv) must be fast or the intermediate would mainly be converted via a proton-shift into a mono-substituted succinic acid. Succinic acid derivatives were produced in these experiments by Nozaki and Ogg but the isomerisation reaction greatly predominated. Since the anion enters into the rate determining step of this mechanism, its nature should effect the observed rates. In Nozaki and Ogg's experiments using HCl, HBr,  $\text{H}_2\text{SO}_4$ ,  $\text{HClO}_4$ , KCNS,  $\text{NH}_4\text{CNS}$  and NaBr, large differences in catalytic activity were observed but insufficient data were obtained to correlate the results with the anion's characteristics. The activation energy of step (i) is much greater for fumaric acid than

maleic acid and subsequently, although reconversion of fumaric acid to maleic acid is possible, nearly all the fumaric acid remains unaffected.

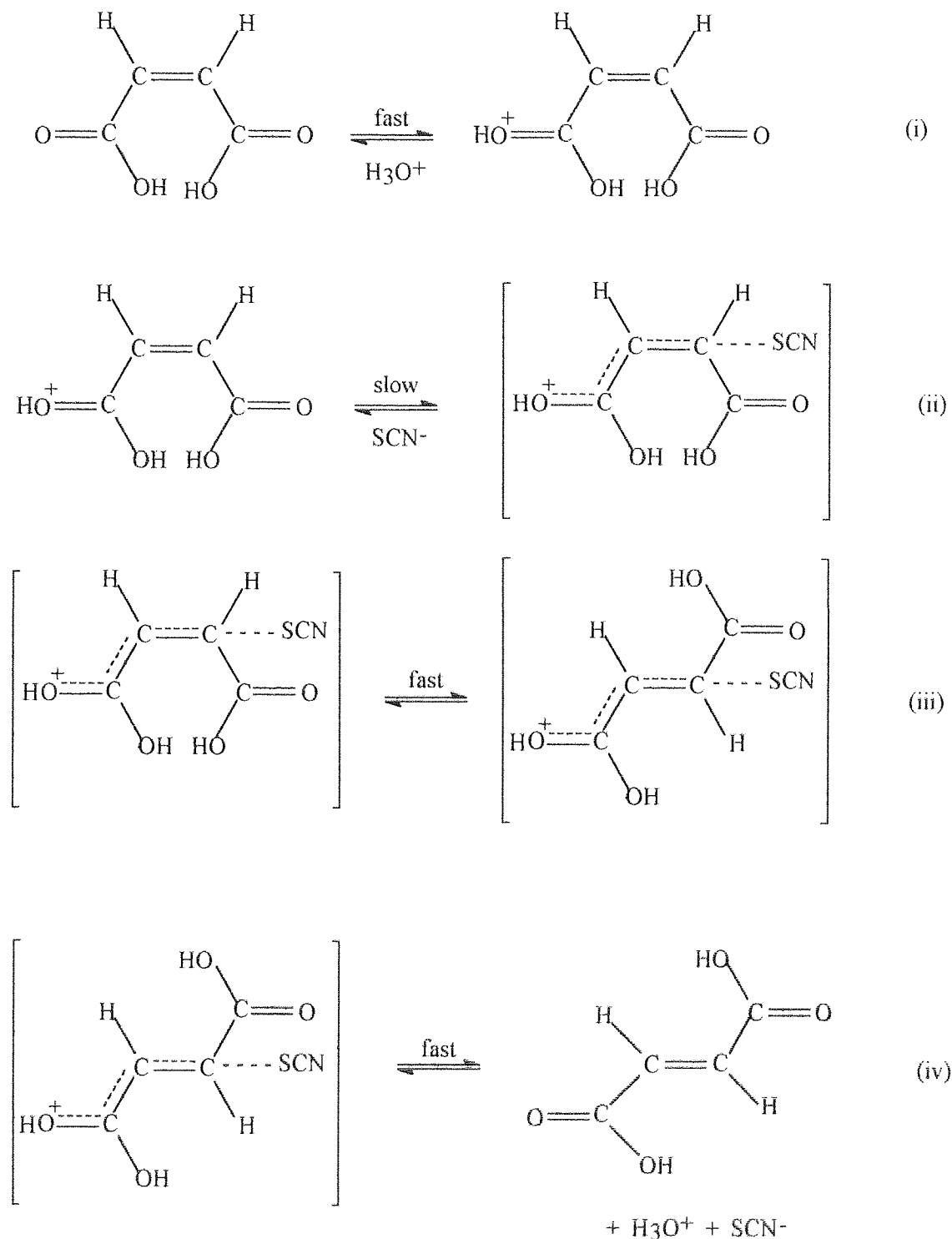


Fig 8.2.1 - Mechanism for the isomerisation of maleic acid to fumaric acid using KCNS.<sup>84</sup>

The reaction is also catalysed by inorganic salts and in this case the necessary protons are provided by the ionisation of other maleic acid molecules. This is born out by the much greater catalytic activity for acids compared to salts - in every case the acids are much better catalysts than the salts derived from them.

Rearrangement or isomerisation reactions are well known within transition metal chemistry and recently details were published in the literature of the Ru(II) catalysis of olefin isomerisation in fully aqueous media<sup>76</sup>.

There are two established pathways for transition metal catalysed isomerisation of olefins. The more common one is a metal-hydride addition-elimination mechanism. The first step is the co-ordination of free olefin to a metal hydride species via the double bond (i). The proton then adds to the double bond producing a secondary metal-alkyl (ii). Subsequent rotation and  $\beta$ -elimination produces the isomerised olefin-metal co-ordination complex (iii). The olefin can then deco-ordinate regenerating the original metal-hydride (iv). A non-productive side reaction (ii') also occurs to a large extent. This is the formation and subsequent  $\beta$ -elimination of a primary metal alkyl and this process is thermodynamically favourable. (Fig 8.2.2). Due to the reversibility of all the steps the reaction eventually leads to a thermodynamic equilibrium of olefins. Various catalyst systems have been reported to isomerise olefins via this mechanism, some of which consist of stable metal-hydrides e.g.  $\text{RhH}(\text{CO})(\text{PPh}_3)_3$  and  $\text{RuHCl}(\text{PPh}_3)$  but some of which do not e.g.  $\text{RhCl}_3$  and  $\text{Ni}[\text{P}(\text{OEt})_3]_4$ . These systems therefore require co-catalysts such as acids for the generation of the initial metal-hydride.<sup>76</sup>

The other, less commonly observed, mechanism for olefin isomerisation is the  $\Pi$ -allyl hydride mechanism. In this mechanism, free olefin co-ordinates to a non-hydride transition metal species (i). Oxidative addition of an allylic C-H bond forms a  $\Pi$ -allyl metal-hydride (ii). Rotation and transfer of the proton to the opposite end of the olefin yields the isomerised olefin (iii) which can then disassociate leaving the original non-hydride transition metal species (iv). (Fig 8.2.3). As with the metal-hydride addition-elimination mechanism, the reversibility of the steps leads to an equilibrium mixture of olefin products.



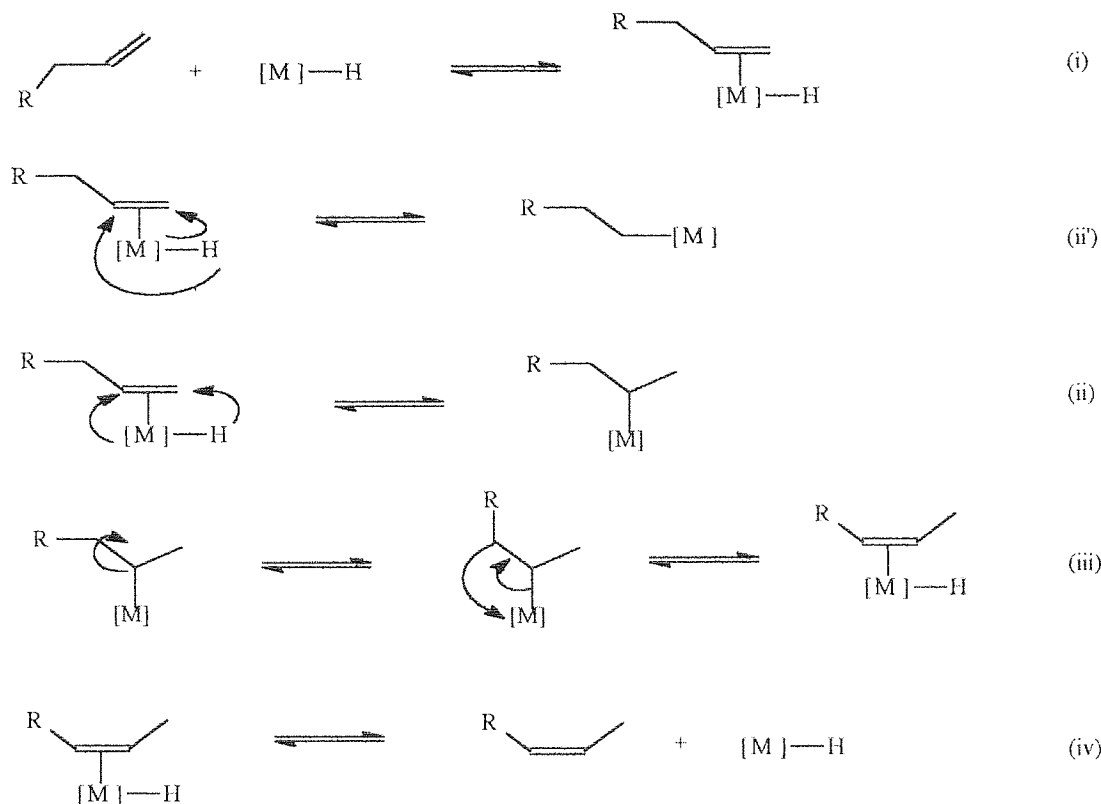


**Fig 8.2.2 - Metal-hydride addition-elimination mechanism for olefin isomerisation.**

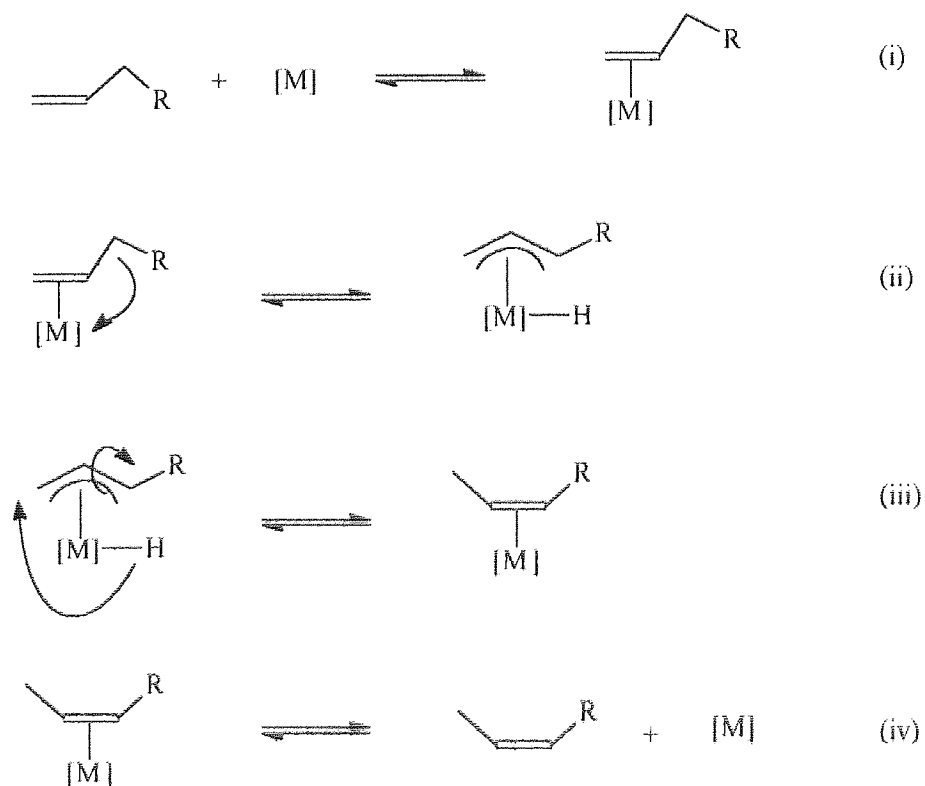


**Fig 8.2.3 -  $\pi$ -allyl hydride mechanism for olefin isomerization**

Although both mechanisms produce the same products, they can be distinguished by labelling studies. The metal-hydride addition-elimination mechanism can produce a 1,2-hydrogen shift via a primary metal alkyl and then a secondary metal alkyl. The  $\Pi$ -allyl hydride mechanism involves a 1,3-hydrogen shift via a mediating metal hydride as shown in Fig 8.2.4.

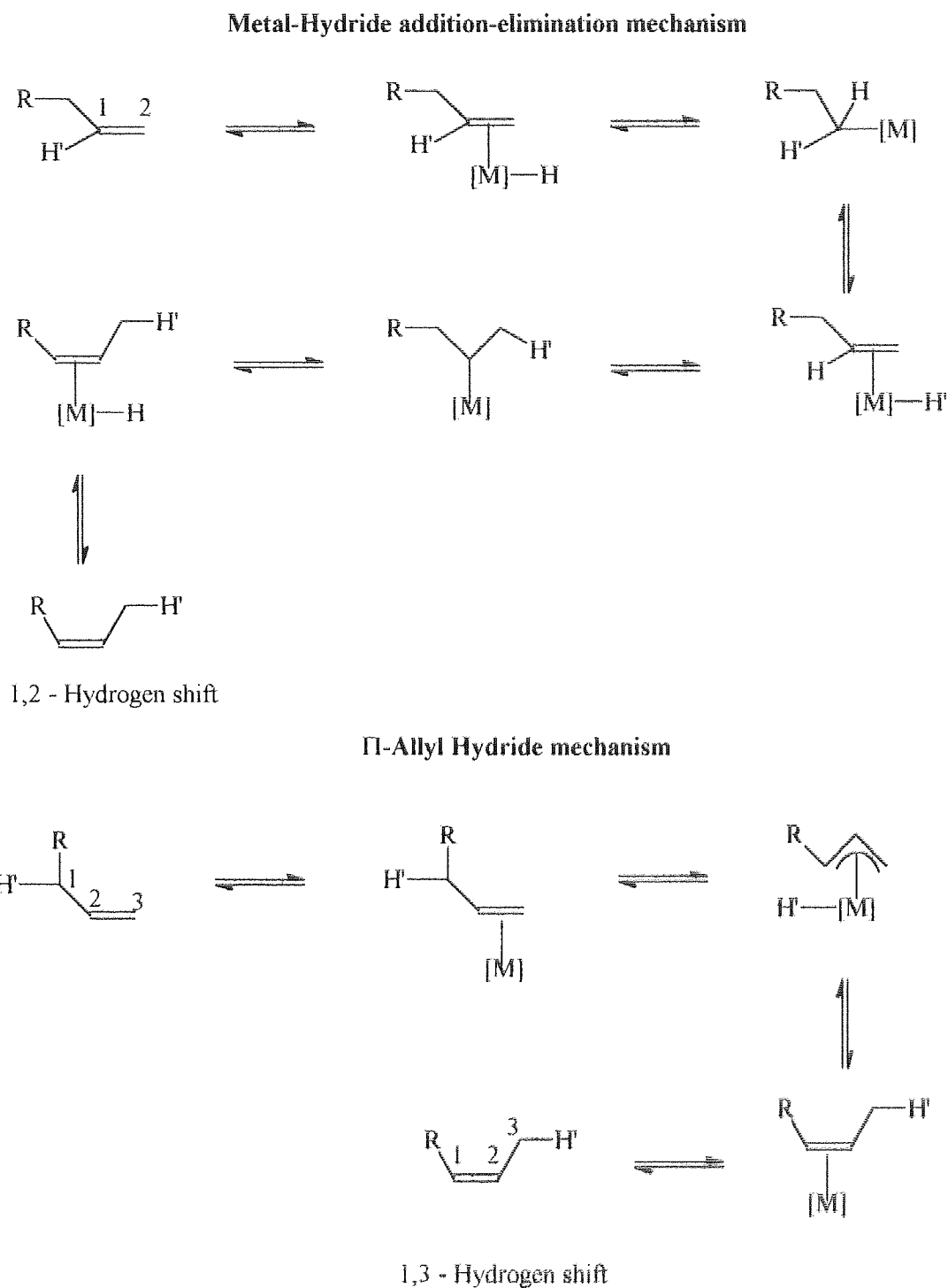


**Fig 8.2.4 - Hydrogen shifts by different isomerization mechanisms.**

The other distinguishing feature of the two mechanisms is that the addition-elimination mechanism is intermolecular i.e. hydrogen atoms from one olefin molecule can be transferred from one olefin molecule to another via the metal catalyst, whereas the  $\Pi$ -allyl mechanism is entirely intramolecular.

The aqueous Ru(II) catalysed isomerization of functionalised olefins was found to proceed via a metal hydride intermolecular mechanism.<sup>76</sup> The lack of a 1,2 - hydrogen shifted product was explained by the olefin's being directed in its co-ordination to the metal by pre-coordination of the pendant oxygen function. This forces the metal into the correct position to form the secondary metal alkyl only so that the addition is exclusively Markovnikov in character i.e. the hydrogen will add to that carbon already bearing the greatest number of hydrogen atoms (the terminal carbon) and therefore no primary metal alkyl is formed. (Fig 8.2.5)

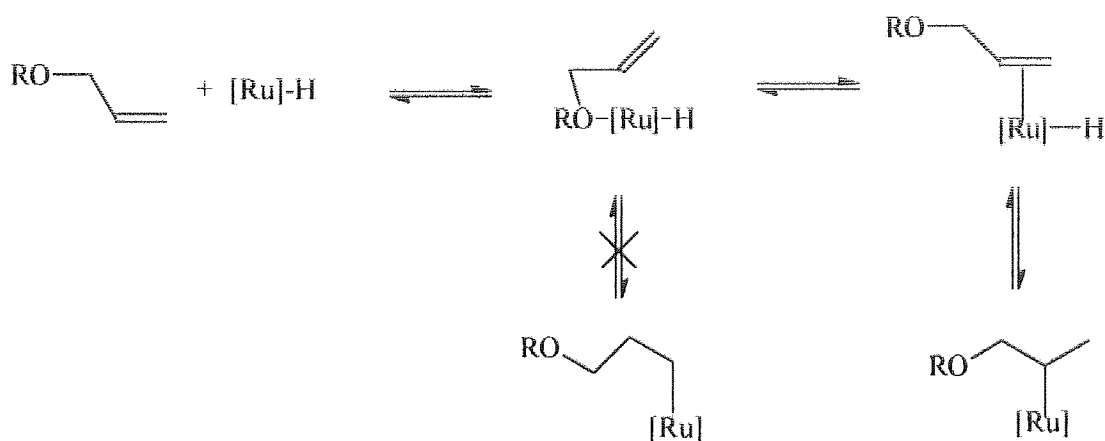


**Fig 8.2.5 - Exclusive Markovnikov addition in isomerisation by a Ru (II) catalyst.**

Such directing effects have also been observed in other systems, for example M<sup>C</sup>Kinney observed a nitrile directed olefin co-ordination in the selective isomerisation of 3-pentenenitrile to 4-pentenenitrile by HNi[P(OR)<sub>3</sub>]<sub>4</sub><sup>+</sup>.<sup>77</sup>

Isomerisation of unfunctionalised olefins by Ru(II) in aqueous media has been investigated by Karlen and Ludi<sup>78</sup>. They found that in the absence of directing groups, rotation in the metal alkyl selectively produced the *trans*- product unless a substituent provides a substantial barrier to rotation. Since rotation is fast compared to the β-elimination, the elimination will take place from the energetically most favourable conformer, therefore producing the *trans*- product. (Fig 8.2.6)

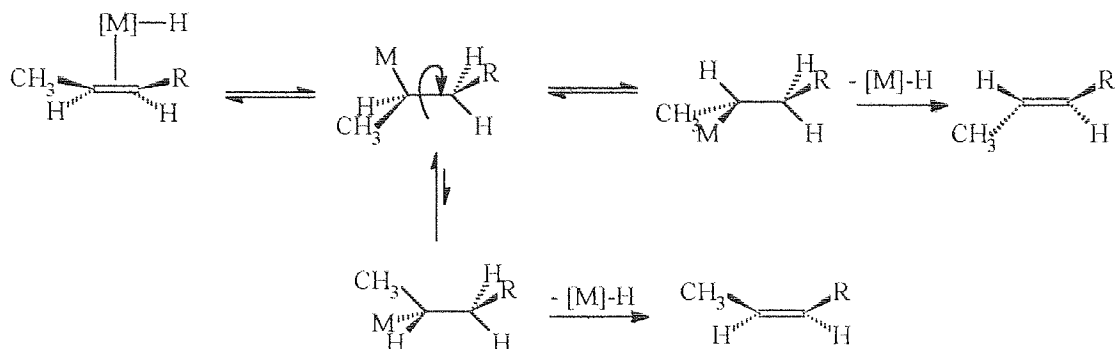


**Fig 8.2.6 - Selective formation of *trans*- products due to bond rotation**

However, when chelating groups are present, the directing behaviour can overcome favourable rotation so that for the isomerisation of 4-penten-1-ol, the *cis:trans* ratio of the product 3-penten-1-ol is 73:27, and the *cis*- product is the major one.<sup>78</sup>

All the isomerisation mechanisms described here share a common feature - the transformation of a  $\Pi$  bond into a  $\sigma$  bond either by the formation of a metal alkyl bond or oxidation of the double bond by an ionic species. The  $\sigma$  bond allows rotation, usually to the energetically more favourable *trans*- conformation before the  $\Pi$  bond is reformed, releasing the *trans*- product.

From the experimental work carried out during this study, it was found that with both  $\text{Ru}(\text{CO})\text{Cl}_2(\text{H}_2\text{O})$  and  $\text{RuCl}_2\text{P}(\text{CH}_2\text{OH})_3$ , precipitation of fumaric acid occurred only from solutions containing 7-oxanorbornenedicarboxylic acid. No precipitate was formed from solutions containing maleic acid or norbornenedicarboxylic acid. Similarly no fumaric acid precipitation is observed from solutions containing either 7-oxanorbornenedicarboxylic acid or maleic acid alone in the absence of any ruthenium complex. Therefore any mechanism for the production of fumaric acid in these cases must include an interaction between a ruthenium complex and the bicycle 7-oxanorbornenedicarboxylic acid.

Although the reverse Diels-Alder reaction does occur in such solutions, as has been shown earlier (See Section 7.2), this cannot be an initial stage in this transformation as it would require the interaction of maleic acid with the ruthenium species to produce fumaric acid, which does not occur. The reverse Diels-Alder reaction cannot produce fumaric acid on its own for two reasons. 1/ As the forward reaction is the reaction of maleic anhydride with furan, then by the Principle of Microscopic Reversibility, the most favourable reverse reaction must be back to furan and maleic acid. 2/ As the Diels-Alder

reaction is a concerted bond rearrangement, at no point in the reverse reaction would the stereochemistry required for isomerisation exist. At no time would one end of the 1,2-dicarbonyl ethyl group be detached from the furan group, which must occur for rotation about a single bond to be allowed.

It is reasonable to assume that the first stage of the mechanism which does occur involves the coordination of ruthenium to the double bond of the bicyclic monomer. There are numerous examples of such complexes in the literature and a similar complex has been proposed as a catalytic precursor by Novak and Grubbs in the polymerisation of 2,3-dimethoxymethyl-7-oxanorbornene in solution<sup>10</sup> (See section 1.4 - Fig 1.4.2). Due to the presence of the protons on the double bond and the orientation of the  $\Pi$  bond, it is likely that the ruthenium co-ordinates perpendicularly below the plane of the double bond to minimise steric crowding. Such side-on co-ordination is similarly proposed by McGrath and Grubbs<sup>79</sup>, and confirmed by NMR spectra, for the co-ordination product of the reaction between  $\text{Ru}^{\text{II}}(\text{H}_2\text{O})_6(\text{tos})_2$  and 2,5-dihydrofuran (tos = *p*-toluenesulfonate). (Fig 8.2.7).

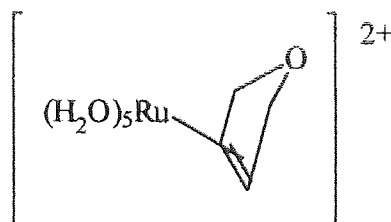


**Fig 8.2.7 - Ru (II) - 2,5-dihydrofuran co-ordination complex.**

That is the complex in the initial stage in this mechanism will be shown in Fig 8.2.8 and Fig 8.2.9.

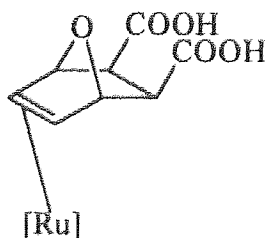


**Fig 8.2.8 - Proposed initial Ru-Monomer complex.**

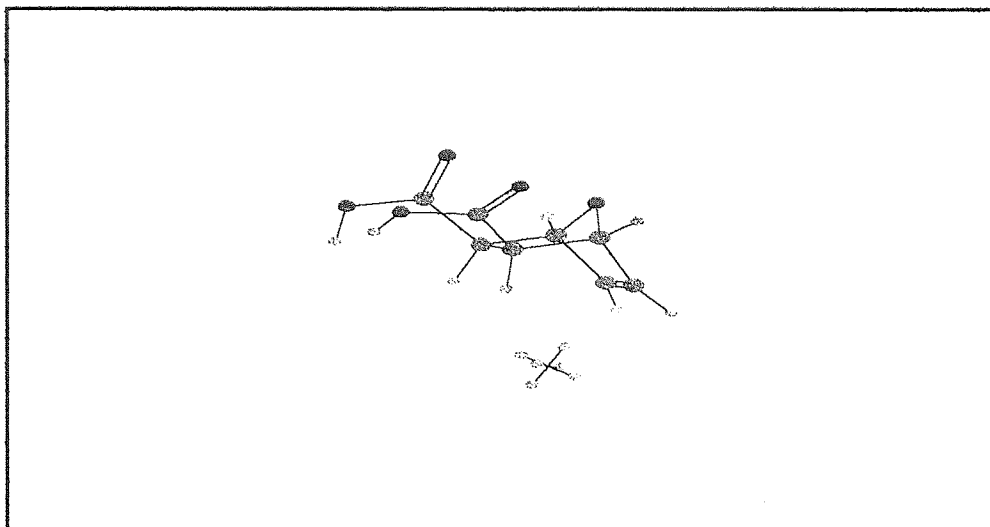


**Fig. 8.2.9 - Proposed initial Ru-monomer complex.  
ChemX molecular modelling software.**

The next stage in the proposed mechanism is the breaking of either of two bonds in the bicyclic ring. This cleavage not only releases some of the ring strain in the molecule but also allows the bond separating the two carboxylic acid groups to rotate. This rotation is energetically favourable as it brings the two -COOH groups into a trans- conformation. It also brings one of the carboxylic acid groups into the correct orientation and separation from the ruthenium atom to allow chelation via its oxygen atom to occur. There is evidence for the preferential formation of such chelate complexes. A bond breaking and chelation mechanism has been proposed by Stone *et al.*<sup>80</sup> (Fig 8.2.10) for the isomerisation of methoxycarbonyl-ruthenium complexes, while cyclic chelate complexes similar to that proposed were isolated.

Even more significantly, a bis-chelate complex formed from the reaction between  $\text{Ru}^{\text{II}}(\text{H}_2\text{O})_6(\text{tos})_2$  and excess 3-pentenoic acid has been isolated and a crystal structure determined showing both co-ordination to the double bond and chelation of the pendant oxygen.<sup>79</sup> (Fig 8.2.11)

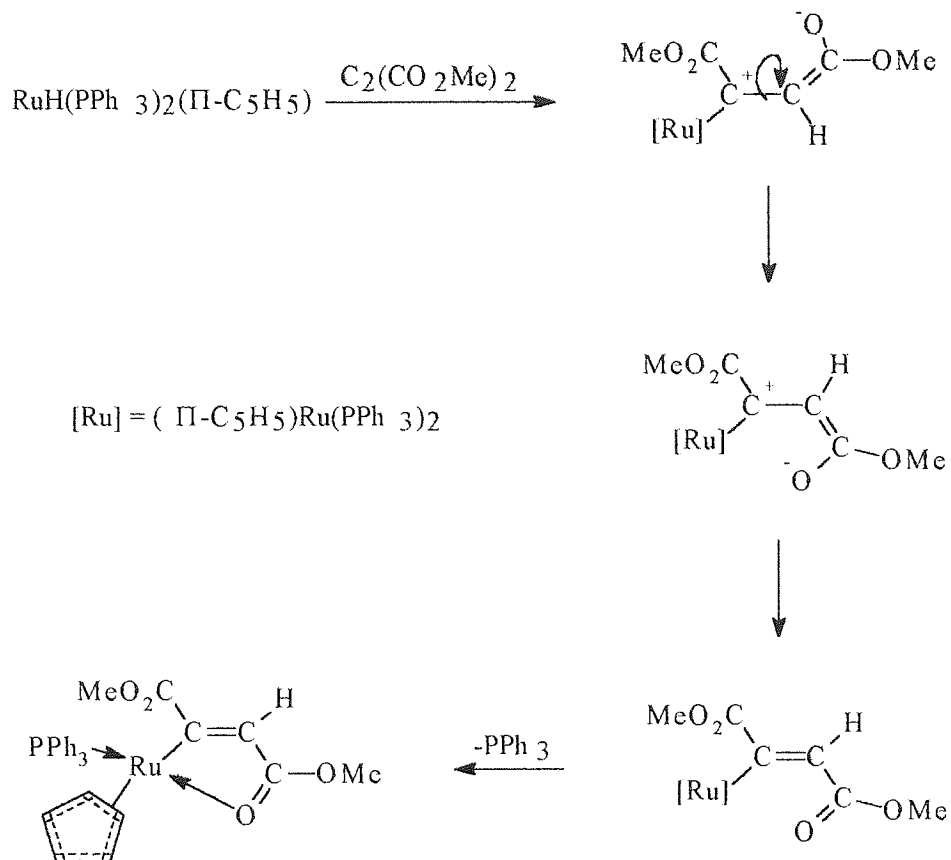


Fig 8.2.10 - Proposed mechanism for the isomerisation of a ruthenium-methoxycarbonyl complex.<sup>80</sup>

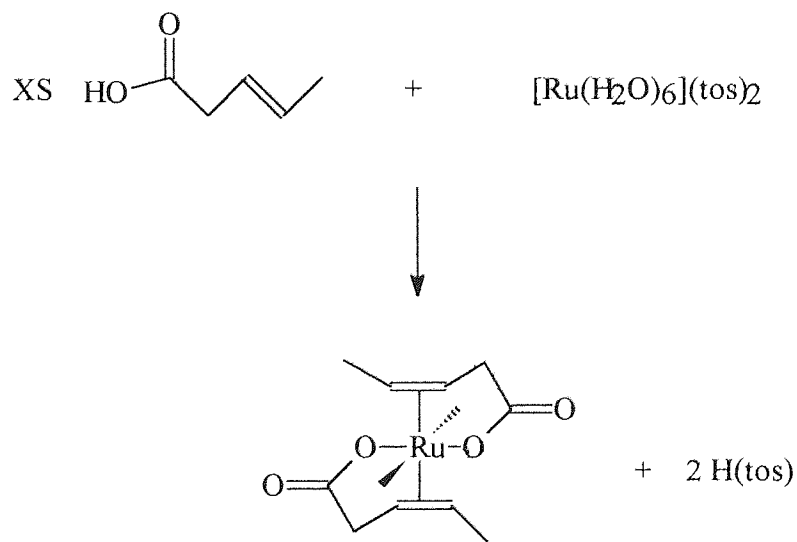
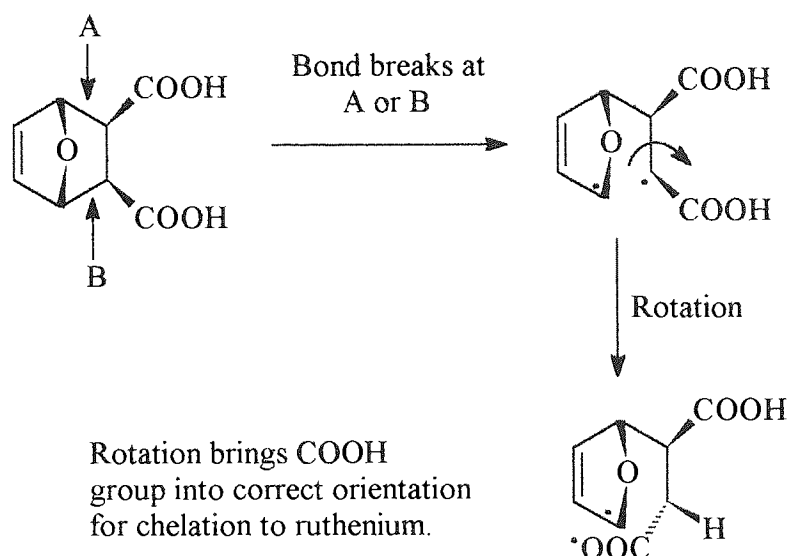


Fig 8.2.11 - Bis-chelate complex -  

$$\text{Ru}(\text{H}_2\text{O})_2(\eta^1(\text{O}):\eta^2(\text{C},\text{C}')\text{-OCOCH}_2\text{CH}=\text{CHCH}_3)_2$$
  
 [H<sub>2</sub>O ligands not shown]

For this chelating bond formation to occur, the carboxylic function must deprotonate, with the proton possibly forming an  $sp^3$  bond to the rotating carbon, see Fig 8.2.12.



**Fig 8.2.12 - Bond breaking and rotation in Ru-Monomer complex.**  
(Co-ordinated ruthenium not shown.)

This rotation brings the two carboxylic acid groups into a *trans*- orientation in relation to each other. A model of the proposed chelate complex has been built using conventional molecular models (Cochranes of Oxford molecular models - Minit size) and visualised using the computer molecular modelling software - ChemX (Fig 8.2.13 and Fig. 8.2.14). Both approaches show that such a chelate complex is feasible even when the original ruthenium complex contains three  $P(CH_2OH)_3$  ligands. Average bond lengths used ( $Ru-[C=C] = 2.1 \text{ \AA}$ ,  $Ru-O = 2.1 \text{ \AA}$ ,  $Ru-P = 2.3 \text{ \AA}$ ) were taken from literature reports of similar compounds.

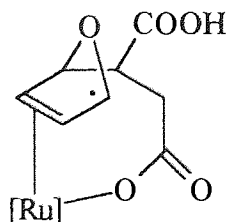


**Fig 8.2.13 - Proposed Ru-Monomer chelate complex.**



The driving force for this isomerisation is thus two-fold; the release of ring strain and the chelation to the metal centre. The complex can then split apart to form furan, fumaric acid and the original ruthenium complex, although it is not clear what is the major driving force for decomposition. There is obviously some entropic advantage in decomposition in going from the chelate complex to three separate molecules but there may also be enthalpic effects.

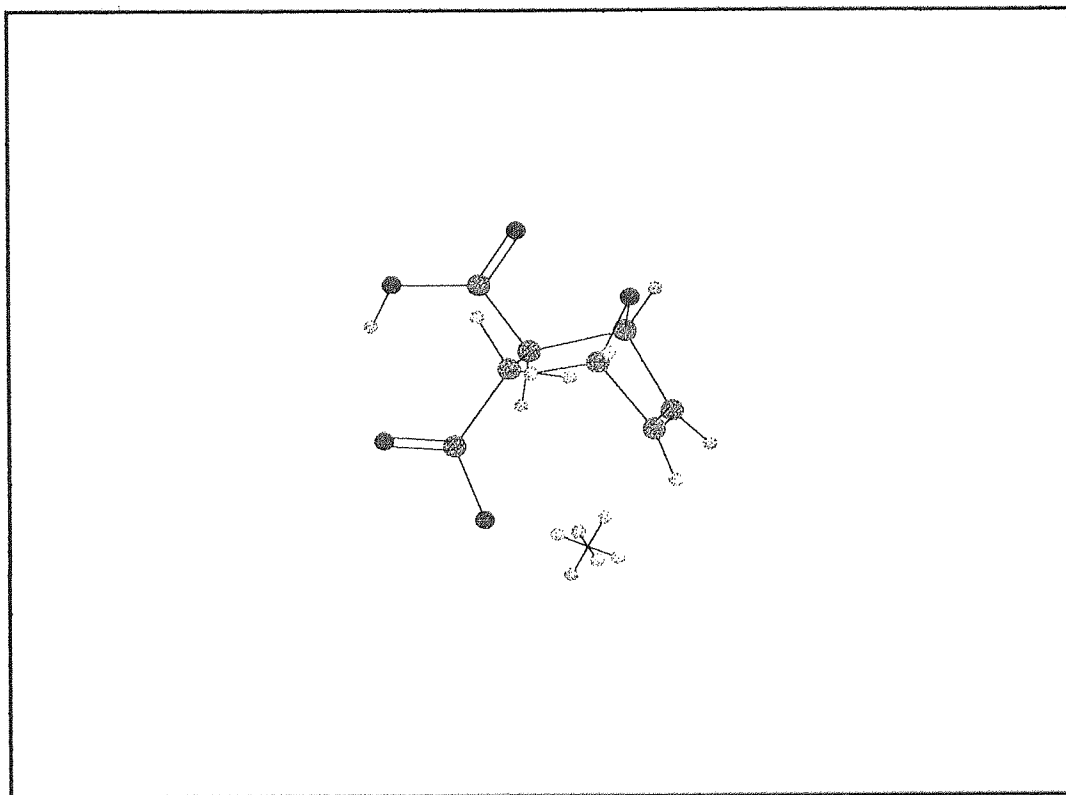
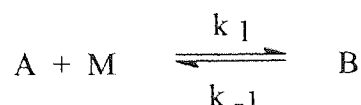


**Fig 8.2.14 - Proposed Ru-Monomer chelate complex.  
ChemX molecular modelling software.**

### 8.3 - The interaction between 7-oxanorbornenedicarboxylic acid and Ru(CO)Cl<sub>2</sub>(H<sub>2</sub>O) monitored by UV spectroscopy.

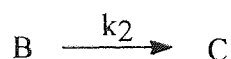
#### Kinetics.

The monitoring of this reaction and the retrieval of kinetic data have been described previously (Sections 6.4 and 7.3). To recap, the data fit a two stage process. The first stage is the establishment of an equilibrium and the early data ( $t < 180$  mins) can be fitted to equation (1).



$$\text{Abs}[B] = \epsilon_B[A]_0 K_1[M] \{1 - e^{-(k_{-1}(1 + K_1[M])t)}\} / (1 + K_1[M]) \quad (1)$$

The second stage suggests a transformation from B to C where both B and C absorb in the same region. The change in absorption for the complete reaction is given by a combination of the two stages and is described by equation (2).



$$\text{Abs} = Z(1 - e^{-k_{\text{obs}}t}) + Yt \quad (2)$$

where Z and Y are the composite constants

$$Z = [A]_0 K_1[M] \{ \epsilon_B - \epsilon_C k_2 / k_{-1} (1 + K_1[M]) \} / (1 + k_1[M])$$

and

$$Y = \epsilon_C [A]_0 K_1[M] k_2 / (1 + k_1[M])$$

For the derivation of the equations see section 7.3.

Tables 8.2.1 and 8.2.2 contains the equilibrium constants for various monomer and Ru(CO)Cl<sub>2</sub>(H<sub>2</sub>O) concentrations.

**Table 8.3.1 - Equation constants for solutions with constant Ru(CO)Cl<sub>2</sub>(H<sub>2</sub>O) concentration (0.025 M) (T=70°C).**

Sample	[M]/ mol dm <sup>-3</sup>	K <sub>1</sub> / mol dm <sup>-3</sup>	10 <sup>4</sup> k <sub>-1</sub> / min <sup>-1</sup>	ε <sub>B</sub> [A] <sub>0</sub> / mol dm <sup>-3</sup>	k <sub>obs</sub> / min <sup>-1</sup>	Z/ mol <sup>1</sup> dm <sup>3</sup>	10 <sup>5</sup> Y/ min <sup>-1</sup>
UV3/4	0.1	7	33	1.03	-	-	-
UV3/3	0.15	6.7	33	0.94	-	-	-
UV3/2	0.2	6.8	26	1.03	-	-	-
UV3/1	0.25	6.5	22	1.07	-	-	-
UV4/3	0.3	6.3	12	1.67	40	0.89	12
UV4/2	0.35	7.2	27	0.89	49	0.9	19
UV4/1	0.4	7.5	26	0.99	73	0.88	15
Average		6.95	27.8 <sup>a</sup>	0.99 <sup>a</sup>	54	0.89	15.3

*Experiment UV3 did not run for long enough to provide data for the complete fit.*

*a) Average does not include value from UV4/3.*

**Table 8.3.2 - Equation constants for solutions with constant monomer concentration (0.01 M) (T=60°C).**

Sample	10 <sup>4</sup> [Ru]/ mol dm <sup>-3</sup>	K <sub>1</sub> / mol dm <sup>-3</sup>	10 <sup>4</sup> k <sub>-1</sub> / min <sup>-1</sup>	ε <sub>B</sub> [A] <sub>0</sub> / mol dm <sup>-3</sup>	k <sub>obs</sub> / min <sup>-1</sup>	Z/ mol <sup>-1</sup> dm <sup>3</sup>	10 <sup>5</sup> Y/ min <sup>-1</sup>
UV2/3	2	7.8	700	1.23	80	0.14	2.7
UV1/4	2.5	-	-	-	24	0.14	1.3
UV1/3	5	-	-	-	19	0.27	2.7
UV2/2	5	7.5	80	1.26	24	0.21	3.3
UV1/2	7.5	-	-	-	19	0.40	4.4
UV1/1	10	-	-	-	26	0.46	4.9
UV2/1	10	12.3	60	2.19	23	0.47	10.3
Average		7.65 <sup>a</sup>	70 <sup>b</sup>	-	22.5 <sup>b</sup>	-	-

*Missing values indicate not enough data points to provide an adequate fit.*

*a) Average does not include UV2/1.*

*b) Average does not include UV2/3.*

With the exception of Z and Y, which increase with increase in [Ru(CO)Cl<sub>2</sub>(H<sub>2</sub>O)], all the constants appear to remain constant with change in monomer and Ru(CO)Cl<sub>2</sub>(H<sub>2</sub>O) concentration.

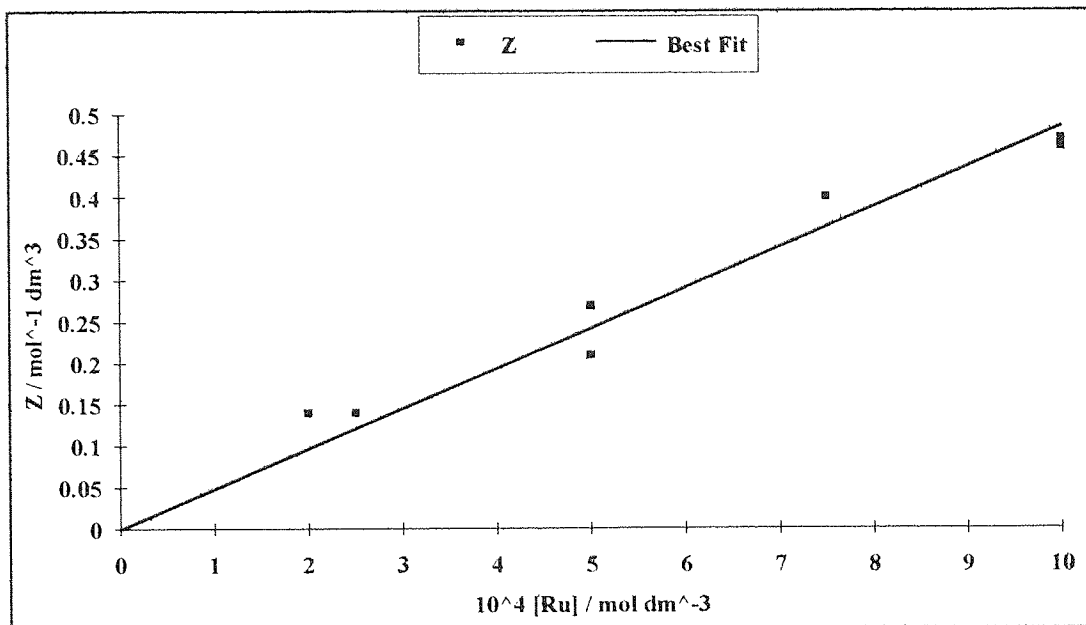


Fig 8.3.1 - Variation of Z with change in  $[\text{Ru}(\text{CO})\text{Cl}_2(\text{H}_2\text{O})]$ .

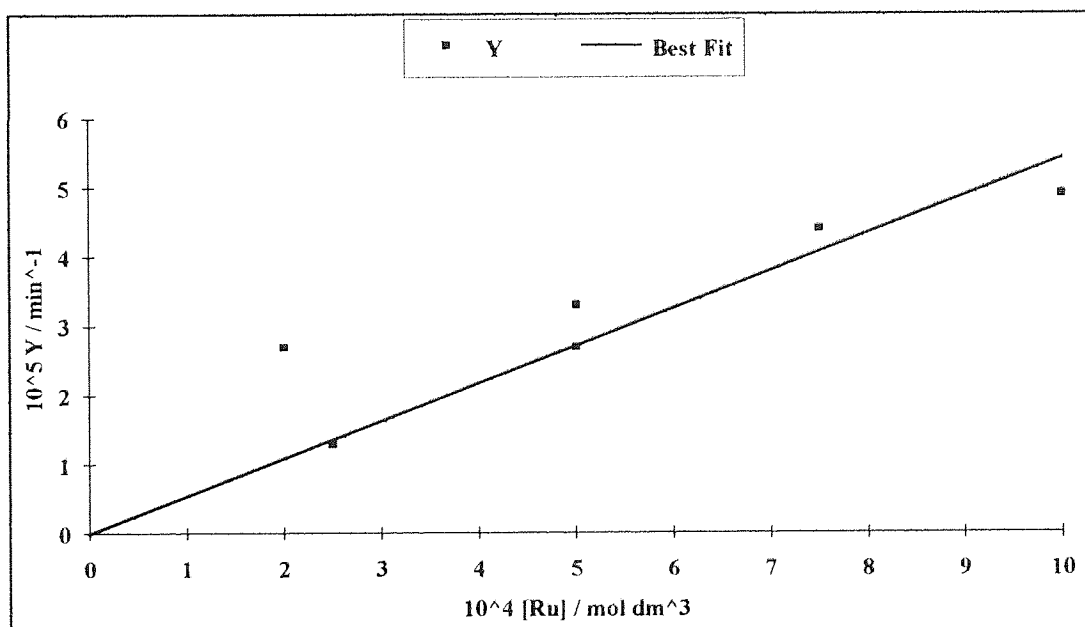


Fig 8.3.2 - Variation in Y with change in  $[\text{Ru}(\text{CO})\text{Cl}_2(\text{H}_2\text{O})]$ .

This increase is explained by the form of the equations for Z and Y.

$$Z = [A]_0 K_1 [M] \{ \epsilon_B - \epsilon_C k_2 / (k_{-1} (1 + K_1 [M])) \} / (1 + K_1 [M])$$

but the term containing  $\epsilon_B$  is the larger such that:-

$$Z \approx \epsilon_B [A]_0 K_1 [M] / (1 + K_1 [M])$$

Similarly for Y

$$Y = [A]_0 k_2 \epsilon_C K_1 [M] / (1 + k_1 [M])$$

$$\therefore Y/Z \approx \epsilon_C k_2 / \epsilon_B$$

For the proposed scheme this value must be much less than 1, and the data agree with this (See Table 8.2.2). The anticipated increase in  $\epsilon_B [A]_0$  with increase in  $[\text{Ru}(\text{CO})\text{Cl}_2(\text{H}_2\text{O})]$  cannot be seen clearly due to the lack of data for the pre-equilibrium stage of the reaction from experiment UV1.

The data presented here, despite not being all encompassing, can be seen to fit the proposed kinetic scheme excellently well. To complete and confirm the observations made additional experiments need to be performed, particularly for the early stages of the reaction.

### **Proposed Mechanism.**

The data fit very well with the kinetic scheme proposed. This scheme must now be rationalised in terms of the reactants involved and the products isolated. The lack of polymeric product, as evidenced by NMR and SEC results negates the possibility of a stepwise polymerisation reaction. It therefore seems reasonable to interpret the results in terms of the mechanism proposed for the production of fumaric acid (Section 8.2).

The nature of the ruthenium species in solution is unknown. Ruthenium(II) species are known to form  $\Pi$ -bonded complexes under similar conditions and the same products are produced when the reaction is performed under argon. Therefore the ruthenium is most likely to exist in the 2+ oxidation state in its reactive form, and a disproportionation or oxidation reaction is not envisaged as the first step. In the solid state,  $\text{Ru}(\text{CO})\text{Cl}_2(\text{H}_2\text{O})$  exists as a series of kinked  $\text{Ru}(\text{CO})\text{Cl}_4(\text{H}_2\text{O})$  units. In solution,  $\text{Ru}(\text{CO})\text{Cl}_2(\text{H}_2\text{O})$  reacts with donor ligands to octahedral complexes of the type  $\text{Ru}(\text{CO})\text{Cl}_2(\text{H}_2\text{O})\text{L}_2$ <sup>60</sup>. Since the ruthenium solutions were made up initially in the absence of monomer, the initial form of the ruthenium is  $\text{Ru}(\text{CO})\text{Cl}_2(\text{H}_2\text{O})_3$ . Whether this is the active species [A] is unknown but not unlikely. For the purpose of this proposal that is assumed to be the case.

The first reaction can be envisaged as the coordination of the double bond on the monomer to the ruthenium species in solution. Such complexes are well known and have been proposed as intermediates in other systems of this type<sup>29</sup> (See 8.2) This reaction is seen as the first step of the mechanism i.e.

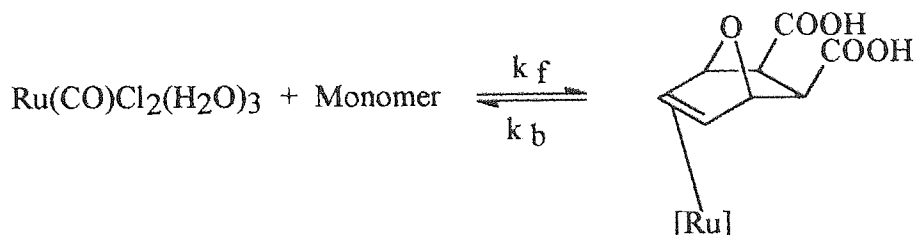


**Fig 8.3.3 - Formation of a Ru-Monomer  $\Pi$ -complex.**

The mechanism then requires the  $\Pi$ -complex to undergo a very slow transformation to some species C. There is no direct evidence for the nature of this species but from the previously proposed mechanism for the production of fumaric acid, three possibilities can be considered.

The most obvious possibility is that the  $\Pi$ -complex undergoes a bond breaking/rotation/chelation process as proposed in the earlier mechanism for formation of fumaric acid (See 8.2). The chelate-complex then undergoes a slow decomposition reproducing the original ruthenium species and fumaric acid, which is therefore the strongly absorbing species C (the other product of decomposition, furan, will be lost from solution rapidly due to both its insolubility and its low boiling point). Although much of the observed product, fumaric acid, precipitates from solution, NMR spectra of the residues obtained by reducing the filtered reaction solution showed the presence of more fumaric acid still in solution (See Section 7.3 and Appendix B - Figs B36 and B37). It is reasonable therefore to assume that an adequate proportion of fumaric acid remains in solution for it to be a candidate for the species C. However spectrophotometric evidence discounts this possibility. UV spectrophotometric data from the literature<sup>81</sup> show that fumaric acid absorbs at 323nm only at high concentrations. An estimate of the extinction coefficient from the spectral data gives  $\epsilon \approx 20 \text{ mol}^{-1}\text{dm}^3$ . As discussed previously, the kinetic mechanism requires the slow production of an absorbing species with a very large extinction coefficient, so fumaric acid is unlikely to be the species observed.

Another possibility is that the  $\Pi$ -complex undergoes a bond breaking/rotation/chelation process which then quickly undergoes a partial degradation, releasing a furan molecule and leaving fumaric acid co-ordinated to the ruthenium centre (Fig. 8.3.3).

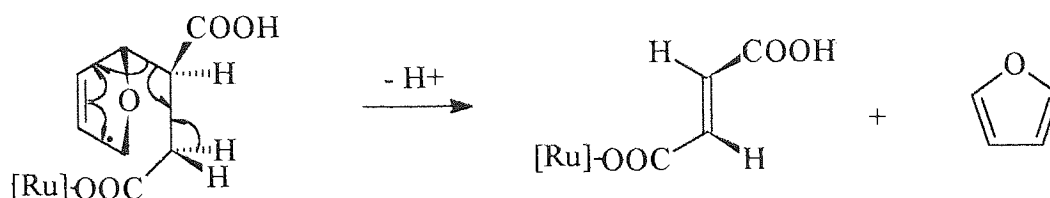
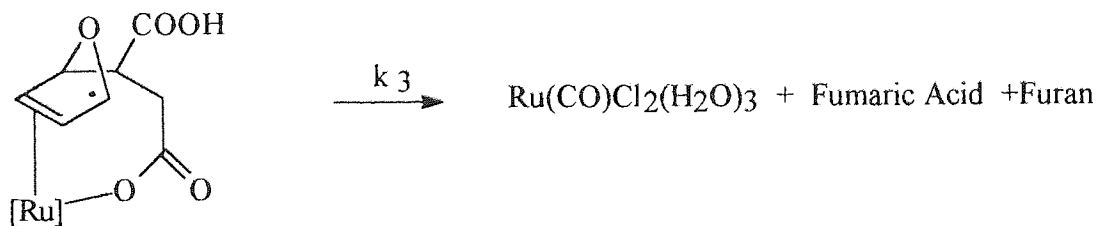
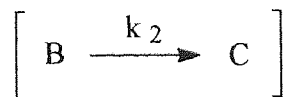
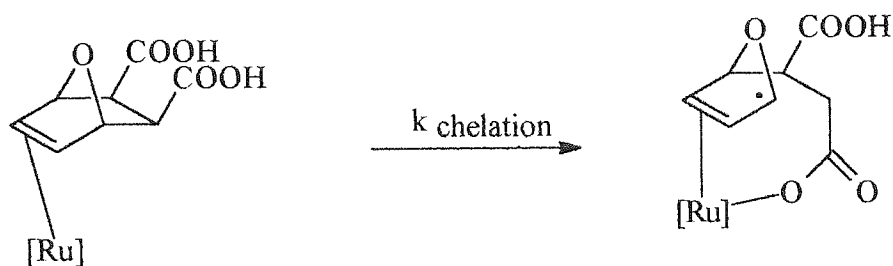
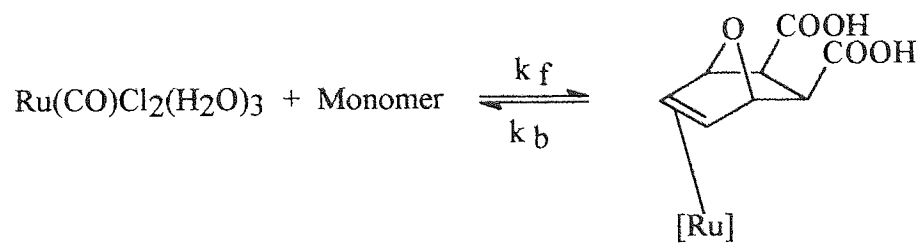


**Fig 8.3.4 - Partial degradation of ruthenium chelate complex.**  
(Co-ordination to double bond not shown)

This ruthenium-fumaric acid complex would then be identified as the strongly absorbing species C. There are no spectrophotometric data for Ru-fumarate complexes published in the literature. However, there are a large number of published reports on the spectrophotometric behaviour of similar Co(III) complexes - such complexes were used in the investigation of inner- and outer- sphere redox reactions.<sup>82</sup> As Co(III) is also low spin  $d^6$  it is not unreasonable to compare extinction coefficient values for such compounds with the expected value for the complex suggested above. In one such reference, Sebera and Taube<sup>83</sup> show that  $\text{Co}(\text{NH}_3)_5(\text{fumarate})$  and  $\text{Co}(\text{NH}_3)_5(\text{maleate})$  to have  $\epsilon = 53 - 79 \text{ mol}^{-1}\text{dm}^3$  at 350 nm. Thus, an analogous ruthenium complex is unlikely to have the high extinction coefficient required by the kinetic scheme for the product C.

The negation of the two options described above leaves a final and more likely possibility. This is that the  $\Pi$ -complex slowly undergoes a bond breaking/rotation/chelation process and the chelate-complex is itself the strongly absorbing species C. For this to be the case a further step, beyond the rate determining step, is necessary to provide the observed product, fumaric acid - for the concentration of C to build up steadily and therefore for the absorbance to increase linearly, as is indicated by the experimental data, the rate of this decomposition must be slower than the rate of formation of C. Unfortunately, confirmation of this proposal cannot be obtained as no UV spectrophotometric data for such chelate complexes exists in the literature. The overall proposed mechanism is summarised below (Fig. 8.3.4). The equivalent step in the kinetic scheme is given in parentheses.



where  $k_2 > k_3$ .

Fig 8.3.5 - Proposed isomerisation mechanism and associated kinetic scheme.



#### 8.4 - Aqueous ROMP using Ruthenium Complex Catalysts - Conclusions.

The aim of this body of research was to produce well defined, water soluble, ruthenium complexes to polymerise bicyclic monomers in 100% aqueous systems. It was hoped that the retrieval of kinetic data from such systems would provide useful information into the mechanism of aqueous ROMP. The failure to achieve polymerisation with any of the discrete Ru(II) complexes investigated and the isolation of fumaric acid from these same systems is indicative of the problems associated with investigations in this area - that is the lack of information on the nature of the co-ordinating species and therefore the mechanism of the carbene forming reaction which is presumed to be the initiating species in the ROMP reaction.

The first observations of aqueous ROMP<sup>10</sup> utilised  $\text{RuCl}_3 \cdot 3\text{H}_2\text{O}$  as the catalyst precursor. However, as has been mentioned previously (See 5.2),  $\text{RuCl}_3 \cdot 3\text{H}_2\text{O}$  is a nominal description of a compound which is in reality a mixture of Ru(IV) polynuclear species. The active species in solution was hypothesised to be a Ru(II)-monomer complex (See Fig 1.4.2) and this species would then presumably have to be transformed into a Ru-carbene complex to act as the initiating species in the polymerisation. However, the difficulties inherent in studying  $\text{RuCl}_3 \cdot 3\text{H}_2\text{O}$  systems is evidenced by the difference in results obtained by two separate groups when investigating the same system<sup>24, 27</sup> - the 100% aqueous polymerisation of oxanorbornenedicarboxylic acid (See 1.4).

If we accept that the first step in these systems is the  $\Pi$ -co-ordination of the monomer to the ruthenium in solution (and the production of fumaric acid described herein would support the formation of such a species) then sufficient differences must exist between the systems investigated here and those quoted in the literature<sup>10, 24, 27</sup> to prevent the formation of a polymerisation initiating species in my experiments. It is not unreasonable to suggest that the presence of other ruthenium species in solution (inherent in the use of  $\text{RuCl}_3 \cdot 3\text{H}_2\text{O}$ ) could play an important part in the formation of the initiating species. It could be the use of single discrete ruthenium complexes which has prevented the formation of an initiating species in this case.

The direction that research into this area has taken has bypassed the need to understand and therefore manipulate the mechanism of carbene formation in the  $\text{RuCl}_3 \cdot 3\text{H}_2\text{O}$  catalysed system. The work of Grubbs *et al.*<sup>15</sup> on the synthesis of well defined ruthenium-carbene catalysts has shown that the unusual stability of the catalysts to deactivation by protic media and functional groups can be extended beyond the poorly

defined  $\text{RuCl}_3 \cdot 3\text{H}_2\text{O}$  system (See 1.3.1). However the move away from the 100% aqueous system means that there exists scant information directly relevant to the mechanism of catalyst formation. Undoubtedly the only way for progress to be made in researching such 100% aqueous systems is (in the absence of the actual isolation and characterisation of the active carbene species in the  $\text{RuCl}_3 \cdot 3\text{H}_2\text{O}$  system) to mimic the approach of Grubbs *et al.* by looking into the synthesis of a stable, *water-soluble* ruthenium-carbene complex. However, this in itself would still be by-passing the actual problem - that of understanding and defining the actual mechanism of carbene formation in these systems. This can only be arrived at by more detailed studies into the co-ordination chemistry of ruthenium in the presence of olefins in general and bicyclic monomers in particular. As has been shown by the isolation of fumaric acid here, the chemistry involved after the initial ruthenium-monomer co-ordination is unclear and possibly only leads to carbene formation and subsequent polymerisation when  $\text{RuCl}_3 \cdot 3\text{H}_2\text{O}$  or the  $\Pi$ -bonded complex postulated previously (Fig 1.4.2) is the ruthenium source.

## REFERENCES

- 1 - **Olefin Metathesis and Ring-Opening Polymerization of Cyclo-Olefins.**  
Valerian Dragutan, Alexandru T. Balaban & Mihai Dimonie.  
Published by John Wiley & Sons Ltd., (1985)
- 2 - **Metathesis polymerisation: Chemistry.**  
A.J. Amass.  
Comp. Poly. Sci., 4(6), 109-135, (1989)
- 3 - **Catalyse de transformation des olefins par les complexes du tungstene.**  
J.L. Herisson & Y. Chauvin.  
Makromol. Chem., 141, 161, (1970)
- 4 - **The mechanism of the olefin metathesis reaction.**  
Thomas J. Katz & James McGinnis  
J. Am. Chem. Soc., 97, 1592-1594, (1975).
- 5 - **Consideration of the mechanism of the olefin metathesis reaction.**  
Robert R. Grubbs, Patrick L. Burk & Dale D. Carr  
J. Am. Chem. Soc., 97, 3265-3267, (1975).
- 6 - **Mechanism for the Olefin Metathesis Reaction.**  
E.I. Muettterties  
Inorg. Chem., 14(4), 951-953, (1975).
- 7 - **Possible role of Hydido-Metal Complexes in Metathesis, Isomerisation, Dimerisation and Polymerisation of Alkenes.**  
D. Theodore Lavery, John R. Rooney & Allan Stewart.  
J. Cat., 45, 110-113, (1976).
- 8 - **Role of dioxygen as an activator in Olefin Metathesis.**  
Kenneth J. Ivin, Boreddy S. R. Reddy & John R. Rooney.  
J. Chem. Soc., Chem. Comm., 1062-1064, (1981).
- 9 - **On the mechanism of the metal catalysed disproportionation of olefins.**  
Glenn S. Lewandos & R. Pettit  
J. Am. Chem. Soc., 93, 7087-7087, (1971)
- 10 - **Catalytic organometallic chemistry in water: The aqueous ring opening metathesis polymerisation of 7-oxanorbornene derivatives.**  
Bruce M. Novak & R.H. Grubbs  
J. Am. Chem. Soc., 110, 7542-7543, (1988)

- 11 - **Selectivity in the olefin metathesis of unsymmetrically substituted ethylenes.**  
Thomas J. Katz, James M<sup>C</sup>Ginnis & Samuel Hurwitz  
J. Am. Chem. Soc., 98, 605, (1976)
- 12 - **Generation and reaction of (Phenylmethylcarbene)pentacarbonyl-tungsten (0).**  
Charles P. Casey, Loren D. Albin & Terry J. Burkhardt  
J. Am. Chem. Soc., 99, 2533-2539, (1977).
- 13 - **Alkylidene Complexes of Niobium and Tantalum.**  
Richard R. Schrock  
Acc. Chem. Res., 12, 98-104, (1979)
- 14 - **Tungsten-Oxo Alkylidene Complexes as Olefin Metathesis catalysts and the crystal structure of W(O)(CHCMe<sub>3</sub>)(PEt<sub>3</sub>)Cl<sub>2</sub>.**  
Jeffery H. Wengrovius, Richard R. Schrock, Melvyn Rowen Churchill, Joseph R. Missert & Wiley J. Youngs.  
J. Am. Chem. Soc., 102, 4515-4516, (1980)
- 15 - **Ring opening metathesis polymerisation (ROMP) of norbornene by a Group VIII carbene complex in protic media.**  
SonBinh T. Nguyen, Lynda K. Johnson & Robert H. Grubbs  
J. Am. Chem. Soc., 114, 3974-3975, (1992)
- 16 - **Syntheses and activities of new single-component ruthenium-based olefin metathesis catalysts.**  
SonBinh T. Nguyen, Robert H. Grubbs & Joseph W. Ziller.  
J. Am. Chem. Soc., 115, 9858-9859, (1993).
- 17 - **Catalytic Ring-Closing Metathesis of Funtionalized Dienes by a Ruthenium Carbene Complex.**  
Gregory C. Fu, SonBinh T. Nguyen & Robert H. Grubbs.  
J. Am. Chem. Soc., 115, 9856-9857. (1993)
- 18 - **Olefin Metathesis I. Acyclic Vinylenic Hydrocarbons.**  
Nissim Calderon, Eilert A. Ofstead, John P. Ward, W Allen Judy & Kenneth W. Scott.  
J. Am. Chem. Soc., 90, 4133-4140, (1968).
- 19 - **Metathesis of 2-Pentene by a binary catalyst system of tungsten hexachloride and n-buylithium.**  
Jin-Liang Wang & H. R. Menapace.  
J. Org. Chem., 33, 3794, (1968)
- 20 - **Homogeneous catalysts for olefin disproportionation.**  
E. A. Zuech  
J. Chem. Soc., Chem. Comm., 1182, (1968).

- 21 - A.W Anderson and N.C. Merckling  
U.S Patent. 2,721,189. 18/10/1955.
- 22 - **Stereospecific ring cleavage homopolymerisation of cycloolefins and structural examination of the resulting homologous series of linear crystalline *trans*-polyalkenamers.**  
Guilio Natta, Gino Dall'Asta, Ivano Walter Bassi & Giovanna Carella.  
Makromol. Chem., 91, 87-106, (1966)
- 23 - **Olefin Metathesis - A novel reaction for skeletal transformations of unsaturated hydrocarbons.**  
Nissim Calderon, Hung Yu Chen & Kenneth W. Scott.  
Tet. Lett., 3327, (1967)
- 24 - **Aqueous ring-opening Metathesis polymerisations of heteropolycyclic carboxylic acids with transition-metal chlorides.**  
W. James. Feast & David B. Harrison  
Polymer, 32 (No.3), 558-563, (1991)
- 25 - **Aqueous metathesis polymerisations of heteropolycyclic alkenes using transition metal chloride catalysts.**  
W. James Feast & David B. Harrison.  
J. Mol. Cat., 65, 63-72, (1991).
- 26 - **Chain transfer during the aqueous ring-opening metathesis polymerisation of 7-oxanorbornene derivatives.**  
Marcia B. France, Robert H. Grubbs, Dominic V. McGrath & Rocco A. Paciello.  
Macromolecules, 26, 4742-4747, (1993)
- 27 - **Aqueous ring-opening metathesis polymerisation and copolymerisation of 2,3-dicarboxylic acid anhydride, 2,3-bis(methoxymethyl) and 2,3-dicarboxylic acid mono-methyl ester derivatives of 7-oxanorbornene.**  
Shui-Yu Lu, Peter Quayle, Frank Heatley, Colin Booth, Stephen G. Yeates & John C. Padget.  
Eur. Polym. J., 29(Nos. 2/3), 269-279, (1993).
- 28 - **Aqueous ring-opening metathesis polymerisation of 7-oxanorbornene derivatives with oxygen containing functionalities.**  
Shui-Yu Lu, Judith M. Amass, Nazia Majid, Dermott Glennon, Andrew Byerley, Frank Heatley, Peter Quayle, Colin Booth, Stephen G. Yeates & John C. Padget.  
Macromol. Chem. Phys., 195, 1273-1288, (1994)
- 29 - **Aqueous Ring opening metathesis polymerisation of *exo, exo* - 2,3 - bis(methoxymethyl) - 7 - oxanorbornene catalysed by ruthenium trichloride.**  
Shui-Yu Lu, Peter Quayle, Frank Heatly & Colin Booth  
Macromol., 25, 2692-2697, (1992)

- 30 - **Topics in inorganic and general chemistry. Vol 19 - The chemistry of Ruthenium.**  
E. A. Seddon and K. R. Seddon  
Elsevier Science Publishers, New York, (1984)
- 31 - **The Ring Opening Polymerisation of Ring Strained Cyclic Ethers.**  
Davinder Paul Singh Riat  
PhD Thesis, Aston University, Pg 112-115, (1992)
- 32 - **Advanced Organic Synthesis : Methods and Techniques**  
R. S. Monson  
Published Academic Press Ltd., 78, (1971)
- 33 - **Synthesis and pharmacological evaluation of 5,6-*exo*-epoxy-7-oxabicyclo[2.2.1]heptane derivatives.**  
Jagabandhu Das, Truc Vu, Don N. Harris & Martin L Ogletree  
J. Med. Chem., 37, 930-935, (1988)
- 34 - **The reaction of furan with maleic anhydride.**  
R.B Woodward & Harold Baer  
J. Am. Chem. Soc., 70, 1161-1166, (1948)
- 35 - **The rearrangement of *endo*-3,6-methylene-1,2,3,6-tetrahydro-*cis*-phthalic anhydride.**  
David Craig  
J. Am. Chem. Soc., 73, 4889-4892, (1951)
- 36 - **Water Soluble, zero-valent, Platinum-, Palladium-, and Nickel- $P(CH_2OH)_3$  complexes : Catalysts for the addition of  $PH_3$  to  $CH_2O$ .**  
Karl.M. Harrison, Peter.A.T. Hoye, A.Guy Orpen, Paul.G. Pringle & Martin.B. Smith.  
J.Chem.Soc-Chem.Comm., 1096-1097, (1989)
- 37 - **Carbonyl Rhodium (I) and Ruthenium (II) complexes with water soluble phosphines.**  
F. P. Pruchnik, P. Smolenski & I. Raksa  
Pol. J. Chem., 69, 5-8, (1995)
- 38 - **Synthesis of watersoluble (tri(hydroxymethyl)phosphine) gold (I) complexes containing a nucleoside ligand.**  
Sanshiro Komiya, Hiroko Awata, Shigeyuki Ishimatsu & Atsushi Fukuoka  
Inorg. Chim. Acta, 217, 201-202, (1994)
- 39 - **Tris(hydroxymethyl)phosphine Platinum metal complexes. Catalysts for water based reactions.**  
Paul.G. Pringle & M.B. Smith.  
Plat.Met.Rev., 34 (No. 2), 74-76, (1990)

- 40 - **Preparation of tris(hydroxymethyl)phosphine.**  
Albright and Wilson Ltd.  
Albright and Wilson product information literature.
- 41 - **Procédé de préparation de triarylphosphines sulfonées.**  
Rhone-poulenc chimie de base - Fr.  
Fr Patent 2 532 318
- 42 - **Comments on the synthesis of Trisulphonated Triphenylphosphine:  
Reaction monitoring by NMR spectroscopy.**  
Tamás Bartik, Berit Bartik, Brian E. Hansen, Tom Glass & William Bebout.  
Inorg. Chem., 31, 2667-2670., (1992)
- 43 - **Homogeneous catalysis in water.**  
Emile G. Kuntz  
Chemtech., 570, (1987)
- 44 - **Homogeneous catalysis in water. Part II. Synthesis and  
characterization of ruthenium water-soluble complexes.**  
E. Fache, C. Santini, F. Senocq & J.M. Basset  
J. Mol. Cat., 72, 331-336, (1992)
- 45 - **Homogeneous catalysis in water. Part III. The catalytic  
hydrogenation of propionaldehyde with (RuCl<sub>2</sub>L<sub>2</sub>)<sub>2</sub>, RuHClL<sub>3</sub>,  
RuH(OAc)L<sub>3</sub>, RuH<sub>2</sub>L<sub>4</sub>, RuHIL<sub>3</sub>, RuCl<sub>2</sub>(CO)<sub>2</sub>L<sub>2</sub> and  
[Ru(OAc)(CO)<sub>2</sub>L]<sub>2</sub> (L=P(C<sub>6</sub>H<sub>4</sub>-*m*-SO<sub>3</sub>Na)<sub>3</sub>.3H<sub>2</sub>O): a kinetic  
investigation of the salt effect in water.**  
E. Fache, C. Santini, F. Senocq & J.M. Basset  
J. Mol. Cat., 72, 337-350, (1992)
- 46 - **The chemistry of the rarer Platinum metals (Os, Ru, Ir and Rh).**  
W.P Griffith  
Interscience Publishers, (1967)
- 47 - **Ruthenium-catalysed ring-opening metathesis polymerisation of  
cyclo-olefins initiated by diazoesters.**  
Albert Demonceau, Alfred F. Noels, Eric Saive & Andre J. Hubert  
J. Mol. Cat., 76, 123-132, (1992).
- 48 - **Homogenous catalysis: A Ruthenium-based Lewis-acid catalyst for the  
Diels-Alder reaction.**  
William Odenkirk, Arnold L. Rheingold & B. Bosnich.  
J. Am. Chem. Soc., 114, 6392-6398, (1992).
- 49 - **Kinetic and Mechanism of reactions of Transition metal complexes.  
(2<sup>nd</sup> Edition).**  
Ralph G. Wilkins  
VCH Publishers, (1991)

- 50 - **A Comparison of the Rates of Electron Exchange Reactions of Ammine Complexes of Ruthenium(II) and (III) with the Predictions of Adiabatic, Outer-Sphere Electron Transfer Models.**  
Glibert M. Brown & Norman Sutin.  
J. Am. Chem. Soc., 101(4), 883-892, (1979).
- 51 - **Synthesis and Properties of the Ru(tacn)<sub>2</sub><sup>3+/2+</sup> Couple and NMR Study of the Electron Self-Exchange (tacn=1,4,7-Triazacyclononane).**  
Paul Bernhard & Alan M. Sargeson.  
Inorg. Chem., 27, 2582-2587, (1988).
- 52 - **Variable-Temperature and Variable-Pressure NMR Kinetic Study of Solvent Exchange on Ru(H<sub>2</sub>O)<sub>6</sub><sup>3+</sup>, Ru(H<sub>2</sub>O)<sub>6</sub><sup>2+</sup> and Ru(CH<sub>3</sub>CN)<sub>6</sub><sup>2+</sup>.**  
Irina Rapaport, Lothar Helm, Andre E. Merbach, Paul Bernhard & Andreas Ludi.  
Inorg. Chem., 27, 873-879, (1988).
- 53 - **Preparation of infra-red spectra of some ammine complexes of Ruthenium (II) and Ruthenium (III).**  
A.D. Allen & C.V. Senoff  
Can.J.Chem, 45, 1338-1341, (1967)
- 54 - **Carbonyl Halides of the Group VIII transition metals. Part V. Halocarbonyl derivatives of Ruthenium III and Ruthenium II.**  
R. Colton & R. H. Farthing  
Aust J Chem., 24 (No.5), 903-909, (1971)
- 55 - **Ammine Complexes of Ruthenium.**  
F.M. Lever & A.R. Powell  
J.Chem.Soc.- Sect. (A), 1477-1482, (1969),
- 56 - **The infrared spectra of some ammine nitrosyl compounds of ruthenium.**  
M.B. Fairy R.J Irving  
Spectrochemica Acta, 22, 359 - 366, (1966)
- 57 - **Infrared spectra of inorganic and coordination compounds.**  
Kazuo Nakamoto  
Published John Wiley and Sons, 105, (1963)  
Lester H. Vogt Jr., J. Lawrence Katz & Stephen E. Wiberley.  
Inorg. Chem., 4 (No. 8), 1162, (1965)
- 58 - **Ruthenium Ammines**  
J. E. Fergusson & J. L. Love  
Inorg Synth., 13, 208 - 213, (1972)
- 59 - **Carbonyl Halides of the Group VIII transition metals. Part I. Dicarboxyldihalogenruthenium(II) and related compounds.**  
R. Colton & R. H. Farthing  
Aust J Chem., 20, 1283, (1967)



- 60 - **Carbonyl Halides of the Group VII transition metals. Part III. Dichloroaquocarbonylruthenium (II).**  
R. Colton & R.H. Farthing  
Aust. J. Chem., 22, 2011-2012, (1969)
- 61 - **Tetrakis(triphenylphosphinedichlororuthenium(II) and tris(triphenylphosphine)dichlororuthenium(II).**  
P.S. Hallman, T.A. Stephenson & G. Wilkinson.  
Inorg. Synth., 12, 237-238, (1975)
- 62 - **Dinuclear Ruthenium (II) carboxylate complexes.**  
M. O. Albers, E. Singleton & J.E. Yates  
Inorg. Synth., 26, 249-258, (1989)
- 63 - **Transition-metal complexes containing phosphorus ligands. Part III. Convenient syntheses of some triphenylphosphine complexes of the platinum metals.**  
J. J. Levinson & S.D. Robinson  
J. Chem. Soc., 2947-2954, (1970)
- 64 - **Olefin co-ordination compounds. Part V. Some diene complexes of Palladium(II) and their alkoxy - derivatives.**  
J. Chatt, L. M. Vallarino & L.M. Venanzi  
J. Chem. Soc., 3413-3416, (1957)
- 65 - **Cyclic diolefin complexes of platinum and palladium.**  
D. Drew & J. R. Doyle.  
Inorg. Synth., 28, 346-349, (1990)
- 66 - **Water soluble Tris(hydroxymethyl)phosphine complexes with Nickel, Palladium and Platinum. Crystal structure of [Pd{P(CH<sub>2</sub>OH)<sub>3</sub>}<sub>4</sub>].CH<sub>3</sub>OH.**  
James W. Ellis, Karl N. Harrison, Peter A. T. Hoyer, A. Guy Orpen, Paul G. Pringle & Martin B. Smith  
Inorg. Chem., 31, 3026-3033, (1992)
- 67 - **Préparation, description et constitution des ruthenium-III-trioxalates.**  
R. Charonnat  
Ann. Chim. (France), 16, 123-250, (1931)
- 68 - **The synthesis and characterisation of diacidobis(ethylenediamine)-ruthenium(III) complexes and related compounds.**  
John A. Brotherhood & L. A. P. Kane-Maguire  
J. Chem. Soc.- Sect. (A), 546-553, (1967)
- 69 - **trans-Carbonylchlorobis(triphenylphosphine)Iridium.**  
J. P. Collman, C. T. Sears & M. Kubota.  
Inorg. Syn., 28, 92, (1991)

- 70 -  **$^{13}\text{C}$  NMR Data for organometallic compounds.**  
 Brian E. Mann and Brian F. Taylor  
 Publ: Academic Press Inc. (London) Ltd
- 71 - **Kinetics of nitrogen uptake by Ruthenium(II) aquo species.**  
 L.A.P. Kane-Maguire  
 J. Inorg. Nucl. Chem., 33, 3964-3966, (1971)
- 72 - **Some reactions of Hydrazine with Ruthenium compounds.**  
 F. Bottomley  
 Can.J.Chem, 48, 351-355, (1970)
- 73 - **Hydrophosphination of formaldehyde catalysed by tris(hydroxymethyl)phosphine complexes of platinum, palladium or nickel.**  
 Peter A. T. Hoye, Paul G. Pringle, Martin B. Smith and Kerry Warboys.  
 J. Chem. Soc., Dalton Trans., 269-275, (1993)
- 74 - **Crystal and Molecular Structure of Dinitrosylbis(triphenylphosphine)ruthenium-Hemibenzene,  $\text{Ru}(\text{NO})_2(\text{P}(\text{C}_6\text{H}_5)_3)_2 \cdot 1/2\text{C}_6\text{H}_5$ .**  
 Arthur P. Gaughan Jr., Brian J. Corden, Richard Eisenberg and James A. Ibers.  
 Inorg. Chem., 13 (4), 786-791, (1974)
- 75 - ***cis-trans* Isomerisation I) The mechanism of a catalysed isomerisation of maleic acid to fumaric acid.**  
 Kenzie Nozaki & Richard Ogg Jr.  
 J. Am. Chem. Soc., 63, 2583-2586, (1941).
- 76 - **The Mechanism of Aqueous Ruthenium (II)-Catalysed olefin isomerisation.**  
 Dominic V. McGrath and Robert H. Grubbs.  
 Organomet., 13, 224-235, (1994).
- 77 - **Kinetic control in catalytic olefin isomerisation: An explanation for the apparent contrathermodynamic isomerisation of 3-pentenenitrile.**  
 R. J. McKinney  
 Organomet., 4, 1142-1143, (1985)
- 78 - **Mechanistic studies on the rearrangement activity of a Ring-Opening Metathesis Polymerisation catalyst: Reaction of  $[\text{Ru}(\text{H}_2\text{O})_6]^{2+}$  with unfunctionalized olefins.**  
 Thomas Karlen and Andreas Ludi  
 J. Am. Chem. Soc., 116, 11375-11378, (1994)
- 79 - **Aqueous Ruthenium (II) Complexes of functionalized Olefins: The X-ray structure of  $\text{Ru}(\text{H}_2\text{O})_2(\eta^1(\text{O}):\eta^2(\text{C},\text{C}')\text{-OCOCH}_2\text{CH}=\text{CHCH}_3)_2$ .**  
 Dominic V. McGrath, Robert H. Grubbs and Joseph W. Ziller.  
 J. Am. Chem. Soc., 113, 3611-3613, (1991)

- 80 - **Cyclopentadienylruthenium phosphine complexes Part II. Reactions between Hydridobis(triphenylphosphine)( $\eta$ -cyclopentadienyl)ruthenium and acetylenes.**  
Timothy Blackmore, Michael I. Bruce and F. Gordon A. Stone.  
J. Chem. Soc. - Dalton. Trans., 106-112, (1974)
- 81 - - **The ultraviolet spectrum of (E)-Butenedioic acid.**  
Ed. K.N. Marsh, Micheal Frenkel.  
TRC Spectral Data, 1, Spec. No. 156, (1993)
- 82 - **Bridging and non-bridging ligand effects in redox reactions of metal ions.**  
Henry Taube.  
Can. J. Chem., 37, 129-137, (1959)
- 83 - **Organic anions as bridging groups in oxidative-reduction reactions.**  
D.K. Sebera and H. Taube.  
J. Am. Chem. Soc., 83, 1785-1791, (1961)
- 84 - **Secondary  $\alpha$ -Deuterium Isotope effect. The mechanism of the *cis-trans* catalysed isomerisation of maleic acid.**  
Stanley Seltzer  
J. Am. Chem. Soc., 83, 1861-5, (1961)
- 85 - **The Aldrich Library of  $^{13}\text{C}$  and  $^1\text{H}$  FTNMR Spectra. Edition 1.**  
Ed. Charles J. Pouchert and Jacquelyn Behuke.  
Aldrich Chemical Company Inc., (1993)

## APPENDIX A - DATA TABLES.

Table A1 - List of chemicals and suppliers.

CHEMICAL	SUPPLIER	CHEMICAL	SUPPLIER
Acetone	Fisons	Maleic Anhydride	Aldrich
Acetonitrile	Fisons	Methanol	Fisons
Ammonia	Fisons	Mercury	Elgar Phosphors and Chemicals Ltd.
Ammonium Chloride	BDH	Mesitylene	Aldrich
Argon	BOC	<i>N</i> -Methyl- <i>N</i> -nitroso toluene- <i>p</i> -sulfonamide (Diazald)	Aldrich
Barium Chloride	Hopkins and Williams Ltd	Nitrogen (Gaseous) Nitrogen (Liquid)	BOC Cryoservice
Cyclooctadiene	Aldrich	60/40 Pet. Ether	Fisons
Dichloromethane	Fisons	Phosphorus Pentoxide	Aldrich
<i>o</i> -Dichlorobenzene	Aldrich	Potassiumtetrachloro pallidate (II)	Johnson Mathey
Dicyclopentadiene	Aldrich	Potassium Oxalate	Aldrich
Diethyl ether	Fisons	Propan-2-ol	Fisons
Dimethylformamide	Aldrich	Ruthenium Trichloride (Hydrated)	Johnson Mathey
Ethanol	Fisons	Silica Gel	Vickers
Ethyl Acetate	Fisons	Sodium Borohydride	Aldrich
Ethyl Diazoacetate	Aldrich	Sodium Hydroxide	Fisons
Ethylenediamine	Aldrich	Sodium Sulfate	Aldrich
Formic Acid	BDH	Fuming Sulfuric Acid (Oleum)	Aldrich
Furan	Aldrich	Tetrahydrofuran	Fisons
Hexane	Fisons	Tetra(Hydroxymethyl) phosphonium Chloride	Albright and Wilson
Hydrazine Monohydrate	Aldrich	Toluene	Fisons
Conc. Hydrochloric Acid	Fisons	Triethylamine	Aldrich
Iridium	Johnson Mathey	Triphenylphosphine	Aldrich
Lithium Aluminium Hydride	Aldrich	Water	Distilled on site
Magnesium Sulfate	Aldrich	Zinc Dust	Aldrich

**Table A2 - Dilatometry data for DIL1**

Time / mins	Drop in meniscus height / mm	Time / mins	Drop in meniscus height / mm	Time / mins	Drop in meniscus height / mm	Time / mins	Drop in meniscus height / mm
0	0	1277	-3.4	2814	-10.4	4474	-17.6
6	0.6	1289	-3.4	2869	-9.2	4501	-17.1
36	0.1	1321	-4.3	2929	-9.8	4512	-17.4
55	-0.3	1390	-4.1	2992	-10.2	4588	-18.5
68	0.1	1477	-5.7	3017	-11	4593	-18.2
77	-0.5	1530	-4.9	3101	-11	5719	-20.7
94	-0.2	1560	-6	3127	-12.6	8424	-29.7
118	-0.8	1577	-6.1	3145	-12.6	8469	-30.2
186	-0.8	1593	-5.3	4146	-15.6	8517	-30.2
229	-1.8	1658	-6.3	4160	-14.9	8577	-30
254	-1.5	1682	-7.1	4212	-15.9	8617	-30.5
275	-1.1	1715	-4.6	4247	-15.5	8625	-30.5
293	-1.1	2762	-11.4	4341	-16.2		
307	-1.7	2783	-8.9	4392	-15.3		
321	-1.4	2804	-9.9	4425	-15.9		

**Table A3 - Dilatometry data for DIL2**

Time / mins	Drop in meniscus height / mm	Time / mins	Drop in meniscus height / mm	Time / mins	Drop in meniscus height / mm	Time / mins	Drop in meniscus height / mm
0	0	1287	-3.3	2946	-8.4	4450	-14
17	-0.1	1367	-3.8	3069	-8.8	4488	-14.3
73	-0.1	1433	-4.2	3090	-9	5450	-17.9
85	0	1463	-4.2	4044	-12.9	5488	-18.1
108	0.3	1536	-4.6	4073	-13.1	5510	-18.1
130	0	1562	-4.3	4133	-13.1	5555	-18.2
142	0	2557	-7.9	4168	-13.1	5635	-18.2
1094	-3.1	2580	-7.9	4266	-13.3	5741	-18.5
1122	-2.9	2724	-7.9	4346	-13.4	5780	-18.8
1162	-3.2	2780	-8.2	4368	-14	5800	-18.5
1208	-3.3	2800	-7.9	4378	-13.9		
1227	-3.3	2819	-8.2	4423	-13.8		

Table A4 - Dilatometry data for DIL3.

Time / mins	Drop in meniscus height / mm						
	Sample 1	Sample 3	Sample 4	Sample 5	Sample 6	Sample 7	Sample 8
0	0		0	0	0	0	0
145	2		-8	-16	-18	-14	-10
1108	-8	0	-13	-20	-36	-26	-39
1170	-9	-5	-20	-28	-45	-32	-43
1223	6	6	-8	-14	-31	-22	-40
1289	3	10	-8	-11	-28	-18	-36
1345	-12	-10	-26	-33	-47	-34	-48
1403	4	2	-9	-13	-31	-23	-43
1470	-7	-11	-19	-23	-38	-22	-45
1531	-8	-10	-26	-29	-50	-37	-59
1588	1	-5	-15	-24	-40	-29	-54
2495	-8		-42	-37	-78		-91
2655	-10	-52	-45	-40	-75	-51	-85
2716	-5	-45	-45	-38	-79	-51	-83
2817	-11	-52	-43	-34	-70	-46	-81
2905	-2	-39	-35	-31	-71	-52	-91
2957	-10	-53	-44	-35	-76	-48	-83
4007	-14	-93	-48	-72	-114	-78	-119
4098	-13	-78	-28	-57	-98	-76	-117
4165	-6	-81	-29	-58	-102	-82	-120
4243	-17	-80	-26	-56	-94	-71	-114
4439	2	-78	-29	-61	-102	-79	-121
5462	-19	-109	-36	-86	-134	-90	-135
5548	-8	-100	-36	-92	-129	-97	-144
5594	-18	-111	-49	-107	-143	-106	-143
5703	-12	-103	-36	-95	-128	-98	-141
5788	-22	-118	-55	-108	-141	-100	-143
5860	-6	-100	-34	-94	-130	-91	-141

**Table A5 - Dilatometry data for DIL4.**

Time / mins	Drop in meniscus height / mm			Time / mins	Drop in meniscus height / mm		
	Sample 3	Sample 6	Sample 7		Sample 3	Sample 6	Sample 7
0	0	0	0	2941	-7.5	-9.1	-8.8
94	0	0.6	1.7	3097	-6.4	-14.8	-9.6
203	0	1.4	1.2	4027	-8.8	-14.8	-13.4
1242	-4.4	-5.9	-4.8	4186	-9.1	-14.1	-14.2
1345	-1.9	-3.3	-3.1	4520	-9.7	-13.4	-13
1510	-2.8	-3.8	-4	5554	-13.2	-18.1	-17.6
1646	-3.5	-3.7	-3.4	5704	-13.9	-20.9	-19.5
2679	-5.1	-8.2	-8.3	5970	-11.9	-18.9	-19.5
2784	-6.3	-7.5	-6.6				

**Table A6 - Dilatometry data for DIL5**

Time / mins	Drop in meniscus height / mm					
	Sample 3	Sample 4	Sample 5	Sample 6	Sample 7	Sample 8
0	0	0	0	0	0	0
100	-0.4	0	0.6	0.2	0.2	0.3
1130	-0.15	0.95	1.65	0.95	0.35	0.25
1400	0	-0.2	-0.1	0.1	0.3	0.5
1540	0.2	0.1	0.3	0	-0.3	-0.4
2540	1.2	1.3	1.5	-0.1	-0.3	-0.4
2965	0.15	0.05	0.55	-0.25	-1.35	-0.65
4090	-0.2	0.3	0.3	0.2	-1.4	0.1
5309	0.5	0.4	0.8	-0.2	-0.7	-1
11235	-0.8	0.5	0	-0.1	-2.9	-1.7
12456	-1.5	-1.8	-1.3	-2.2	-5.4	-3.5
13975		-2.2	-2.4	-2.3	-5.6	-3.1
15405	-1.8	-1.4	-1.4	-1.5	-5.4	-2.8
15495	-2.3	-1.3	-1.2	-1.3	-5.1	-3.3
20135	-5.95	-6.45	-5.55	-3.45	-10.15	-5.35
21165	-5.1	-5.5	-5.7	-4.2	-10.9	-5.5
22605	-5.45	-5.45	-5.35	-3.65	-10.35	-5.35
24045	-5.9	-5.6	-5.4	-3.7	-10.6	-5.5

**Table A7 - Dilatometry data for DIL6**

Time / mins	Drop in meniscus height / mm				
	Sample 1	Sample 2	Sample 3	Sample 4	Sample 5
0	0	0	0	0	0
1000	-0.04	0.06	-1.9	-3.9	-3.2
1290	-0.05	0.01	-3.3	-5.4	-3.6
1450	-0.04	-0.05	-2.9	-5.2	-4.2
2465	-0.05	-0.06	-4.2	-6.6	-5.1
2745	-0.04	-0.02	-4	-6.5	-6.1
2900	-0.01	-0.1	-5	-6.4	-5
3950	-0.02	-0.13	-4.5	-7.5	-5.4
4220	0.01	0.04	-4.1	-6.6	-5.4
4425	0.01	-0.01	-4.4	-7.1	-5
5385	0.06	0.05	-3.5	-6.3	-4.1
5520	0.09	0.07	-3.4	-5.9	-4.1
5630	0.03	0.17	-2.5	-5.2	-3.7
6795	-0.19	-0.25	-5.6	-7.2	-4.4

**Table A8 - Dilatometry data for DIL7**

Time / mins	Change in meniscus height / mm				
	Sample 1	Sample 2	Sample 3	Sample 4	Sample 5
0	0	0	0	0	0
60	-0.5	-6.2	-1.4	-6.8	-8
86	0.74	3.1	8.2	3	1.8
166	0.67	1.4	6.6	0.8	0.1
234	0.67	1.9	7	1.9	1.6
370	0.71	2.1	7.3	1.9	0.9
1290	0.75	2.6	7.3	2	0.7
1425	0.68	2	7	1.7	0.6
1505	0.72	2.6	8.1	2.7	1.7
1645	0.73	2.7	7.8	1.9	1.2
2710	0.63	2.4	7.9	2.8	2.1
3685	0.83	2.2	7.5	2.6	1.2
4725	0.95	2.2	7.6	2	0.9
7545	1.03	2	7.2	2.3	1.2
9000	1	2.6	7.9	3.4	2.1
13650	1.47	3	8.2	4.2	



**Table A9 - Dilatometry data for DIL8**

Time / mins	Change in meniscus height / mm				
	Sample 1	Sample 2	Sample 3	Sample 6	Sample 7
0	0	0	0	0	0
145	0.3	-0.3	0.6	14.4	8.1
230	1.2	1.1	2.6	17.8	11.3
1260	1.9	1.5	7.1	21.2	18.3
1335	0.7	0.5	7.4	22	18.5
1435	0.8	0.8	7.2	21.1	18.5
1535	1	1.1	8.1	21.7	19.7
1550	1.7	1.6	8.5	21.7	19.7
1610	1.4	1	7.9	21.2	18.4
1670	1.3	0.8	7.9	21.3	18.7
1765	1.2	0.5	8.2	21.6	18.8
2700	1.6	2	10.9	22.1	19.2
2715	1.2	0.7	10	21.4	18.7
2725	0.3	0.6	10.6	22.3	19.3
2785	0.6	0.4	10	21.3	19.1
2890	1.6	1.2	11.2	22.2	19
3015	0.8	1.3	10.6	21.9	18.9
3155	1.3	1.4	11.7	22.2	19.4
4120	1.4	1.3	12.6	21.8	19
4285	1	0.8	12.1	21.8	19.7
8430	-0.9	0.3	13.6	22.3	19.4
9900	-0.8	0.5	13.8	22.1	19.2
10200	-0.8	1.7	14.9	22.4	19.4
11360	-1	0.7	14.5	21.5	19
12810	-1.5	0.2	13.6	21.4	20.3
13065	-0.5	1.3	14.6	21.5	19.1

**Table A10 - Dilatometry data for DIL9**

Time / mins	Change in meniscus height / mm				
	Sample 1	Sample 2	Sample 4	Sample 5	Sample 6
0	0	0	0	0	0
20	-0.5	3.9	3	2.2	2.1
30	-0.5	4.8	4.4	3.1	3
60	-0.9	8.8	6.5	4.6	4.8
85	0.2	10.9	8.5	6.2	5.9

**Table A11 - Dilatometry data for DIL10**

Time / mins	Change in meniscus height / mm		
	Control	Sample 1	Sample 3
0	0	0	0
25	-0.6	0.1	0.9
75	-0.9	-0.3	3.9
255	-0.3	1.1	10.3
1335	-0.7	3.1	12
1515	-0.1	3.3	12.2
1620		3.9	12.4

**Table A12 - Absorbance data for UV1**

Time / mins	Absorbance			
	Sample 1	Sample 2	Sample 3	Sample 4
0	0	0	0	0
60	0.07	0.025	0	0.015
120	0.16	0.085	0.055	0.025
180	0.19	0.12	0.095	0.05
240	0.22	0.16	0.11	0.075
300	0.24	0.14	0.12	0.08
1260	0.52	0.475	0.28	0.13
2700	0.59	0.485	0.355	0.19
6930	0.765	0.665	0.43	0.225
11040	1.01	0.905	0.585	0.15

**Table A13 - Absorbance data for UV2**

Time / mins	Absorbance			Time / mins	Absorbance		
	Samp. 1	Samp. 2	Samp. 3		Samp. 1	Samp. 2	Samp. 3
0	0	0	0	130	0.13	0.06	0.11
10	0.03	0.02	0.05	140	0.15	0.07	0.11
20	0.04	0.02	0.07	150	0.16	0.06	0.09
30	0.06	0.02	0.07	160	0.17	0.09	0.09
40	0.08	0.06	0.09	180	0.17	0.09	0.11
50	0.08	0.03	0.09	190	0.17	0.07	0.12
60	0.08	0.03	0.09	200	0.19	0.07	0.12
70	0.08	0.04	0.09	210	0.2	0.09	0.11
80	0.08	0.04	0.08	220	0.21	0.08	0.1
90	0.1	0.06	0.08	230	0.22	0.08	0.11
100	0.12	0.04	0.07	240	0.23	0.1	0.11
110	0.12	0.06	0.07	250	0.24	0.1	0.11
120	0.12	0.05	0.09	260	0.24	0.1	0.11

Table A13 (cont.) - Absorbance data for UV2

Time / mins	Absorbance			Time / mins	Absorbance		
	Samp 1	Samp 2	Samp 3		Samp 1	Samp 2	Samp 3
270	0.25	0.12	0.12	640	0.43	0.18	0.16
280	0.26	0.12	0.12	650	0.43	0.18	0.16
290	0.26	0.11	0.12	660	0.44	0.19	0.16
300	0.27	0.12	0.13	670	0.44	0.19	0.16
310	0.27	0.13	0.13	680	0.45	0.19	0.16
320	0.28	0.12	0.12	690	0.45	0.19	0.16
330	0.29	0.12	0.13	695	0.45	0.2	0.16
340	0.29	0.12	0.13	720	0.47	0.2	0.16
350	0.3	0.12	0.13	735	0.47	0.2	0.17
360	0.31	0.13	0.14	750	0.47	0.2	0.17
370	0.31	0.14	0.13	765	0.48	0.2	0.17
380	0.33	0.14	0.14	780	0.47	0.2	0.17
390	0.33	0.14	0.14	795	0.47	0.2	0.16
400	0.33	0.14	0.14	810	0.47	0.2	0.17
410	0.34	0.14	0.14	825	0.48	0.2	0.17
420	0.35	0.15	0.14	840	0.48	0.21	0.17
430	0.35	0.15	0.14	855	0.49	0.21	0.17
440	0.36	0.15	0.14	870	0.49	0.21	0.17
450	0.35	0.15	0.14	885	0.5	0.21	0.17
460	0.36	0.15	0.14	900	0.5	0.21	0.17
470	0.37	0.16	0.14	915	0.5	0.21	0.17
480	0.37	0.16	0.15	930	0.51	0.22	0.17
490	0.37	0.16	0.14	945	0.51	0.22	0.17
500	0.38	0.16	0.15	960	0.51	0.22	0.17
510	0.38	0.16	0.15	975	0.52	0.22	0.18
520	0.39	0.16	0.15	990	0.52	0.22	0.17
530	0.39	0.16	0.15	1010	0.53	0.22	0.17
540	0.39	0.17	0.15	1025	0.53	0.22	0.17
550	0.4	0.17	0.15	1040	0.53	0.22	0.17
560	0.4	0.17	0.15	1055	0.54	0.22	0.18
570	0.41	0.17	0.15	1070	0.54	0.22	0.18
580	0.41	0.17	0.16	1085	0.55	0.23	0.18
590	0.42	0.17	0.15	1100	0.55	0.23	0.18
600	0.42	0.18	0.15	1115	0.56	0.22	0.18
610	0.42	0.18	0.15	1130	0.56	0.22	0.18
620	0.43	0.18	0.16	1145	0.56	0.23	0.18
630	0.43	0.18	0.16	1160	0.57	0.23	0.18

**Table A13(cont) - Absorbance data for UV2**

Time / mins	Absorbance			Time / mins	Absorbance		
	Samp 1	Samp 2	Samp 3		Samp 1	Samp 2	Samp 3
1175	0.57	0.23	0.18	1940	0.67	0.27	0.19
1190	0.57	0.23	0.18	1955	0.67	0.27	0.19
1205	0.58	0.23	0.18	1970	0.67	0.27	0.19
1220	0.58	0.24	0.18	1985	0.68	0.27	0.19
1235	0.59	0.24	0.18	2000	0.68	0.27	0.19
1745	0.64	0.26	0.19	2015	0.68	0.27	0.19
1760	0.65	0.26	0.19	2030	0.68	0.27	0.19
1775	0.65	0.26	0.19	2045	0.69	0.27	0.19
1790	0.65	0.26	0.19	2060	0.69	0.27	0.19
1805	0.66	0.26	0.19	2075	0.69	0.27	0.19
1820	0.66	0.27	0.19	2090	0.67	0.27	0.19
1835	0.66	0.27	0.19	2105	0.67	0.27	0.19
1850	0.66	0.27	0.19	2120	0.67	0.27	0.19
1865	0.66	0.27	0.19	2135	0.68	0.27	0.19
1880	0.67	0.27	0.19	2150	0.68	0.27	0.19
1895	0.67	0.27	0.19	2165	0.68	0.27	0.19
1910	0.67	0.27	0.19	2180	0.68	0.27	0.19
1925	0.67	0.27	0.19				

**Table A14 - Absorbance data for UV3**

Time / mins	Absorbance			
	Sample 1	Sample 2	Sample 3	Sample 4
0	0	0	0	0
5	0.02	0.02	0.01	0.01
10	0.04	0.04	0.04	0.05
15	0.08	0.07	0.06	0.06
20	0.09	0.08	0.06	0.07
25	0.11	0.1	0.08	0.06
30	0.11	0.1	0.1	0.06
35	0.14	0.13	0.12	0.09
40	0.16	0.14	0.13	0.09
45	0.15	0.17	0.15	0.11
50	0.15	0.18	0.15	0.13
55	0.19	0.18	0.16	0.13
60	0.19	0.19	0.16	0.12
65	0.22	0.2	0.18	0.13
70	0.25	0.23	0.2	0.16

**Table A14(cont) - Absorbance data for UV3**

Time / mins	Absorbance			
	Sample 1	Sample 2	Sample 3	Sample 4
75	0.26	0.25	0.21	0.16
80	0.27	0.26	0.21	0.17
85	0.28	0.27	0.23	0.18
90	0.3	0.28	0.23	0.19
95	0.28	0.26	0.21	0.17
100	0.28	0.26	0.21	0.19
105	0.32	0.29	0.25	0.21
110	0.33	0.28	0.25	0.18
115	0.33	0.32	0.27	0.22
120	0.34	0.33	0.27	0.22
125	0.35	0.31	0.28	0.23
130	0.36	0.32	0.29	0.23
135	0.37	0.33	0.28	0.24
140	0.34	0.34	0.28	0.23
145	0.37	0.34	0.29	0.23
150	0.37	0.35	0.29	0.24
155	0.38	0.35	0.3	0.25
160	0.38	0.38	0.32	0.26
165	0.4	0.36	0.31	0.25
170	0.41	0.39	0.32	0.26
175	0.41	0.39	0.32	0.27
180	0.43	0.4	0.34	0.28
185	0.44	0.41	0.34	0.28
190	0.45	0.42	0.35	0.29
195	0.45	0.42	0.35	0.29
200	0.46	0.43	0.36	0.3
205	0.47	0.44	0.37	0.31
210	0.49	0.45	0.37	0.31

Table A15- Absorbance data for UV4

Time/ mins	Absorbance			Time / mins	Absorbance		
	Samp 1	Samp 2	Samp 3		Samp 1	Samp 2	Samp 3
0	0	0	0	440		0.86	
5	0.04	0	0	445		0.86	
10	0.09	0.03	0.02	1355			1.04
15	0.13	0.07	0.04	1365			1.04
20	0.16		0.06	1375			1.04
25	0.18	0.14	0.09	1385			1.05
30	0.2	0.17	0.12	1430		1.19	
35	0.23	0.19	0.14	1440		1.19	
40	0.25	0.21		1450		1.2	
45	0.28	0.23		1460		1.2	
50	0.3	0.25		1470		1.2	
60		0.28		1480		1.2	
65		0.3		1490		1.2	
70		0.32		1500		1.2	
75	0.4			1620			1.08
80	0.41			1630			1.09
85	0.43			1640			1.09
100		0.4		1650			1.09
105		0.41		1660			1.09
110		0.42		1670			1.09
120			0.39	1680			1.09
125		0.46	0.4	1690			1.09
135			0.42	1700			1.1
140	0.58	0.49	0.42	1725		1.23	
145	0.59	0.5	0.43	1735		1.25	
150	0.6		0.44	1745		1.25	
155			0.45	1755		1.25	
210			0.53	1765		1.25	
215			0.53	2825			1.22
230			0.55	2855			1.23
240	0.75		0.56	2860		1.45	
245	0.76		0.57	2885			1.23
250	0.76		0.57	2890		1.45	
255	0.77			2915			1.23
260	0.78		0.59	2920		1.46	
265	0.78		0.59	2950		1.47	
270	0.79		0.59	3090			1.25
300		0.73		3155		1.48	
305		0.74		4170			1.36
310		0.74		4335		1.68	

**Table A15 (Cont) - Absorbance data for UV4**

Time/ mins	Absorbance			Time / mins	Absorbance		
	Samp 1	Samp 2	Samp 3		Samp 1	Samp 2	Samp 3
315		0.75		48250	1.605		
320	0.83	0.75		4430	1.61		
325		0.76		4640	1.66		
335	0.84			4735	1.68		
355	0.84			5725	1.81		
415		0.84		6145	1.87		
420		0.84		7150	1.93		
425		0.85		7515	1.99		
430		0.85		8600	2.14		
435		0.86					

**Table A16 - Absorbance data for UV5**

Time / mins	Absorbance			Time / mins	Absorbance		
	Samp 1	Samp 2	Samp 3		Samp 1	Samp 2	Samp 3
0	0	0	0	1275	0.43		
10	0.04	0.095	0.06	1388			0.455
20	0.06	0.18	0.09	1418			0.46
30	0.078	0.255	0.13	1448			0.465
40	0.09	0.335	0.16	1478			0.47
50	0.103	0.38	0.18	1541		1.145	
60	0.11		0.195	1571		1.145	
70		0.475	0.21	2665	0.46		
80		0.515	0.235	2695	0.46		
90		0.545	0.26	2725	0.46		
100		0.575	0.28	2853			0.565
110		0.605	0.31	2873			0.57
120		0.635		2913			0.575
130		0.655		2943			0.575
140		0.675		4122	0.455		
1225	0.415			4152	0.455		
1235	0.42			4268			0.65
1245	0.42			4298			0.655
1255	0.425			5589		1.495	
1265	0.425						

## APPENDIX B - NMR AND IR SPECTRA.

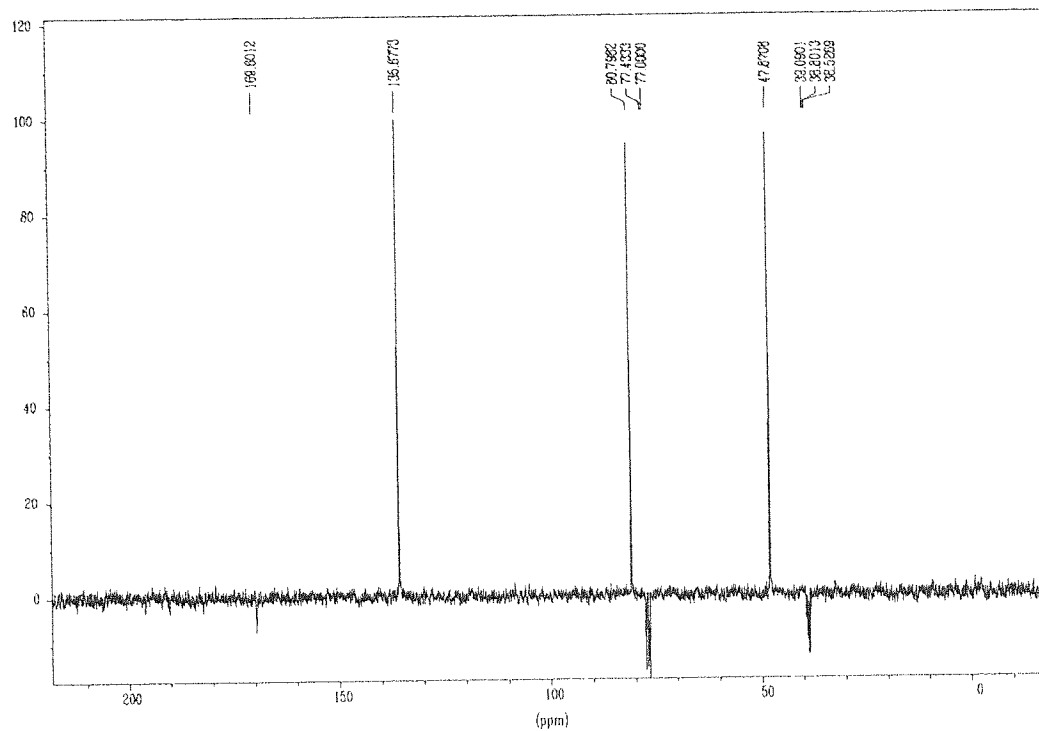


Fig B1 -  $^{13}\text{C}$  NMR of oxanorbornenedicarboxylic anhydride

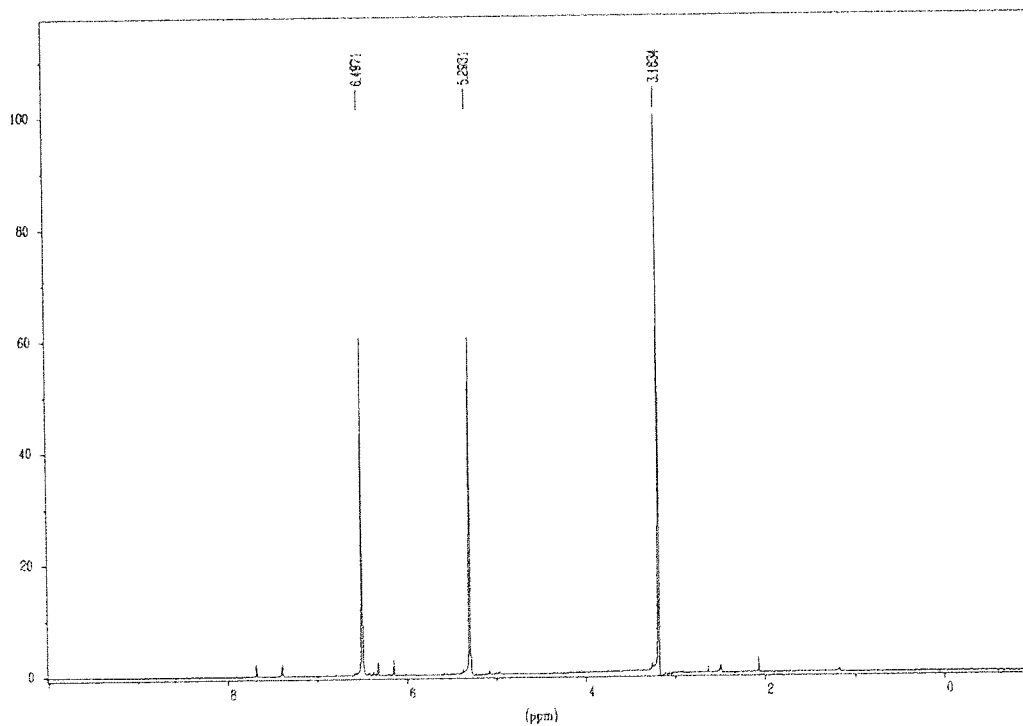


Fig B2 -  $^1\text{H}$  NMR of oxanorbornenedicarboxylic anhydride.



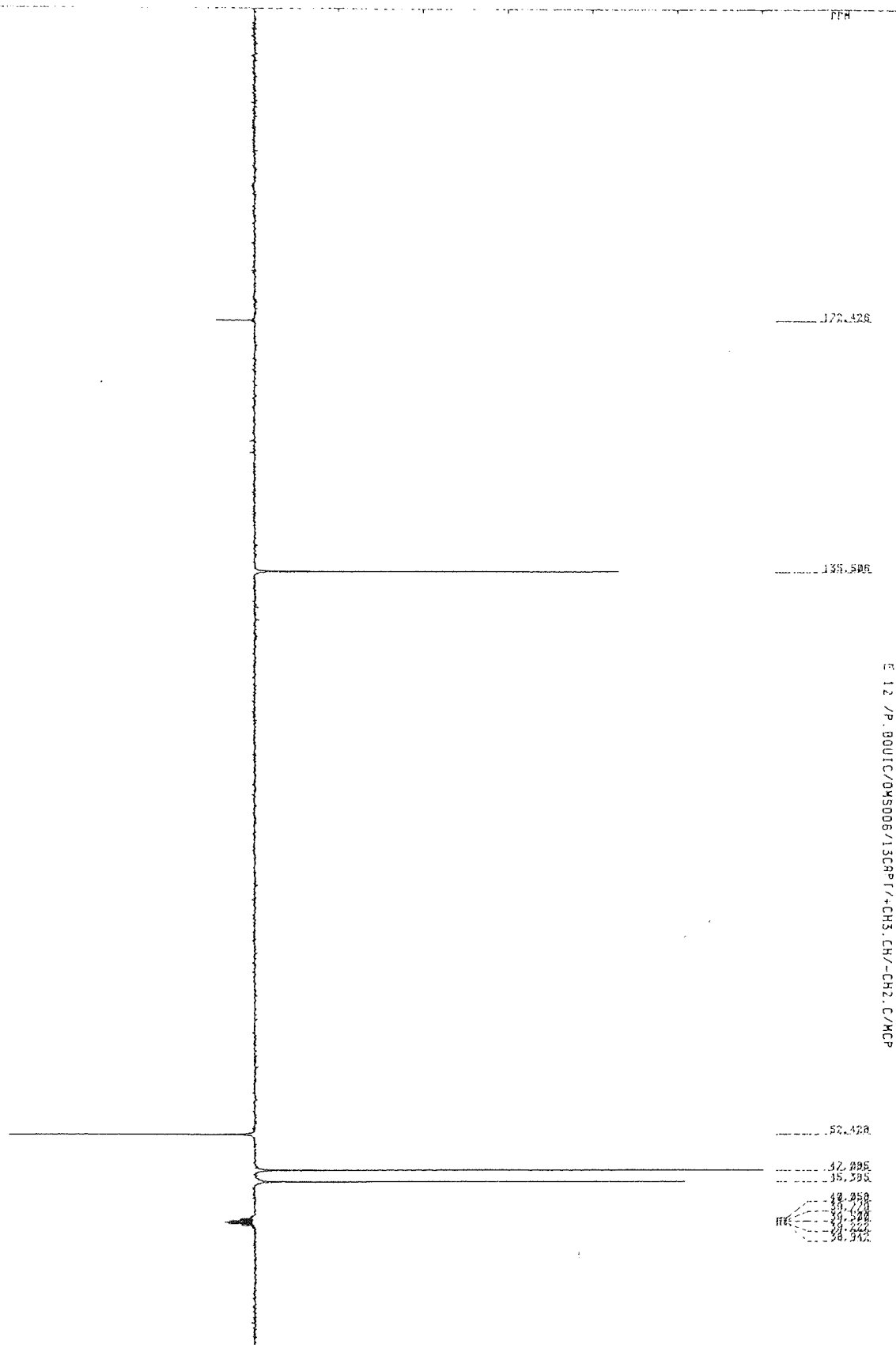


Fig B3 -  $^{13}\text{C}$  NMR of *endo*-norbornenedicarboxylic anhydride

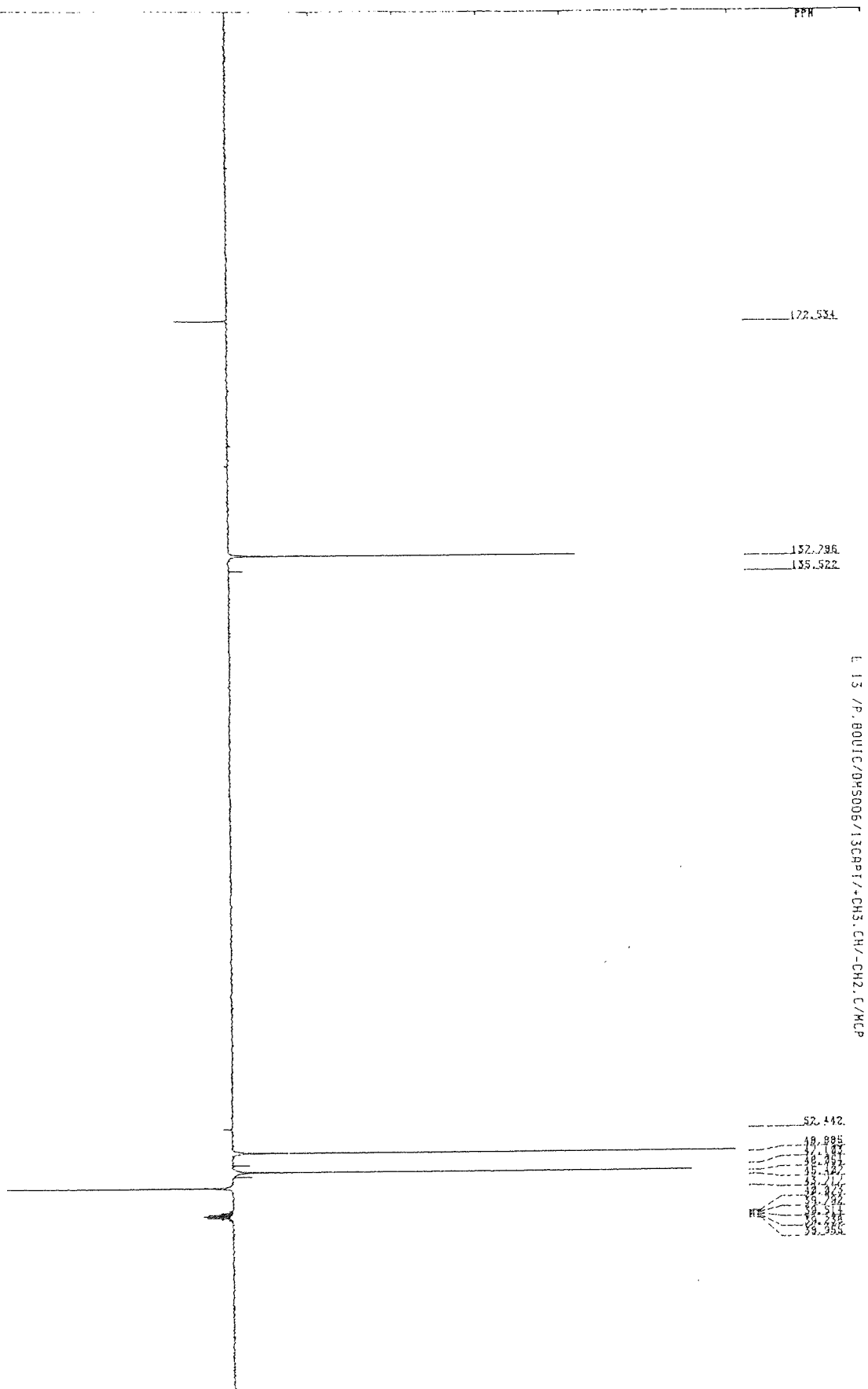


Fig B4 -  $^{13}\text{C}$  NMR of exo-norbornenedicarboxylic anhydride.

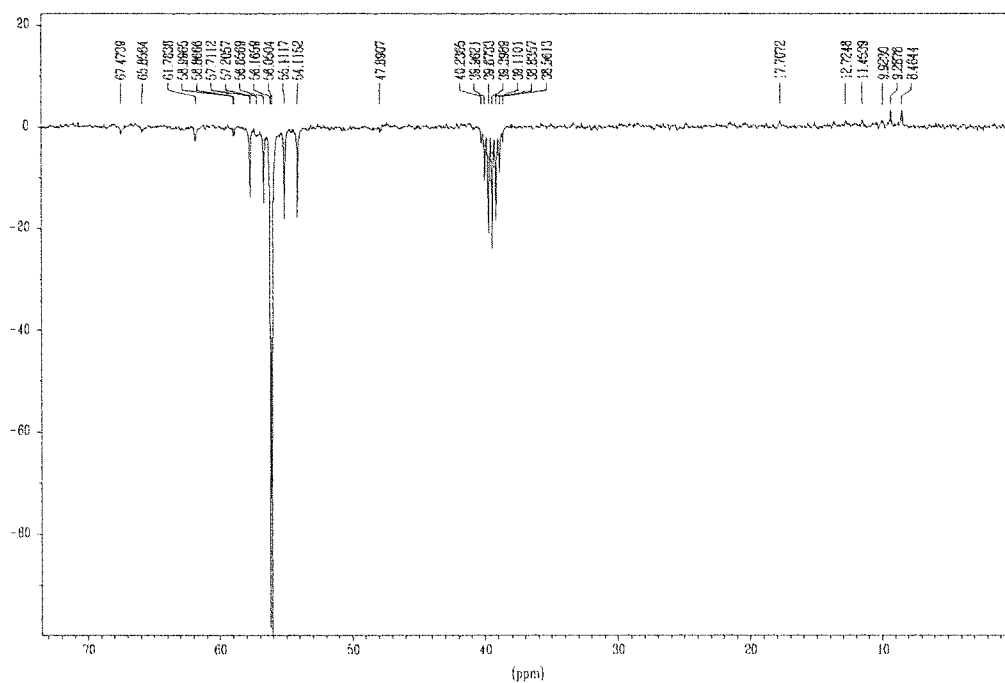


Fig B5 -  $^{13}\text{C}$  NMR of THMP.

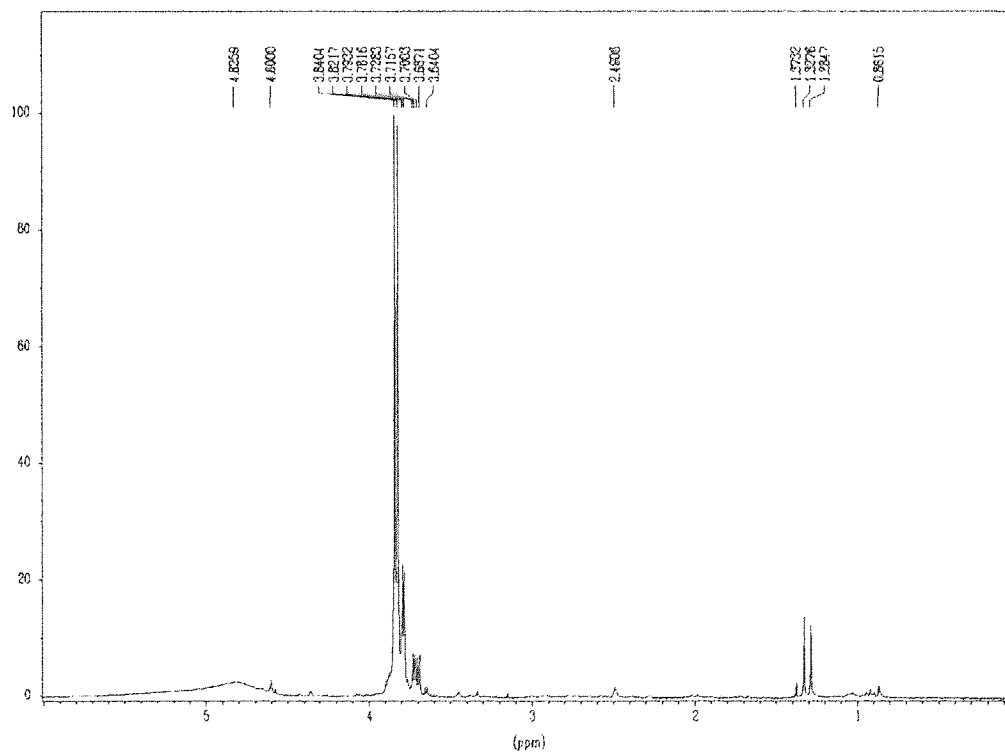


Fig B6 -  $^1\text{H}$  NMR of THMP.

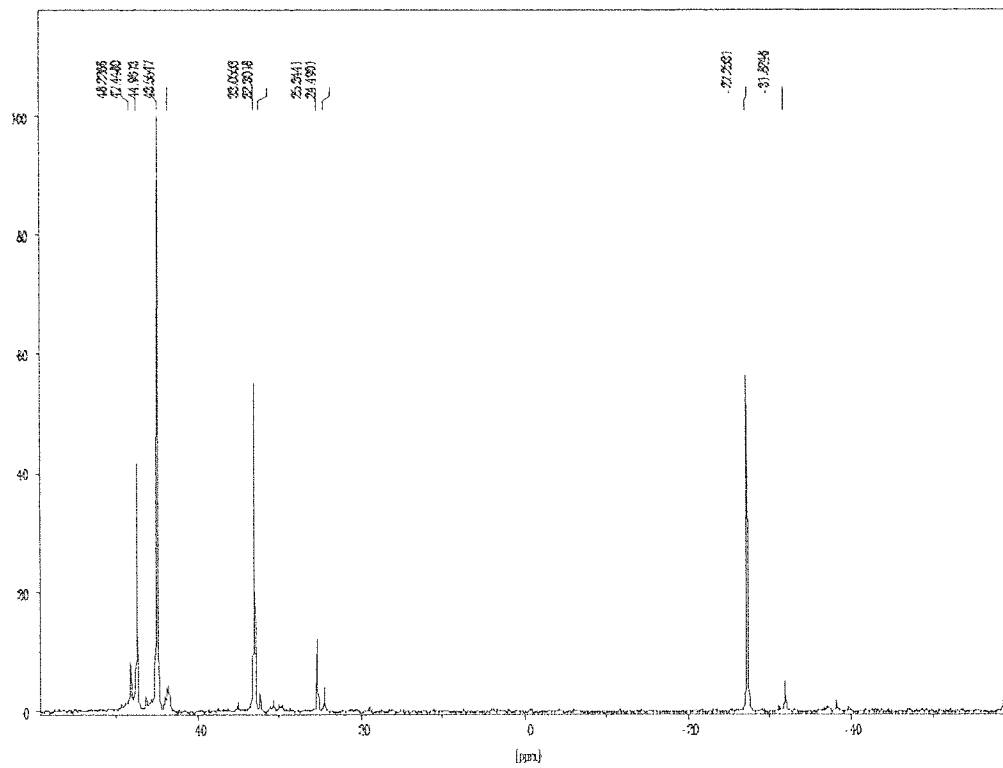


Fig B7 -  $^{31}\text{P}$  NMR of THMP

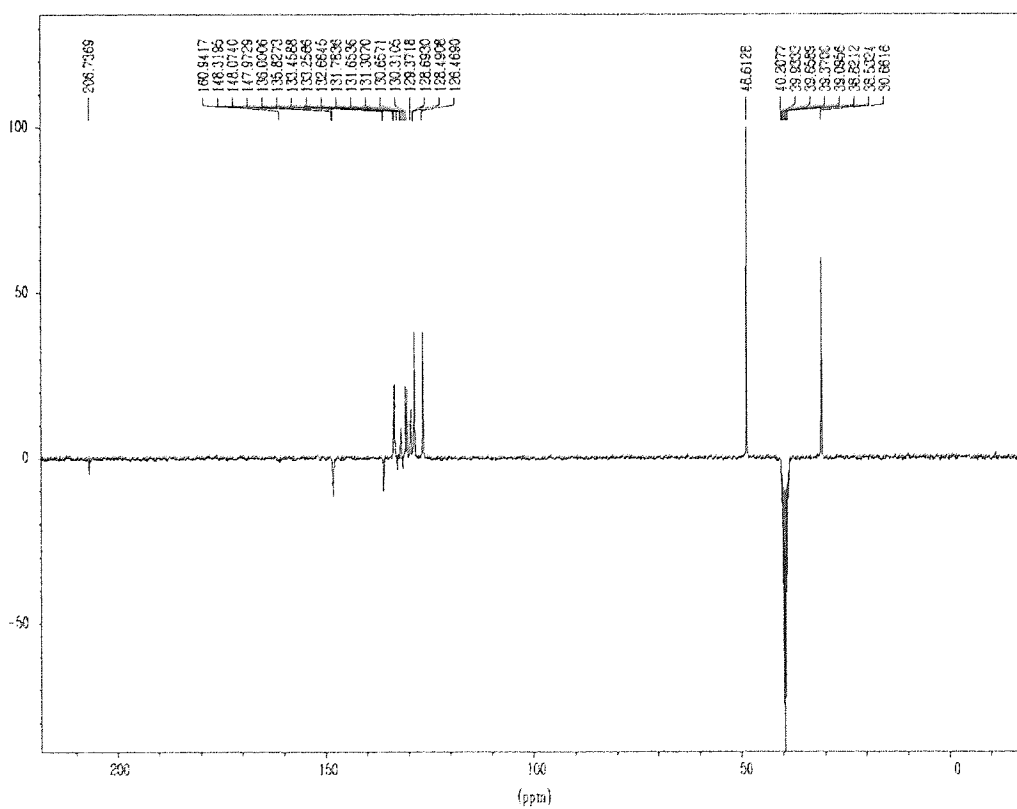


Fig B8 -  $^{13}\text{C}$  NMR of TPPTS

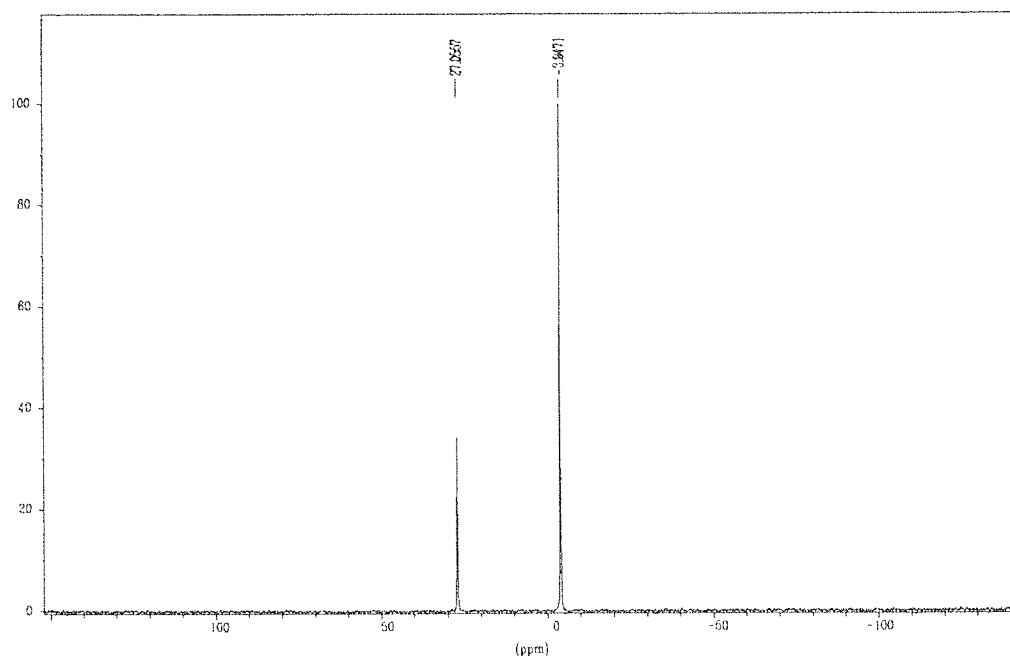


Fig B9-  $^{31}\text{P}$  NMR of TPPTS

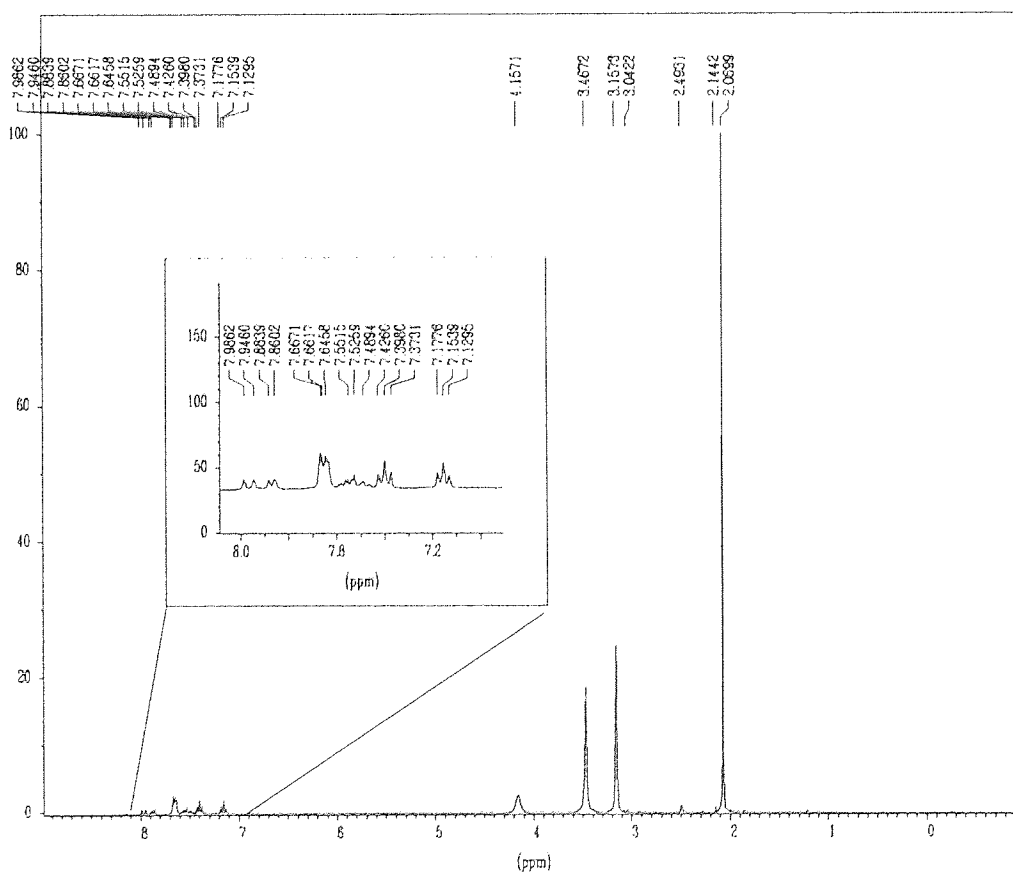


Fig B10 -  $^1\text{H}$  NMR of TPPTS

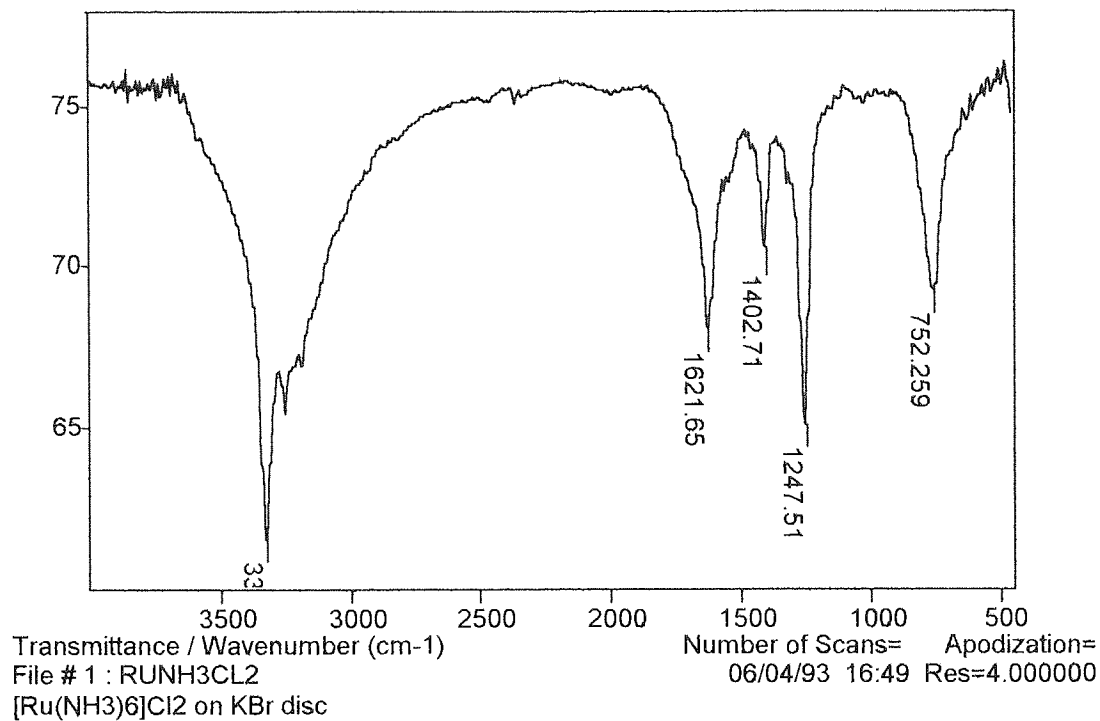


Fig B11- FTIR of [Ru(NH<sub>3</sub>)<sub>6</sub>]Cl<sub>2</sub>

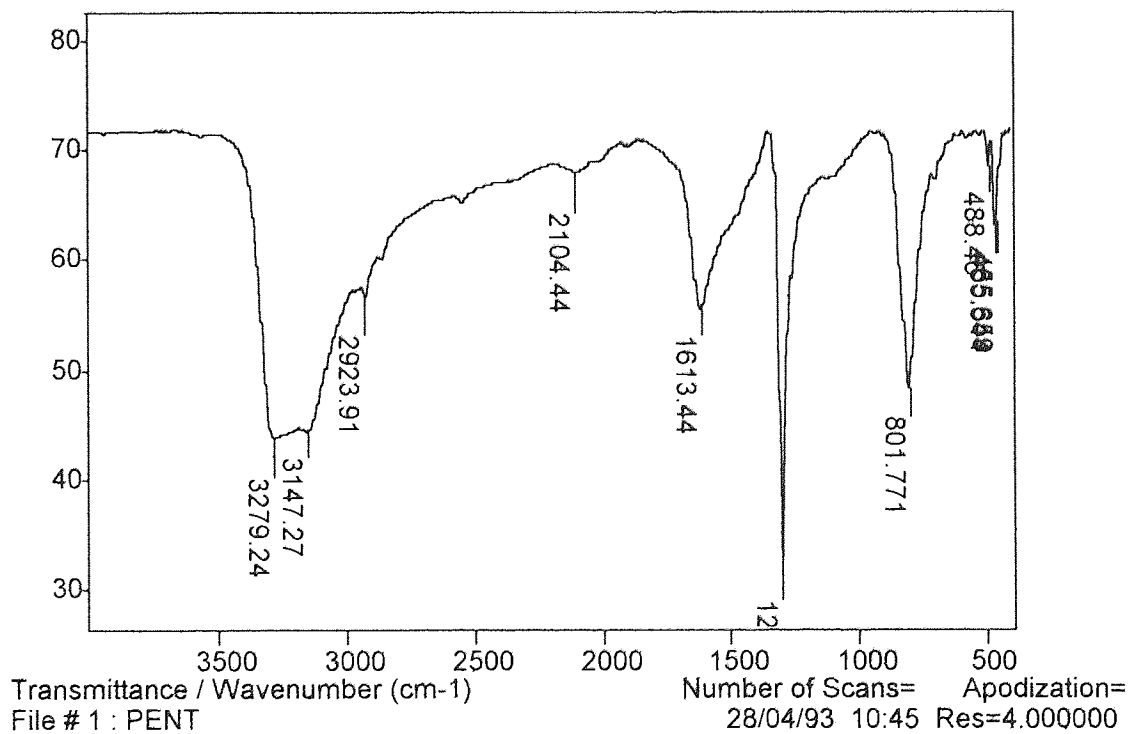


Fig B12 - FTIR spectrum of [Ru(NH<sub>3</sub>)<sub>5</sub>Cl]Cl<sub>2</sub>

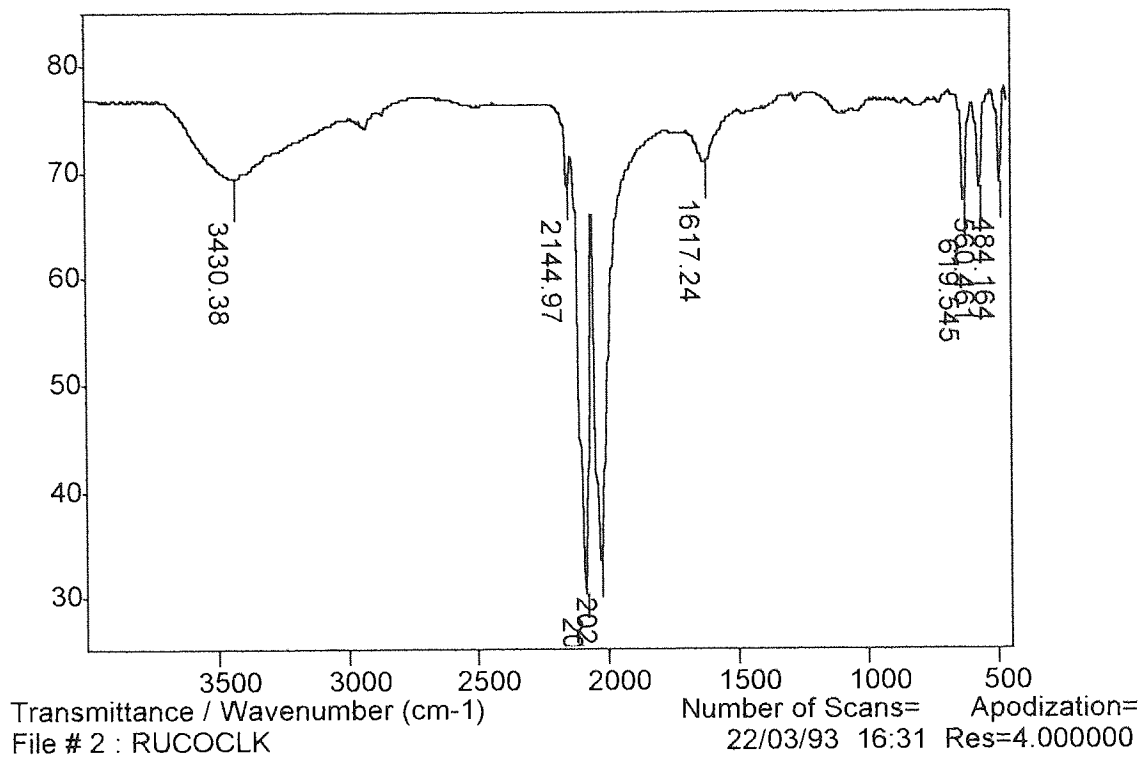


Fig B13- FTIR of Ru(CO)<sub>2</sub>Cl<sub>2</sub> - KBr disk

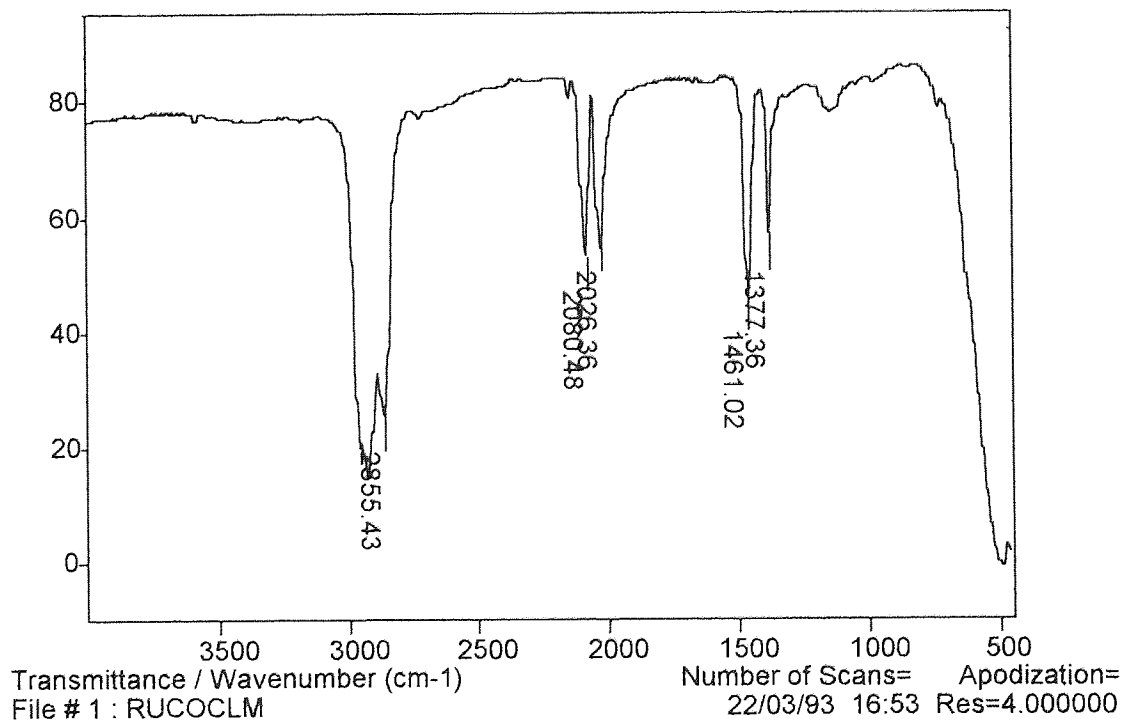


Fig B14 - FTIR of Ru(CO)<sub>2</sub>Cl<sub>2</sub> - Nujol Mull

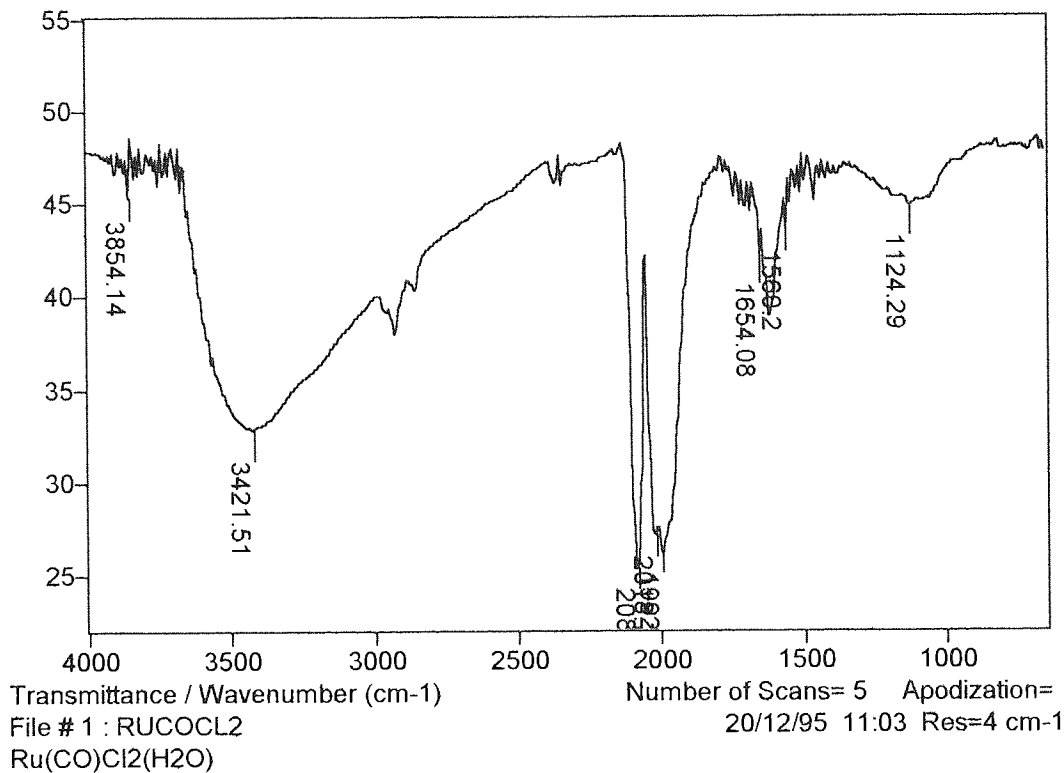


Fig B15 - FTIR of Ru(CO)Cl<sub>2</sub>(H<sub>2</sub>O)

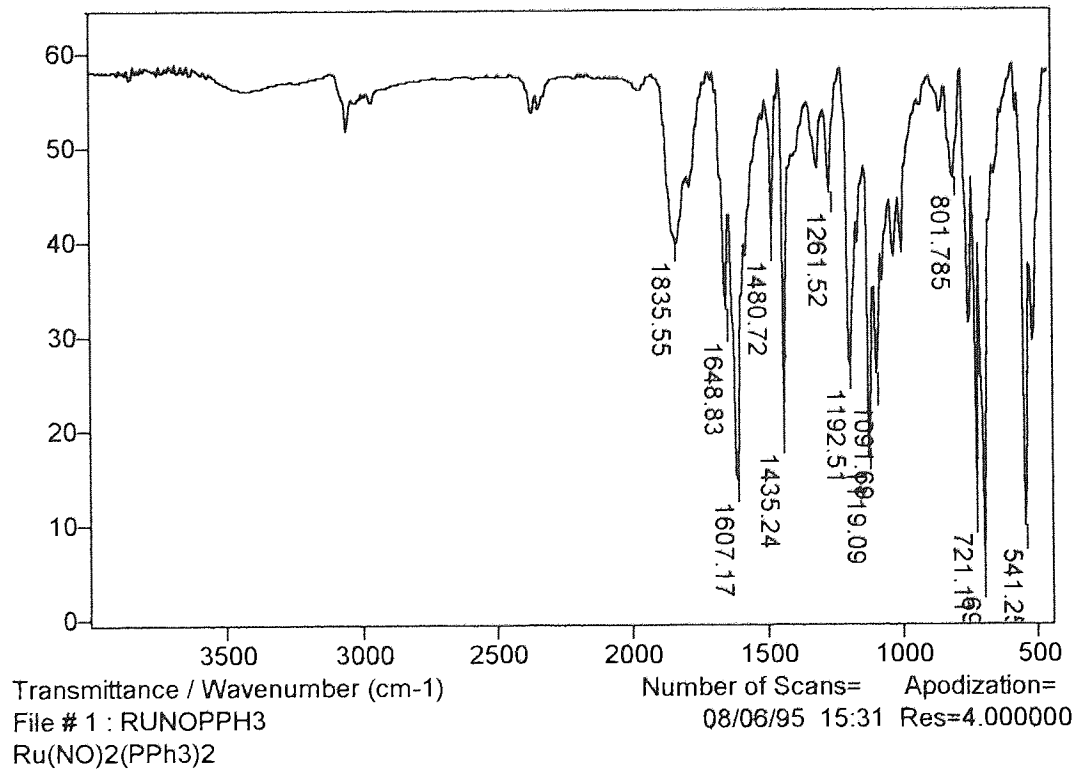


Fig B16 - FTIR of Ru(NO)<sub>2</sub>(PPh<sub>3</sub>)<sub>2</sub>



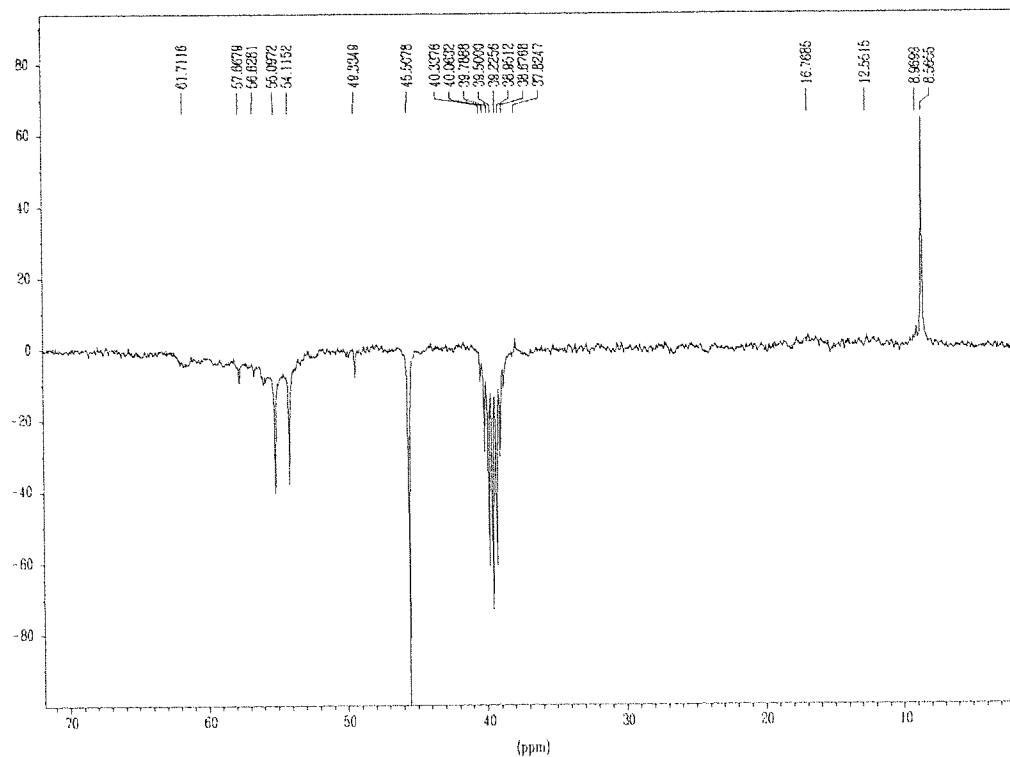


Fig B17-  $^{13}\text{C}$  NMR of Ru-P(CH<sub>2</sub>OH)<sub>3</sub> complex - Method 2

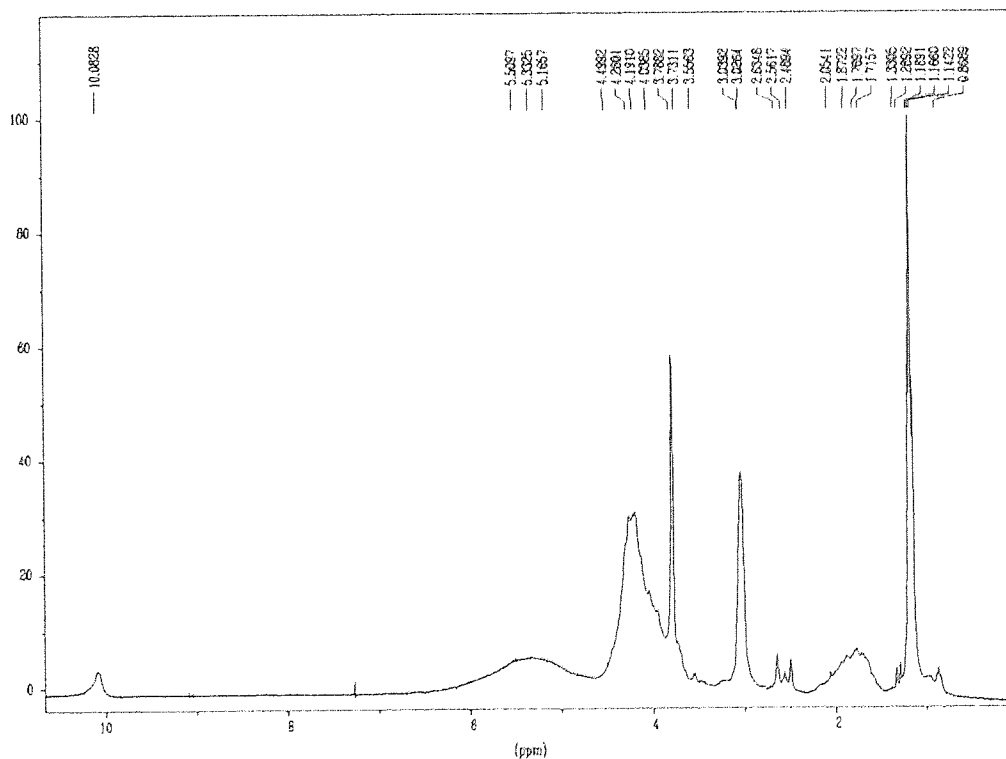


Fig B18 -  $^1\text{H}$  NMR of Ru-P(CH<sub>2</sub>OH)<sub>3</sub> complex - Method 2

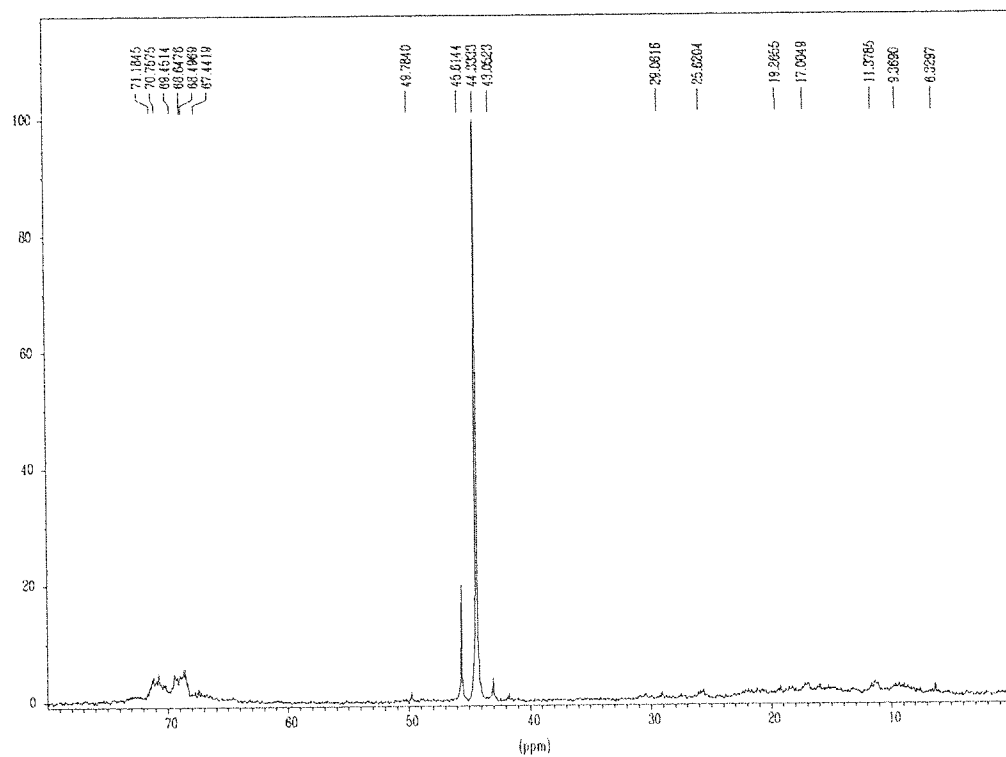


Fig B19 - <sup>31</sup>P NMR of Ru-P(CH<sub>2</sub>OH)<sub>3</sub> complex - Method 2

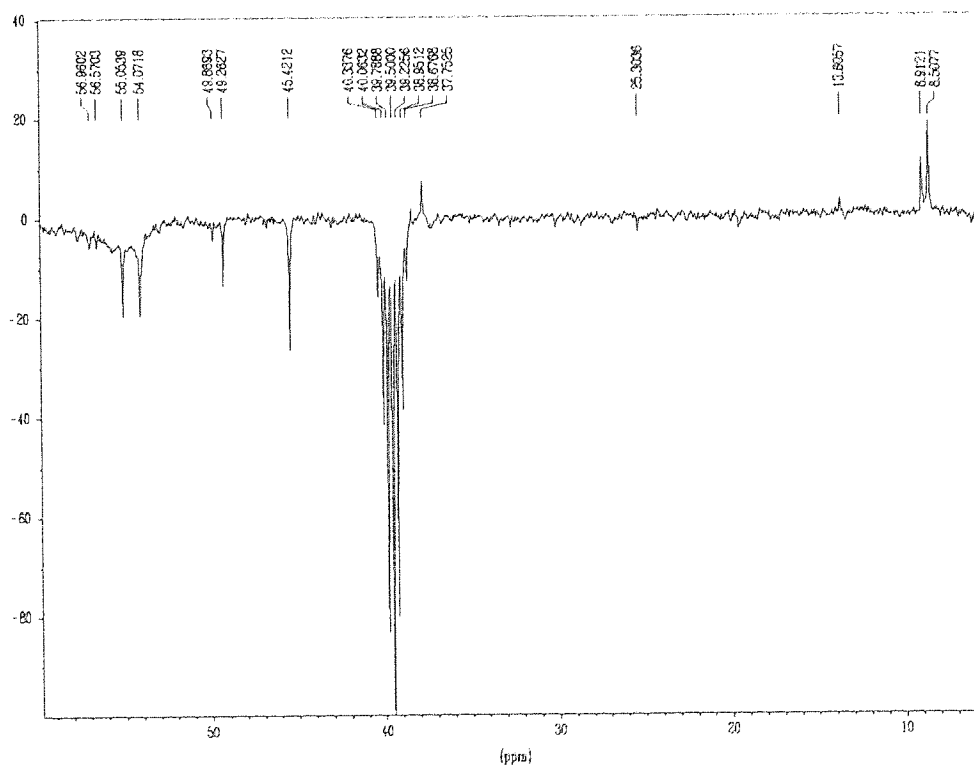


Fig B20 - <sup>13</sup>C NMR of Ru-P(CH<sub>2</sub>OH)<sub>3</sub> complex - Method 3

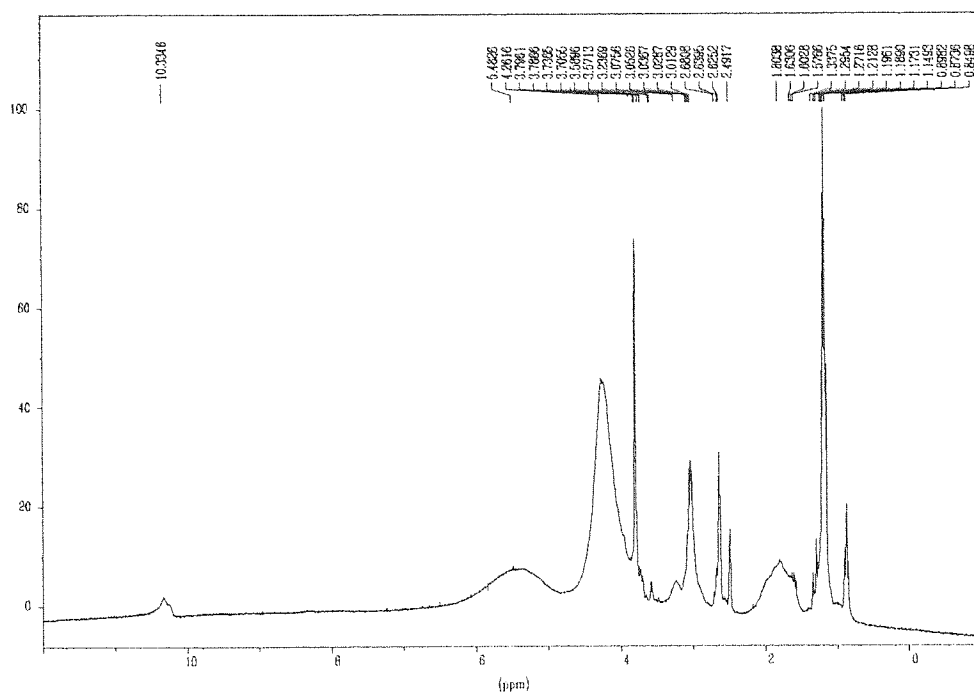


Fig B21 -  $^1\text{H}$  NMR of  $\text{Ru-P}(\text{CH}_2\text{OH})_3$  complex - Method 3

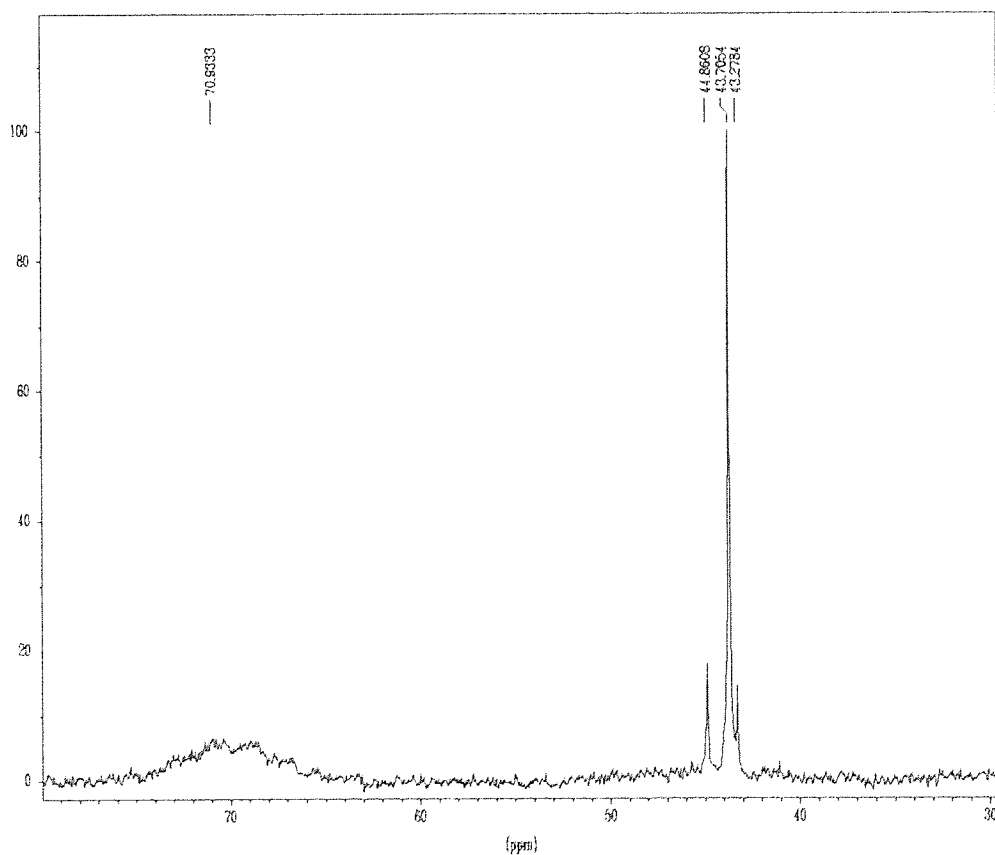


Fig B22 -  $^{31}\text{P}$  NMR of  $\text{Ru-P}(\text{CH}_2\text{OH})_3$  complex - Method 3

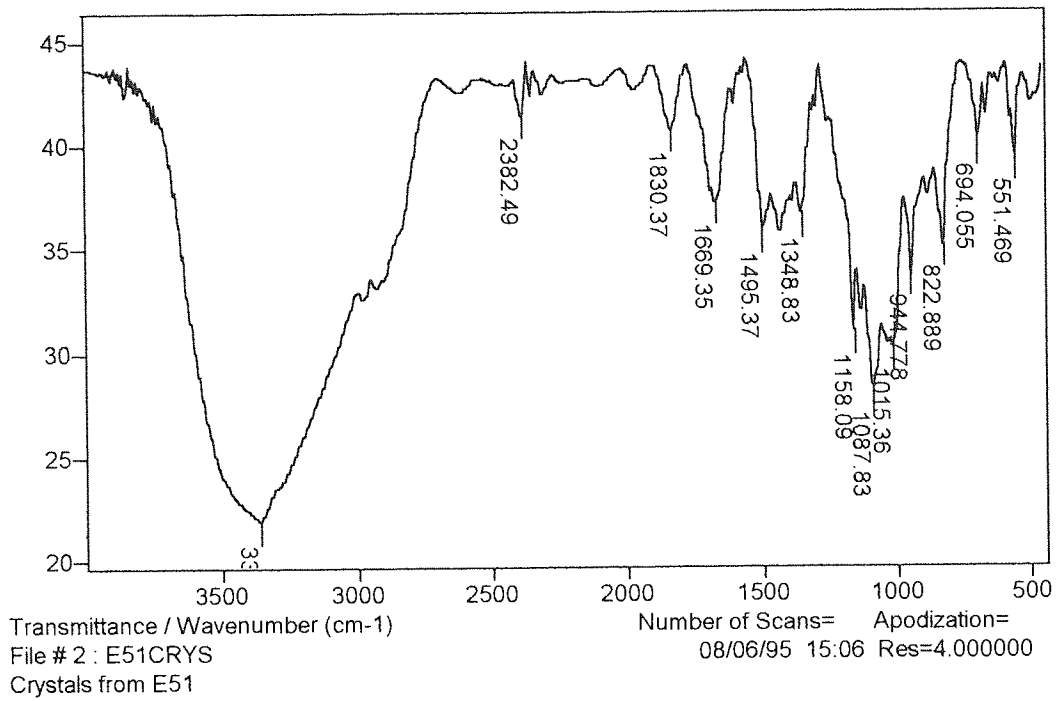


Fig B23 - FTIR of crystals from attempted synthesis of  $\text{Ru}(\text{NO})_2(\text{P}(\text{CH}_2\text{OH})_3)_2$

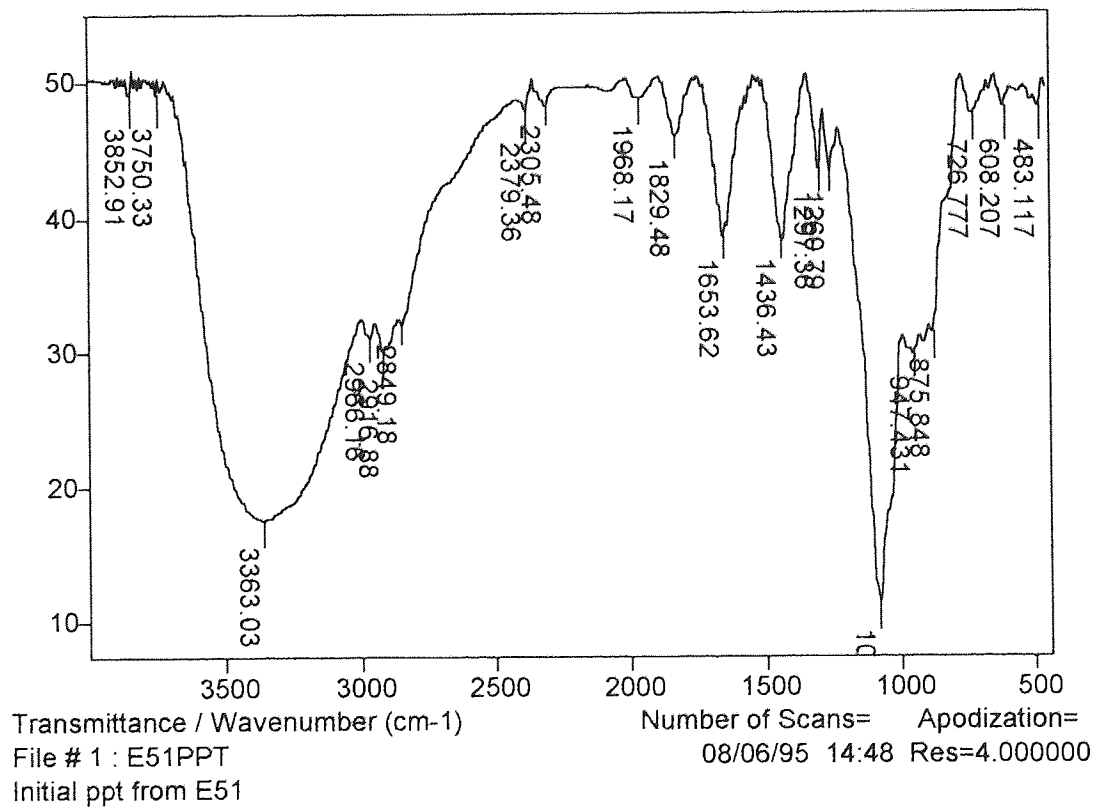


Fig B24 - FTIR of ppt from attempted synthesis of  $\text{Ru}(\text{NO})_2(\text{P}(\text{CH}_2\text{OH})_3)_2$



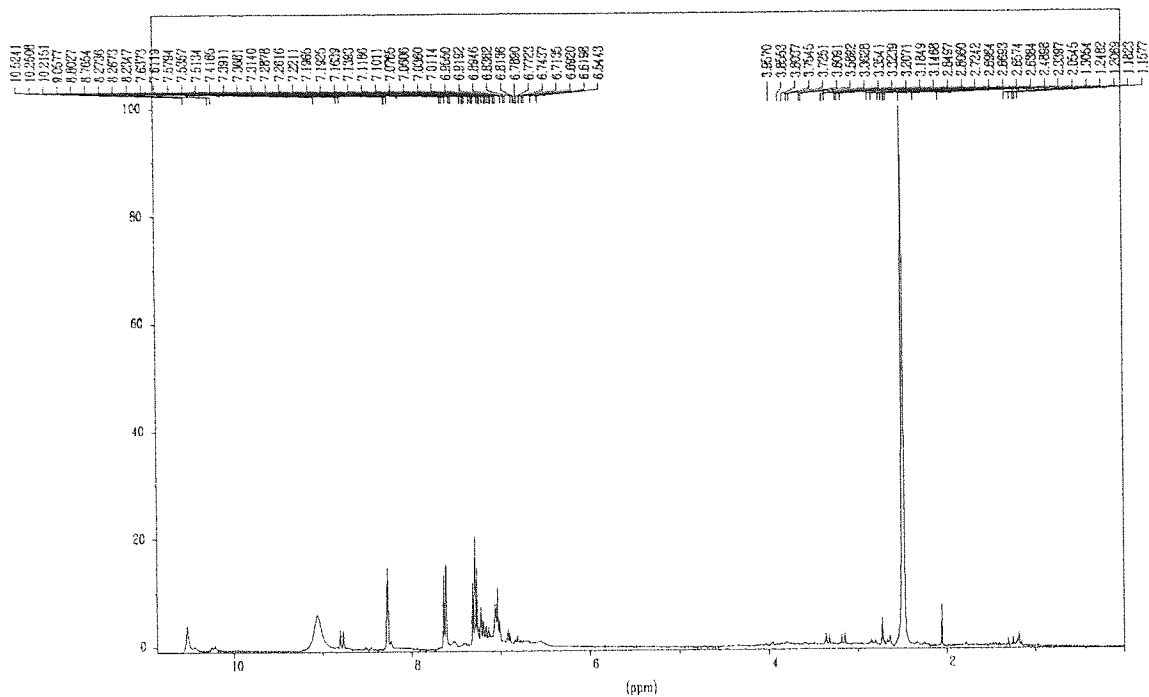


Fig B27 -  $^1\text{H}$  NMR of orange residue from  $\text{Ir-P}(\text{CH}_2\text{OH})_3$  synthesis.

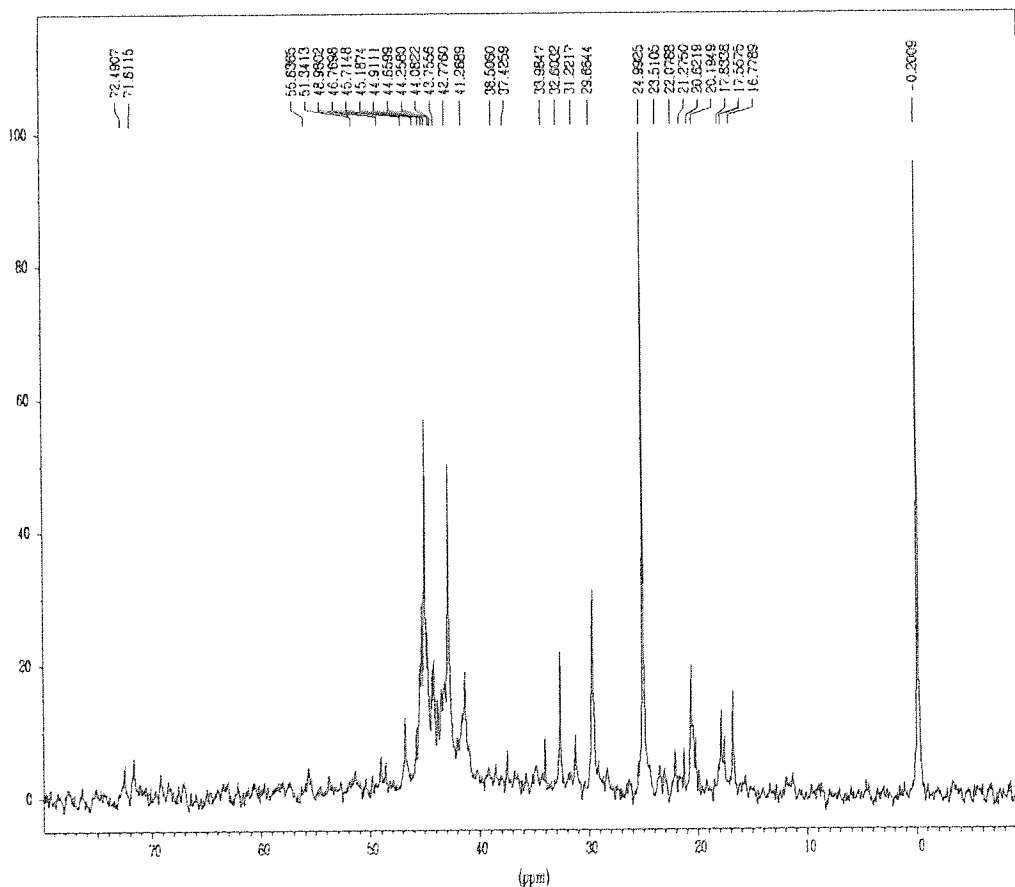


Fig B28 -  $^{31}\text{P}$  NMR of orange residue from  $\text{Ir-P}(\text{CH}_2\text{OH})_3$  synthesis.

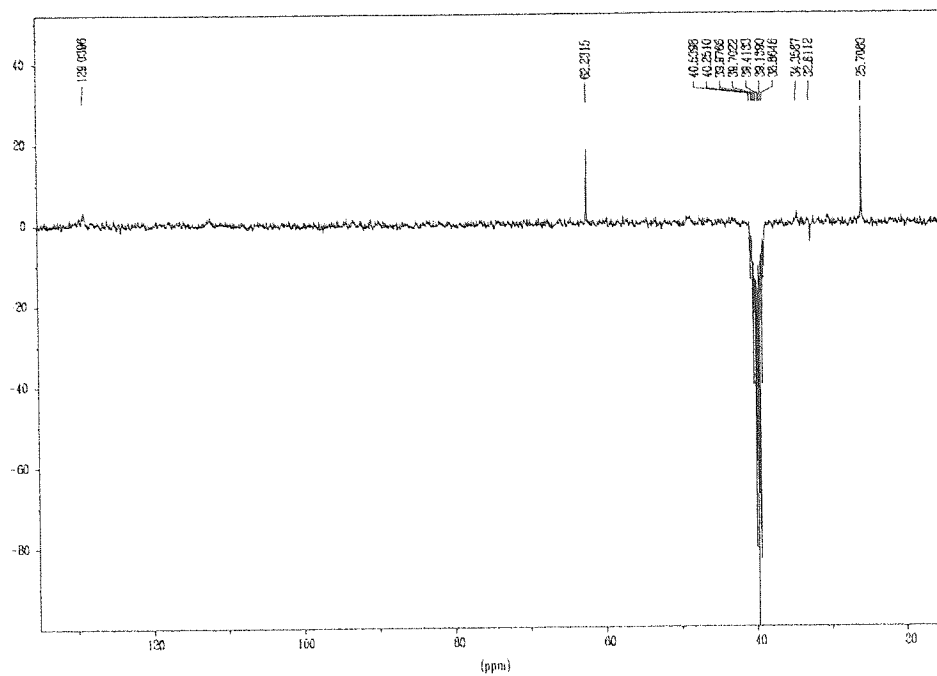


Fig B29 -  $^{13}\text{C}$  NMR of precipitate of  $\text{Ir-P}(\text{CH}_2\text{OH})_3$  synthesis.

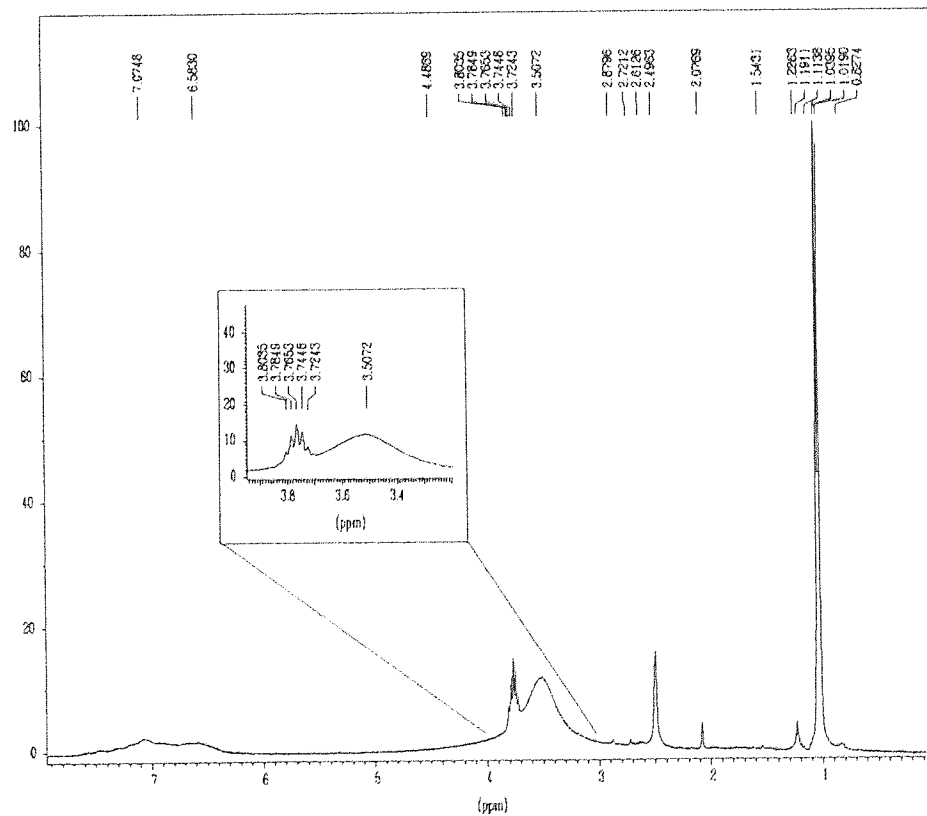


Fig B30 -  $^1\text{H}$  NMR of precipitate from  $\text{Ir-P}(\text{CH}_2\text{OH})_3$  synthesis.

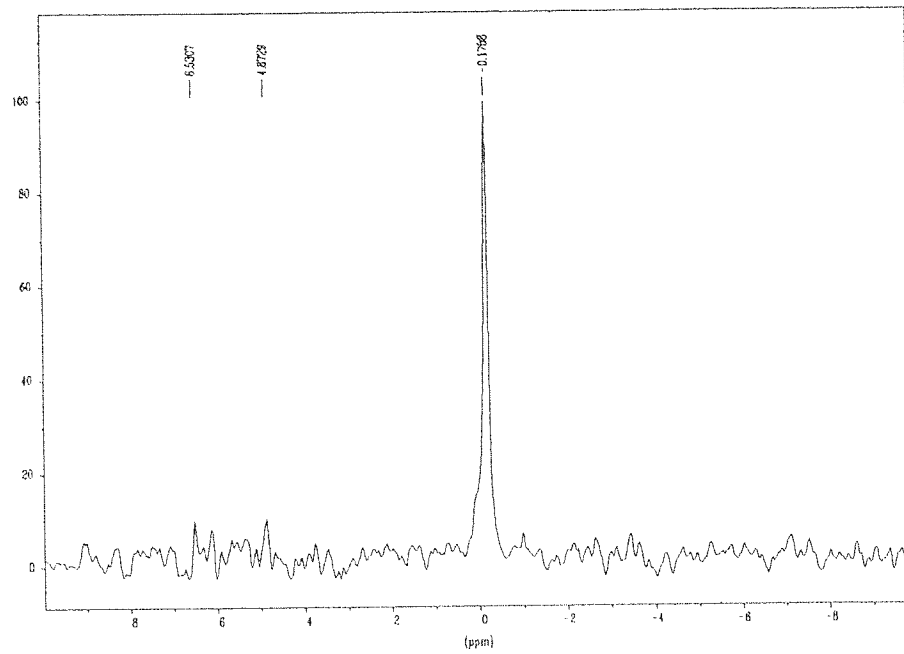


Fig B31 - <sup>31</sup>P NMR of precipitate from Ir-P(CH<sub>2</sub>OH)<sub>3</sub> synthesis.

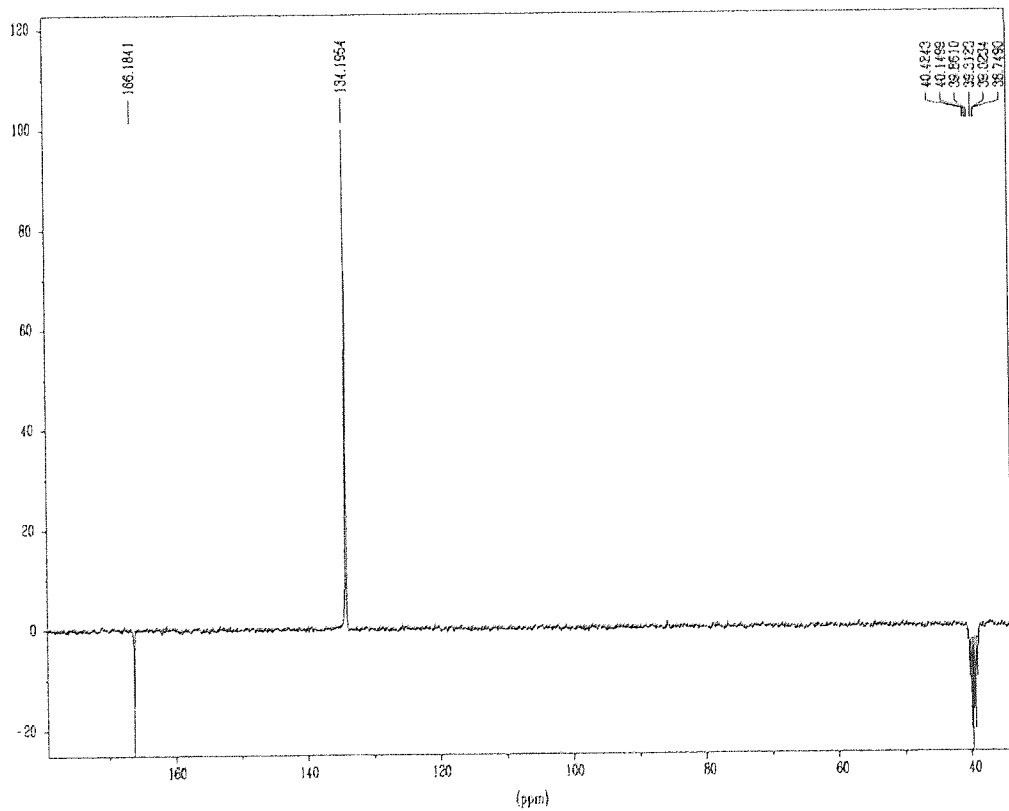


Fig B32 - <sup>13</sup>C NMR of precipitate from reaction between monomer and Ru(CO)Cl<sub>2</sub>(H<sub>2</sub>O) - Run 4



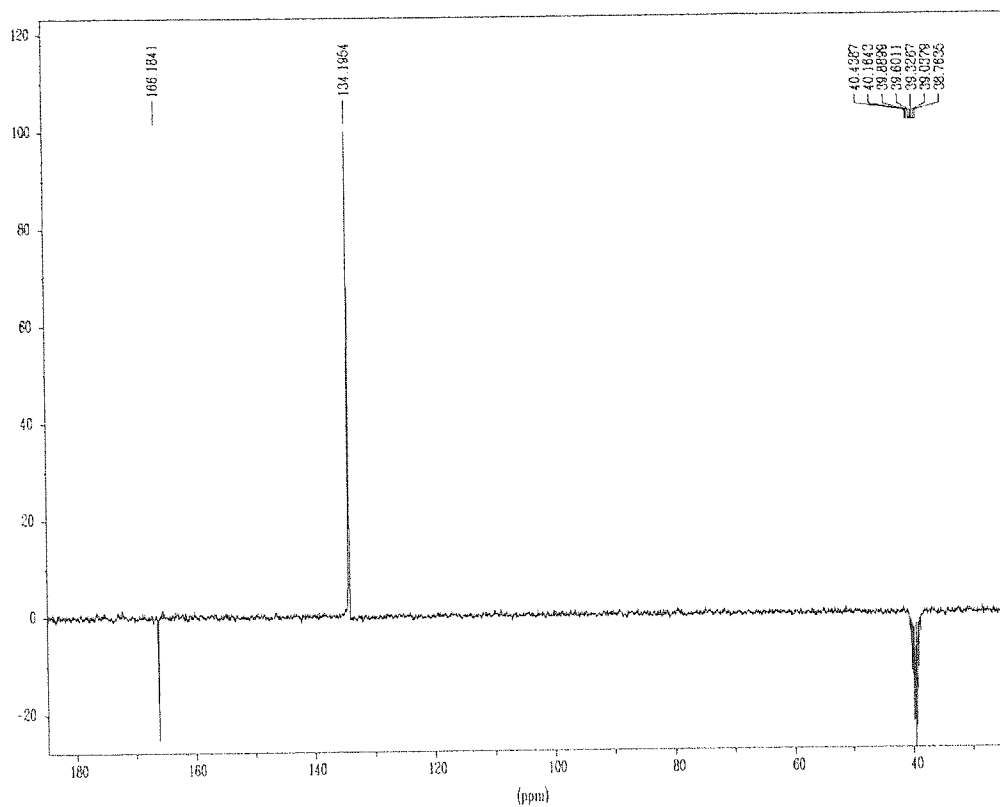


Fig B33-  $^{13}\text{C}$  NMR of precipitate from reaction between monomer and  $\text{Ru}(\text{CO})\text{Cl}_2(\text{H}_2\text{O})$  - Run 5

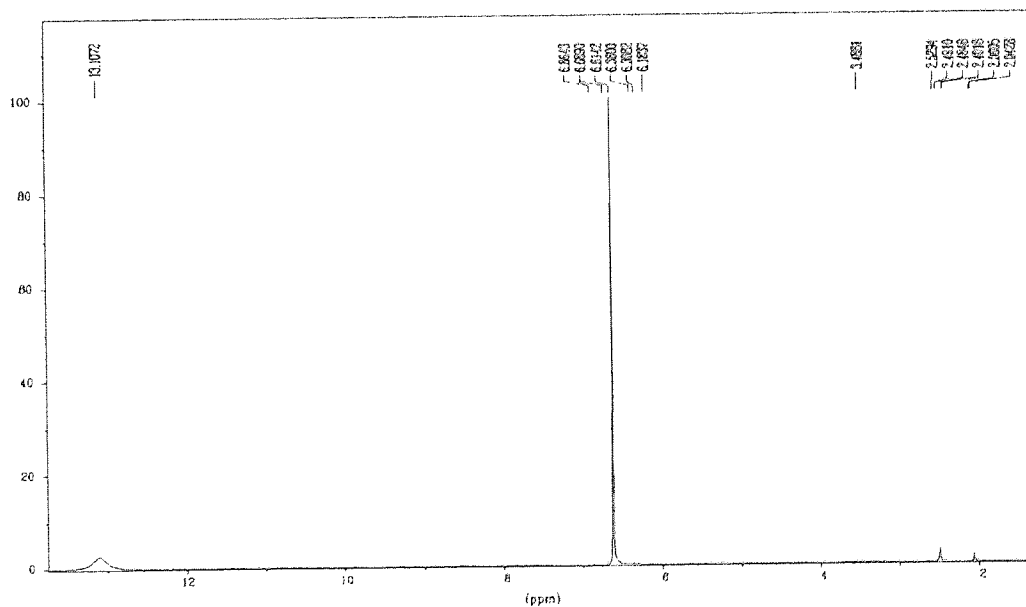


Fig B34 -  $^1\text{H}$  NMR of precipitate from reaction between monomer and  $\text{Ru}(\text{CO})\text{Cl}_2(\text{H}_2\text{O})$  - Run 4

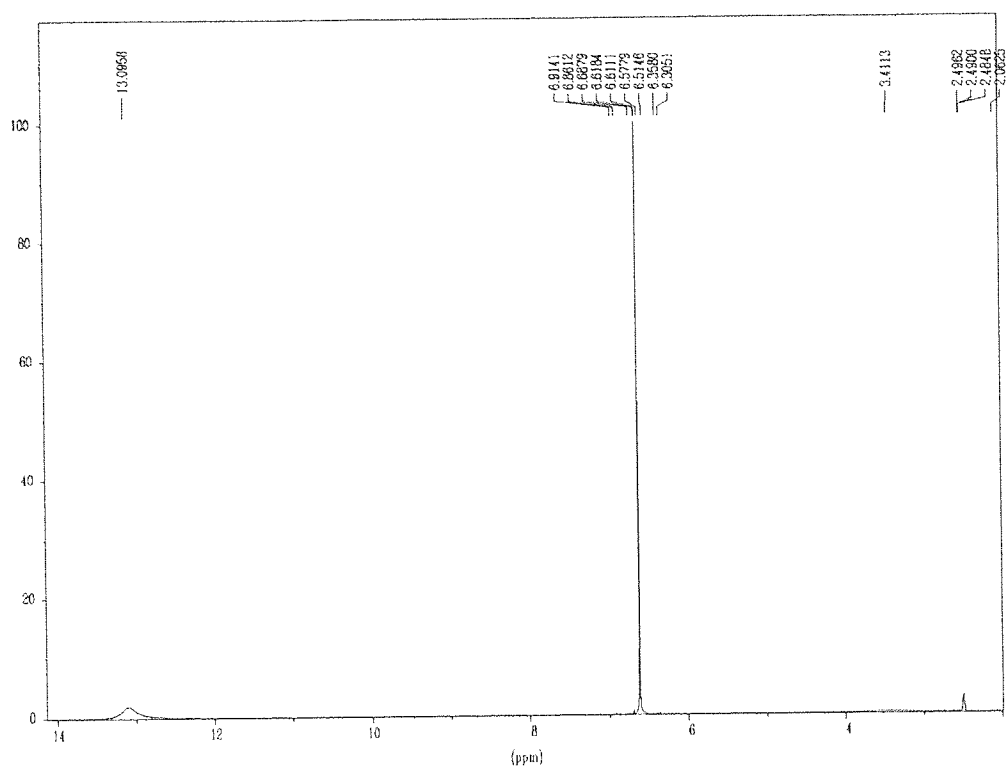


Fig B35 -  $^1\text{H}$  NMR of precipitate from reaction between monomer and  $\text{Ru}(\text{CO})\text{Cl}_2(\text{H}_2\text{O})$  - Run 5

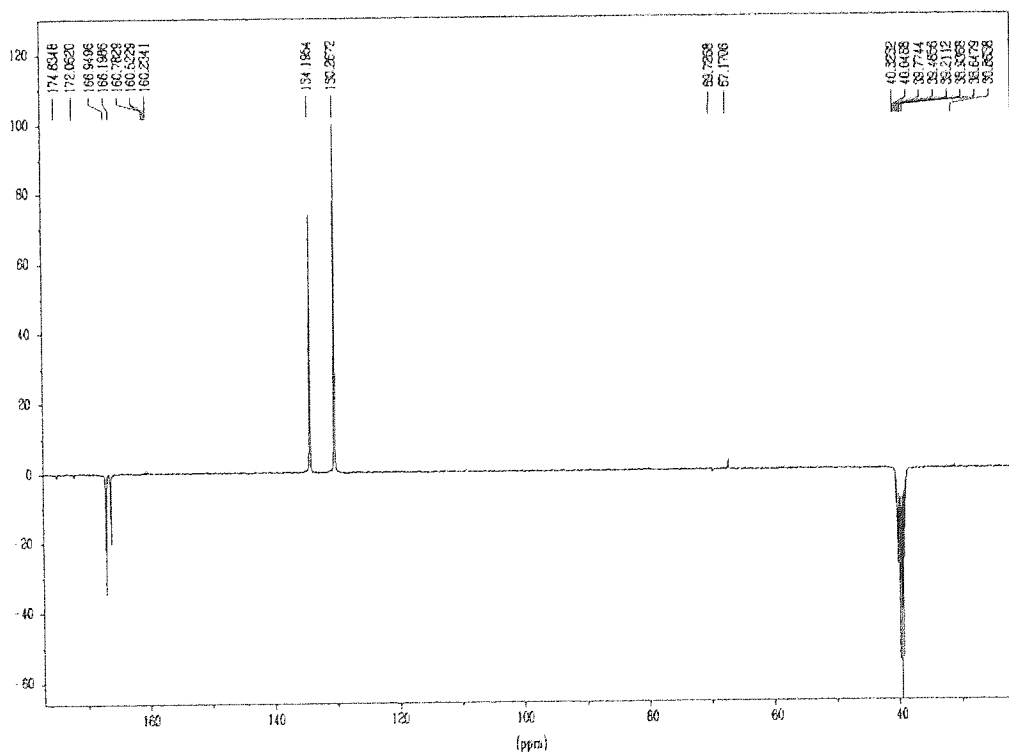


Fig B36 -  $^{13}\text{C}$  NMR of residue from reaction between monomer and  $\text{Ru}(\text{CO})\text{Cl}_2(\text{H}_2\text{O})$  - Run 4

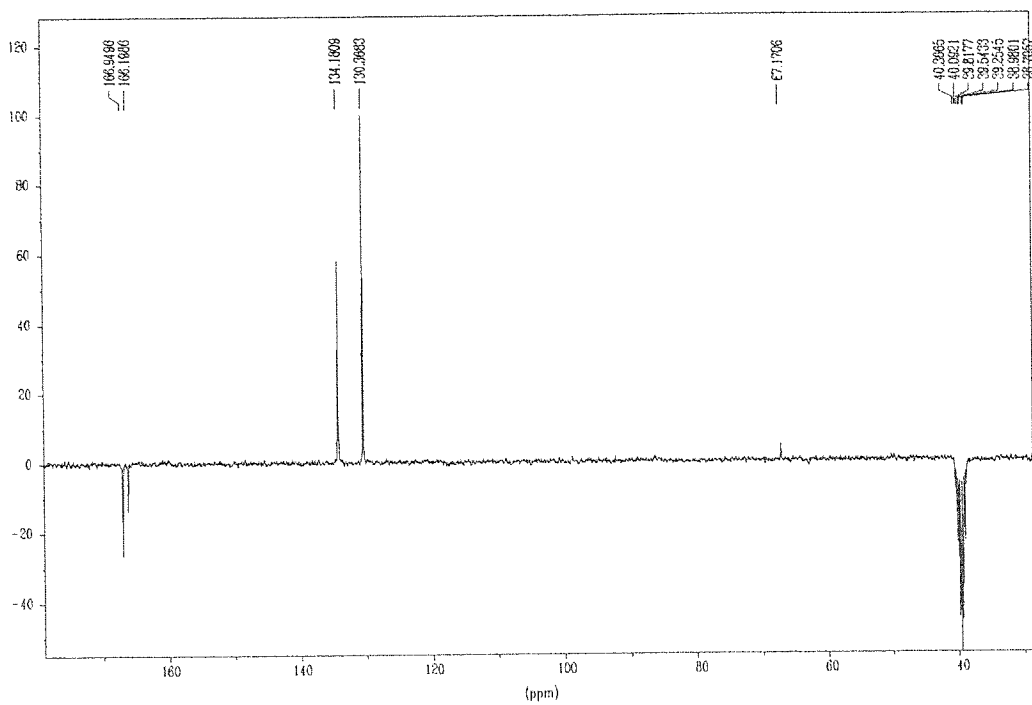


Fig B37 -  $^{13}\text{C}$  NMR of residue from reaction between monomer and  $\text{Ru}(\text{CO})\text{Cl}_2(\text{H}_2\text{O})$  - Run 5

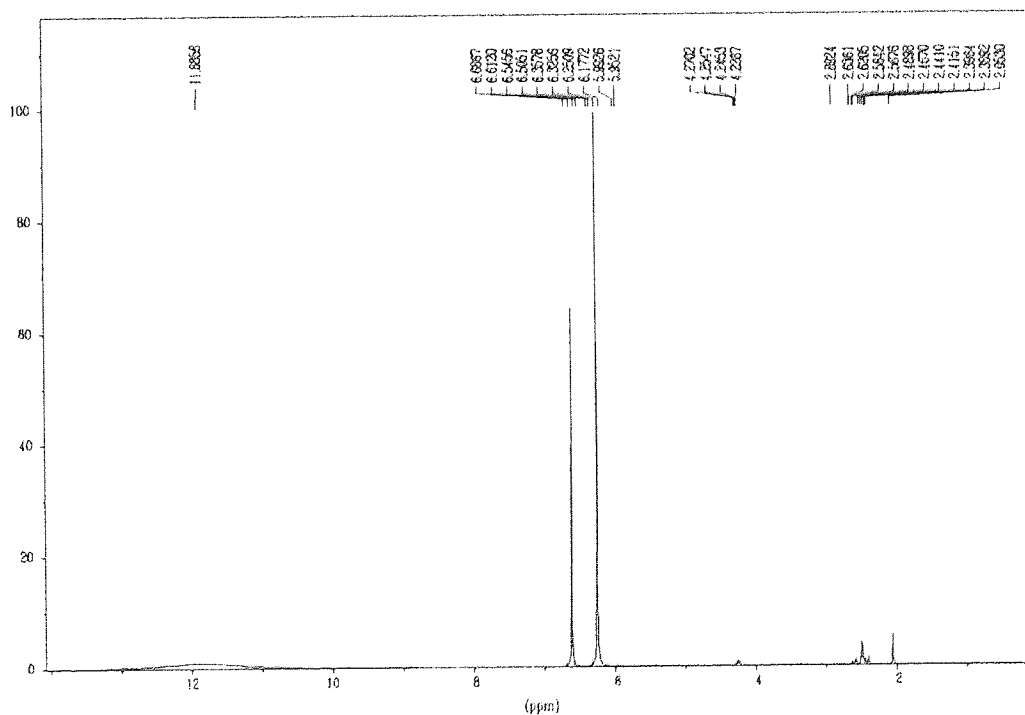


Fig B38 -  $^1\text{H}$  NMR of residue from reaction between monomer and  $\text{Ru}(\text{CO})\text{Cl}_2(\text{H}_2\text{O})$  - Run 4

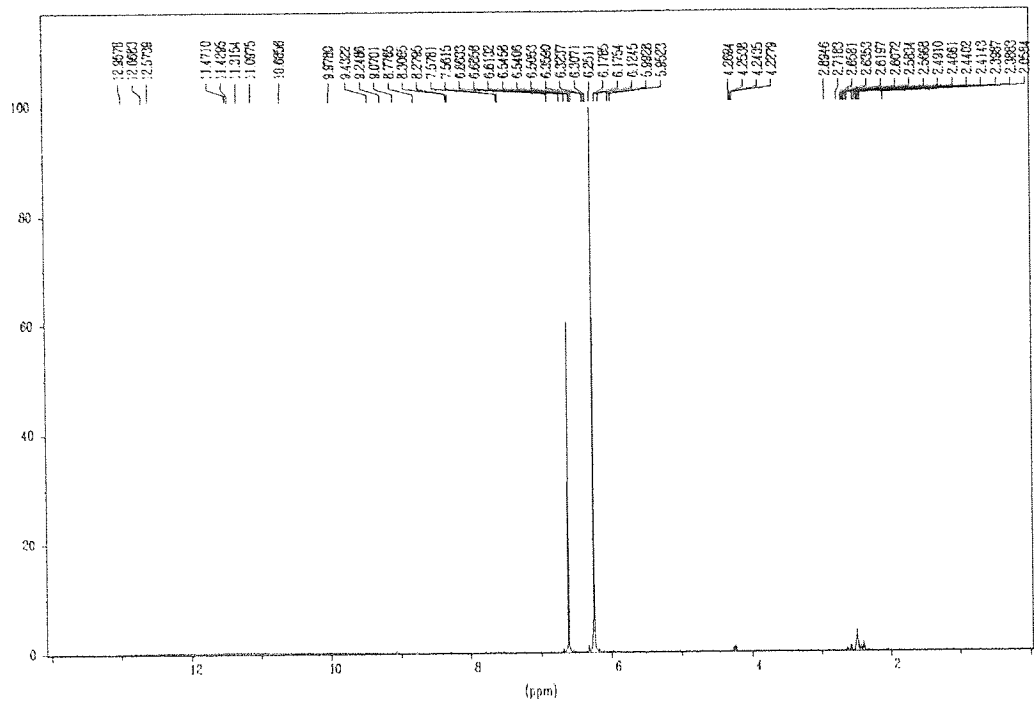


Fig B39 - <sup>1</sup>H NMR of residue from reaction between monomer and Ru(CO)Cl<sub>2</sub>(H<sub>2</sub>O) - Run 5

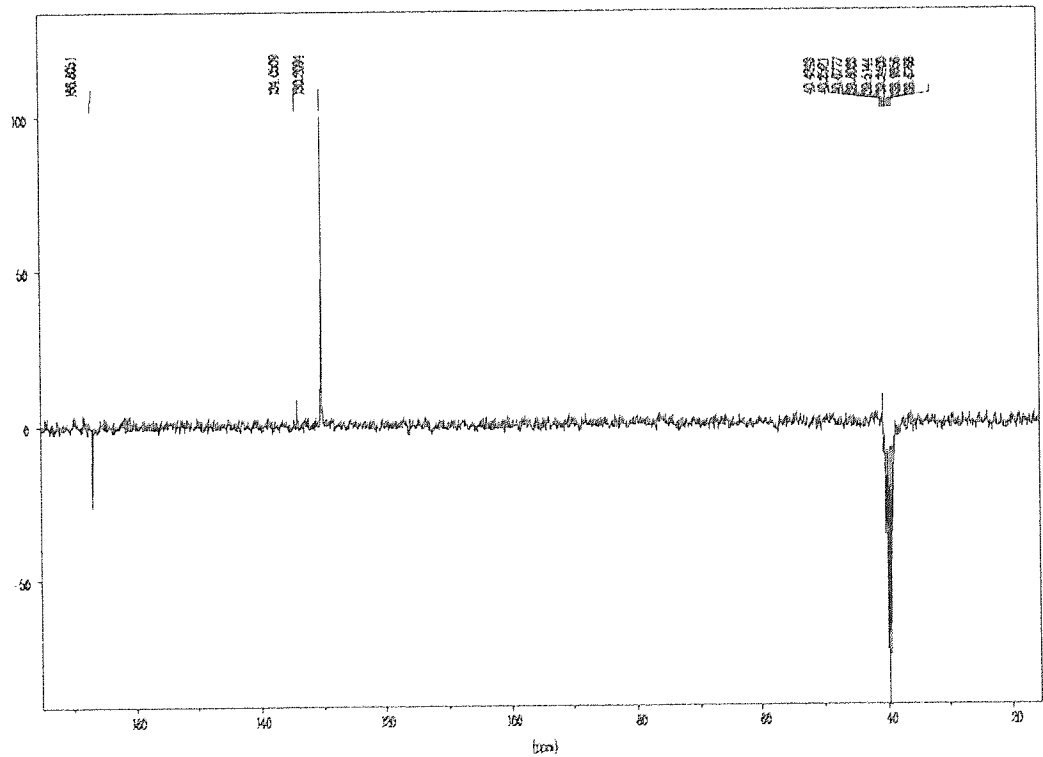


Fig B40 - <sup>13</sup>C NMR of product of reaction between monomer and Ru-P(CH<sub>2</sub>OH)<sub>3</sub> complex.

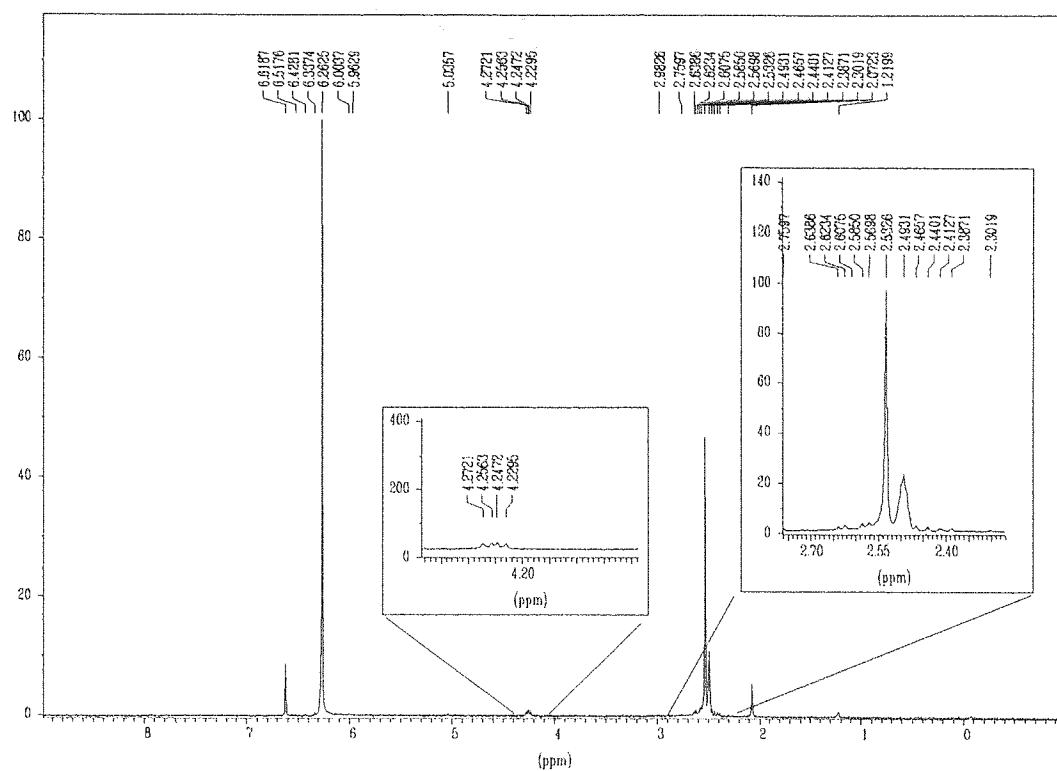


Fig B41 -  $^1\text{H}$  NMR of product of reaction between monomer and  $\text{Ru-P}(\text{CH}_2\text{OH})_3$  complex.